# Experimental analysis of Calcium Looping CO$_2$ capture in coal-fired power plants

vorgelegt von
**Joseba Moreno Mendaza**
aus Estella-Lizarra, Spanien

# Erklärung

Hiermit versichere ich, Joseba Moreno Mendaza, die vorliegende Arbeit ohne Hilfe Dritter und nur mit den angegebenen Quellen und Hilfsmitteln angefertigt zu haben. Alle Stellen, die Quellen entnommen wurden, sind als solche kenntlich gemacht worden. Diese Arbeit hat in gleicher oder ähnlicher Form noch keiner Prüfungsbehörde vorgelegen. In der abgegebenen Arbeit stimmen die schriftliche und elektronische Fassung überein.

To my wife, my sister, and my parents.
For their unconditional support.

# Acknowledgments

# Contents

# List of Symbols

## Latin symbols

| Symbol | Unit | Meaning |
|---|---|---|
| $d_p$ | µm, mm | particle size |
| E | mol/mol, % | $CO_2$ capture efficiency |
| $e_i$ | $mg/MJ_{th}$ | (fuel-specific) emission factor of component "i" |
| $f_{active}$ | | active/reacting particle fraction |
| h | m | height |
| k | | sorbent deactivation constant |
| $k_S$ | $s^{-1}$ | surface reaction rate constant |
| $n_{cycles}$ | | number of calcination and carbonation cycles |
| $\dot{N}_i$ | mol/s | molar flow rate of component "i" |
| $N_i$ | mol, kmol | molar amount of component "i" |
| p | bar, MPa | pressure |
| $p_i$ | bar | partial pressure of component "i" |
| $Q_3$ | $m^3/m^3$ | cumulative volume particle size distribution |
| $q_3$ | $m^3/(m^3\,µm)$ | frequency volume particle size distribution |
| t | s, min, h | time |
| T | °C | temperature |
| $u_0$ | m/s | superficial gas velocity |
| $W_s$ | $kg/m^2$, kg | solid inventory |
| X | mol/mol | sorbent conversion |
| $X_{ave}$ | mol/mol, g/g | average $CO_2$ carrying capacity |
| $X_{calc}$ | mol/mol | sorbent carbonate content in/after the calciner |
| $X_{carb}$ | mol/mol | sorbent carbonate content in/after the carbonator |
| $X_{CO_2}$ | mol/mol | sorbent carbonation conversion |
| $x_i$ | kg/kg | mass fraction of component "i" |
| $X_{n_{cycles}}$ | mol/mol | sorbent conversion at "n" cycles |
| $X_r$ | mol/mol, g/g | sorbent residual activity |
| $y_i$ | $m^3/m^3$ | volume fraction of component "i" |

## Greek symbols

| Symbol | Unit | Meaning |
|---|---|---|
| $\varphi$ | | gas-solid contact factor |
| $\xi_{LR}$ | mol/mol | looping ratio |
| $\xi_{MR}$ | mol/mol | make-up ratio |
| $\eta_i$ | mol/mol | absorption efficiency of component "i" |
| $\tau_{active}$ | s | active space time |
| $\nu_{recycled}$ | $m^3/m^3$ | fraction of recirculated flue gas |

## Miscellaneous symbols

| Symbol | Unit | Meaning |
|---|---|---|
| $k_S\varphi$ | $s^{-1}$ | apparent carbonation rate constant |
| $\Delta p$ | mbar | differential pressure |

## Subscripts

| Symbol | Meaning |
|---|---|
| 0 | sorbent (exception: $u_0$) |
| CaL | Calcium Looping |
| calc | calciner / calcination |
| carb | carbonator / carbonation |
| eq | equilibrium |
| FG | Flue Gas |
| fuel | fuel |
| in | inlet |
| loop | loop |
| norm | normalized |
| out | outlet |
| th | thermal |

## Abbreviations

| Symbol | Meaning |
|---|---|
| 0D | 0-Dimensional |
| 1D | 1-Dimensional |
| ASU | Air Separation Unit |

| Symbol | Meaning |
|---|---|
| BECCS | Bio-Energy with Carbon Capture and Storage |
| BFB | Bubbling Fluidized Bed |
| BPB | By-Product of Biodiesel |
| CaL | Calcium Looping |
| CCS | Carbon Capture and Storage |
| CFA | Coal Fly Ash |
| CFB | Circulating Fluidized Bed |
| COP21 | 21st (climate) Conference Of the Parties |
| DFB | Dual Fluidized Bed |
| FGD | Flue Gas Desulfurization |
| HEX | Heat EXchanger |
| IEA | International Energy Agency |
| IPCC | Intergovernmental Panel on Climate Change |
| LS | Loop Seal |
| MSW | Municipal Solid Waste |
| NGCC | Natural Gas Combined Cycle |
| PSD | Particle Size Distribution |
| RFCS | Research Fund for Coal and Steel |
| SRF | Solid Recovered Fuel |
| TFB | Turbulent Fluidized Bed |
| TG | Thermo-Gravimetry (also Thermo-Gravimetric) |
| TGA | Thermo-Gravimetric Analyzer |
| TRL | Technology Readiness Level |
| WtE | Waste-to-Energy |

# Abstract

The Calcium Looping (CaL) technology has recently emerged as a viable option for efficiently decarbonizing power plant flue gases. The process is based on the sequential calcination and carbonation of a calcium-based sorbent, usually limestone. Although CaO-based sorbents offer many advantages, they typically suffer from a rapid decline in $CO_2$ capture during cyclic operation. This latter aspect has remained an urgent issue to be addressed for CaL power plant application. Besides, coal-fired power stations are expected to operate in a load-following mode due to the growing share of renewable energy. Moreover, the usage of alternative fuels in existing coal-fired power units is envisaged to ensure sustainable energy generation and to avoid an overshoot of $CO_2$ emissions into the atmosphere.

This thesis aims at addressing each of the previously anticipated challenges individually. A range of experimental investigations studying the cycling conversion of three originally distinct limestones – Rheinkalk, Riyadh, and Saabar – were conducted by thermogravimetric analysis (TGA). To this end, several carbonation routines were employed, including $SO_2$ and steam. The Saabar metamorphosed limestone showed to be negatively influenced by the presence of steam, while limited sulfation positively affected its $CO_2$ capture performance. This unusual behavior can be ascribed to pore blocking during carbonation. Besides, Rheinkalk and Riyadh behaved similarly, resembling the typical behavior of common unmetamorphosed limestones. The decay in Rheinkalk conversion upon cycling was further explored at a 20 $kW_{th}$ CaL facility setting different carbonation conditions. A mathematical expression is proposed to compare the results obtained in both facilities, correlating them with adequate accuracy. In the following, an alternative reactor concept based on a bubbling fluidized bed (BFB) carbonator was employed for flexible load operation. Within the first phase of the tests, a parametric study was conducted at the 20 $kW_{th}$ CaL facility to evaluate the influence of temperature, $CO_2$ loading, and steam concentration upon the BFB carbonator performance. Hereafter, investigations at a 200 $kW_{th}$ semi-industrial CaL plant were conducted to evaluate the flexible behavior of the suggested carbonator setting. It was demonstrated that the BFB carbonator can be operated stably with gas superficial velocities ranging from 0.8 to 2.0 m/s without affecting the solid circulation between reactors. The latter range corresponds to a maximum reduction in the flue gas load of 60 % with respect to the nominal operation case. A simple carbon material balance was applied for preliminary validation of the carbonator performance. In addition, a carbonator model

approach based on the active space time ($\tau_{active}$) was proposed for a more detailed result interpretation. According to the results, an active space time value of 41 s was identified as sufficient to achieve an equilibrium normalized capture efficiency ($E_{norm}$) of 90 %. Moreover, the circulating fluidized bed (CFB) calciner operation appeared independent from the flue gas load set in the carbonator. The reactor could be successfully operated with recirculation rates as low as 27 %, reaching inlet dry oxygen concentrations as high as 0.55 m$^3$/m$^3$. Within the next phase of the experiments, the impact of fuel selection in the calciner was evaluated. Oxy-combustion of hard coal, wheat straw, and solid recovered fuel (SRF) was demonstrated during more than 43 h of continuous operation. A range of experiments was conducted to address the influence of fuel blending and inlet oxygen concentration on pollutant formation (i.e., $NO_x$, $SO_2$, HCl) and hydrodynamic behavior. The calciner inlet $O_2$ concentration appeared to barely affect the pollutant formation process. In contrast, biomass substitution influenced gaseous emissions by modifying the fuel mixture's nitrogen and chlorine content. Concurrently, specific HCl emissions were significantly reduced by the presence of Ca-species in the calciner solid inventory, yielding chlorine retention rates above 0.90 mol/mol with at least 30 % biomass substitution. Besides, ash accumulation led to elevated pressure drops over the CFB riser when operating with alternative fuels. Although this was not a limiting aspect in this work, results anticipate that ash accumulation might constitute a key challenge to be addressed in fluidized beds employing combustion of low-grade quality fuels.

# Kurzfassung

Die Calcium-Looping-Technologie (CaL) hat sich in jüngster Zeit als vielversprechende Option für die effiziente Dekarbonisierung von Kohlekraftwerken erwiesen. Das Verfahren basiert auf der sequentiellen Kalzinierung und Karbonisierung eines kalkbasierten Sorbens, meist Kalkstein. Obwohl CaO-basierte Sorbentien viele Vorteile bieten, leiden sie in der Regel unter einer schnellen Abnahme der $CO_2$-Aufnahmefähigkeit während des zyklischen Betriebs. Dieser letzte Aspekt ist nach wie vor ein dringendes Problem für die Anwendung von CaL-Kraftwerken. Zudem sollen Kohlekraftwerke aufgrund des wachsenden Anteils erneuerbarer Energien im Lastfolgebetrieb betrieben werden, sodass ein flexibler Betrieb des CaL Prozesses sichergestellt werden muss. Darüber hinaus ist die Verwendung alternativer Brennstoffe in bestehenden Kohlekraftwerken vorgesehen, um eine nachhaltige Energieerzeugung zu gewährleisten und eine Überschreitung der $CO_2$-Emissionen in die Atmosphäre zu vermeiden.

Das Ziel dieser Dissertation ist es, die daraus resultierenden Herausforderungen im Einzelnen zu untersuchen. Die zyklische Umwandlung von drei Kalksteinen unterschiedlicher Herkunft – Rheinkalk, Riyadh und Saabar – wurde mittels Thermogravimetrie (TGA) untersucht, um unter anderem den Einfluss von $SO_2$ und Wasserdampf auf das Sorbensverhalten zu charakterisieren. Wasserdampf wirkte sich bei dem metamorphen Saabar Kalkstein negativ auf die $CO_2$-Aufnahme des Sorbens auf, wohingegen $SO_2$ einen positiven Effekt hatte. Dieses ungewöhnliche Verhalten kann der Porenblockierung während der Karbonisierung zugeschrieben werden. Außerdem zeigten Rheinkalk und Riyadh ein ähnliches Verhalten, das dem typischen Verhalten von nicht-metamorphen Kalksteinen entspricht. Darüber hinaus wurde die Abnahme der Aufnahmefähigkeit in Abhängigkeit der Zyklenzahl in einer 20 kW$_{th}$ CaL-Anlage bei unterschiedlichen Karbonisierungsbedingungen untersucht. Zudem wurde ein mathematischer Ansatz vorgeschlagen, um die in beiden Versuchsanlagen erhaltenen Ergebnisse zu vergleichen. Im weiteren Versuchsverlauf wurde ein alternatives Reaktorkonzept auf Basis eines blasenbildenden Wirbelschichtkarbonators (BFB) für einen flexiblen Lastfolgebetrieb eingesetzt. In der ersten Testphase wurde an der 20 kW$_{th}$ CaL-Anlage eine Parameterstudie durchgeführt, um den Einfluss von Temperatur, $CO_2$-Beladung und Wasserdampfkonzentration auf die BFB-Karbonatorleistung zu bewerten. Die Eignung des Reaktorkonzepts für den flexiblen Betrieb einer CaL-Anlage wurde anhand von Versuchen an einer 200 kW$_{th}$ semi-industriellen Versuchsanlage nachfolgend beurteilt.

Es wurde gezeigt, dass der BFB-Karbonator stabil mit Gasgeschwindigkeiten von 0,8 bis 2,0 m/s betrieben werden kann, ohne die Feststoffzirkulation zwischen den Reaktoren zu beeinträchtigen. Der untere Bereich entspricht einer maximalen Reduzierung der Abgaslast von 60 % gegenüber der Nennleistung. Der Versuchsbetrieb wurde durch eine vereinfachte Kohlenstoffbilanz validiert. Zusätzlich wurde ein Karbonator-Modellansatz basierend auf der aktiven Verweilzeit ($\tau_{active}$) für eine detailliertere Ergebnisinterpretation angewendet. Nach den Ergebnissen wurde eine aktive Verweilzeit von 41 Sekunden als ausreichend identifiziert, um eine normalisierte $CO_2$-Abscheidung ($E_{norm}$) von 90 % zu erreichen. Darüber hinaus wurde der zirkulierende Wirbelschichtbetrieb (CFB) des Kalzinators nicht von der im Karbonator eingestellten Abgaslast beeinflusst. Der Kalzinator konnte mit niedrigen Rauchgasrezirkulationsraten von bis zu 27 % erfolgreich betrieben werden und erreichte Eingang-Sauerstoffkonzentrationen von bis zu 0,55 $m^3/m^3$. In der nächsten Phase der Experimente wurde der Einfluss der Brennstoffauswahl im Kalzinator bewertet. Die Machbarkeit der Oxy-Verbrennung von Steinkohle, Weizenstroh und Ersatzbrennstoff (SRF) wurde in Dauerbetrieb nachgewiesen. Eine Reihe von Experimenten wurde durchgeführt, um den Einfluss der Brennstoffmischung und der Eingang-Sauerstoffkonzentration auf die Schadstoffbildung ($NO_x$, $SO_2$, HCl) und das hydrodynamische Verhalten zu untersuchen. Die Eingang-Sauerstoffkonzentration schien den Prozess der Schadstoffbildung kaum zu beeinflussen. Im Gegensatz dazu beeinflusste die Substitutionsrate der Biomasse die gasförmigen Emissionen, indem sie den Stickstoff- und Chlorgehalt des Brennstoffgemisches veränderte. Gleichzeitig wurden die spezifischen HCl-Emissionen durch das Vorhandensein von Ca-Spezies im Kalzinator-Feststoffinventar signifikant reduziert, was Chlorabscheideraten von über 0,90 mol/mol bei Biomassesubstitutionsraten von über 30 % ergab. Außerdem führte die Aschenanreicherung im Betrieb mit alternativen Brennstoffen zu einem erhöhten Druckverlust im CFB-Kalzinator. Obwohl die Aschenanreicherung den Betrieb des Kalziners in dieser Arbeit nicht einschränkte, deuten die Ergebnisse darauf hin, dass die Ascheansammlung in ersatzbrennstoffgefeuerten Wirbelschichten eine wichtige Herausforderung darstellen könnte.

# 1 Introduction

## 1.1 Motivation for $CO_2$ capture from coal-fired power plants

Global energy-related $CO_2$ emissions grew $1.7\%$ in 2018 to reach a historic high of $33.1\,\text{GJ}$ [115]. During that period, the power sector accounted for nearly two-thirds of emissions growth [115]. Besides, coal use in power generation surpassed $10\,\text{Gt}$ $CO_2$ [115]. Although the share of coal for heat and power generation slowly continues to decrease, the latter fuel remains the largest source of electricity and the second-largest source of primary energy [116]. Hence, a portfolio of technologies and approaches will be needed to address the 2050 decarbonization challenge while supporting energy accessibility [199]. Carbon Capture and Storage (CCS) technologies are being increasingly recognized as the only alternative to enable the continued operation of existing fossil-fueled plants with significantly reduced $CO_2$ emissions [112, 120]. According to the International Energy Agency (IEA), about $300\,\text{GW}$ of existing coal-fired power capacity meet several basic criteria for being suitable for a retrofit [113]. This number increases as new coal plants are commissioned, and the new plants are all sufficiently large for retrofitting. Moreover, detailed engineering studies show that retrofitting a coal-fired power plant today will entail $CO_2$ avoidance costs of around \$45/t [122]. With further research, development, and growing practical experience, there is considerable potential to reduce energy needs and costs. In addition, CCS can contribute to energy security objectives by supporting greater diversity in generation options and integrating growing shares of variable renewable sources with flexible dispatchable power. Concurrently, CCS can accelerate the retirement of existing power and industrial sites or re-purpose them to operate at lower capacity utilization rates or with alternative fuels.

## 1.2 Motivation for Calcium Looping $CO_2$ capture

Calcium Looping (CaL) is gaining increasing attention as a viable post-combustion CCS technology for the decarbonization of power and industrial sites. In the process, $CO_2$ is separated from the flue gas and subsequently transferred into a $CO_2$-rich gas stream by

sequential calcination (i.e., sorbent regeneration) and carbonation (i.e., sorbent loading) of a calcium-containing sorbent. The process is mainly characterized by its high exergy level due to the high temperatures needed for efficient sorbent calcination. Simultaneously, the high temperatures involved in the cycle enable additional electrical generation by means of a relatively efficient Rankine cycle. In addition, the process relies on the mature fluidized bed technology, which has already been demonstrated in facilities of hundreds of MW in size. Other major advantages of CaL include (i) operation in a very high-temperature level, (ii) inexpensive sorbent feedstock, (iii) high $CO_2$ capacity of CaO, (iv) and a relatively small efficiency penalty.

Although the technology was initially conceived to decarbonize fossil-fueled power plants, its retrofit potential to the cement industry has recently received increased attention. Due to the synergies arising from the share of common feedstock (i.e., $CaCO_3$), the CaL technology appears to be highly suitable for an application in the cement sector. The inherent utilization of $CaCO_3$ enables the re-utilization of spent sorbent from the CaL process within the clinker manufacturing process, allowing increased make-up rates that eventually enhance the sorbent's $CO_2$ capture capacity. In addition, the potential of utilizing biogenic fuels or fuels with a large biogenic content in the CaL calciner has been recently addressed. Thereby, net negative $CO_2$ emissions may be feasible due to the capture and long-term storage of biogenic based $CO_2$. Moreover, the use of waste-derived fuels with low or even negative fuel prices can lead to significantly improved process economics.

## 1.3 Objectives of this thesis

The process integration of Calcium Looping in coal-fired power plants has been often addressed in the last two decades. Many authors have identified a major challenge on the sorbent reactivity, which decays relatively fast upon the sequential calcination and carbonation cycles. So far, most experimental investigations have been performed at thermogravimetric (TG) scale. However, the process characteristics attained in TG and dual fluidized bed (DFB) systems differ greatly, making results difficult to compare. Furthermore, most CaL studies often ignore the presence of gas species other than $CO_2$ during carbonation (e.g., steam and/or $SO_2$). Indeed, $SO_2$ and steam deserve consideration as they affect the sorbent carrying capacity decay leading to significant consequences on CaL system design. At the time being, process feasibility has been demonstrated up to the $MW_{th}$ scale with several pilot plants worldwide. Nevertheless, most research has focused on investigating the process performance at baseload operating conditions, overlooking the flexibility potential of CaL systems coupled to mid-merit fossil-fueled power units. CaL plants retrofitted to existing power stations are expected to exhibit a high degree of versatility in terms of load

variations, which ultimately results in drastic process implications. Besides, the potential of fuel flexibility in the CaL calciner has often been neglected. The Calcium Looping process represents one option to capture $CO_2$ from Waste-to-Energy (WtE) plant exhaust gases. Hence, CaL systems might also be expected to operate with alternative fuels to pursue the achievement of net-negative $CO_2$ emissions. The key objectives of this thesis are listed as follows:

1. Assessment on multicyclic conversion of various limestones at TG level under the influence of realistic and scarcely investigated flue gas constituents such as steam and/or $SO_2$ upon carbonation. Selection of a suitable sorbent candidate for subsequent sorbent analysis under continuous DFB operation.

2. Experimental assessment and demonstration (TRL6) of a unique Calcium Looping system for enhanced carbonator load flexibility in mid-merit power plants.

3. Experimental assessment and demonstration (TRL6) of fuel flexibility options in a Calcium Looping calciner under a wide range of process conditions.

## 1.4 Scientific publications

### 1.4.1 List of publications

This thesis is based on the work contained in the following peer-reviewed journals:

(A) Moreno, J.; Homsy, S. L.; Schmid, M.; Scheffknecht, G.: Calcium Looping: Sorbent and Process Characterization in a 20 $kW_{th}$ Dual Fluidized Bed. *Energy & Fuels* 35(20): 16693-16704, 2021. https://doi.org/10.1021/acs.energyfuels.1c01734.

(B) Moreno, J.; Hornberger, M.; Schmid, M.; Scheffknecht, G.: Part-Load Operation of a Novel Calcium Looping System for Flexible $CO_2$ Capture in Coal-Fired Power Plants. *Industrial & Engineering Chemistry Research* 60(19): 7320-7330, 2021. https://doi.org/10.1021/acs.iecr.1c00155.

(C) Moreno, J.; Hornberger, M.; Schmid, M.; Scheffknecht, G.: Oxy-Fuel Combustion of Hard Coal, Wheat Straw, and Solid Recovered Fuel in a 200 $kW_{th}$ Calcium Looping CFB Calciner. *Energies* 14(8): 2162, 2021. https://doi.org/10.3390/en14082162.

### 1.4.2 Other publications (not included in the thesis)

(D) Moreno, J.; Schmid, M.; Scharr, S.; Scheffknecht, G.: Oxy-combustion of solid recovered fuel in a semi-industrial CFB reactor: on the implications of gas at-

mosphere and combustion temperature. *ACS omega* 7(10): 8950–8959, 2022. https://doi.org/10.1021/acsomega.1c07334.

(E) Homsy, S. L.; Moreno, J.; Dikhtiarenko, A.; Gascon, J.; Dibble, R. W.: Calcium Looping: On the Positive Influence of $SO_2$ and the Negative Influence of $H_2O$ on $CO_2$ Capture by Metamorphosed Limestone-Derived Sorbents. *ACS omega* 5(50): 32318–32333, 2020. https://doi.org/10.1021/acsomega.0c04157.

(F) Hornberger, M.; Moreno, J.; Schmid, M.; Scheffknecht, G.: Experimental investigation of the carbonation reactor in a tail-end Calcium Looping configuration for $CO_2$ capture from cement plants. *Fuel Processing Technology* 210, 106557, 2020. https://doi.org/10.1016/j.fuproc.2020.106557.

(G) Hornberger, M.; Moreno, J.; Schmid, M.; Scheffknecht, G.: Experimental investigation of the calcination reactor in a tail-end calcium looping configuration for $CO_2$ capture from cement plants. *Fuel* 284, 118927, 2021. https://doi.org/10.1016/j.fuel.2020.118927.

In addition to the listed journal publications, intermediate results were partly disseminated at scientific conferences [152, 153] and workshops [151].

## 1.4.3 Statement of contribution

The author of this thesis has contributed to the aforementioned publications ((A)-(G)) in the following manner:

(A) Conceptualization, Methodology, Validation, Investigation, Data Curation, Writing – Original Draft, and Visualization

(B) Conceptualization, Methodology, Validation, Investigation, Data Curation, Writing – Original Draft, and Visualization

(C) Conceptualization, Methodology, Validation, Investigation, Data Curation, Writing – Original Draft, and Visualization

(D) Conceptualization, Methodology, Validation, Investigation, Data Curation, Writing – Original Draft, and Visualization

(E) Conceptualization, Methodology, Validation, Investigation, Review, and Editing

(F) Review and Editing

(G) Review and Editing

# 2 State of the art

## 2.1 Carbon Capture and Storage technologies

Carbon Capture and Storage is expected to play an important role in meeting the global warming targets set by the Conference of the Parties (COP21) [199]. There are numerous technology options that are generally compatible with CCS activity. However, three routes are generally accepted as suitable for commercial plant deployment in the near to medium term. These can be classified according to their order of occurrence as follows (see figure 2.1): (i) pre-combustion, (ii) oxy-fuel, and (iii) post-combustion.
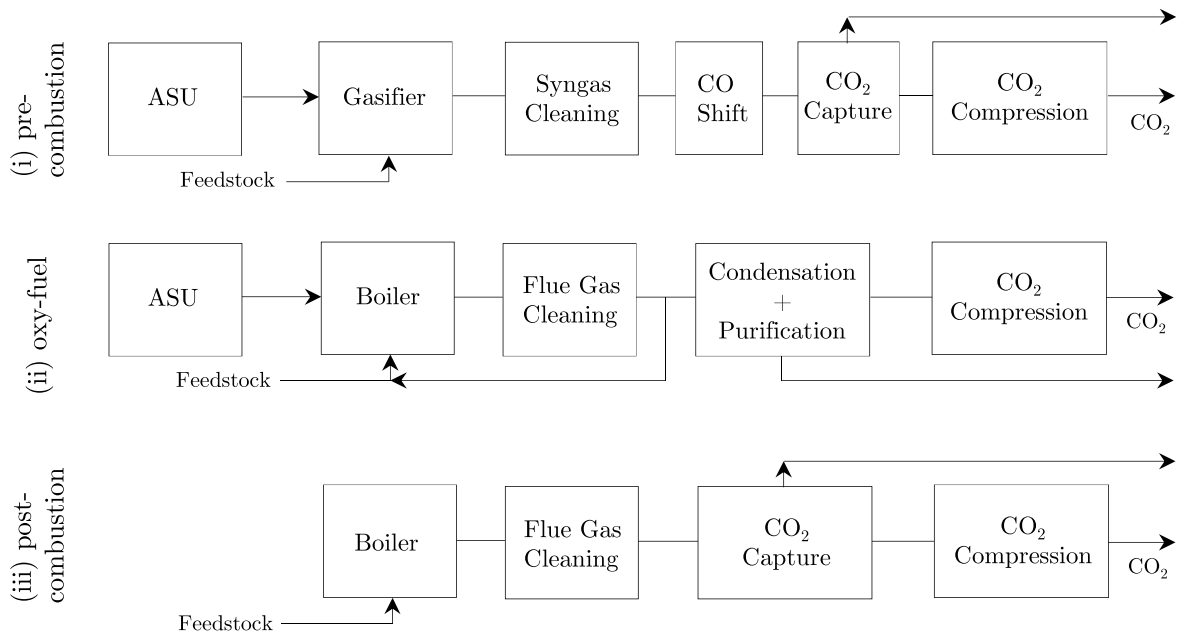


Figure 2.1: Overview of Carbon Capture and Storage technologies

Pre-combustion capture separates $CO_2$ from gasification and reforming technologies. The generated syngas is subsequently burned or utilized downstream the process to generate a carbon-free flue gas. In contrast, oxy-fuel solutions are based on the combustion of a carbonaceous fuel in a nearly pure oxygen environment. With the purpose of controlling the flame temperature, the combustion flue gas is partly recycled to the boiler. The combus-

tion flue gas consists mainly of $CO_2$, steam, and excess oxygen. Besides, post-combustion carbon capture usually separates $CO_2$ by utilizing solvents or sorbents. The $CO_2$ capture medium binds the $CO_2$ from the flue gas by physical or chemical absorption. In the following, the sorbent (or solvent) is directed to a second reactor for regeneration, releasing the captured $CO_2$ into a carbon-rich gas stream. Pre-combustion and oxy-fuel technologies can be applied to gasification and new-built power plants. Instead, post-combustion capture is particularly well-suited to retrofit already existing power sites due to its "end-of-pipe" approach. Recently, many post-combustion capture technologies have been proposed, including chemical absorption [136, 198], adsorption [131], membrane separation [174], solid looping [69, 73], or cryogenic fractionation [128]. Among the latter options, $CO_2$ capture using high-temperature solid sorbents has recently attracted much research attention. The process is commonly referred to as "Carbonate Looping" or "Calcium Looping" and is introduced in the next section of this chapter.

## 2.2 Calcium Looping $CO_2$ capture

### 2.2.1 Process development

The roots of the Calcium Looping cycle in a fluidized bed environment date back to the $CO_2$ acceptor process proposed by Curran et al. in 1967 [62]. At that time, the release of $CO_2$ during calcination was not considered an issue, and the heat for calcination was supplied by combusting part of the fuel with air. It was not until 1999 that Shimizu et al. proposed a dual fluidized bed CaL cycle for combustion applications involving sorbent regeneration under high $CO_2$ atmospheres [189]. In the following years, multiple thermo-gravimetric studies were reported on the feasibility of CaO to capture $CO_2$ under characteristic carbonation conditions [2, 89, 90, 190, 194, 201]. First process demonstrations began in electrically heated fluidized bed reactors, usually operated in a batch mode [3, 175]. Subsequently, continuous DFB operation was demonstrated using different reactor concepts such as bubbling (BFB) and circulating (CFB) fluidized beds [10, 44, 134, 170]. From here on, the Calcium Looping technology has experienced significant development, being its feasibility demonstrated up to the $MW_{th}$-scale in several pilot facilities worldwide [15, 17, 44, 45, 72, 74, 102, 193].

Process modeling activities have also experienced much development in the last two decades. Particle reaction models were first deployed to thoroughly characterize the carbonation [3, 11, 100, 125, 146] and calcination [24, 57, 145, 146] kinetics. Also, the influence of side effects such as sorbent sulfation [172] and degradation [137, 196, 202] was addressed. In addition, reactor hydrodynamics were described through several reactor models ranging from 0D [11, 145], over 1D [125, 208, 209] up to full CFB studies [156, 157]. More re-

cently, the performance and cost estimation of different integration possibilities has been discussed [23, 65, 66]. Current efforts on CaL are dedicated to retrofitting the technology to mid-merit or back-up power stations [22, 68, 155] as well as cement plants [15, 105, 106]. Furthermore, the possibility of operating the calciner with alternative fuels to enable net-negative CO$_2$ emissions is being explored [96, 150].

## 2.2.2 Process description

Calcium Looping is a high-temperature technology based on the reversible calcination and carbonation of a calcium-containing sorbent, usually raw limestone:

$$CaO_{(s)} + CO_{2(g)} \leftrightarrow CaCO_{3(s)} \tag{2.1}$$

The process is carried out under continuous operation of two fluidized bed reactors, which are interconnected by means of solid transfer lines. As indicated in figure 2.2, the CO$_2$ is exothermically absorbed from the flue gas using CaO in a carbonator reactor. Meanwhile, the CO$_2$-depleted exhaust gas is vented to the environment, and the partly carbonated solids are transferred to a calcination reactor (i.e., calciner or regenerator). In the calciner, the CO$_2$ bound in the solid phase is released into a highly concentrated CO$_2$ gas stream, while the regenerated CaO is returned to the carbonator to close the solid loop.
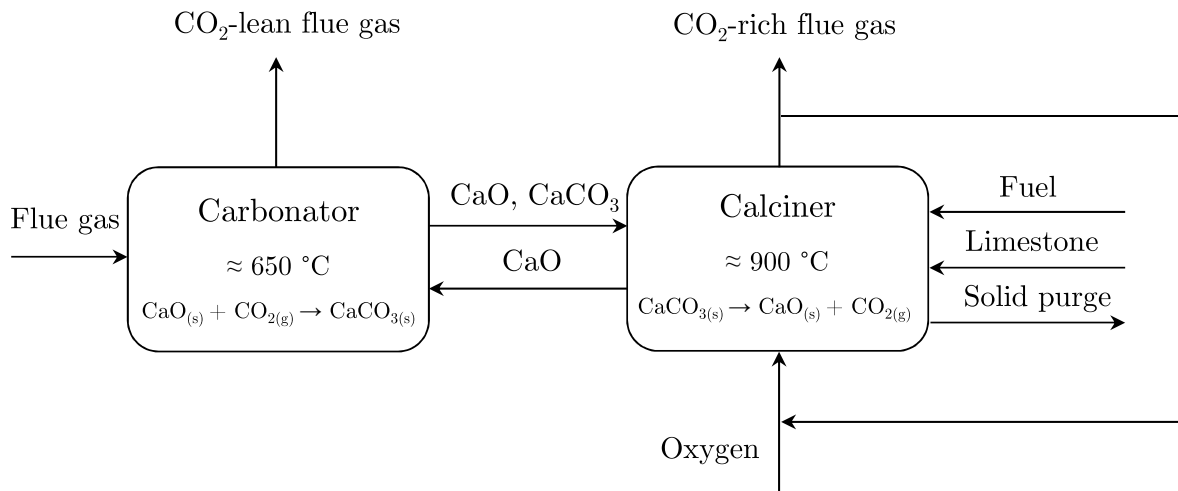


Figure 2.2: Simplified schematic of the Calcium Looping cycle

The energy required for sorbent regeneration is generally provided by burning supplementary fuel with oxygen from an air separation unit (i.e., oxy-fuel). The CO$_2$-rich flue gas can be partly recirculated to the regenerator to adjust the combustion temperature. Due to sorbent deactivation upon cycling, a continuous flow of fresh limestone make-up is fed

to the process. The latter is compensated by an equivalent sorbent purge to avoid the accumulation of inerts in the system (e.g., fuel ash and $CaSO_4$). Moreover, the high energy integration of the process necessitates and facilitates energy recuperation. The high exothermicity of the carbonation reaction, as well as energy recovery from outlet gas and solid streams, can be utilized in a Rankine cycle to minimize the electric efficiency penalty incurred by the $CO_2$ capture process [101, 171].

## 2.2.3 The CaO-CO$_2$-CaCO$_3$ equilibrium system

The operating conditions of the calciner and carbonator are imposed by the thermodynamics of the $CaO$-$CO_2$-$CaCO_3$ equilibrium system. The carbonator is generally operated at temperatures around 650 °C as a trade-off between the limitations imposed by the reaction kinetics and the equilibrium driving forces. In contrast, the calciner is typically operated above 900 °C to allow fast sorbent regeneration in a $CO_2$-rich atmosphere.

The equilibrium $CO_2$ partial pressure as a function of temperature can be described using the expression introduced by Stanmore and Gilot in a previous publication [192].

$$p_{CO_2,eq} \ (\text{bar}) = 4.192 \cdot 10^7 \exp\left(-\frac{20474}{T}\right) \qquad (2.2)$$
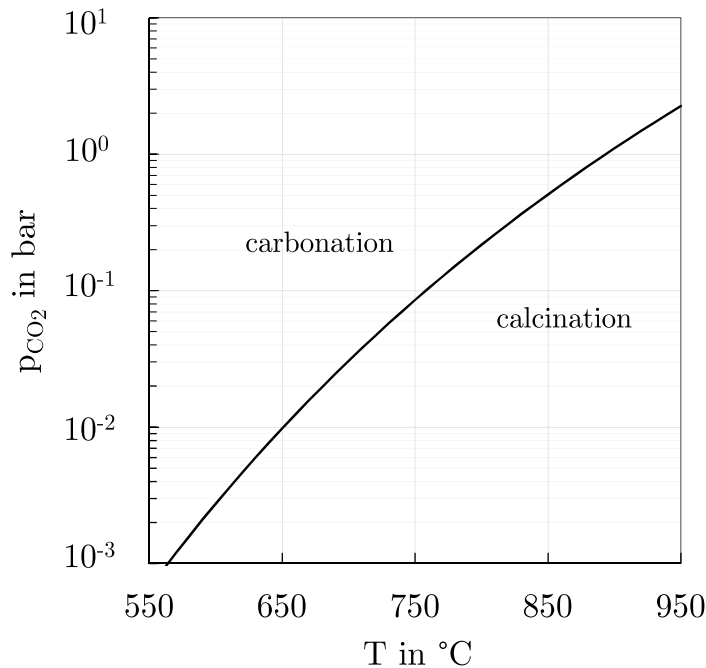


Figure 2.3: Equilibrium partial pressure of $CO_2$ as a function of temperature

Equation 2.2 is graphically represented in figure 2.3 for the temperature range 550 °C-950 °C. As can be observed, the equilibrium CO$_2$ partial pressure increases with increasing temperature. CO$_2$ absorption is favored at partial pressures above the equilibrium level, whereas CO$_2$ desorption (i.e., sorbent calcination) is achieved at pressures below the equilibrium line. Considering a typical power plant flue gas with about 0.14 m$^3$/m$^3$ of CO$_2$, a carbonation temperature of around 650 °C can lead to carbonator CO$_2$ capture efficiencies as high as 95%, depending on the carbonator design and sorbent activity. On the other hand, temperatures above 900 °C are required for effective sorbent calcination and regeneration in a pure CO$_2$ atmosphere.

## 2.2.4 Key process indicators

The Calcium Looping process can be characterized by means of several key evaluation parameters. A number of them are revealed through material balance equations, including the CO$_2$ capture efficiency and the carbonator design equation.
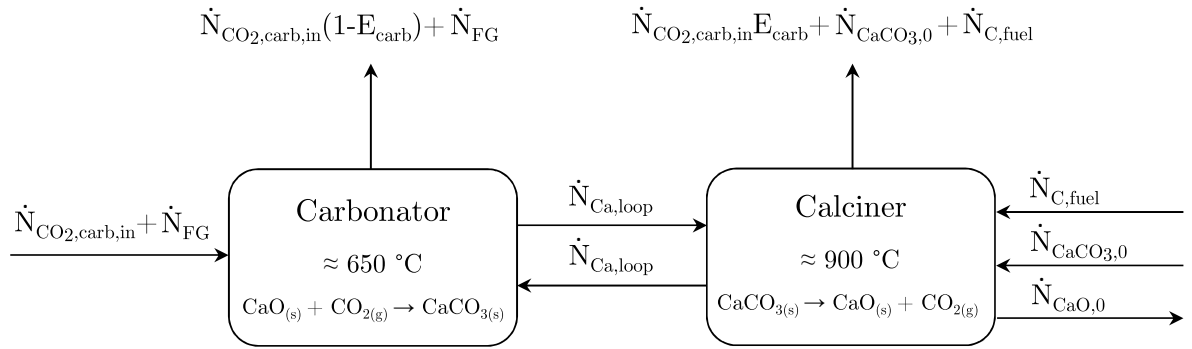


Figure 2.4: Schematic of the Calcium Looping carbon molar balance

The carbon molar balance of a CaL facility is introduced in figure 2.4. CO$_2$ enters the system from three different sources, namely (i) the combustion flue gas, (ii) the continuous supply of limestone make-up, and (iii) the carbon content of the auxiliary fuel.

In the carbonator, part of the CO$_2$ contained in the flue gas is absorbed by CaO according to equation 2.1. The carbonator CO$_2$ capture efficiency (E$_{carb}$) can be then expressed as follows:

$$E_{carb} = \frac{\dot{N}_{CO_2,carb,in} - \dot{N}_{CO_2,carb,out}}{\dot{N}_{CO_2,carb,in}} = 1 - \frac{\dot{N}_{CO_2,carb,out}}{\dot{N}_{CO_2,carb,in}} \tag{2.3}$$

Where $\dot{N}_{CO_2,carb,in}$ and $\dot{N}_{CO_2,carb,out}$ refer to the carbonator inlet and outlet CO$_2$ molar streams, respectively. In some cases, E$_{carb}$ may also be referred to the maximum achievable, equilibrium limited CO$_2$ capture efficiency (E$_{carb,eq}$). This latter term refers to as

equilibrium normalized $CO_2$ capture efficiency ($E_{norm}$) and can be used to compare different steady states which may occur at slightly different carbonation temperatures:

$$E_{norm} = \frac{E_{carb}}{E_{carb,eq}} \tag{2.4}$$

In addition to the carbonator $CO_2$ absorption efficiency (see equation 2.3), the overall $CO_2$ capture efficiency of the CaL reactor system ($E_{CaL}$) is calculated according to equation 2.6:

$$E_{CaL} = \frac{\dot{N}_{CO_2,carb,in}E_{carb} + \dot{N}_{CaCO_3,0} + \dot{N}_{C,fuel}}{\dot{N}_{CO_2,carb,in} + \dot{N}_{CaCO_3,0} + \dot{N}_{C,fuel}} \tag{2.5}$$

$$E_{CaL} = 1 - \frac{\dot{N}_{CO_2,carb,out}}{\dot{N}_{CO_2,carb,in} + \dot{N}_{CaCO_3,0} + \dot{N}_{C,fuel}} \tag{2.6}$$

Where $\dot{N}_{CaCO_3,0}$ and $\dot{N}_{C,fuel}$ indicate the molar calcium flows of sorbent make-up and fuel, respectively.

Among the different operating parameters of the CaL cycle, the looping and the make-up ratios deserve special consideration. The looping ratio ($\xi_{LR}$) is defined as the quotient between the molar flow of calcium transferred to the carbonator ($\dot{N}_{Ca,loop}$) and the $CO_2$ entering the carbonator (see equation 2.7). $\xi_{LR}$ influences the heat demand in the calciner required to regenerate the sorbent and to heat up the circulating solids. A low looping ratio is beneficial in terms of energy consumption, although this needs to be balanced with the criteria of $CO_2$ capture efficiency in the carbonator. In contrast, the make-up ratio ($\xi_{MR}$) is the relation between the molar flow of fresh sorbent fed to the CaL system and the $CO_2$ entering the carbonator (see equation 2.8). Increased $\xi_{MR}$ values lead to lower sorbent residence times in the system. Consequently, the sorbent undergoes less calcination and carbonation cycles, which in turn leads to higher $CO_2$ sorbent capture capacities. However, this second term is also subjected to optimization. High $\xi_{MR}$ values increase the sorbent regeneration efforts in the calciner significantly and are not desirable from an economic perspective unless the spent sorbent can be used as a by-product (e.g., for clinker manufacture at nearby cement plants).

$$\xi_{LR} = \frac{\dot{N}_{Ca,loop}}{\dot{N}_{CO_2,carb,in}} \tag{2.7}$$

$$\xi_{MR} = \frac{\dot{N}_{CaCO_3,0}}{\dot{N}_{CO_2,carb,in}} \tag{2.8}$$

Another procedure for characterizing the performance of a CaL cycle is based on assessing the efforts in $CO_2$ capture. A widely adopted approach is based on the SPECCA coefficient ($e_{SPECCA}$), which evaluates the energy consumption per kilogram of $CO_2$ avoided [85,

162]. $e_{SPECCA}$ calculates the primary energy demand of a capture technology based on its type of energy employed and a given electricity generation efficiency. For matured post-combustion amine technologies, a $e_{SPECCA}$ of $4\,MJ/kg$ has been proposed [39]. According to recent studies, the CaL process has the potential to further reduce this value to around 2-3 MJ/kg [23, 161, 173].

## 2.2.5 Carbonator material balance and reactor design

An essential tool for the validation of the carbonation process is the closure of the $CO_2$ material balance. During steady-state operation, where there is no accumulation of $CaCO_3$ in the reactor bed, the mass of $CO_2$ disappearing from the gas phase has to equal the mass of $CO_2$ being bound as carbonate in the Ca stream circulating between the two reactors ($\dot{N}_{Ca,loop}$):

$$\dot{N}_{CO_2,carb,in}E_{carb} = \dot{N}_{Ca,loop}(X_{carb} - X_{calc}) \tag{2.9}$$

The amount of $CO_2$ captured from the gas phase ($\dot{N}_{CO_2,carb,in}E_{carb}$) can be calculated by continuously measuring volume flow and gas composition at carbonator inlet and outlet. For calculating the amount of $CO_2$ appearing in the solid phase, the looping rate is estimated according to the measured solid circulation rate and the circulating solids' calcium content. Once $\dot{N}_{Ca,loop}$ is known, it is possible to calculate the amount of solids entering the carbonator with a molar carbonate content $X_{calc}$ after regeneration (i.e., $\dot{N}_{Ca,loop}X_{calc}$) and those leaving the carbonator after $CO_2$ absorption with a molar carbonate content $X_{carb}$ (i.e., $\dot{N}_{Ca,loop}X_{carb}$), assuming that both reactors are perfectly mixed. The comparison between both equation terms is a useful indicator of the experimental information's consistency, which is the basis for analyzing the carbonator performance.

Another relevant methodology for assessing the carbonation process is based on a basic reactor model and simplified particle reaction rate model [45]:

$$\left(\frac{dX_{carb}}{dt}\right) = k_S\,\varphi X_{ave}\left(\overline{y_{CO_2,carb} - y_{CO_2,carb,eq}}\right) \tag{2.10}$$

In equation 2.10, $k_S$ is the surface reaction rate constant for the utilized limestone, while $(\overline{y_{CO_2,carb} - y_{CO_2,carb,eq}})$ refers to the difference between the logarithmic average and the equilibrium $CO_2$ volume fraction in the carbonator. In parallel, $\varphi$ indicates the gas-solid contacting factor and $X_{ave}$ states for the sorbent's average maximum $CO_2$ carrying capacity. This simplified approach allows to solve the following mass balance for the amount of $CO_2$ removed in the gas phase and the $CO_2$ captured by the CaO particles in the carbonator bed (see [45] for more details):

$$\dot{N}_{CO_2,carb,in}E_{carb} = N_{Ca,carb}f_{active}k_S\,\varphi X_{ave}\left(\overline{y_{CO_2,carb} - y_{CO_2,carb,eq}}\right) \tag{2.11}$$

The apparent carbonation rate constant $(k_S\varphi)$ can be calculated as a fitting parameter from equation 2.11, whereas $k_S$ can be determined by thermogravimetric analysis. $N_{Ca,carb}$ refers to the carbonator calcium inventory, and $f_{active}$ corresponds to the fraction of active particles reacting in the fast reaction rate (where $X_{carb}<X_{ave}$). Equation 2.11 constitutes a reactor design model and links all CaL parameters directly or indirectly with $E_{carb}$ for the given set of operating conditions. The key parameter of this model is the active space time $(\tau_{active} = N_{Ca,carb}f_{active}X_{ave}/\dot{N}_{CO_2,carb,in})$, which is indicative of both the sorbent inventory and the reaction rate of such inventory.

## 2.2.6 The carbonation reaction

The $CO_2$ capture efficiency attained in a carbonator is governed by the relationship between carbonation kinetics and thermodynamics. The kinetics of carbonation are related to the required residence time of a sorbent to fully transform and reach a certain equilibrium conversion. It is generally accepted that the carbonation of lime follows a two-stage reaction pattern [1, 25, 30, 90]. The initial stage occurs fast and is kinetically controlled. Then, the reaction experiences a sharp transition to a slow diffusion-limited step on the formed product layer.
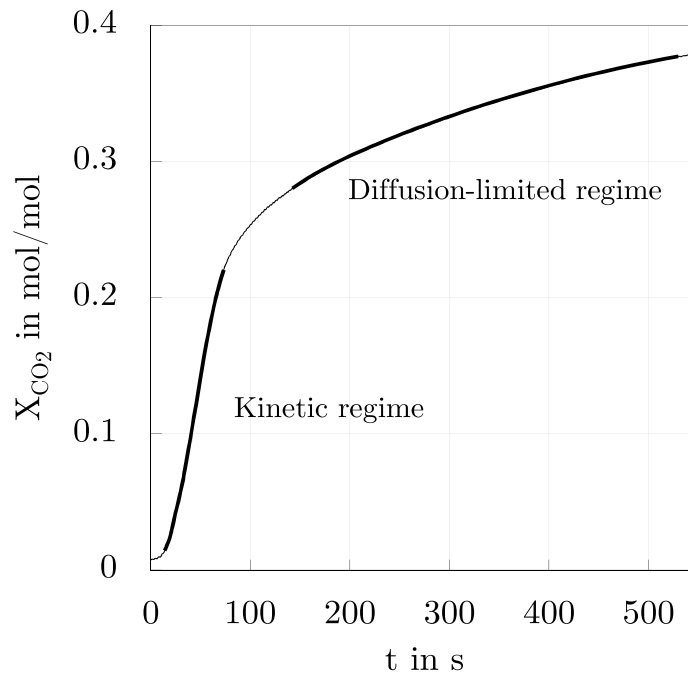
Figure 2.5: Exemplary evolution of the carbonation conversion with time

Figure 2.5 introduces a graphical visualization of an exemplary carbonation conversion curve obtained with the use of a thermogravimetric analyzer (TGA). The conversion ex-

tent of a particle ($X_{CO_2}$) is defined as the quotient between the absorbed $CO_2$ and the total Ca contained in the sample, usually expressed in molar terms (i.e., mol $CO_2$/ mol Ca). Commonly, a first-order carbonation reaction is proposed to describe the dependency of the partial pressure of $CO_2$ with respect to its equilibrium value [30, 91]. Nevertheless, different reaction orders have also been reported, based on the distinct reaction mechanisms considered [3, 11, 36, 132]. Generally, only the fast reaction regime is taken as relevant for $CO_2$ capture, as exploitation of the diffusion-limited step would comprehensively increase the sorbent residence time and the reaction design efforts [1]. Moreover, it has been postulated that the shape of the carbonation curve can be strongly influenced by the utilized experimental setup [11]. Therefore, caution is advised to avoid diffusional limitations that might hinder the determination of kinetic data. Also, it should be recalled that the achieved overall conversion is highly dependent on the cycle number, as the latter diminishes due to sorbent deactivation upon cycling [90].

### 2.2.7 Multicycle sorbent conversion

The conversion extent of CaO to $CaCO_3$ is often defined as the maximum carbonation conversion attained during the fast, kinetically controlled reaction regime. In a cycling environment, this maximum carbonation conversion decreases with each calcination and carbonation step ($X_{n_{cycles}}$), reaching an asymptotic threshold for an infinite number of cycles [1, 25, 90, 194, 201]. The decay in sorbent deactivation can be described by a semi-empirical approach suggested by Grasa and Abanades in an early study [89]:

$$X_{n_{cycles}} = \frac{1}{\dfrac{1}{1 - X_r} + k \cdot n_{cycles}} + X_r \tag{2.12}$$

Where k corresponds to the sorbent deactivation constant and $X_r$ refers to the residual sorbent conversion after an infinite number of cycles. The authors showed that the sequential decay in carbonation capacity is a common feature in all types of limestones and process conditions, suggesting reference values of k=0.52 and $X_r$=0.075.

So far, the decay in sorbent reactivity has been mostly addressed at thermogravimetric scale. Nonetheless, the use of a dual interconnected fluidized bed system also constitutes a favorable framework for investigating the evolution of sorbent activity upon cycling since it ensures improved gas-solid interaction as well as heat and mass transfer characteristics. Chapter 4 presents a procedure for estimating the theoretical number of cycles ($n_{cycles}$) under continuous fluidized bed operation. The suggested approach is based on the equation introduced by Charitos et al. in a previous publication [45], incorporating an amendment for the cycling history of the particles prior to the beginning of the calcination and

carbonation experiments.

**Implications of sorbent deterioration**

It is generally accepted that the rapid stage reaction rate is largely dependent on both the surface area of the reacting particle and the thickness of the formed product layer [2, 94, 109]. The $CaCO_3$ formed during carbonation fills up the available porosity of small pores and a small fraction of the large voids [90]. The product layer grows accordingly until a critical thickness is reached that marks the onset of the slow carbonation period [13]. The diffusion of $CO_2$ in the product layer can also be compromised by textural changes arising in the sorbent matrix during the repetitive calcination and carbonation cycles. Such modifications lead to sorbent deterioration and thus to a decrease in sorbent reactivity. The following section of this chapter introduces each of these phenomena separately.

*Sintering*    Sintering can be defined as the change in pore shape, pore shrinkage, and grain growth that particles endure while heating [31]. During the process, the growth and co-alescence of CaO grains lead to a reduction of the sorbent's surface area and porosity, which in turn hinder the potential conversion of $CO_2$ and other flue gas components (see figure 2.6). Sintering is of special relevance during the calcination step, as the deactivation rate has shown to be promoted within a relatively short time scale (i.e., 15 min) at temperatures above 900 °C [34]. Moreover, particle sintering is negatively affected by other factors such as (i) calcination time, (ii) $CO_2$ partial pressure, (iii) the presence of steam, and (iv) sorbent impurities [33–35]. In parallel, the negative effect of carbonation time of sorbent sintering has been postulated to be of minor relevance [25, 179, 196]. Furthermore, the latter studies suggest that increasing carbonation times might result in a higher sorbent reactivity towards $CO_2$, as the reaction is allowed to proceed to the diffusion-controlled step. However, it must be acknowledged the extended carbonation period may be impractical for industrial operation. In the last years, both the manufacture of synthetic-based Ca-based sorbents [37, 97, 182] and sorbent reactivation steps [20, 28, 70] have been suggested as effective measures to substantially reduce the decay in carbonation capacity. However, there is a need to study the scalability of these complex processes as well as the sorbent manufacture costs [80]. For an overview of current sorbent manufacture and reactivation techniques, please refer to chapter 3.

*Attrition*    Attrition is related to unwanted particle breakage and is influenced by the reactor design, sorbent properties, and reaction environment [26]. Sorbent attrition can be categorized into three groups: (i) primary fragmentation, (ii) secondary fragmentation, and (iii) attrition by abrasion [54, 80]. While (i) is mainly caused by thermal stresses and
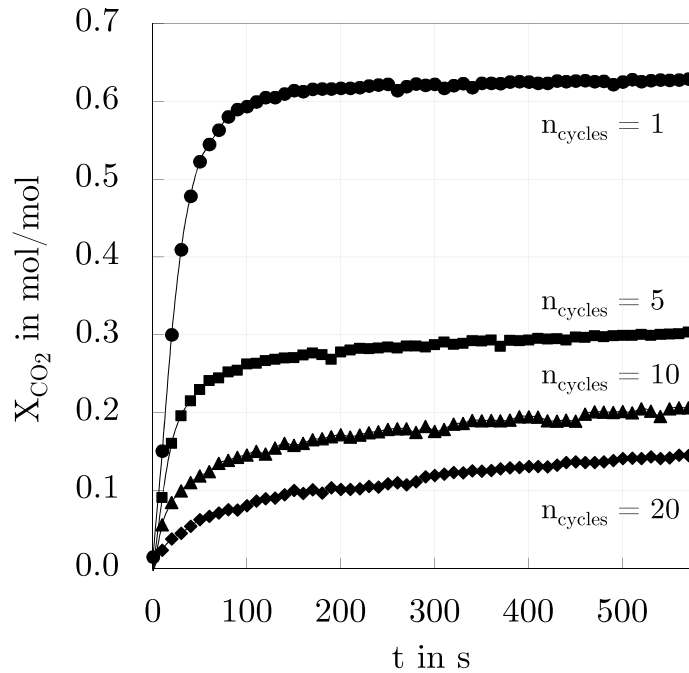
Figure 2.6: Effect of sintering time on cyclic carbonation of CaO

overpressures due to $CO_2$ release during calcination, (ii) and (iii) are related to mechanical stresses from impacts between particles and the reactor. Besides, while (ii) typically leads to similar coarse fragments, (iii) takes place exclusively on the particle surface, leading to a finer size fraction. During fluidized bed operation, CaO attrition is of particular relevance due to the fast environmental changes the particles are subjected to [8]. The extent of sorbent attrition in a fluidized bed environment has been assessed by several authors in the last years [8, 50, 78, 86, 134]. With a marked variability between limestones, the latter studies reveal higher attrition in the first calcination and carbonation cycles, where the particle size shrinks rapidly. From this point on, the particle size shows a rather constant behavior upon cycling. In a recent study, Alonso et al. postulated that primary fragmentation dominated during the period of maximum sorbent calcination rates [8]. Concurrently, abrasion of CaO particles after calcination was detected by monitoring the evolution in particle size with time. Besides, Saastamoinen et al. reported that the sudden $CO_2$ release driven by the first calcination of limestone is the main contributor to sorbent decrepitation (i.e., primary fragmentation) rather than abrupt thermal variations [177]. In parallel, the authors concluded that sulfation of CaO greatly reduces the generation of fines from abrasion, as the formed sulfate layer strengthens the particle [176, 177]. Also, the history of particles has proven to play a major role. According to a study by Scala et al., raw limestone and recarbonated sorbents are most resistant to secondary fragmentation, whereas calcined sorbents are more susceptible to attrition by abrasion [183]. Recently,

granulation has been postulated as a promising technique to produce sorbents with both enhanced chemical and mechanical properties [168]. Nevertheless, as attrition depends on both experimental setup and operating conditions [31], there is still much scope for further work on the topic.

*Competing reactions* The sorbent carrying capacity can also be negatively affected by chemical reactions occurring between CaO and other gas molecules rather than $CO_2$. Here, the reaction with sulfur dioxide ($SO_2$) is the most important. At specific process conditions, the $SO_2$ originating from the flue gas and the combustion of the auxiliary fuel in the calciner can irreversibly react with the Ca-containing sorbent, forming calcium sulfate via two reaction pathways [31]. Direct sulfation (equation 2.13) occurs when the $CO_2$ partial pressure in the reactor is above the chemical equilibrium $CO_2$ pressure. Instead, if the $CO_2$ partial pressure is lower than the equilibrium value, indirect sulfation proceeds (equation 2.14). Consequently, the last route dominates at the conditions typically prevailing in the calciner. According to an early work by Anthony and Granatstein, the sulfation reaction usually takes place at the external surface, around the pores of the sorbent particles [14]. Since the molar volume of $CaSO_4$ is higher than the molar volume of $CaCO_3$ or CaO, the pores become blocked, and the inner part of the particle core remains unreacted.

$$CaCO_{3(s)} + SO_{2(g)} + \frac{1}{2}O_{2(g)} \rightarrow CaSO_{4(s)} + CO_{2(g)} \qquad (2.13)$$

$$CaO_{(s)} + SO_{2(g)} + \frac{1}{2}O_{2(g)} \rightarrow CaSO_{4(s)} \qquad (2.14)$$
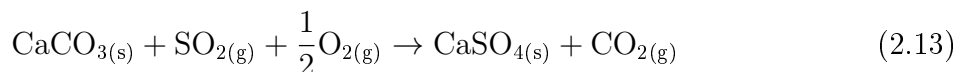
The affinity of both $SO_2$ and $CO_2$ towards CaO has been addressed by several authors in the past [9, 16, 92, 167, 175, 194]. Both Grasa et al. and Ryu et al. concluded that $SO_2$ can also react with deactivated CaO resulting from multiple calcination and carbonation cycles, as the resulting large pores are less subject to pore blockage during sulfation. Consequently, the solid purge of a CaL cycle could constitute a more effective desulfurization medium than fresh limestone-derived CaO. Moreover, the high make-up rates enabled by process synergies with cement plants allow counteracting sorbent deactivation by sulfation considerably [105]. In this last case, sorbent sulfation can be taken as a sorbent degradation mechanism which can be corrected by simple process tailoring. Besides, and particularly when utilizing alternative fuels in the CaL process, the effects of additional fuel species (e.g., Cl) on sorbent deactivation are of particular interest. For a detailed explanation on the absorption of HCl by limestone, please refer to chapter 6.

**Implications of process conditions**

The influence of carbonation temperature on $CO_2$ absorption has been investigated by various authors in the past [30, 61, 127, 143, 214]. As anticipated previously, the carbonator temperature is defined as a trade-off between reaction kinetics and thermodynamics. While higher temperatures are desirable to increase the efficiency of heat recovery within the CaL loop, lower temperatures are required to achieve higher $CO_2$ capture levels and push the technology towards the "zero emissions" target. Li et al. investigated the effect of increasing the carbonation temperature at the end of the diffusion-controlled stage and reported an increase in $CO_2$ carrying capacity [127]. According to the authors, higher temperatures favor the formation of lower density, larger-sized $CaCO_3$ product islands that simultaneously ease CaO mobility through the pore network. Consequently, sorbent conversion is enhanced. The increase in sorbent capacity with increasing temperature was also reported by Criado et al. [61]. The authors also attributed the latter effect to the formation of a thicker product layer resulting from the formation of larger product islands on the surface of the CaO. Besides, Manovic and Anthony postulated that the positive effect of temperature on sorbent conversion might be significantly reduced when operating at temperatures above 650 °C [143] in the presence of steam. In practice, the standard operation of a CaL carbonator is carried out between 600-700 °C, although the application of lower carbonation temperatures could be interesting for novel CaL solutions based on the use of a low-cost thermochemical energy storage system [22, 61].

The $CO_2$ partial pressure has also been reported to significantly affect the extent of the sorbent conversion [30, 89, 158, 160, 205]. According to Ortiz et al., increased $CO_2$ partial pressures enhance carbonation kinetics in the fast reaction regime, as the higher $CO_2$ availability increases the reaction driving force [160]. However, carbonation in the diffusion-controlled regime looses relevancy as the inlet volume fraction of $CO_2$ is increased. Grasa et al. made a similar observation when investigating the effect of $CO_2$ partial pressure on the carbonation reaction with values between 0.002-0.1 MPa [90]. The authors observed that the slopes of the fast carbonation reaction period were strongly affected by the concentration of the reactant, demonstrating a first-order dependency of the carbonation reaction with respect to the $CO_2$ concentration.

The presence of steam in the flue gas has been widely reported to greatly enhance solid-state diffusion and, consequently, carbonation of CaO [19, 73, 77, 93, 143]. Manovic and Anthony supported the latter assertion by (i) the observed temperature dependency of the carbonation rate in the presence of steam, (ii) the influence of $Na^+$ ions in the sorbent, and (iii) the sorbent morphology attained during carbonation with and without steam presence [143]. The authors also claimed that steam is more helpful under conditions where the product layer diffusion becomes reaction-rate limiting (i.e., at low temperatures and/or

with more sintered sorbents). Donat et al. made a similar observation, reporting enhanced sorbent reactivities in the presence of steam [77]. Besides, the authors conducted a systematical analysis of steam concentration, both during carbonation and calcination [77]. Donat et al. claimed that at low concentrations, the effect of steam on the sorbent carrying capacity depended on the amount of steam available. However, above a certain concentration point, no further improvement was observed. On the other hand, Manovic and Anthony postulated a marginal increase in sorbent conversion during carbonation at $600\,°C$ with increasing steam concentration from 0.10 to 0.20 m$^3$/m$^3$ [143]. It is evident that further research is required to fully characterize the systematical effect of steam concentration on sorbent conversion, particularly in a fluidized bed environment. The investigations included in chapter 4 aim at improving the understanding of the latter aspect.

# 3 Calcium Looping CO$_2$ capture from coal-fired power plants

## 3.1 Sorbent development for Calcium Looping

As already discussed in chapter 2, there are several properties that characterize the performance of a CaL sorbent, such as its (i) CO$_2$ capture capacity, (ii) stability upon cycling, (iii) attrition resistance, and (iv) chemical stability towards side reactions. Moreover, a promising sorbent candidate should be (i) widely available, (ii) economically affordable, and (iii) easy to regenerate. Limestone-derived CaO fulfills the latter specifications to a great extent, making it particularly attractive as a sorbent for high-temperature CO$_2$ capture applications [178]. CaO-based sorbents can be mainly put into three groups, namely (i) natural-based sorbents, (ii) doped natural-based sorbents, and (iii) artificial (or synthetic) sorbents. While group (i) has been widely addressed in the past, the most recent work is being devoted to developing sorbents contained in the categories (ii) and (iii). Nevertheless, the solution is not straightforward since it needs to be balanced by the criteria of both sorbent reactivity and economic feasibility at a large scale. In addition, deactivated natural-based sorbents may undergo an additional recycling step to increase the resulting low residual reactivity, thereby avoiding the necessity of disposal. The following section of this chapter gives an overview of recent efforts achieved in the development of Calcium Looping sorbents.

### 3.1.1 Natural-based sorbents

CaO-based natural solid sorbents benefit from (i) the initially high theoretical absorption capacity, (ii) fast reaction kinetics, and (iii) wide precursor abundance [27].

In the last decades, many investigations have been devoted to exploiting the characteristics of unmetamorphosed limestones and dolomites. However, naturally-occurring metamorphosed (i.e., marble) sorbents also deserve consideration due to their comparatively high accessibility and affordability [104]. Contrary to unmetamorphosed sorbents, marble materials are exposed to elevated temperatures and pressures during the geological process. Under these circumstances, the limestone deforms and recrystallizes, resulting in

a variety of metamorphic morphologies. While the specific metamorphic characteristics depend mainly on the geological conditions, limestone metamorphism usually derives in increased grain sizes. In the following, the most relevant studies on unmetamorphosed limestones are discussed. For a detailed discussion of metamorphosed limestones, please refer to chapter 4. Limestone (CaCO$_3$) embraces carbonate rocks or fossils with a high calcium and magnesium content, including varying amounts of impurities such as silica and alumina [31]. So far, calcite-rich limestones have received the largest focus for CO$_2$ capture activities, as it allows the highest uptake of CO$_2$ per unit mass [31]. However, natural limestones show a high variation concerning their attrition and sulfation resistance, which ultimately affects their CO$_2$ capture performance (see figure 3.1). A second sorbent group is related to the dolomites (CaMg(CO$_3$)$_2$), which are also naturally occurring. Compared to limestones, dolomites (i.e., MgO) do not undergo carbonation under typical CaL conditions, and hence the stoichiometric capture capacity is lower than that of limestone [31, 48]. Nonetheless, Blamey et al. reported that certain dolomites might display a higher long-term CO$_2$ uptake than limestone-derived CaO [31]. According to the authors, the latter effect is related to the preservation of the unreacted MgO porosity network and the increased MgO melting point compared to CaO (i.e., reduced sintering). The decay in CO$_2$ carrying capacity of natural-based limestones has been widely addressed in the last two decades. So far, most of these studies have been carried out using a TGA apparatus [2, 25, 90, 190, 194], although fluidized bed reactors have also been employed on some occasions [45, 50, 175]. In an early work by Coppola et al., the CO$_2$ capture performance and attrition behavior of limestone and dolomite were assessed using a lab-scale fluidized bed [54, 55]. In the absence of SO$_2$, the authors showed that dolomite performed better upon cycling despite its lower calcium content. The residual capture capacity of dolomite was 0.12 g/g compared to 0.02-0.07 g/g yielded with limestone operation. The latter effect was attributed to the large magnesium fraction of the dolomite, which reduces sintering [31]. Nevertheless, the experiments showed that dolomite is less resistant to attrition and fragmentation, particularly upon the first calcination stage.

Although with some exceptions [104], carbonation of CaO in the presence of SO$_2$ has been found to promote sorbent deactivation [16, 56, 79, 175]. The additional sorbent degradation incurred by SO$_2$ has shown to differ significantly for different types of limestones, despite showing a similar carbonation behavior in the absence of sulfur [92]. In any case, it seems evident that natural sorbents face major challenges that compromise their application in large-scale systems. Hence, several procedures have been proposed to reduce the impact on sorbent deactivation.
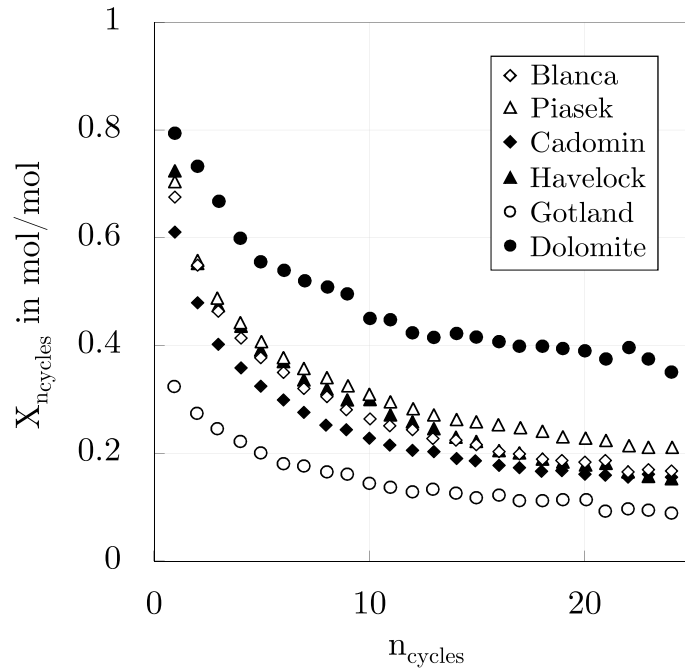
Figure 3.1: Conversion vs number of cycles for different types of natural-based sorbents. Adapted from [89]

## 3.1.2 Enhancement of natural-based sorbents

Sorbent enhancement techniques represent a midpoint between the use of natural materials and the utilization of complex procedures for the synthesis of new materials. In consequence, sorbent reactivation is expected to be generally less costly than the production of new sorbents. Currently, there is a broad range of techniques that can be applied to improve sorbent properties [80]. The following chapter briefly summarizes the most promising procedures suggested to date.

**Thermal pre-treatment**

According to several studies, thermal pre-treatment can improve the conversion of CaO in long sequential calcination and carbonation cycles [7, 140, 144]. When subjected to temperatures between 800-1300 ℃, the continuous cycling of the sorbent leads to the formation of a skeleton of interconnected CaO, which in turn acts as an outer reactive CaO layer and stabilizes the sorption capacity [137]. An experimental investigation by Manovic and Anthony further revealed that in the early cycles, only the less reactive hard skeleton exists, although conversion increases as the soft structure develops [140].
Thermal pre-treatment is considered to be straightforward and inexpensive. However, it should be noted that it will incur additional energy efforts as the material needs to be

heated up before its final use. In addition, thermal pre-treatment has been reported to influence sorbent reactivation unequally [21, 46, 144]. Hence, it is probable that the different types of natural sorbents will require other reactivation conditions due to the differences in impurity composition and internal structure.

## Hydration

Hydration of spent CaL sorbents has also been proposed as a promising reactivation strategy [82, 109, 195]. Sorbent hydration is beneficial due to the formation of cracks in the CaO particles, which concurrently create new reaction paths and improve CO$_2$ capture [204]. Sorbent reactivation by hydration also leads to the formation of larger pores, making the particle less susceptible to pore blockage [211].

Hydration can be achieved using water [53, 207], steam, or a mixture of both [20, 80]. Among all possibilities, steam hydration has received particular attention due to the high spent sorbent's reactivity towards steam. According to several studies, sorbent reactivity upon cycling is preserved by this method due to the enhanced carbonation rate in the diffusion-controlled regime [148].

The benefits of using hydration as a means to reactivate sorbent are numerous. However, it must be noted that the placement of an extra reactor will increase the cost and complexity of the plant. Also, the tendency to attrition might be enhanced with hydrated particles [32, 141, 204], which could require the implementation of additional sorbent processing steps (e.g., granulation or extrusion) to overcome their weaker mechanical stability.

## Re-carbonation

The following method is based on the re-carbonation of carbonated particles by extending the time the solids spend in the slow diffusion stage [80]. The first sorbent re-carbonation study for CaL application was proposed by Sun et al. [196]. The authors showed that an increase in the carbonation time positively affected the capture capacity over several subsequent CaL cycles. Chen et al. also made a similar observation, claiming that the samples that experienced extended carbonation displayed a better performance than those that did not [46]. A few years later, Arias et al. introduced a re-carbonation reactor concept for CaL application [21], suggesting that the sorbent properties can be mostly preserved if re-carbonating with pure CO$_2$ coming from the regenerator. The design of such a reactor was proposed in a latter study [71].

Nonetheless, re-carbonation can have an adverse effect since it might accelerate the decay of CaO conversion [80, 142]. Valverde et al. confirmed the latter observation, suggesting that re-carbonation of carbonated solids might cause defects due to intense bulk stresses [200]. Despite the potential of this process, further studies are required to thoroughly characterize

the implications of re-carbonation on sorbent properties, particularly at increased CaL cycles.

### 3.1.3 Doped natural-based sorbents

Doped sorbents refer to natural-based materials whose properties have been enhanced by additives. The idea behind this technique is the production of a sinter-resistant material with a high carrying capacity at affordable costs.
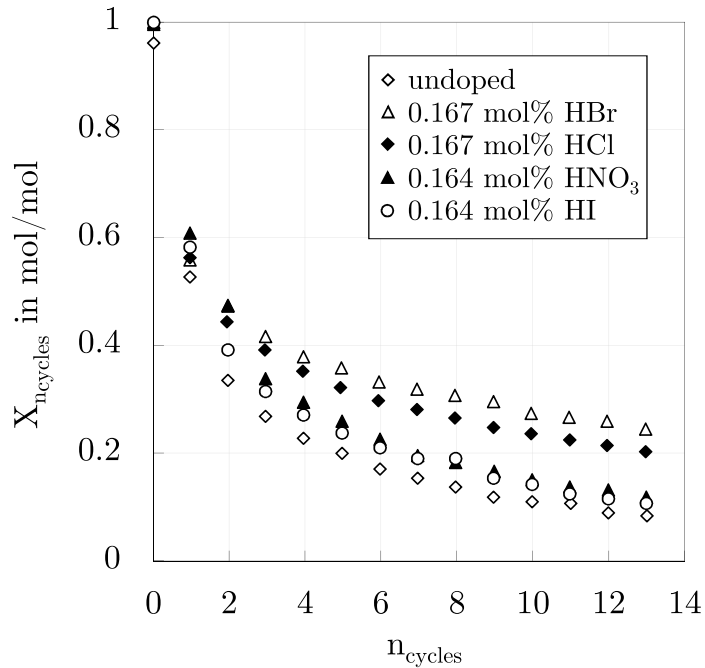


Figure 3.2: Conversion vs number of cycles for Havelock limestone using different dopant solutions. Adapted from [5]

Currently, the primary method associated with sorbent doping is wet impregnation [80]. In an early TGA study, Salvador et al. studied the impregnation of Ca-based sorbents with sodium chloride (NaCl) and sodium carbonate ($Na_2CO_3$) [179]. According to the authors, the addition of NaCl led to an enhanced capture capacity, maintaining it at $40\,\%$ of overall capacity over 13 cycles. In contrast, impregnation with $Na_2CO_3$ had no apparent effects. Years later, Fennell et al. conducted investigations on wet impregnation with $Na_2CO_3$ in a fluidized bed facility [83]. The authors reported that doping small quantities of $Na_2CO_3$ with very low molarity led to a slight improvement in the carrying capacity. However, increased doping quantity solutions showed a detrimental effect and decreased the reactivity of the tested limestone. Moreover, investigations with other impregnating solutions (e.g., KCl [87], $K_2CO_3$ [87], $MgCl_2$ [6], $CaCl_2$ [6], $Mg(NO_3)_2$ [6, 197]) have also confirmed

the benefit of utilizing low dopant concentrations [80]. Al-Jeboori et al. demonstrated the positive effects of mineral-acid doping on the long-term reactivity of limestone-based sorbents (see figure 3.2). The authors explored the cyclic activity of three different limestones doped with a range of inorganic mineral acids (HCl, HBr, HI, and $HNO_3$) in a fluidized bed reactor [5]. At low dopant molarity concentrations, the performance yielded during the experiments showed to be highly dependent on the type of limestone used. For the Havelock limestone, the best results were obtained with HBr and HCl, followed by HI and $HNO_3$.

Provided a careful selection of materials and methods, sorbent doping has shown to entail positive effects on the pore structure, pore volume, and pore size, which ultimately benefit the carrying capacity [80]. However, the costs related to doping solutions need to be carefully assessed, considering the large amounts of sorbent required for application at industrially relevant scale.

### 3.1.4 Artificial sorbents

The main difference between doped sorbents and artificial (i.e., synthetic) sorbents lies in the origin of the calcium source. Artificial materials do not have any naturally occurring components, and they rely on the dispersion of an active compound onto a porous inert matrix [133]. Synthetic sorbents hold the premise of reducing the decrease in capture capacity. The addition of an inert material can help preserve the $CO_2$ capture capacity, while it may also entail an increase in sorbent costs [27]. Therefore, a relatively new field in sorbent development has emerged that aims at synthesizing low-cost sorbents, which also benefit from high stability and high cycling capacity [80]. Recently, Saccia et al. developed a sorbent containing CaO and coal fly ash cenospheres (i.e., CaO-CFA900) [182]. The authors reported the creation of a highly stable and inexpensive sorbent, which yielded a residual activity of 0.22 g/g after 200 calcination and carbonation cycles in a TGA apparatus. In another study, Ma et al. explored the properties of waste product carbide slag, alumina cement, and glucose [138]. Best results for the proposed sorbent (i.e., CaO and $Ca_{12}Al_{14}O_{33}$) were found with an alumina cement content of 5 wt%, yielding a capture capacity of 0.37 g/g and 0.29 g/g after 20 cycles under mild and severe calcination conditions, respectively. Although with increased manufacturing costs, CaO with sepiolite as an inert matrix (i.e., CaO, MgO, and $Ca_2SiO_4$) has also proved to perform adequately [188]. According to Shi et al., the latter candidate yielded a capture capacity of 0.37 g/g after ten sequential calcination and carbonation cycles. According to the authors, this is about 39 % and 56 % higher than the values reported for hydrated CaO and original CaO, respectively. The carrying capacities and test conditions of selected artificial sorbents are summarized in tables 3.1 and 3.2, respectively. As can be observed, the residual activity after repeated

calcination and carbonation cycles is mostly maintained if compared to that of natural-based sorbents. Still, there is a need to study the scalability of these relatively complex processes. The preferred techniques will be, at least at an initial stage of deployment, techniques that are already proven in the industry (e.g., granulation and extrusion) [80]. Moreover, the suitability of the particles for use in fluidized beds requires careful consideration. In addition, the cost of sorbent processing should not be ignored.

Table 3.1: Overview of selected artificial sorbents for CaL application

| Sorbent | Initial carrying capacity | Long-term carrying capacity | No. cycles | Ref. |
|---|---|---|---|---|
| CaO-sepiolite | - | 0.37 g/g | 10 | [188] |
| BPB-CaO | 0.7 g/g | 0.5 g/g | 20 | [47] |
| CaO-Ca$_{12}$Al$_{14}$O$_{33}$ | - | 0.29 g/g | 20 | [138] |
| CaO-CFA900 | 0.33 g/g | 0.22 g/g | 20-200 | [182] |

Table 3.2: Operation conditions of sorbents presented in table 3.1

| Sorbent | Reactor | Carbonation conditions | Calcination conditions | Ref. |
|---|---|---|---|---|
| CaO-sepiolite | DFB | 650 °C; 0.15 m$^3$/m$^3$ CO$_2$ | 850 °C; 1 m$^3$/m$^3$ N$_2$ | [188] |
| BPB-CaO | TFB | 700 °C; 0.2 m$^3$/m$^3$ CO$_2$ | 850 °C; 1 m$^3$/m$^3$ N$_2$ | [47] |
| CaO-Ca$_{12}$Al$_{14}$O$_{33}$ | DFB | 700 °C; 0.15 m$^3$/m$^3$ CO$_2$ | 920 °C; 0.70 m$^3$/m$^3$ CO$_2$ | [138] |
| CaO-CFA900 | TGA | 600 °C; 0.40 m$^3$/m$^3$ CO$_2$ | 900 °C; 1 m$^3$/m$^3$ N$_2$ | [182] |

## 3.2 Load flexibility potential of Calcium Looping systems

Future energy scenarios are expected to be mainly dominated by renewable energy sources [114]. However, the behavior of most renewable technologies is still intermittent and will require the implementation of back-up or mid-merit power plants to balance energy supply and demand [111].

Existing coal-fired power blocks operated in a back-up mode could be favored in such electricity portfolios, as they usually introduce low fuel costs and can be largely amortized [111, 121, 149]. Still, flexible power plant operation alone is incompatible with the long-term sustainability goals to achieve deep decarbonization in energy supply. Consequently, load-following power stations equipped with CCS technology are required to

accomplish the ambitious $CO_2$ emission reduction targets [199]. Originally, CCS facilities were designed for base-load operation. Rapid fluctuations in electricity demand further exacerbate the challenges associated with load-flexible CCS plants, increasing process complexity and the associated costs [40, 63, 76, 119, 139].

Due to the inherent advantages of the CaL cycle, the suitability of this technology for flexible $CO_2$ capture has been recently addressed. At the time of writing, several process layouts have been proposed to increase the flexibility of CaL systems. Some of them rely on the usage of a thermo-chemical energy storage system [22, 23, 60, 98, 159]. In contrast, other studies focus on the assessment of flexible pilot plant operation [68, 155] as well as alternative process schemes [98, 213]. The following section of this chapter briefly summarizes the current state-of-the-art of flexible CaL units.

## 3.2.1 Thermo-chemical energy storage

Energy storage technologies are expected to play a crucial role in energy system decarbonization by (i) improving energy resources (i.e., efficiency), (ii) increasing energy access, and (iii) improving electricity grid stability and flexibility, among others [118].

To date, several studies have addressed the feasibility of implementing energy storage solutions for the flexible decarbonization of power systems. The storage of a fraction of rich solvent has been studied in post-combustion amine-based $CO_2$ capture systems [4, 181]. Such investigations concluded that the latter approach could reduce power consumption in the regeneration and $CO_2$ compression units during the peak power demand periods. Consequently, the latter operations can be postponed to when there is less power demand. For oxy-fuel combustion systems, the storage of $O_2$ in cryogenic tanks during low power demand periods has been proposed, operating the air separation unit (ASU) in base mode [99]. Similarly, the storage of $H_2$ in pre-combustion $CO_2$ processes has been addressed to decouple the generation of power from $H_2$ production [64]. The latter approaches aim at covering short peaks characterized by a fast response [22]. Therefore, such systems will be mostly penalized in case of seasonal back-up (i.e., operating a few weeks per year) due to the large capacity required to store costly materials or solvents as well as large-scale storage equipment (i.e., cryogenic $O_2$ or pressurized $H_2$).

In the last years, CaL-based thermo-chemical energy storage systems have been often proposed to improve the flexibility for $CO_2$ capture. The latter approach takes advantage of the low specific costs of solids required for large-scale storage (i.e., CaO and $CaCO_3$). An early study from Hanak et al. explored different routes for energy storage in Calcium Looping systems, namely (i) CaO-$CaCO_3$, (ii) CaO-Ca(OH)$_2$, and (iii) cryogenic $O_2$ storage [98]. The comparison between (i) and (iii) revealed that the latter would result in a higher turndown of the entire system, thereby leading to increased energy densities and

lower capital costs. Also, (ii) was suggested as a promising option to increase the energy density of the $CaO$-$CaCO_3$ storage system by about $57\%$. In another work, Criado et al. proposed a $CaO$-$CaCO_3$ storage concept that could be integrated into existing power plants operating as back-up in renewable energy systems [60]. The authors claimed that electricity costs between 0.13-0.15 \$ per $kWh_e$ could be feasible, as carbonator solids could be stored at low temperatures ($< 250\,°C$) in large solid piles. Astolfi et al. performed a more detailed assessment of the previous thermo-chemical storage unit, focusing on optimizing the size of the calciner and the storage system to minimize the cost of electricity [23]. From the logistic viewpoint, sizing the calciner on the average daily load and the storage system to manage the daily cycling appeared to be most feasible, incurring minor economy penalty compared with the optimal plant design. The latter scenario revealed a reduction in the cost of avoided $CO_2$ in the range of 16-26\% compared to the reference low capacity factor scenario without solids storage. The practical feasibility of the thermo-chemical $CaO$-$CaCO_3$ concept has been recently explored by Arias et al. [22]. According to the latter study, a small oxy-fired calciner of about $8\%$ of the total thermal capacity could be sufficient to effectively regenerate the sorbent while capturing $90\%$ of the $CO_2$ in the carbonator. Moreover, the authors suggested using the steam cycle of the existing power plant in order to improve the capture flexibility and to minimize the increase of $CO_2$ capture costs. In this way, the electrical power output might be preserved while reducing the thermal input to the power plant by $12\%$. In addition, the possibility of including such a thermo-chemical energy storage method in concentrated solar power plants has been recently discussed [159].

While some energy storage technologies are close to maturity, most are still in the early stages of development, struggling to compete with other non-storage technologies due to increased costs [118]. Consequently, they will require additional efforts before their potential can be fully reached.

## 3.2.2 Conventional CFB carbonator arrangement

One major reason for the rapid progress experienced by the CaL process is ascribed to the resemblance of the carbonator and calciner to commercial CFB reactors. CaL systems coupled to load-following power plants are expected to accommodate frequent variations in the flue gas flow rate and, therefore, in the carbonator inlet gas velocity. This has a direct implication on the hydrodynamics of the reactor, which in turn leads to changes in the solids' circulation rate and bed inventories of the reactors [68]. Consequently, the residence time of the particles inside the carbonator is affected, thereby impacting on the attained $CO_2$ capture efficiency.

Originally, CFB carbonators were designed to capture the $CO_2$ emitted from base-load op-
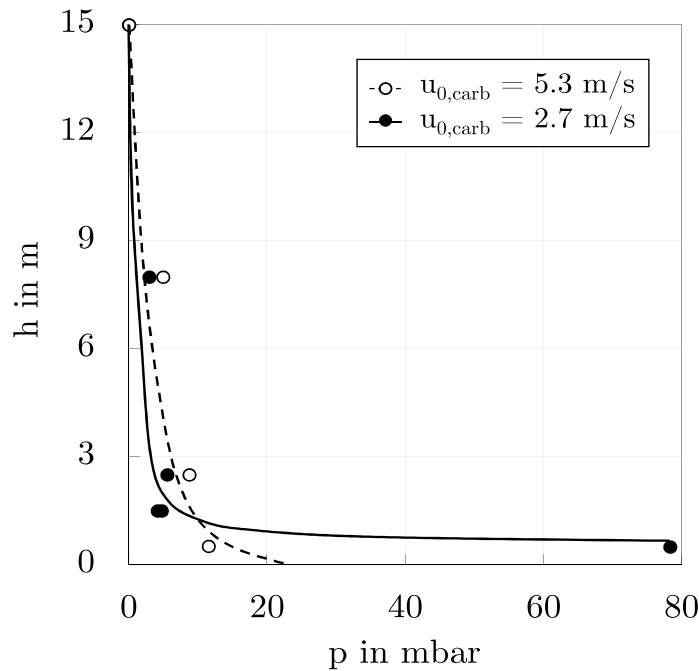
Figure 3.3: Pressure profile of solids in a CFB carbonator during part-load operation at a 1.7 $MW_{th}$ pilot plant. Adapted from [68]

erated power plants. At high superficial gas velocities, the solid entrainment rate achieved in the reactor is beyond the solid circulation rate required to achieve the $CO_2$ capture targets [68]. In consequence, the surplus of entrained solids is often recirculated back towards the carbonator. During part-load operation, the situation reverses. There is a threshold in the case of low superficial gas velocities, beyond which the entrainment rate is below the required values. In this context, Ylätalo et al. proposed a strategy to mix the flue gas arriving from the power plant with a recycled fraction of the lean $CO_2$ stream exiting the carbonator [210]. While the proposed approach might guarantee a stable solids circulation between reactors, it reduces the $CO_2$ concentration in the inlet gas stream, thus affecting the carbonation kinetics. Moreover, the integration of CaL cycles with power plants during steady-state and flexible operation has been numerically investigated. Lara and Romeo proposed a scheme for integrating CaL cycles with power plants at load scenarios as low as 30 %, concluding that $CO_2$ capture systems defined for nominal load conditions might be oversized when operating at part-load [124]. In another study, Cormos developed a 1-D dynamic model of both CFB reactors (i.e., carbonator and calciner) operated in fast and turbulent operation regimes [58]. The study concluded that the effect of the disturbance propagated with delay for the solid phase compared with the gas phase. However, the ramp perturbation was found not to destabilize the process as a step change. Recently, the load flexibility potential of a 1.7 $MW_{th}$ CFB carbonator has been experimentally invest-

igated [68]. The study aimed to explore the CaL plant's performance during steady-state operation, both under full- and part-load conditions (see figure 3.3). According to the authors, an increase in the carbonator gas velocity from 2.0 to 5.3 m/s led to a rise in the particles entrainment rate from 3.4 to 13.4 kg/(m$^2$ s). However, Diego and Arias concluded that superficial gas velocities lower than 2.0 m/s might not be feasible without substantial modifications due to inefficient circulation of solids between reactors. The authors proposed implementing a flue gas staging procedure to improve the flexible performance of the system. Nevertheless, this would negatively affect the overall $CO_2$ capture efficiency of the system due to the lower amount of flue gas passing through the lower dense solid bed in the carbonator [45]. Furthermore, the latter study suggests that maximum load reductions of up to 50 % can be attained with the conventional setup, which is less than the reduction rates expected for coal-fired power plants operated at minimum load cases [119]. Therefore, further research is required to confirm whether or not conventional CFB carbonators have the potential to cope with the low load capacity factors expected in flexibly operated power plants.

### 3.2.3 Novel BFB carbonator approach

An alternative process scheme for improving the load-flexibility behavior of CaL systems was proposed by Dieter et al. in an early work [73]. The authors suggested the possibility of utilizing a BFB carbonator with a bottom interlink to decouple flue gas load and sorbent circulation, thus enabling operation in a wide range of fluidization regimes (see figure 3.4). Although the concept has been successfully demonstrated on several occasions [72, 73, 106], its load flexibility behavior has not been explored until lately. In the context of the recent European RFCS research project "FlexiCaL" Moreno et al. have conducted investigations to assess the flexibility potential of the proposed reactor setting [155]. The results showed that part-load cases as low as 40 % can be attained with the suggested CaL configuration. It was demonstrated that the facility can be operated stably with carbonator superficial gas velocities ranging from 0.8 m/s to 2.0 m/s without affecting the solid circulation between reactors. Moreover, the calciner operation appeared to be independent of the flue gas load set in the carbonator. Hence, it is envisaged that the calciner of such a system (i.e., BFB-CFB) can operate over a wide range of process conditions without posing a significant impact on the reactor coupling. Besides, load case scenarios below 40 % may still be feasible using the proposed layout. Nonetheless, the latter case is not straightforward as it needs to be balanced by criteria of reactor hydrodynamics and $CO_2$ capture efficiency. In any case, the reactor concept proposed here deserves attention as it appears to be suitable for both existing and newly built power plants, considering the typical size (i.e., 200 MW) of medium-scale boiler blocks available in the market [153]. For a further assessment of the

flexible behavior of the BFB-CFB reactor system, please refer to chapter 5.
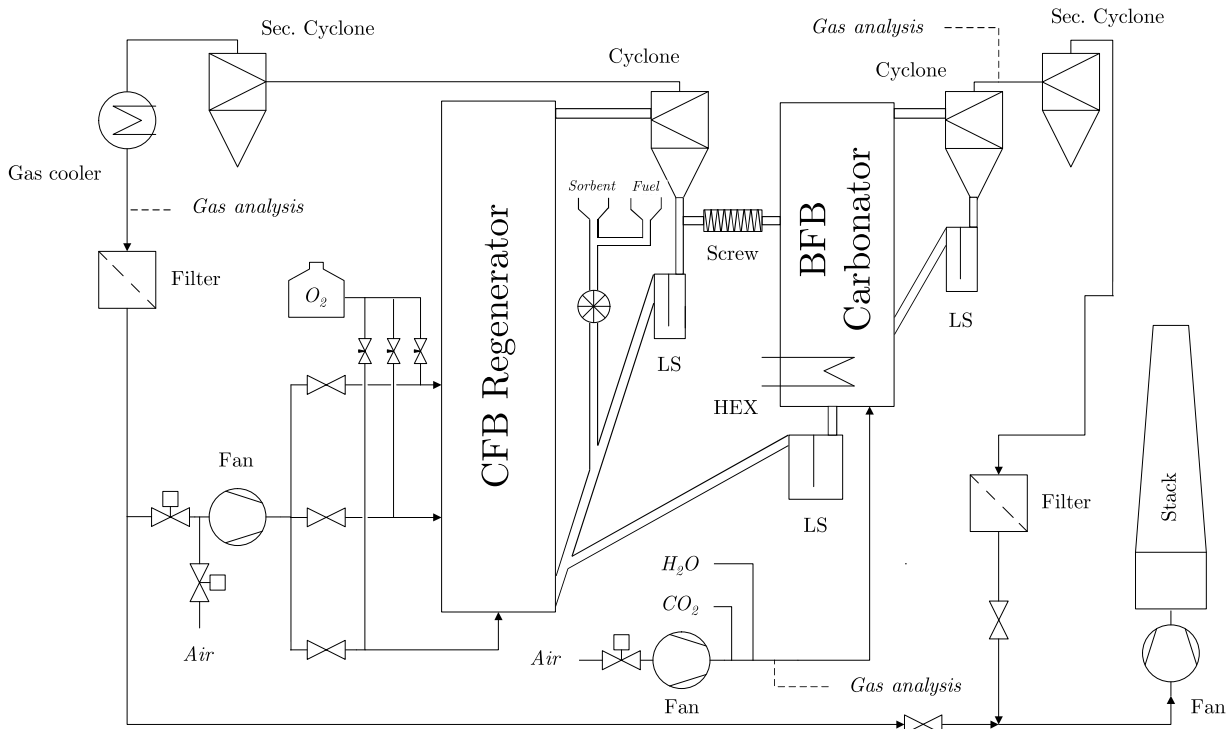


Figure 3.4: Schematic of the 200 kW$_{\text{th}}$ CaL pilot plant using the BFB carbonator arrangement. Adapted from [155]

## 3.3 Fuel flexibility potential of Calcium Looping systems

In the last century, coal has emerged as a major source for electric power generation due to (i) its high heating value, (ii) homogeneous composition, (iii) favorable heat transfer characteristics, and (iv) relatively low costs. Although an increasing amount of power plants has started to co-fire less carbon-intensive fuels, coal is still a dominant resource used for power generation [117]. Consequently, coal has also remained a preferable fuel for CaL units retrofitted to existing power plants [186]. However, additional coal consumption can significantly affect the environmental footprint, as emissions related to coal production and transport are reported to influence the life cycle impact of a CaL system notably [110]. The following section of this chapter offers the latest achievements in CaL systems driven by alternative fuels.

### 3.3.1 Calcium Looping powered by natural gas

The use of natural gas in the CaL cycle can avoid the environmental repercussions associated with coal usage [186]. To date, several numerical studies have been reported on the performance of natural gas-fired CaL units both for power plant [29, 59] and industrial [49, 147] application. According to Berstad et al., the advantages of applying CaL instead of chemical solvents to capture $CO_2$ from natural gas combined cycle (NGCC) power plants narrow down to the possibility of using the process by-product (i.e., lime) at nearby cement plants [29]. On the contrary, Cormos and Simon postulated that NGCC units retrofitted with CaL give significantly better environmental and economic performances than chemical solvent-based solutions [59]. Despite introducing a slightly higher capture energy penalty, the authors claimed that CaL systems allow for higher carbon capture rates, increased heat recovery potential, and lower sorbent make-up costs. Regarding $H_2$ production, Martinez et al. claimed that CaL could lead to significantly higher $CO_2$ capture efficiencies than amine-based CCS options [147]. At the same time, Connell et al. concluded that the retrofit of the CaL process into a hydrogen production plant might result in a substantial co-production of electricity [49]. Recently, the possibility of using natural gas in the BFB calciner of a CaL cycle has been evaluated at pilot-scale [81]. Erans et al. concluded that calciner operation under pure-oxygen conditions is feasible and economically promising as flue gas recycling is decreased or even eliminated. Since less oxygen is required, both the air separation unit and the size of the calciner could be significantly reduced. However, the authors reported that small particle size distributions (i.e., 100-200 $\mu$m) might not be applicable using the suggested setting, as most of the bed inventory was collected in the calciner's cyclone catch-pot. Therefore, further research is required to ratify whether or not CaL can develop as a leading $CO_2$ capture option in NGCC plants.

### 3.3.2 Biomass combustion within the Calcium Looping cycle

The use of biomass in energy production is considered to be carbon neutral. Furthermore, the combination of biomass with carbon sequestration techniques enables net-negative carbon emissions by sequestration of biogenic $CO_2$. The latter approach is usually referred to as bioenergy with CCS (i.e., BECCS), which is gaining increasing popularity as a feasible solution to meet the 2050 zero-carbon emission targets [38, 88, 212]. The feasibility of applying Calcium Looping to biomass-fired power plants has been analyzed by several authors. In 2011, Alonso et al. explored the concept of in situ $CO_2$ capture from biomass combustion by CaO in a 30 kW interconnected fluidized bed rig [12]. Three biomass feeds were evaluated over a wide range of operating conditions, yielding $CO_2$ capture efficiencies over 80 % in some cases. Years later, the concept was further explored in a 300 kW$_{th}$

pilot reactor at 700 °C [67]. In this work, combustion efficiencies close to 100 % were reported, yielding capture efficiencies between 70 and 95 % with wood pellet combustion. In a separate study, the same group proposed a concept for a large-scale ($>$ 100 MW$_e$) biomass-fired power plant with in situ CO$_2$ capture by CaL [163]. With a heat exchanger network, the authors suggested that this system could lead to a higher net power generation efficiency than that of a oxy-fuel biomass combustion plant. In addition, a CO$_2$ purification and compression unit should allow achieving CO$_2$ streams with a molar purity higher than 95 %. Ozcan et al. further indicated that the CO$_2$ avoidance cost estimates for the biomass oxy-fired and in situ CaL plants were close, although the gap widened with different process integration possibilities. In parallel, the cost of biomass and revenue from green certificates were shown to influence the CO$_2$ avoided cost calculations significantly. More recently, a concept for in situ CO$_2$ capture from biomass combustion in a pressurized spout fluidized bed reactor has been proposed [206]. Yao et al. reported CO$_2$ capture levels over 70 % in a temperature range between 550-750 °C at 1.5 bar. Furthermore, the authors observed that an increase in temperature and O$_2$ partial pressure led to lower capture capacities as a result of the rapid combustion and the CO$_2$ release rates. On the contrary, the total pressure did not pose a significant impact on the system. Despite the potential benefits of the process, future studies were recommended to assess its overall life-cycle carbon emissions. Also, additional work on process modeling should enable a better correlation between the release and absorption rates of CO$_2$ at elevated pressures.

### 3.3.3 Combustion of waste-derived fuels in a Calcium Looping calciner

The deployment of CCS in the waste management sector can make municipal and industrial waste a strategic resource for climate change mitigation [135]. The use of CCS with WtE could create a negative carbon sink over the life cycle of (waste) materials [165]. Despite the increasing attention being paid to the utilization of alternative fuels in a CaL cycle, little research has been devoted to experimentally investigating the performance of waste-derived fuels at realistic CaL process conditions. Recently, Haaf et al. demonstrated the feasibility of mono-combusting solid recovered fuels (SRF) under oxy-fuel conditions in a 1 MW$_{th}$ CaL pilot plant [95, 96]. Over a wide range of operation conditions, carbonator CO$_2$ capture efficiencies close to 80 % were reported, yielding total CO$_2$ capture rates over 90 %. Furthermore, the authors established a chlorine balance over the CaL system, identifying the calciner fly ash as the major chlorine effluent [96]. Haaf et al. emphasized that SRF as CaL supplementary fuel has no significant disadvantages on the CO$_2$ capture performance [95]. Nonetheless, the authors observed that the enrichment of coarse ash within the solid phase could negatively affect the hydrodynamics of the CaL system.

Hence, further research on the influence of SRF on solid phase and calciner gaseous emissions was recommended. At the University of Stuttgart's 200 kW$_{th}$ CaL pilot facility, the combustion characteristics of hard coal, wheat straw, and SRF were investigated to derive implications on the formation of gaseous pollutants and reactor hydrodynamics [150]. Setting industrially relevant process conditions (TRL6), the latter work explored the performance of the CFB calciner under different hard coal and biomass blending ratios and inlet oxygen concentrations in the oxidant gas. Additionally, the feasibility of the process under stand-alone SRF combustion was assessed. While fuel blending hardly influenced the pollutant formation process, biomass substitution directly affected the pollutants emission by modifying the fuel mixture's nitrogen and chlorine content. Besides, ash accumulation was found to significantly increase the pressure drop along the CFB riser, not only at high biomass substitution rates but also during mono-combustion of SRF. Similar to the conclusions drawn by Haaf et al. [95, 96], the authors indicated that ash accumulation constitutes a key challenge to be addressed in fluidized beds employing low-grade quality fuels. For a further assessment of the impact of fuel selection for a CaL calciner, please refer to chapter 6.

# 4 Calcium Looping: Sorbent and Process Characterization in a 20 kW$_{th}$ Dual Fluidized Bed

## 4.1 Original publication

# energy&fuels

Article

# Calcium Looping: Sorbent and Process Characterization in a 20 kW$_{th}$ Dual Fluidized Bed

Joseba Moreno,* Sally L. Homsy, Max Schmid, and Günter Scheffknecht

Cite This: *Energy Fuels* 2021, 35, 16693−16704

Read Online

ACCESS | Metrics & More | Article Recommendations

**ABSTRACT:** This paper presents an experimental investigation at a 20 kW$_{th}$ calcium looping (CaL) facility with a twofold focus. The first objective is on assessing the multicyclic behavior of limestone under continuous dual fluidized bed (DFB) operation. Different carbonation conditions were employed to derive a mathematical expression that is valid to compare the results from DFB and thermogravimetric analysis (TGA) with adequate accuracy. A preliminary screening of three morphologically distinct limestones was conducted by TGA including exposure to $SO_2$ and $H_2O$ during carbonation. The second objective is to analyze the influence of multiple process variables (i.e., temperature, $CO_2$ loading, and $H_2O$ concentration) on the performance of the 20 kW$_{th}$ CaL facility's bubbling fluidized bed carbonator. Within the investigated range of operating conditions, the chosen carbonator design allowed for $CO_2$ capture efficiencies as high as 0.99 mol/mol, yielding an apparent carbonation rate $(k_S\varphi)$ of 0.09 s$^{-1}$. Paving the way to a more flexible usage of CaL systems, the proposed carbonator design could be integrated into the existing load-following power plants, in preference to a conventional circulating fluidized bed carbonator that is heavily penalized when forced to operate under low capacity factors.
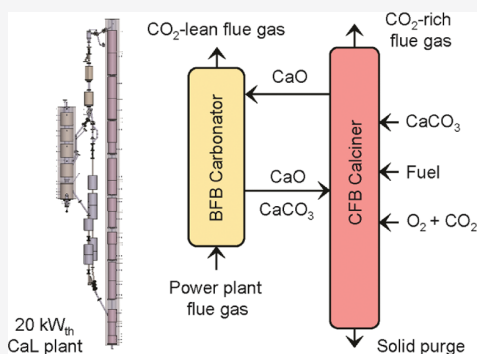
## 1. INTRODUCTION

The calcium looping (CaL) technology has gained considerable attention in recent years as a viable solution for the decarbonization of fossil-intensive power and industrial sites. The process is carried out in a dual fluidized bed (DFB) system. $CO_2$ is absorbed from the flue gas of an existing power plant using limestone-derived CaO in a carbonator (see Figure 1). Subsequently, the resulting $CaCO_3$ is regenerated in a calciner while producing a rich stream of $CO_2$. The operating conditions of the calciner and carbonator are imposed by thermodynamic equilibrium.[1] The carbonator is generally operated at temperatures around 650 °C as a trade-off between the limitations imposed by the reaction kinetics and the equilibrium driving forces,[2−5] while the calciner is typically operated above 900 °C to allow fast sorbent regeneration in a $CO_2$-rich atmosphere.[6,7] The energy required for sorbent regeneration is generally provided by burning supplementary fuel with oxygen from an air separation unit (i.e., oxy-fuel). The $CO_2$-rich regenerator flue gas can be partly recirculated into the system to adjust the combustion temperature. Due to sorbent deactivation upon cycling, a continuous flow of fresh limestone make-up (i.e., $CaCO_3$) is fed to the process. This is compensated by an equivalent sorbent purge to avoid accumulation of inerts in the system (e.g., fuel ash and $CaSO_4$).

The roots of the CaL technology, namely, using a calcium-containing sorbent for $CO_2$ capture, date back to the $CO_2$ acceptor process proposed by Curran et al. in 1967.[8] In 1999, Shimizu et al. further developed the idea to a full fluidized bed CCS process by switching the regenerator operation from air to oxy-fuel.[2] Early thermogravimetric analysis (TGA) studies proved the feasibility of exploiting the reversible reaction between CaO and $CO_2$ at characteristic process conditions.[9,10] First process demonstrations began in electrically heated fluidized bed facilities that were operated in a batch mode.[11,12] Hereafter, continuous DFB operation was assessed using diverse electrically heated reactor concepts,[13,14] prior to successful demonstration in fuel-powered pilot plants up to the MW$_{th}$ scale.[15−18]

Although CaO-based sorbents offer many advantages, for example, wide availability, relative low cost, and high theoretical $CO_2$ uptake, they typically suffer from a rapid decline in $CO_2$ capture performance during cyclic operation (see Figure 2). This latter aspect has remained an urgent issue required to be addressed for CaL industrial and power applications.[6,7,19] The loss of reactivity is usually ascribed to

16693
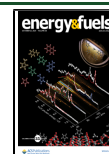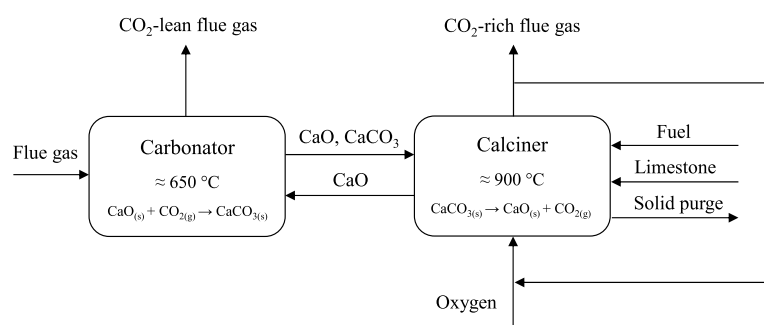
**Figure 1.** Basic schematic of the CaL process.
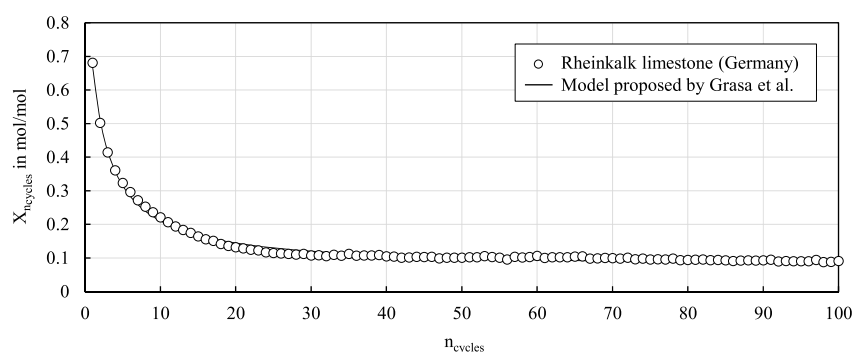


**Figure 2.** Sorbent capacity ($X_{n_{cycles}}$) against the number of cycles ($n_{cycles}$) for the Rheinkalk limestone. The solid line corresponds to the model proposed by Grasa et al.;[7] $k = 0.59$ and $X_r = 0.067$. Carbonation conditions: $T_{carb} = 650\ °C$, $t_{carb} = 10\ min$, $y_{CO_2,carb,in} = 0.15\ m^3/m^3$, and $y_{N_2,carb,in} = 0.85\ m^3/m^3$. Calcination conditions: $T_{calc} = 850\ °C$, $t_{calc} = 10\ min$, and $y_{N_2,calc,in} = 1\ m^3/m^3$.

the reduction of suitable pore volume and pore surface area due to several mechanisms such as sintering (i.e., grain growth) and competing reactions (e.g., sulfation).[20,21] The influence of sulfation, both with and without steam addition, has been previously investigated for CaL systems. While most work has been completed at TGA[21,22] and at the laboratory scale,[23,24] some pilot investigations have been reported using limestone[15,25] as well as synthetic sorbents.[26]

To date, several semi-empirical methods have been proposed to describe the decay of a sorbent's carrying capacity with the number of cycles.[7,19,27] While most early studies considered gas atmospheres consisting of $CO_2$, $N_2$, $O_2$, and/or air,[2,6,7,10,28] the current focus is on exploring more realistic carbonation conditions that include the influence of $H_2O$ and/ or $SO_2$.[29,30] In fact, $SO_2$ and $H_2O$ deserve consideration as they affect the sorbent carrying capacity decay, leading to significant consequences on the CaL system design.[22,31,32]

Despite the significant development achieved in this field in recent years, most research has focused on investigating the process performance at baseload operating conditions, overlooking the flexible operation of CaL systems coupled to load-following power units. In this context, the conventional CaL configuration relying on two interconnected circulating fluidized bed reactors (i.e., CFB−CFB) might not be a preferable option at minimum thermal loads, where the resulting low gas superficial velocities might constrain efficient solid entrainment and circulation within the CaL system.[33] The combination of a bubbling fluidized bed (BFB) carbonator with a bottom interlink has been recently proposed as a viable option to enhance the load flexibility of CaL systems.[34,35] Such a design offers the unique possibility of

decoupling solid circulation from the carbonator flue gas load, thus enabling the BFB carbonator to be operated in a broad range of fluidization regimes ranging from bubbling, over turbulent, to circulating conditions. Furthermore, BFB units might serve power plants with a maximum electric power output of roughly 200 MW,[36] which represents the typical size of currently available medium-scale power boiler blocks.

In this work, we evaluate the influence of several carbonation variables (i.e., temperature, $CO_2$ loading, and $H_2O$ concentration) on the BFB carbonator performance of a 20 kW$_{th}$ CaL facility as a preliminary step for subsequent flexible demonstration at a larger scale (TRL6). The carbonator performance has been preliminarily validated using a general carbon mass balance. In the following, a simplified reactor model approach implemented in experimental facilities of different sizes has been applied for a more detailed result interpretation.[14,16,37−39] The sorbent selected for fluidized bed experiments derived from the TGA of three limestone candidates with distinct origin and morphological structure. Sorbents were subjected to cyclic experiments to determine the decay in cyclic carrying capacity with flue gas compositions expected to prevail in coal-fired power plants (i.e., presence of $SO_2$ and/or $H_2O$).

## 2. METHODOLOGY AND VALIDATION

**2.1. Experimental Section.** The chemical composition of the three limestones utilized in this work is given in Table 1. The metamorphosed Saabar limestone and the unmetamorphosed Riyadh limestone were obtained from Saudi Arabia, from the Red Sea coastal plane and the Arabian platform, respectively. Both sorbents were provided by United Mining

**Table 1. Chemical Composition of the Utilized Sorbents**

|  | $x_{CaO}$ | $x_{MgO}$ | $x_{SiO_2}$ | $x_{Al_2O_3}$ | $x_{CO_2}$ | $x_{others}$ |
|---|---|---|---|---|---|---|
|  | kg/kg, wf | | | | | |
| Rheinkalk | 0.551 | 0.007 | 0.004 | 0.001 | 0.435 | 0.002 |
| Saabar | 0.512 | 0.006 | 0.039 | 0.002 | 0.416 | 0.025 |
| Riyadh | 0.518 | 0.004 | 0.032 | 0.003 | 0.426 | 0.017 |

Investments Co. and subsequently milled and sieved by BHS-Sonthofen GmbH and Allgaier Process Technology GmbH, respectively. The unmetamorphosed German limestone "Messinghausener Sand" from Lhoist Germany Rheinkalk GmbH was also obtained. The particle size distribution of each limestone ranged between 100 and 400 $\mu$m and was measured using a Malvern Mastersizer 3000 equipped with an Aero S dry particle dispersion unit. A detailed morphological characterization of these three sorbents is presented elsewhere.[30]

A custom-built TGA (Linseis PT1100) equipped with a gas mixing manifold was used for a preliminary assessment of the multicyclic activity decay of the three limestones analyzed in this work. The TGA experiments were performed on 12 mg samples of raw limestone by calcining them in pure nitrogen at 850 °C for 10 min and subsequently carbonating them at 650 °C for 10 min in different gas atmospheres (see Table 2). The

**Table 2. TGA Carbonation Routines Investigated in This Work**

|  | gas composition ($m^3/m^3$) | | | |
|---|---|---|---|---|
|  | $y_{CO_2,carb,in}$ | $y_{N_2,carb,in}$ | $y_{H_2O,carb,in}$ | $y_{SO_2,carb,in}$ |
| routine (a): $CO_2$ | 0.150 | 0.850 | 0.000 | 0.000 |
| routine (b): $CO_2$, $H_2O$ | 0.150 | 0.700 | 0.150 | 0.000 |
| routine (c): $CO_2$, $SO_2$ | 0.150 | 0.848 | 0.000 | 0.002 |
| routine (d): $CO_2$, $H_2O$, $SO_2$ | 0.150 | 0.698 | 0.150 | 0.002 |

TGA apparatus was operated with a total gas flow of 100 sccm/min. The applied heating and cooling rates were 200 °C/min and 50 °C/min, respectively. The recorded changes in sample mass were used to calculate the attained sorbent conversion.

The University of Stuttgart's 20 kW$_{th}$ laboratory scale facility consists of two electrically heated fluidized beds (see Figure 3). The two reactors can be operated separately or coupled. When coupled, the fluidized beds are interconnected via two loop seals. The CFB reactor has a total height of 12 m and an internal diameter of 70 mm, whereas the BFB unit consists of a 3.5 m reactor with an internal diameter of 150 mm in the bed and 200 mm in the freeboard region.

In this study, the CFB unit is operated as a calciner, whereas the BFB reactor is utilized as a carbonator. The flue gas of each reactor is separated from the entrained solids in a high-efficiency, primary cyclone. Subsequently, a protective cyclone and a candle filter are employed for separating finer particles before the flue gas is vented to the atmosphere. Solids separated by the high-efficiency cyclones are directed back to the reactors via loop seals, whereas solids removed by the protective cyclones and candle filters are collected in bins. Solids separated by the CFB's primary cyclone are either recirculated internally to the riser or externally to the BFB reactor. The respective share of external and internal circulation is controlled via a cone valve in the reactor's loop seal. The transfer of solids from the carbonator to the calciner

is achieved by means of an overflow pipe. Fluidization gases such as $N_2$, $CO_2$, and steam are preliminarily heated, whereas $SO_2$ is fed to the preheated mixture as needed before injection to the gas distributor. The dry gas composition of each reactor is continuously measured between the protective cyclone and the candle filter. The carbonator is equipped with an ABB Advance Optima 2020 for continuous $CO_2$, $O_2$, and $SO_2$ analysis. Concurrently, the calciner employs an ABB EL 3020 to monitor the volume fractions of $O_2$ and $CO_2$ in the off-gas. Although $O_2$ was not added to the gas distributor, volume fractions up to 0.02 $m^3/m^3$ were measured after each reactor due to the supply of air required for the continuous flushing of the diverse pressure transducers. Both fluidizing beds are equipped with gravimetric dosing systems for solids. The solid circulation between reactors is manually determined by means of solid accumulation in a dedicated measuring section. The solids sampled from the loop seals, protective cyclones, and candle filters of each reactor are subsequently analyzed in terms of chemical composition, sorbent carrying capacity, and particle size distribution. The facility is equipped with thermocouples and pressure transducers along all gas and solid lines. Moreover, the electrical heating of the fluidized bed system enables independent assessment of operation parameters detached from the complex interaction at considerably higher scale.[35,40]

During the DFB experiments, the BFB carbonator was operated with a gas superficial velocity of 0.5 m/s. As postulated by diverse authors, the ratio of solid inventory (i.e., bed height) to flue gas velocity yielded in a carbonator is of particular interest since it poses a major influence on both heat recovery and $CO_2$ capture efficiency.[2,5,13,41] In CaL, the latter parameter is commonly referred to as carbonator space time ($\tau$). Considering the bed height attained in the 20 kW$_{th}$ BFB carbonator (i.e., 0.5 m), a bed height to gas velocity ratio of approximately 1 s can be calculated for this study. Generally, the $CO_2$ removal efficiencies yielded in the present work are in good agreement with the results reported by other authors under similar process conditions.[2,13] Furthermore, Charitos et al. performed complementary investigations at flue gas velocities up to 1.2 m/s (i.e., lower space time values), reporting considerably lower $CO_2$ capture efficiencies due to a decreased residence time.[13]

**2.2. Evaluation of Sorbent Deactivation in a TGA Environment.** It is well known that CaO-based sorbents experience a considerable reduction in carrying capacity with increasing number of sequential calcination and carbonation cycles, especially in the first 20 cycles. Although several semi-empirical models have been proposed to describe the multicyclic decay in sorbent activity,[19,27] particularly one approach has received considerable attention in the last years, as it is valid for describing the evolution in capture capacity for a wide number of limestones and operating conditions[7]

$$X_{n_{cycles}} = \frac{1}{(1/(1 - X_r)) + kn_{cycles}} + X_r \qquad (1)$$

Grasa and Abanades proposed a second-order decay equation in which sorbent conversion ($X_{n_{cycles}}$) can be calculated as a function of the number of cycles ($n_{cycles}$) under the consideration that the particles reach the point of maximum conversion during the fast reaction regime. $k$ corresponds to the sorbent deactivation constant and $X_r$ refers to the sorbent residual conversion after an infinite number of cycles.
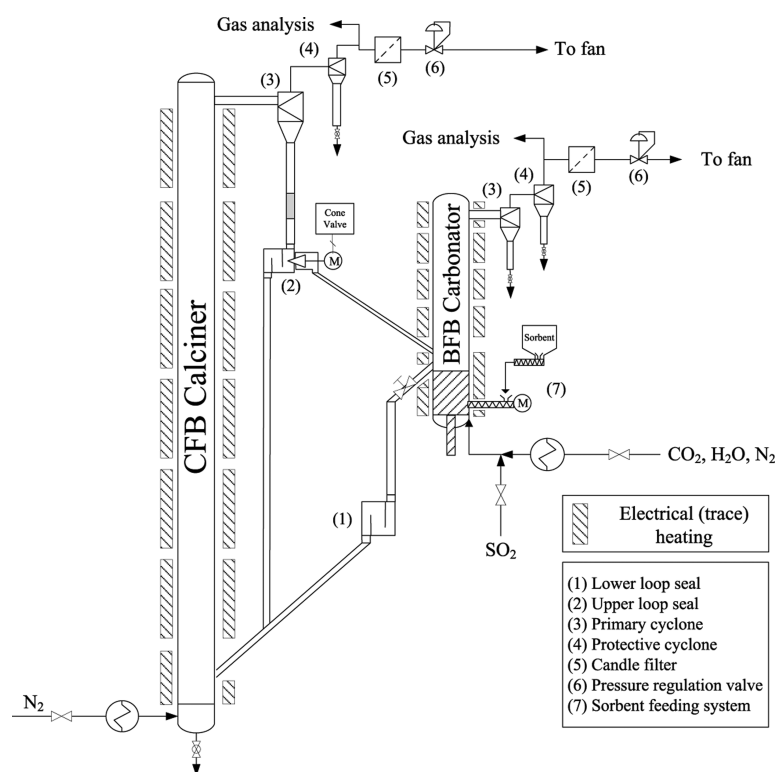
**Figure 3.** Schematic of the University of Stuttgart's 20 kW$_{th}$ CaL facility.

**2.3. Evaluation of Sorbent Deactivation in a Continuous DFB Environment.** The use of a dual interconnected fluidized bed system constitutes a favorable framework for investigating the evolution of sorbent activity upon cycling, as it ensures improved gas–solid interaction as well as heat- and mass-transfer characteristics. In the absence of make-up, the sorbent average activity decays with time. This decay is ascribed to the increasing number of cycles that the average particle has experienced in the system. Under these conditions, the theoretical number of calcination and carbonation cycles ($n_{cycles}$) can be estimated by introducing an amendment accounting for the cycling history of the particles prior to the beginning of the calcination and carbonation experiments $\left( 0 < t < t_1 \right)$ to the equation previously proposed by Charitos et al.[38]

$$n_{cycles} = \int_0^{t_1} \frac{\dot{N}_{Ca,loop}(t)}{N_{Ca,total}} \, dt + \int_{t_1}^{t_2} \frac{\dot{N}_{CO_2,carb,in} E_{carb}(t)}{N_{Ca,total} X_{ave}} \, dt \tag{2}$$

where $\dot{N}_{Ca,loop}(t)$ indicates the instantaneous molar flow rate of calcium between reactors, $\dot{N}_{CO_2,carb,in}$ refers to the molar flow rate of $CO_2$ at the carbonator inlet, and $E_{carb}(t)$ refers to the instantaneous $CO_2$ carbonator capture efficiency. In addition, $N_{Ca,total}$ and $X_{ave}$ represent the total molar calcium inventory in the system and the average carrying capacity of the sorbent, respectively.

**2.4. Validation of the Carbonator Carbon Mass Balance.** An essential tool for the validation of the carbonation process is the closure of the carbon mass balance. During steady-state operation, where there is no accumulation of $CaCO_3$ in the reactor bed, the mass of $CO_2$ disappearing from the gas phase has to equal the mass of $CO_2$ being bound as carbonate in the CaO stream circulating between the two reactors

$$\dot{N}_{CO_2,carb,in} E_{carb} = \dot{N}_{Ca,loop}(X_{carb} - X_{calc}) \tag{3}$$

The amount of $CO_2$ captured from the gas phase $\left( \dot{N}_{CO_2,carb,in} E_{carb} \right)$ can be calculated by means of the measured gas composition and volume flow. For calculating the amount of $CO_2$ appearing in the solid phase, the CaL rate is estimated according to the measured solid circulation rate and the circulating solids' calcium content. Once $\dot{N}_{Ca,loop}$ is known, it is possible to calculate the amount of solids entering the carbonator with a molar carbonate content $X_{calc}$ after regeneration (i.e., $\dot{N}_{Ca}X_{calc}$) and those leaving the carbonator after $CO_2$ absorption with a molar carbonate content $X_{carb}$ (i.e., $\dot{N}_{Ca}X_{carb}$), assuming that both reactors are perfectly mixed. The comparison between both equation terms is a useful indicator of the experimental information's consistency, which is the basis for analyzing the carbonator performance.

Another relevant methodology for assessing the carbonation process is based on a basic reactor model and simplified particle reaction rate model[38]

$$\left( \frac{dX}{dt} \right)_{carb} = k_s \varphi X_{ave} \left( \overline{y_{CO_2,carb}} - y_{CO_2,carb,eq} \right) \tag{4}$$

In eq 4, $k_s$ is the surface reaction rate constant for the utilized limestone, $\left( \overline{y_{CO_2,carb}} - y_{CO_2,carb,eq} \right)$ refers to the difference between the logarithmic average and the equilibrium $CO_2$ volume fraction in the carbonator, and $\varphi$ indicates the gas–solid contacting factor. This simplified approach allows us to solve the following mass balance for the amount of $CO_2$
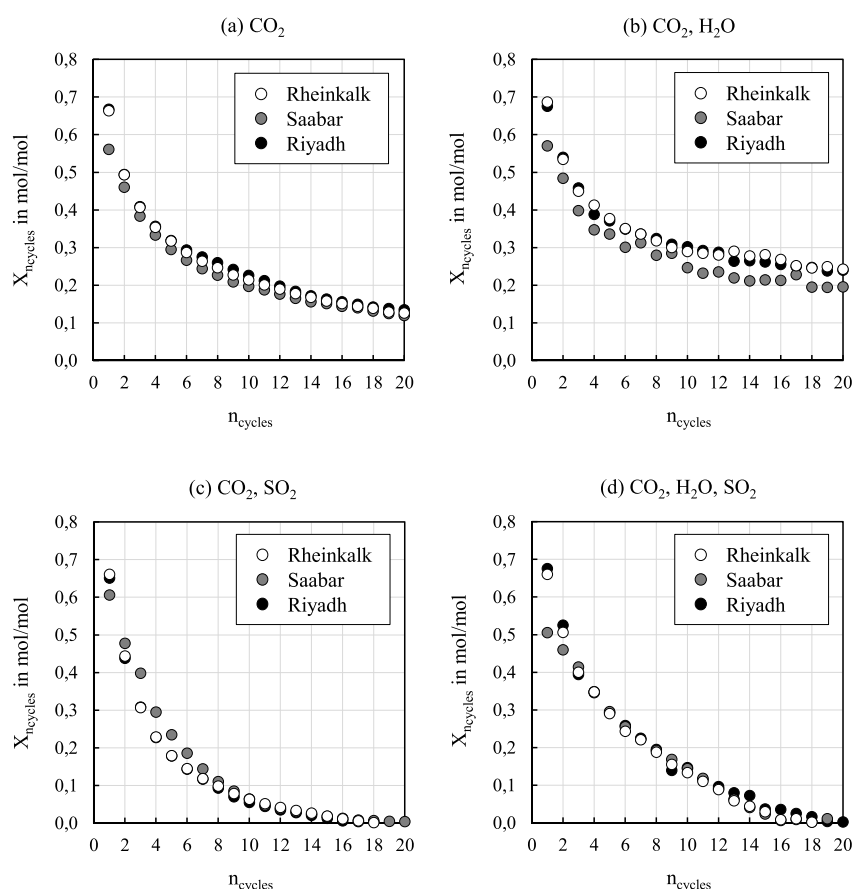
**Figure 4.** Sorbent capacity ($X_{n_{cycles}}$) against the number of cycles ($n_{cycles}$) for all investigated TGA routines and limestones. (a) $CO_2$; (b) $CO_2$ and $H_2O$; (c) $CO_2$ and $SO_2$; and (d) $CO_2$, $H_2O$, and $SO_2$. Carbonation conditions: $T_{carb}$ = 650 °C, $t_{carb}$ = 10 min. Calcination conditions: $T_{calc}$ = 850 °C, $t_{calc}$ = 10 min, and $y_{N_2,calc,in}$ = 1 $m^3/m^3$.

**Table 3. Compilation of Deactivation Constants ($k$) and Residual Conversions ($X_r$) for All Investigated Limestones and Carbonation Routines**

| | (a) $CO_2$ | (b) $CO_2$, $H_2O$ | (c) $CO_2$, $SO_2$ | (d) $CO_2$, $H_2O$, $SO_2$ |
|---|---|---|---|---|
| Rheinkalk | $k$ = 0.593 ± 0.004, $X_r$ = 0.069 ± 0.003 | $k$ = 0.822 ± 0.012, $X_r$ = 0.187 ± 0.002 | $k$ = 0.472 ± 0.004, $X_r$ = −0.116 ± 0.004 | $k$ = 0.312 ± 0.009, $X_r$ = −0.126 ± 0.002 |
| Saabar | $k$ = 0.780 ± 0.003, $X_r$ = 0.078 ± 0.002 | $k$ = 1.032 ± 0.022, $X_r$ = 0.161 ± 0.003 | $k$ = 0.392 ± 0.002, $X_r$ = −0.128 ± 0.002 | $k$ = 0.401 ± 0.015, $X_r$ = −0.019 ± 0.003 |
| Riyadh | $k$ = 0.583 ± 0.003, $X_r$ = 0.059 ± 0.001 | $k$ = 0.834 ± 0.008, $X_r$ = 0.192 ± 0.002 | $k$ = 0.470 ± 0.003, $X_r$ = −0.112 ± 0.002 | $k$ = 0.307 ± 0.005, $X_r$ = −0.140 ± 0.003 |

removed in the gas phase and the $CO_2$ captured by the CaO particles in the carbonator bed (see ref 38 for more details)

$$\dot{N}_{CO_2,carb,in}E_{carb} = N_{Ca,carb}f_{active}k_s\varphi X_{ave}\left(\overline{y_{CO_2,carb}} - y_{CO_2,carb,eq}\right) \quad (5)$$

The apparent carbonation rate constant ($k_s\varphi$) can be calculated as a fitting parameter from eq 5, whereas $k_s$ can be determined by TGA. $N_{Ca,carb}$ refers to the carbonator calcium inventory and $f_{active}$ corresponds to the fraction of active particles reacting in the fast reaction regime (where $X_{carb} < X_{ave}$). Equation 5 constitutes a reactor design equation model and links all CaL parameters directly or indirectly with the carbonator $CO_2$ capture efficiency ($E_{carb}$) for the given set of operating conditions. The key parameter of this model is the active space time ($\tau_{active} = N_{Ca,carb}f_{active}X_{ave}/\dot{N}_{CO_2,carb,in}$), which is

indicative of both the sorbent inventory and the reaction rate of such inventory.

## 3. RESULTS AND DISCUSSION

The present work focuses on the experimental assessment of a 20 $kW_{th}$ CaL facility using a BFB carbonator, which is operated under boundary conditions similar to those applied in coal-fired power plants. In a preliminary phase, the decay in capture capacity of three distinct limestones over multiple calcination and carbonation cycles has been evaluated using a thermogravimetric analyzer. Subsequently, the activity decay behavior of the selected limestone type has been investigated in a continuous DFB environment. In the following, the BFB carbonator performance has been assessed in terms of reactor bed temperature, $CO_2$, and $H_2O$ loading. The evaluation of the calciner performance is out of the scope of this study.

**3.1. Sorbent Deactivation in a TGA Environment.** The evolution of the sorbent capture capacity ($X_{n_{cycles}}$) over 20 sequential calcination and carbonation cycles is displayed in Figure 4. When $SO_2$ is absent during carbonation, the attained sorbent conversion equals the $CO_2$ conversion experienced by the sorbent. However, when $SO_2$ is added to the process, the decay in capture capacity also includes the deactivation extent incurred by CaO sulfation.

Under pure $CO_2$ carbonation conditions (see Figure 4a), all three limestones reveal a similar behavior. Saabar shows a higher deactivation tendency upon the first calcination/carbonation cycles, although it eventually converges to a similar residual value as for the other two investigated limestones. The derived deactivation information from such data series (see Table 3) correlates well with the observations made by Grasa et al., who suggested values of $k = 0.52$ and $X_r = 0.075$ to describe a general activity decay behavior under pure $CO_2$ carbonation conditions with adequate accuracy.[7]

In the presence of steam (see Figure 4b), all three limestones exhibit a positive effect upon carbonation. The influence of steam on carbonation efficiency was also investigated by Manovic et al. and Donat et al., who attributed the enhanced carbonation to an improvement of solid-state diffusion in the product layer.[42,43] In the current study, Saabar seems to be less positively influenced by steam addition when compared to Rheinkalk and Riyadh. As postulated by Homsy et al. in a recent publication, metamorphosed Saabar presents large, relatively pure, and highly crystalline monomineralic $CaCO_3$ grains.[30] Such morphologic structure is responsible for the evolution of relatively narrow uniform pores and high-purity crystalline CaO with low overall porosity upon calcination. This is ultimately translated into a higher surface reactivity and increased susceptibility to pore blockage during carbonation, which correlates well with the trend shown by Saabar in Figure 4a. Besides, the pore narrowing effect achieved by humid carbonation conditions further exacerbates Saabar's pore blockage, which ultimately results in a lower carbonation conversion upon cycling. Homsy et al. concluded that the introduction of a limited amount of impurities such as $SO_2$ may contribute to enhancing resistance against mesopore blockage during the first CaL cycles due to fast surface carbonation. By this way, the sorbent porosity may be preserved, while the sorbent's grain and pore size concurrently increases. The results presented in Figure 4c corroborate this hypothesis. In the absence of $H_2O$, $SO_2$ positively influences the capture performance of the Saabar limestone during the first 10 calcination and carbonation cycles. In consequence, Saabar yields a lower deactivation constant when compared to Rheinkalk and Riyadh (see Table 3). With increasing cycle number, sorbent deactivation is greatly exacerbated for all three limestones due to exposure to $SO_2$. As can be observed in Figure 4c, the residual sorbent activity after 20 sequential calcination and carbonation cycles approaches zero for all three investigated limestones. The negative values included in Table 3 are inconceivable based on the definition of $X_r$ and are ascribed to extrapolation of the data for an infinite number of CaL cycles. Besides, steam addition to a sorbent carbonated under $SO_2$ further magnifies the influence of steam on each limestone (see Figure 4d). Rheinkalk and Riyadh present a substantial improvement in the sorbent capture capacity compared to the previous case (Figure 4c), which is again attributed to the enhanced CaO reactivity with $CO_2$ achieved

by steam addition. As for Saabar, the positive effect achieved by $SO_2$ addition is compensated by the presence of $H_2O$, which leads to a similar decay behavior as for Rheinkalk and Riyadh.

In conclusion, Rheinkalk and Riyadh show a similar activity decay for all investigated TGA routines. The capture performance of both limestones aligns well with a recent work from Coppola et al., who reported a positive and negative influence by flue gas $H_2O$ and $SO_2$, respectively.[44] Saabar exhibits anomalous behavior, where the sorbent activity during the first cycles is positively and negatively affected by the presence of $SO_2$ and water vapor, respectively. Since dry sulfurous flue gas is uncommon, further exploration of Saabar was not completed. Moreover, the possibility of utilizing Riyadh at the 20 $kW_{th}$ CaL facility was finally discarded due to the additional costs entailed by the increased sorbent and logistic efforts. In consequence, Rheinkalk was selected for further investigation by DFB experiments.

**3.2. Sorbent Deactivation in a Continuous DFB Environment.** The evolution of Rheinkalk's capture capacity with time was investigated in the DFB 20 $kW_{th}$ CaL facility. For these experiments, the carbonator and calciner were electrically preheated up to 650 and 900 °C in pure nitrogen conditions, respectively. When the desired target temperatures were achieved, a total amount of 40 kg of Rheinkalk was gradually added to the system, monitoring the sorbent calcination degree at each step by continuously measuring the outlet $CO_2$ concentration in the calciner. After the last batch of limestone was calcined, the carbonator gas atmosphere was switched to the desired carbonation conditions. The solid circulation rate between reactors was adjusted to maintain an adequate residence time of the sorbents in the carbonator and averaged at 8.5 mol/mol. Throughout the experiments, no limestone make-up was added. From this point onward, solids were regularly sampled from the loop seals of each reactor for subsequent analysis. Each experiment was investigated for about 5 h of continuous operation.

The degradation behavior experienced by Rheinkalk under two distinct carbonation gas atmospheres is presented in Figure 5. The depicted cycle number was calculated according to eq 2, as solids were continuously circulated for up to 1 h before the calcination and carbonation experiments initiated. As can be observed in the illustration, the calculated activity decay at the 20 $kW_{th}$ facility correlates reasonably well with the results obtained from the thermogravimetric analyzer (i.e., model curves). In both cases, sorbents exhibited an exacerbated deactivation when carbonated in the presence of $SO_2$, with a more pronounced decay in the subsequent CaL cycles. As previously anticipated, this is a typical behavior in most unmetamorphosed limestones, where the formation of $CaSO_4$ in the product layer leads to pore blockage, limiting the degree of sorbent utilization.[45,46] In any case, the suggested expression seems to estimate the theoretical CaL cycles with adequate accuracy, considering the inherent uncertainties in the determination of some of the involved parameters (i.e., $X_{ave}$ and $\dot{N}_{Ca,loop}$).

**3.3. Parametric Study of the 20 $kW_{th}$ CaL Facility's BFB Carbonator.** The carbonator $CO_2$ capture efficiency is affected by diverse process variables such as carbonator space time, carbonation temperature, looping ratio, and make-up ratio. From an operational standpoint, the looping ratio and make-up ratio are of particular interest, as they can be set
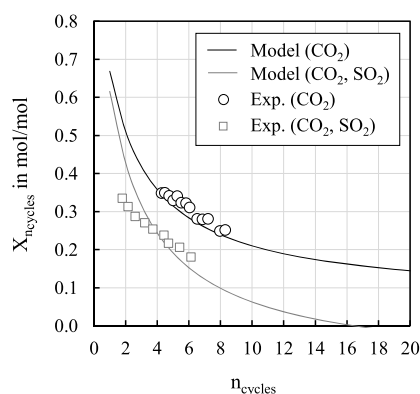
**Figure 5.** Sorbent capacity ($X_{n_{cycles}}$) against the number of cycles ($n_{cycles}$) for Rheinkalk during DFB experiments. Black circles: $T_{carb}$ = 650 °C, $y_{CO_2,carb,in}$ = 0.15 m$^3$/m$^3$, $y_{N_2,carb,in}$ = 0.85 m$^3$/m$^3$; gray squares: $T_{carb}$ = 650 °C, $y_{CO_2,carb,in}$ = 0.15 m$^3$/m$^3$, $y_{SO_2,carb,in}$ = 0.002 m$^3$/m$^3$, and $y_{N_2,carb,in}$ = 0.848 m$^3$/m$^3$. Calcination conditions: $T_{calc}$ = 850 °C, $y_{N_2,calc,in}$ = 1 m$^3$/m$^3$. Model parameters according to Table 3.

directly by the designer/operator without the control loop implementation. However, an in-depth view of the process requires understanding the effect of other variables such as space time (i.e., carbonator bed inventory and $CO_2$ loading) or carbonation temperature since the latter has a major implication on the carbonation rate and, thus, on the attained $CO_2$ capture efficiency. At the 20 kW$_{th}$ CaL facility, the carbonator solid inventory is controlled by an overflow system and thus cannot be freely defined. In consequence, this study aims at improving process understanding by evaluating the influence of $CO_2$ loading and carbonator temperature on the overall BFB carbonator performance. Also, the role of steam upon carbonation is discussed, as it can influence the design of a CaL process significantly.[22,23,47]

As anticipated in a previous passage, the BFB carbonator was operated at a gas superficial velocity of 0.5 m/s throughout the tests. Based on the findings of a recent study, such gas velocity could be translated into a part-load scenario as low as 25% with respect to the defined nominal case.[35] In consequence, the parametric analysis included in this study can promote a wider understanding of BFB carbonators that are operated at characteristic minimum power plant load conditions.
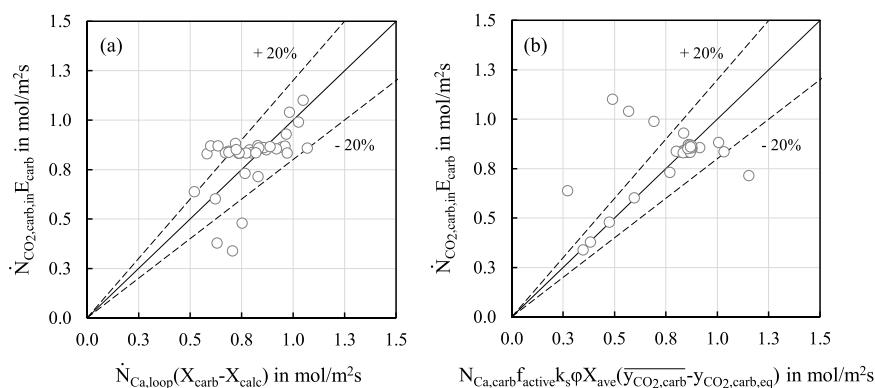
*3.3.1. Closure of the Carbonator Carbon Mass Balance.* The carbonator carbon balance constitutes a key metric for evaluating the CaL process performance. Figure 6a compares the amount of $CO_2$ disappearing from the gas phase with the amount of $CO_2$ appearing as $CaCO_3$ in the circulating solid stream (calculated according to eq 3). Both balances (i.e., gas and solid) are presented with respect to the carbonator's cross-sectional area. The depicted dashed lines in Figure 6 correspond to a standard deviation of 20% with respect to the diagonal line included in the illustration. As can be observed, the gas and solid $CO_2$ balances correlate reasonably well. In Figure 6a, 74% of the depicted data points reveal a standard deviation equal or lower than 20%. Moreover, 50% of them indicate a standard deviation equal or lower than 10%. The latter dispersion can be mainly ascribed to the intrinsic uncertainties in the measurement of the hot circulating solids. Moreover, it should be noted that the sampled solids represent only a minor share of the total solid inventory, which may also influence the analysis of the solid's phase balance. Figure 6b offers a comparison between the $CO_2$ removed from the gas phase and the $CO_2$ reacting with CaO in the carbonator bed as calculated by eq 5. It can be seen that most experiments lead to a satisfactory closure of the mass balance, considering the aforementioned intrinsic uncertainties in the estimation of the solid circulation rate and the sorbent carbonation degree. Only 13% of the points show a standard deviation higher than 20%. Moreover, 79% of all tests indicate a standard deviation equal to or less than 5% with respect to the diagonal line. Note that experimental points that appear to have a higher dispersion when the mass balance is closed using eq 5 have a lower deviation when eq 3 is used and vice versa. This further indicates that the observed deviations are due to the experimental artifacts and that the error can be minimized by selecting the appropriate mass balance approach for each experimental set. As previously anticipated, eq 5 also constitutes a basic carbonator design model, as it links all CaL operating parameters with the carbonator $CO_2$ capture efficiency. For the experiments in this study, $k_s\varphi$ averaged 0.09 s$^{-1}$ with a standard deviation of 0.03. The calculated apparent carbonation rate correlates satisfactorily with the results reported in previous works using a BFB reactor as a carbonator unit.[40,48]

*3.3.2. Influence of Carbonation Temperature.* The carbonation temperature has a direct impact on the carbonator $CO_2$ capture efficiency, as it determines the thermodynamic



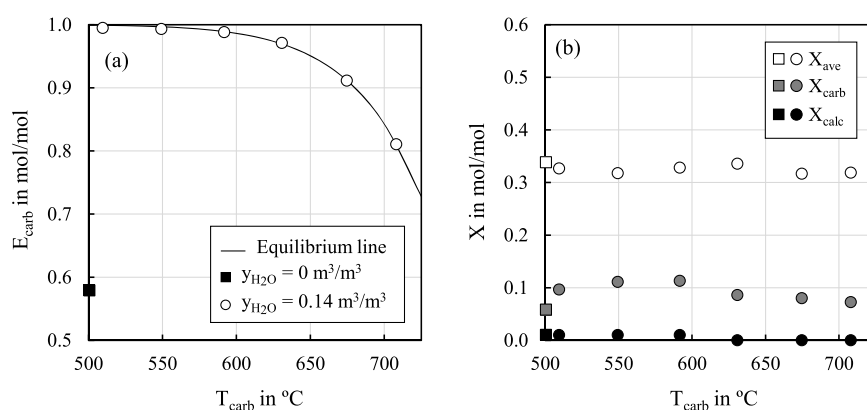**Figure 6.** (a) Comparison between the $CO_2$ removed from the gas phase and the increment in the $CaCO_3$ flow between reactors. (b) Comparison between the $CO_2$ removed from the gas phase and the $CO_2$ reacting with CaO in the carbonator bed.

**Figure 7.** (a) Carbonator $CO_2$ capture efficiency ($E_{carb}$) for different carbonation temperatures ($T_{carb}$) with (white circles) and without (black square) steam addition. Equilibrium $CO_2$ capture efficiency (solid curve) defined according to an inlet $CO_2$ concentration of 0.14 m³/m³. (b) $CO_2$ conversion degree ($X_{carb}$, $X_{calc}$) and maximum average carrying capacity ($X_{ave}$) for different carbonation temperatures with (circles) and without (square) steam addition.
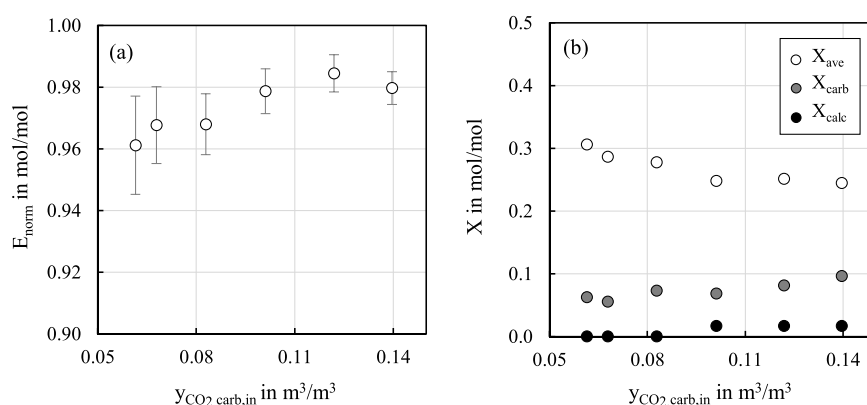


**Figure 8.** (a) Equilibrium-normalized carbonator $CO_2$ capture efficiency ($E_{norm}$) for different inlet $CO_2$ concentrations ($y_{CO_2,carb,in}$) at 650 °C in the presence of steam ($y_{H_2O,carb,in}$ = 0.14 m³/m³). (b) $CO_2$ conversion degree ($X_{carb}$, $X_{calc}$) and maximum average carrying capacity ($X_{ave}$) for different inlet $CO_2$ concentrations.

maximum amount of $CO_2$ that can be absorbed from the gas phase for a given volume flow of $CO_2$ entering the reactor. Furthermore, it plays a major role in the carbonation kinetics, as it specifies the driving force of the carbonation reaction. Figure 7a shows the influence of carbonation temperature on the $CO_2$ capture efficiency, with and without the presence of steam. For the presented experiments, a surplus of active sorbent was circulated between both reactors. Hence, the carbonation efficiency was solely determined by the process temperature and not by the amount of circulating sorbent. The solid curve represents the maximum attainable equilibrium $CO_2$ capture as a function of the system temperature,[49] which is defined for an inlet $CO_2$ concentration of 0.14 m³/m³. As can be observed, the experimentally determined carbonator $CO_2$ capture efficiencies under steam addition correlate satisfactorily with the equilibrium limited $E_{carb}$ values. Carbonator temperatures in the range of 500−600 °C have been reported to improve the $CO_2$ removal efficiency due to the lower achievable $CO_2$ concentration.[9,50] This is also reflected by the results shown in Figure 7a, where $E_{carb}$ increased from 0.81 mol/mol at 708 °C to 0.99 mol/mol at 510 °C when operating under the influence of steam. The standard deviation throughout each test is not presented in the illustration since the respective error bars are consistently

smaller than the depicted individual data points. Under kinetically controlled conditions (i.e., 500−515 °C), the presence of steam enhanced the carbonation rate notably. The addition of $H_2O$ was capable of improving the $CO_2$ capture efficiency in about 41 percentage points as long as $E_{carb}$ was not limited by the amount of circulating solids. This observation is in line with an early work by Dobner et al., who investigated the effect of steam on carbonation of dolomites.[51] The authors postulated that steam can "catalyze" the reaction between $CO_2$ and CaO, particularly at carbonation temperatures as low as 550 °C. The results presented in this section endorse that a BFB carbonator operated under steam addition and sufficient solid circulation can enable near equilibrium capture efficiencies over a wide temperature range. From the load flexibility standpoint, this can also be regarded in a positive light, mainly because of the temperature fluctuations which might be expected during the transient behavior between specific load cases.

The influence of carbonation temperature on the evolution of the sorbent carrying capacity along cycling was assessed by Criado et al. in a recent work.[52] The authors performed a thermogravimetric study of the decay behavior experienced by a high-purity natural Ca-material in a temperature range of 450−725 °C and found a reduction in the carrying capacity of
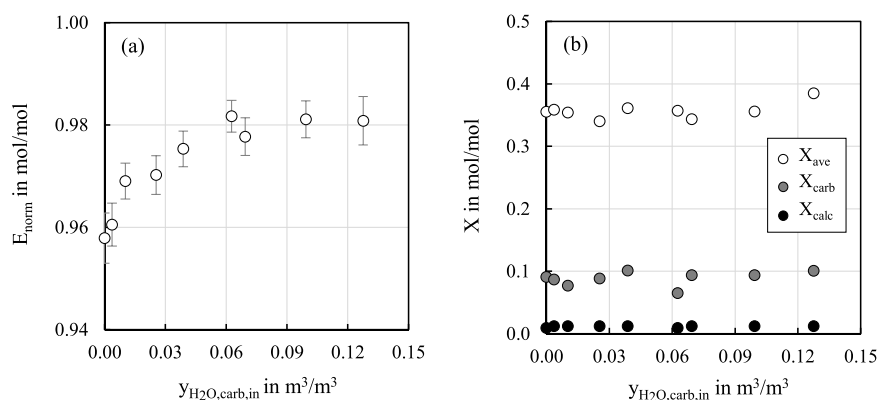
**Figure 9.** (a) Equilibrium-normalized carbonator $CO_2$ capture efficiency ($E_{norm}$) for different inlet $H_2O$ concentrations ($y_{H_2O,carb,in}$) at 650 °C with an inlet $CO_2$ concentration of 0.14 m³/m³. (b) $CO_2$ conversion degree ($X_{carb}$ and $X_{calc}$) and maximum average carrying capacity ($X_{ave}$) for different inlet $H_2O$ concentrations.

CaO over cycling with decreasing temperature. Similar to the conclusions drawn by other authors,[53,54] Criado et al. attributed this effect to a decrease in the product layer thickness at decreasing carbonator temperatures, resulting from the formation of smaller product islands on the CaO surface. The latter observations deviate with the results displayed in Figure 7b, in which $X_{ave}$ showed a constant trend along with increasing carbonator temperature ($T_{carb}$). Although a reduction in $X_{ave}$ with decreasing carbonation temperature might have also been expected in the present study, this effect seemed to be overcome by the aforementioned surplus of the active material being circulated between reactors. Also, the possible effect of continuous make-up addition should not be ignored, as the latter was absent in the previously cited thermogravimetric investigations. Besides, Figure 7b shows the carbonate content of the carbonator ($X_{carb}$) and calciner ($X_{calc}$) solids. $X_{carb}$ decreased with increasing $T_{carb}$ due to the poorer carbonation efficiency achieved as a result. Concurrently, the lower $X_{carb}$ values attained in the carbonator directly influenced $X_{calc}$, as a result of the lower carbonate content of the carbonator solids.

*3.3.3. Influence of Flue Gas $CO_2$ Concentration.* Carbonation performance is favored at higher $CO_2$ partial pressures, as the higher $CO_2$ availability increases the reaction driving force. Nevertheless, as the $CO_2$ capture progresses in time, the outlet $CO_2$ partial pressure reduces toward the equilibrium value, thus limiting the reaction rate. The results presented in Figure 8a reflect well this theory. Throughout the conducted experiments, $CO_2$ inlet volume fractions in the range of 0.06−0.14 m³/m³ were investigated, as these are expected to prevail in flue gases obtained from combustion units employing diverse fuels (e.g., natural gas, heavy fuel oil, or coal). All depicted tests were completed at a carbonator bed temperature of 650 °C in the presence of steam ($y_{H_2O,carb,in}$ = 0.14 m³/m³). From the illustration, it can be seen that higher inlet $CO_2$ partial pressures entailed enhanced equilibrium normalized carbonator $CO_2$ capture efficiencies ($E_{norm}$) as long as a sufficient reactive solid inventory was available. While carbonation performance was particularly enhanced at lower $CO_2$ volume fractions (i.e., 0.06−0.10 m³/m³), the effect diminished at increased $CO_2$ loadings (i.e., 0.12−0.14 m³/m³), as the partial pressure approached its equilibrium value. The latter results are in good agreement with the observations made by Yang et al. in a previous work, in which enhanced

carbonation at increased $CO_2$ partial pressures was reported.[55] Besides, the depicted error bars in Figure 8a represent the standard deviation obtained throughout each experiment. According to the illustration, a higher disparity is achieved at lower $CO_2$ inlet concentrations. The discrepancy here is ascribed to a higher inaccuracy of the utilized mass flow controller, which was operated at the lower end of its range. As the $CO_2$ loading was increased, the standard deviation diminished, averaging at 0.005 at an inlet $CO_2$ concentration of 0.14 m³/m³. Similar to Figure 7, the latter experiments support the assertion that BFB carbonators can enable high $CO_2$ capture efficiencies over a wide range of $CO_2$ concentrations.

Moreover, the improvement in carbonation efficiency entailed an increase in the amount of $CO_2$ being bound as carbonate (see $X_{carb}$ in Figure 8b). Concurrently, as the calcination efficiency was not affected, the increase in $CO_2$ was translated into the calciner solids ($X_{calc}$). The average maximum carrying capacity was found to be negatively influenced by the increased $CO_2$ carbonator loading, despite the continuous flow of limestone being added to the system. As reported by Sun et al., increased $CO_2$ partial pressures tend to accelerate the carbonation reaction, explaining the increase in $CO_2$ uptake.[56] However, as carbonation progresses in time, the partially carbonated solids experience an enhanced carbonation conversion, promoting surface sintering and exacerbating pore blockage. Concurrently, an increase in $CO_2$ concentration might also result in a faster completion of the sequential calcination and carbonation cycles (i.e., lower $X_{ave}$), as more $CO_2$ is captured by the inventory of solids (see eq 2).

*3.3.4. Influence of Flue Gas $H_2O$ Concentration.* The presence of steam in the flue gas has been widely reported to greatly enhance the sorbent carbonation conversion. However, less research has been devoted to systematically investigating the influence of steam partial pressure on carbonation efficiency, particularly at process-relevant temperatures. Even if the partial pressure of steam in the flue gas is intrinsically defined, it is of special relevance to determine which kind of correlation the steam concentration poses on the attained carbonation performance. Figure 9a shows the influence of different inlet steam volume fractions on the equilibrium-normalized carbonator $CO_2$ capture efficiency, at a carbonator temperature of 650 °C and an inlet $CO_2$ concentration of 0.14 m³/m³. The depicted error bars indicate a rather constant

standard deviation throughout the tests, which is basically attributed to the design of the steam generator, particularly conceived for providing low steam flows. The results obtained in this work indicate that $E_{norm}$ is positively influenced by the presence of steam, particularly at low $H_2O$ values (i.e., up to 0.04 $m^3/m^3$). From this point onward, the carbonation efficiency is marginally enhanced with increasing inlet $H_2O$ partial pressure, yielding an improvement of roughly 0.05 mol/mol at $H_2O$ volume fractions between 0.04 $m^3/m^3$ and 0.13 $m^3/m^3$.

The influence of $H_2O$ partial pressure upon carbonation was investigated by Donat et al. in an early work.[43] The authors performed a systematical analysis of steam concentration, both during carbonation and calcination, on the carrying capacity of four distinct limestones through 10 cycles. Donat et al. concluded that at low concentrations, the effect of steam on the carrying capacity was dependent on the amount of steam available. However, above some concentration/saturation point, there was no further improvement. Besides, Manovic and Anthony[42] reported a marginal increase in conversion of one limestone during carbonation at 600 °C with increasing steam concentration from 0.10 to 0.20 $m^3/m^3$, with steam present for carbonation only. The results of this study (see Figure 9b) endorse the latter observation, as $X_{ave}$ was found to increase slightly from 0.34 to 0.38 mol/mol at $H_2O$ values between 0.07 and 0.13 $m^3/m^3$. Assuming a negligible effect of sorbent make-up on $X_{ave}$, the weak influence of steam on sorbent carrying capacity can be presumably attained to the fact that steam does not affect the carbonation rate during the initial, kinetically controlled stage.[57] However, the presence of steam enhances diffusion in the product layer, and that diffusion becomes the controlling step later, when the thicker product layer is formed. In consequence, it can be concluded that steam might be more helpful under conditions where product layer diffusion becomes reaction-rate limiting, that is, lower temperatures and/or more sintered sorbents.

## 4. CONCLUSIONS

Within a preliminary phase of this work, the multicyclic conversion decay of three limestones of distinct origin and morphological structure has been assessed in a TGA apparatus. Sorbent screening experiments have shown that the Saabar metamorphosed limestone is negatively and positively influenced by the presence of steam and $SO_2$, respectively. This unusual behavior can be ascribed to pore blocking during carbonation (Homsy et al., 2020), which results from its high CaO purity, narrow pores, and low porosity. Besides, Rheinkalk and Riyadh have behaved similar, resembling the typical behavior of unmetamorphosed limestones. The activity decay behavior of Rheinkalk at the 20 $kW_{th}$ CaL facility has been subsequently evaluated, adapting the approach proposed by Charitos et al. in a previous publication. The evolution in carrying capacity has been examined using two carbonator gas atmospheres: (i) $CO_2$ and (ii) $CO_2$ with $SO_2$. The resulting deactivation trends in both cases correlate satisfactorily with the behavior observed during the TGA runs, validating the proposed expression for the estimation of the theoretical cycle number. In the following, the influence of temperature, $CO_2$ loading, and steam concentration upon carbonation has been evaluated at the 20 $kW_{th}$ CaL facility. Results have been validated using a general carbon mass balance and a simplified carbonator equation model, respectively. An apparent carbonation rate constant ($k_S\varphi$) of 0.09 $s^{-1}$ is proposed for the

carbonator used in this work, which is consistent with the values reported for BFB reactors in previous publications. The carbonator $CO_2$ capture efficiency has shown to sink with increasing carbonator temperature due to the limitations imposed by the $CaO-CO_2-CaCO_3$ equilibrium. $E_{norm}$ increased with increasing $CO_2$ loading because of the enhanced carbonation driving force. The presence of steam in low concentrations (e.g., $y_{H_2O,carb,in} \approx 0.02$ $m^3/m^3$) has been found to influence $E_{norm}$ significantly due to the improved $CO_2$ diffusivity in the sorbent pore network. Throughout the DFB tests, the BFB carbonator has been operated at a gas superficial velocity of 0.5 m/s, as the latter is expected to prevail in flue gases of coal-fired plants operated at minimum thermal loads (Moreno et al., 2021). Furthermore, the results included in this publication endorse the viability of operating a BFB carbonator over a wide range of process conditions, achieving near-equilibrium capture efficiencies in most investigated cases. Besides, this study contributes to a better understanding of the influence of $SO_2$ and $H_2O$ on scarcely investigated metamorphosed limestones, which may serve to guide future sorbent selection and design efforts.

## ■ AUTHOR INFORMATION

**Corresponding Author**

   **Joseba Moreno** − *University of Stuttgart, Institute of Combustion and Power Plant Technology (IFK), Stuttgart 70569, Germany;* ⊙ orcid.org/0000-0002-6756-4404; Phone: +49 711 685-63562; Email: joseba.moreno@ifk.uni-stuttgart.de

**Authors**

   **Sally L. Homsy** − *Clean Combustion Research Center, King Abdullah University of Science and Technology (KAUST), Thuwal 23955-6900, Saudi Arabia;* ⊙ orcid.org/0000-0003-2767-0031

   **Max Schmid** − *University of Stuttgart, Institute of Combustion and Power Plant Technology (IFK), Stuttgart 70569, Germany*

   **Günter Scheffknecht** − *University of Stuttgart, Institute of Combustion and Power Plant Technology (IFK), Stuttgart 70569, Germany*

Complete contact information is available at:
https://pubs.acs.org/10.1021/acs.energyfuels.1c01734

**Author Contributions**

J.M., S.L.H., M.S., and G.S. were contributed equally. The manuscript was written through contributions of all authors. All authors have given approval to the final version of the manuscript.

## ■ NOMENCLATURE

**Symbols**

   $dX/dt$ = carbonation reaction rate ($s^{-1}$)

$E_{carb}$ = carbonator $CO_2$ capture efficiency (mol/mol)

$E_{norm}$ = equilibrium-normalized carbonator $CO_2$ capture efficiency (mol/mol)

$f_{active}$ = active fraction of particles reacting in the fast reaction regime (-)

$k$ = sorbent deactivation constant

$k_S$ = surface reaction rate constant $(s^{-1})$

$k_S\varphi$ = apparent carbonation rate constant $(s^{-1})$

$N_i$ = molar content of component "i" (kmol)

$\dot{N}_i$ = molar flow of component "i" (kmol/h or kmol/s)

$n_{cycles}$ = number of cycles

$T_{carb}$ = carbonator/carbonation temperature (°C)

$T_{calc}$ = calciner/calcination temperature (°C)

$t$ = time, duration (min, h)

$X$ = sorbent conversion (mol/mol)

$X_{ave}$ = maximum average sorbent (carrying) capacity (mol/mol)

$X_{carb}$ = sorbent carbonate content in/after the carbonator (mol/mol)

$X_{calc}$ = sorbent carbonate content in/after the calciner (mol/mol)

$X_{n_{cycles}}$ = sorbent (carrying) capacity at cycle "$n_{cycles}$" (mol/mol)

$X_r$ = sorbent residual conversion (mol/mol)

$x_i$ = mass fraction of component "i" (kg/kg)

$y_i$ = gas volume fraction of component "i" $(m^3/m^3)$

## Greek letters

$\varphi$ = gas−solid contacting effectivity factor (-)

$\tau$ = space time (s)

$\tau_{active}$ = active space time (s)

## Acronyms

BFB = bubbling fluidized bed

CaL = calcium looping

CFB = circulating fluidized bed

DFB = dual fluidized bed

TGA = thermogravimetric analysis/analyzer

TRL = technology readiness level

## Subscripts

ave = average

carb/calc = carbonator/calciner

eq = equilibrium

in = inlet

wf = water free

## ■ REFERENCES

(1) Baker, E. H. The calcium oxide-carbon dioxide system in the pressure range 1−300 atm. *J. Chem. Soc.* **1962**, 464−470.

(2) Shimizu, T.; Hirama, T.; Hosoda, H.; Kitano, K.; Inagaki, M.; Tejima, K. A Twin Fluid-Bed Reactor for Removal of $CO_2$ from Combustion Processes. *Chem. Eng. Res. Des.* **1999**, 77, 62−68.

(3) Erans, M.; Manovic, V.; Anthony, E. J. Calcium looping sorbents for $CO_2$ capture. *Appl. Energy* **2016**, 180, 722−742.

(4) Lasheras, A.; Ströhle, J.; Galloy, A.; Epple, B. Carbonate looping process simulation using a 1D fluidized bed model for the carbonator. *Int. J. Greenhouse Gas Control* **2011**, 5, 686−693.

(5) Alonso, M.; Rodríguez, N.; Grasa, G.; Abanades, J. C. Modelling of a fluidized bed carbonator reactor to capture $CO_2$ from a combustion flue gas. *Chem. Eng. Sci.* **2009**, 64, 883−891.

(6) Abanades, J. C.; Alvarez, D. Conversion Limits in the Reaction of $CO_2$ with Lime. *Energy Fuels* **2003**, 17, 308−315.

(7) Grasa, G. S.; Abanades, J. C. $CO_2$ Capture Capacity of CaO in Long Series of Carbonation/Calcination Cycles. *Ind. Eng. Chem. Res.* **2006**, 45, 8846−8851.

(8) Curran, G. P.; Fink, C. E.; Gorin, E. $CO_2$ Acceptor Gasification Process. *Fuel Gasification*; American Chemical Society, 1967; Chapter 10, pp 141−165.

(9) Bhatia, S. K.; Perlmutter, D. D. Effect of the product layer on the kinetics of the $CO_2$-lime reaction. *AIChE J.* **1983**, 29, 79−86.

(10) Barker, R. The Reversibility of the Reaction $CaCO_3 \rightleftarrows CaO + CO_2$. *J. Appl. Chem. Biotechnol.* **1973**, 23, 733−742.

(11) Abanades, J. C.; Anthony, E. J.; Lu, D. Y.; Salvador, C.; Alvarez, D. Capture of $CO_2$ from combustion gases in a fluidized bed of CaO. *AIChE J.* **2004**, 50, 1614−1622.

(12) Ryu, H.-J.; Grace, J. R.; Lim, C. J. Simultaneous $CO_2/SO_2$ Capture Characteristics of Three Limestones in a Fluidized-Bed Reactor. *Energy Fuels* **2006**, 20, 1621−1628.

(13) Charitos, A.; Hawthorne, C.; Bidwe, A. R.; Sivalingam, S.; Schuster, A.; Spliethoff, H.; Scheffknecht, G. Parametric investigation of the calcium looping process for $CO_2$ capture in a 10 $kW_{th}$ dual fluidized bed. *Int. J. Greenhouse Gas Control* **2010**, 4, 776−784.

(14) Alonso, M.; Rodríguez, N.; González, B.; Grasa, G.; Murillo, R.; Abanades, J. C. Carbon dioxide capture from combustion flue gases with a calcium oxide chemical loop. Experimental results and process development. *Int. J. Greenhouse Gas Control* **2010**, 4, 167−173.

(15) Arias, B.; Diego, M. E.; Abanades, J. C.; Lorenzo, M.; Diaz, L.; Martínez, D.; Alvarez, J.; Sánchez-Biezma, A. Demonstration of steady state $CO_2$ capture in a 1.7 $MW_{th}$ calcium looping pilot. *Int. J. Greenhouse Gas Control* **2013**, 18, 237−245.

(16) Hilz, J.; Helbig, M.; Haaf, M.; Daikeler, A.; Ströhle, J.; Epple, B. Long-term pilot testing of the carbonate looping process in 1 $MW_{th}$ scale. *Fuel* **2017**, 210, 892−899.

(17) Dieter, H.; Bidwe, A. R.; Varela-Duelli, G.; Charitos, A.; Hawthorne, C.; Scheffknecht, G. Development of the calcium looping $CO_2$ capture technology from lab to pilot scale at IFK, University of Stuttgart. *Fuel* **2014**, 127, 23−37.

(18) Chang, M.-H.; Chen, W.-C.; Huang, C.-M.; Liu, W.-H.; Chou, Y.-C.; Chang, W.-C.; Chen, W.; Cheng, J.-Y.; Huang, K.-E.; Hsu, H.-W. Design and Experimental Testing of a 1.9 $MW_{th}$ Calcium Looping Pilot Plant. *Energy Procedia* **2014**, 63, 2100−2108.

(19) Lysikov, A. I.; Salanov, A. N.; Okunev, A. G. Change of $CO_2$ Carrying Capacity of CaO in Isothermal Recarbonation−Decomposition Cycles. *Ind. Eng. Chem. Res.* **2007**, 46, 4633−4638.

(20) Borgwardt, R. H. Sintering of nascent calcium oxide. *Chem. Eng. Sci.* **1989**, 44, 53−60.

(21) Grasa, G. S.; Alonso, M.; Abanades, J. C. Sulfation of CaO Particles in a Carbonation/Calcination Loop to Capture $CO_2$. *Ind. Eng. Chem. Res.* **2008**, 47, 1630−1635.

(22) Arias, B.; Grasa, G.; Abanades, J. C.; Manovic, V.; Anthony, E. J. The Effect of Steam on the Fast Carbonation Reaction Rates of CaO. *Ind. Eng. Chem. Res.* **2012**, 51, 2478−2482.

(23) Coppola, A.; Gais, E.; Mancino, G.; Montagnaro, F.; Scala, F.; Salatino, P. Effect of steam on the performance of Ca-based sorbents in calcium looping processes. *Powder Technol.* **2017**, 316, 578−584.

(24) Coppola, A.; Montagnaro, F.; Salatino, P.; Scala, F. Fluidized bed calcium looping: The effect of $SO_2$ on sorbent attrition and $CO_2$ capture capacity. *Chem. Eng. J.* **2012**, 207−208, 445−449.

(25) Diego, M. E.; Arias, B.; Abanades, J. C. Evolution of the $CO_2$ carrying capacity of CaO particles in a large calcium looping pilot plant. *Int. J. Greenhouse Gas Control* **2017**, 62, 69−75.

(26) Erans, M.; Jeremias, M.; Zheng, L.; Yao, J. G.; Blamey, J.; Manovic, V.; Fennell, P. S.; Anthony, E. J. Pilot testing of enhanced sorbents for calcium looping with cement production. *Appl. Energy* **2018**, 225, 392−401.

(27) Wang, J.; Anthony, E. J. A Common Decay Behavior in Cyclic Processes. *Chem. Eng. Commun.* **2007**, 194, 1409−1420.

(28) Grasa, G.; Abanades, J. C.; Alonso, M.; González, B. Reactivity of highly cycled particles of CaO in a carbonation/calcination loop. *Chem. Eng. J.* **2008**, 137, 561−567.

(29) He, D.; Gong, H.; Chen, Y.; Jiao, Z.; Liu, Y.; Zhang, X.; Qin, C.; Yin, H. Experimental and density functional theory study of the synergistic effect between steam and $SO_2$ on $CO_2$ capture of calcium-based sorbents. *Fuel* **2021**, 295, 120634.

(30) Homsy, S. L.; Moreno, J.; Dikhtiarenko, A.; Gascon, J.; Dibble, R. W. Calcium Looping: On the Positive Influence of $SO_2$ and the Negative Influence of $H_2O$ on $CO_2$ Capture by Metamorphosed Limestone-Derived Sorbents. *ACS Omega* **2020**, *5*, 32318−32333.

(31) Arias, B.; Cordero, J. M.; Alonso, M.; Diego, M. E.; Abanades, J. C. Investigation of $SO_2$ Capture in a Circulating Fluidized Bed Carbonator of a Ca Looping Cycle. *Ind. Eng. Chem. Res.* **2013**, *52*, 2700−2706.

(32) Coppola, A.; Scala, F. A Preliminary Techno-Economic Analysis on the Calcium Looping Process with Simultaneous Capture of $CO_2$ and $SO_2$ from a Coal-Based Combustion Power Plant. *Energies* **2020**, *13*, 2176.

(33) Diego, M. E.; Arias, B. Impact of load changes on the carbonator reactor of a 1.7 $MW_{th}$ calcium looping pilot plant. *Fuel Process. Technol.* **2020**, *200*, 106307.

(34) FlexiCaL. *Development of Flexible Coal Power Plants with $CO_2$ Capture by Calcium Looping. Research Fund for Coal and Steel (RFCS) Project*, 2016.

(35) Moreno, J.; Hornberger, M.; Schmid, M.; Scheffknecht, G. Part-Load Operation of a Novel Calcium Looping System for Flexible $CO_2$ Capture in Coal-Fired Power Plants. *Ind. Eng. Chem. Res.* **2021**, *60*, 7320−7330.

(36) Moreno, J.; Spörl, R.; Scheffknecht, G. $CO_2$ Capture with a Highly Flexible Calcium Looping System Using a BFB/TFB Carbonator. *SSRN J.* **2019**.

(37) Arias, B.; Alonso, M.; Abanades, C. $CO_2$ Capture by Calcium Looping at Relevant Conditions for Cement Plants: Experimental Testing in a 30 $kW_{th}$ Pilot Plant. *Ind. Eng. Chem. Res.* **2017**, *56*, 2634−2640.

(38) Charitos, A.; Rodríguez, N.; Hawthorne, C.; Alonso, M.; Zieba, M.; Arias, B.; Kopanakis, G.; Scheffknecht, G.; Abanades, J. C. Experimental Validation of the Calcium Looping $CO_2$ Capture Process with Two Circulating Fluidized Bed Carbonator Reactors. *Ind. Eng. Chem. Res.* **2011**, *50*, 9685−9695.

(39) Rodríguez, N.; Alonso, M.; Abanades, J. C. Experimental investigation of a circulating fluidized-bed reactor to capture $CO_2$ with CaO. *AIChE J.* **2011**, *57*, 1356−1366.

(40) Hornberger, M.; Moreno, J.; Schmid, M.; Scheffknecht, G. Experimental investigation of the carbonation reactor in a tail-end Calcium Looping configuration for $CO_2$ capture from cement plants. *Fuel Process. Technol.* **2020**, *210*, 106557.

(41) Lu, D. Y.; Hughes, R. W.; Anthony, E. J. Ca-based sorbent looping combustion for $CO_2$ capture in pilot-scale dual fluidized beds. *Fuel Process. Technol.* **2008**, *89*, 1386−1395.

(42) Manovic, V.; Anthony, E. J. Carbonation of CaO-Based Sorbents Enhanced by Steam Addition. *Ind. Eng. Chem. Res.* **2010**, *49*, 9105−9110.

(43) Donat, F.; Florin, N. H.; Anthony, E. J.; Fennell, P. S. Influence of high-temperature steam on the reactivity of CaO sorbent for $CO_2$ capture. *Environ. Sci. Technol.* **2012**, *46*, 1262−1269.

(44) Coppola, A.; Esposito, A.; Montagnaro, F.; Iuliano, M.; Scala, F.; Salatino, P. The combined effect of $H_2O$ and $SO_2$ on $CO_2$ uptake and sorbent attrition during fluidised bed calcium looping. *Proc. Combust. Inst.* **2019**, *37*, 4379−4387.

(45) Blamey, J.; Paterson, N. P. M.; Dugwell, D. R.; Fennell, P. S. Mechanism of Particle Breakage during Reactivation of CaO-Based Sorbents for $CO_2$ Capture. *Energy Fuels* **2010**, *24*, 4605−4616.

(46) Stanmore, B. R.; Gilot, P. Review—calcination and carbonation of limestone during thermal cycling for $CO_2$ sequestration. *Fuel Process. Technol.* **2005**, *86*, 1707−1743.

(47) Duelli, G.; Charitos, A.; Diego, M. E.; Stavroulakis, E.; Dieter, H.; Scheffknecht, G. Investigations at a 10 $kW_{th}$ calcium looping dual fluidized bed facility: Limestone calcination and $CO_2$ capture under high $CO_2$ and water vapor atmosphere. *Int. J. Greenhouse Gas Control* **2015**, *33*, 103−112.

(48) Charitos, A. Experimental Characterization of the Calcium Looping Process for $CO_2$ Capture. Ph.D. Thesis, University of Stuttgart, 2013.

(49) García-Labiano, F.; Abad, A.; de Diego, L. F.; Gayán, P.; Adánez, J. Calcination of calcium-based sorbents at pressure in a broad range of $CO_2$ concentrations. *Chem. Eng. Sci.* **2002**, *57*, 2381−2393.

(50) Silaban, A.; Harrison, D. P. High temperature capture of carbon dioxide: characteristics of the reversible reaction between CaO (s) and $CO_2$ (g). *Chem. Eng. Commun.* **1995**, *137*, 177−190.

(51) Dobner, S.; Sterns, L.; Graff, R. A.; Squires, A. M. Cyclic Calcination and Recarbonation of Calcined Dolomite. *Ind. Eng. Chem. Process Des. Dev.* **1977**, *16*, 479−486.

(52) Criado, Y. A.; Arias, B.; Abanades, J. C. Effect of the Carbonation Temperature on the $CO_2$ Carrying Capacity of CaO. *Ind. Eng. Chem. Res.* **2018**, *57*, 12595−12599.

(53) Li, Z.-s.; Fang, F.; Tang, X.-y.; Cai, N.-s. Effect of Temperature on the Carbonation Reaction of CaO with $CO_2$. *Energy Fuels* **2012**, *26*, 2473−2482.

(54) Li, Z.; Sun, H.; Cai, N. Rate Equation Theory for the Carbonation Reaction of CaO with $CO_2$. *Energy Fuels* **2012**, *26*, 4607−4616.

(55) Yang, S.; Xiao, Y. Steam Catalysis in CaO Carbonation under Low Steam Partial Pressure. *Ind. Eng. Chem. Res.* **2008**, *47*, 4043−4048.

(56) Sun, P.; Grace, J. R.; Lim, C. J.; Anthony, E. J. Removal of $CO_2$ by Calcium-Based Sorbents in the Presence of $SO_2$. *Energy Fuels* **2007**, *21*, 163−170.

(57) Fennell, P. S.; Pacciani, R.; Dennis, J. S.; Davidson, J. F.; Hayhurst, A. N. The Effects of Repeated Cycles of Calcination and Carbonation on a Variety of Different Limestones, as Measured in a Hot Fluidized Bed of Sand. *Energy Fuels* **2007**, *21*, 2072−2081.

## 4.2 Result discussion and contextualization

Similar to what has been reported in the literature [1, 89, 142], the results displayed in chapter 4.1 indicate that most limestones exhibit a comparable deactivation behavior when cycled in a sulfur-free environment. In the presence of SO$_2$, however, the deactivation rate experienced by the sorbent is strongly dependent on its morphology and microstructure [92, 126, 175, 185].

Aiming at contextualizing the data presented in the last section, figure 4.1 displays the cyclic evolution in sorbent capacity for the three investigated limestones together with the trends obtained for other limestones [19, 51, 175]. An overview of the test conditions selected for each case is given in table 4.1. As already discussed, all limestones introduce a similar loss in sorbent conversion when cycled in the absence of SO$_2$ (see figure 4.1a). The latter behavior can be mostly ascribed to particle sintering, which leads to a rapid decay upon the first sequential calcination and carbonation cycles and tends to stabilize with increasing the cycle number [89]. It must be noted that Rheinkalk, Riyadh, Saabar, and PS were evaluated using a TGA apparatus. On the contrary, Danyang, Strassburg, Luscar, and EnBW were assessed in a fluidized bed reactor. Thus, it can be deduced that the differences introduced by the latter trends can be explained – at least partly – by the distinct contacting degree between gas and solid in each experimental setup. Although with a similar deactivation behavior, the EnBW limestone shows a comparatively lower activity than the rest of the sorbents. A possible explanation for this effect could be the selected calcination conditions (i.e., 940 °C, 20 min), which can negatively affect the sorbent by promoting surface sintering [89]. Moreover, the effect of particle size for Rheinkalk, Riyadh, and Saabar was evaluated (see Appendix A.2). Similar to the conclusions drawn by Grasa and Abanades, the sorbent particle size did not influence the sorption capacity of the sorbent significantly, being the latter determined mainly by the calcination/carbonation cycle number [89]. The addition of steam in the carbonation stage improved X$_{n_{cycles}}$ with respect to the reference case (see figure 4.1b). The positive effect of water vapor upon carbonation can be clearly observed for Rheinkalk, Riyadh, Saabar, and PS. EnBW also experienced an increase in sorbent conversion under steam addition, although to a lesser extent than in the previous limestones. As expected, the presence of SO$_2$ during carbonation produced a more substantial decline in sorbent capacity because of the simultaneous sulfation and carbonation of CaO [51, 52, 175]. Results indicate that the extent of sorbent deactivation by SO$_2$ is strongly dependent on the morphology and microstructure of the material (see figure 4.1c). Opposite to common unmetamorphosed limestones, Saabar benefits from the presence of SO$_2$ at a lower cycle number, as SO$_2$ enhances its resistance against mesopore blockage due to fast surface carbonation [104]. Moreover, Danyang introduces a comparatively lower deactivation than the rest of the limestones. According to

the authors, the latter behavior is attributed to the uniform distribution of sulfur over the particle surface, which facilitates the infiltration of $CO_2$ through the product layer [175]. Altogether, conditions with steam and $SO_2$ improved sorbent performance with respect to the previous case (see figure 4.1d). The latter finding corroborates the positive effect of steam in samples carbonated with and without $SO_2$ addition.

Table 4.1: Cycling conditions for the experiments depicted in figure 4.1

| Symbol | Unit | Ryu et al. | Coppola et al. | Arias et al. | Moreno et al. |
|---|---|---|---|---|---|
| $T_{carb}$ | °C | 700 | 650 | 650 | 650 |
| $t_{carb}$ | min | | 15 | 20 | 10 |
| Carbonation routine (a) | | | | | |
| $y_{CO_2,carb,in}$ | $m^3/m^3$ | 0.1600 | 0.1500 | 0.1000 | 0.1500 |
| $y_{H_2O,carb,in}$ | $m^3/m^3$ | 0 | 0 | 0 | 0 |
| $y_{SO_2,carb,in}$ | $m^3/m^3$ | 0 | 0 | 0 | 0 |
| $y_{N_2,carb,in}$ | $m^3/m^3$ | 0.7900 | 0.6700 | 0.7110 | 0.8500 |
| $y_{O_2,carb,in}$ | $m^3/m^3$ | 0.0500 | 0.1800 | 0.1890 | 0 |
| Carbonation routine (b) | | | | | |
| $y_{CO_2,carb,in}$ | $m^3/m^3$ | - | 0.1500 | 0.1000 | 0.1500 |
| $y_{H_2O,carb,in}$ | $m^3/m^3$ | - | 0.1000 | 0.2000 | 0.1500 |
| $y_{SO_2,carb,in}$ | $m^3/m^3$ | - | 0 | 0 | 0 |
| $y_{N_2,carb,in}$ | $m^3/m^3$ | - | 0.5925 | 0.5530 | 0.7000 |
| $y_{O_2,carb,in}$ | $m^3/m^3$ | - | 0.1575 | 0.1470 | 0 |
| Carbonation routine (c) | | | | | |
| $y_{CO_2,carb,in}$ | $m^3/m^3$ | 0.1600 | 0.1500 | - | 0.1500 |
| $y_{H_2O,carb,in}$ | $m^3/m^3$ | 0 | 0 | - | 0 |
| $y_{SO_2,carb,in}$ | $m^3/m^3$ | 0.0020 | 0.0015 | - | 0.0020 |
| $y_{N_2,carb,in}$ | $m^3/m^3$ | 0.7880 | 0.6703 | - | 0.8480 |
| $y_{O_2,carb,in}$ | $m^3/m^3$ | 0.0500 | 0.1782 | - | 0 |
| Carbonation routine (d) | | | | | |
| $y_{CO_2,carb,in}$ | $m^3/m^3$ | - | 0.1500 | - | 0.1500 |
| $y_{H_2O,carb,in}$ | $m^3/m^3$ | - | 0.1000 | - | 0.1500 |
| $y_{SO_2,carb,in}$ | $m^3/m^3$ | - | 0.0015 | - | 0.0020 |
| $y_{N_2,carb,in}$ | $m^3/m^3$ | - | 0.5913 | - | 0.6980 |
| $y_{O_2,carb,in}$ | $m^3/m^3$ | - | 0.1572 | - | 0 |
| $T_{calc}$ | °C | 850 | 940 | 900 | 850 |
| $t_{calc}$ | min | | 20 | 5 | 10 |
| $y_{CO_2,calc,in}$ | $m^3/m^3$ | 0 | 0.7000 | 0 | 0 |
| $y_{N_2,calc,in}$ | $m^3/m^3$ | 0.7900 | 0.2370 | 0.7900 | 1 |
| $y_{O_2,calc,in}$ | $m^3/m^3$ | 0.2100 | 0.0630 | 0.2100 | 0 |
| Limestone type | | Strassburg Luscar Danyang | EnBW | PS | Rheinkalk Riyadh Saabar |
| Reference | | [175] | [51] | [19] | [154] |

Within the next phase of the experiments, the decay in Rheinkalk conversion was evaluated

in a continuous DFB environment. To this end, two different carbonation routines were employed, namely with and without $SO_2$.
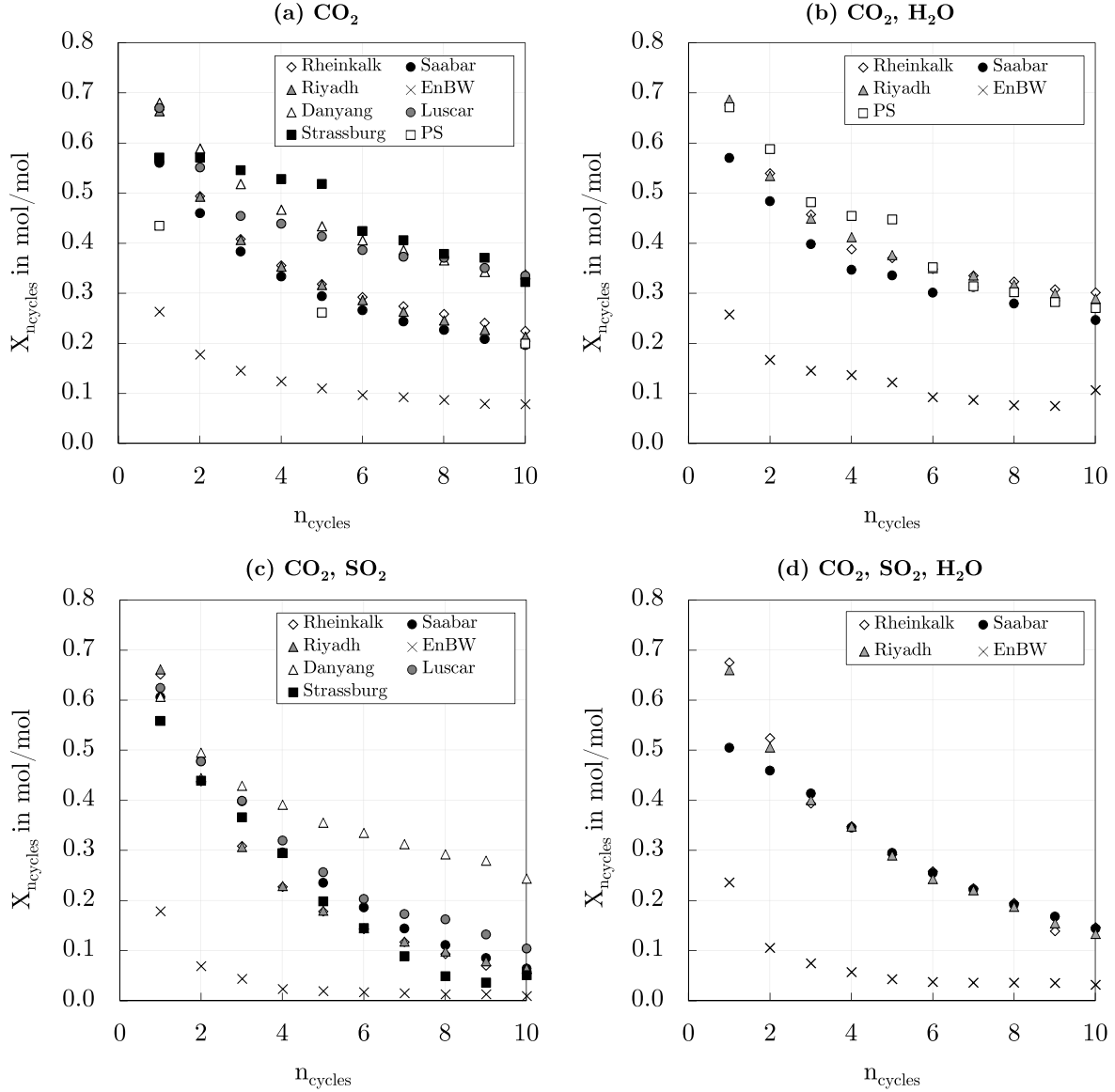


Figure 4.1: Sorbent capacity ($X_{n_{cycles}}$) against number of cycles ($n_{cycles}$) for a wide variety of limestones investigated under different carbonation routines: Danyang [175], Strassburg [175], Luscar [175], EnBW [51], and PS [19]

In a previous work, Charitos et al. proposed an equation to describe the evolution in sorbent conversion with the cycle number in the absence of make-up [45]. In this work, a new expression has been suggested, which introduces an amendment to the equation of Charitos et al. accounting for the cycling history of the particles prior to the calcium looping experiments (see chapter 4.1). The following illustration shows the sorbent capacity evolution

experienced by different limestones when cycled in a continuous DFB environment. The Swabian Alb and Northwest Spain limestone deactivation curves were determined according to the expression developed by Charitos et al. [45]. On the contrary, the data points obtained in this work and the proposed model line refer to the Rheinkalk limestone and were calculated using the methodology presented in chapter 4.1. Observing figure 4.2a, different conclusions can be drawn. Firstly, it can be noted that the methodology proposed in this work to calculate the cycle number can make a difference of up to four additional Calcium Looping cycles with respect to the original expression proposed by Charitos et al. [45]. Thus, results suggest that continuous material cycling at elevated temperatures for long periods can negatively affect the sorbent's carrying capacity. In addition, the data obtained with the latter expression seems to fit the model equation obtained in the TGA adequately. Also, the trend introduced by the Northwest Spain limestone at a higher cycle number seems to correlate well with the proposed model, despite the differences arising from the sorbent composition and the make-up addition during the tests [45]. For a given theoretical cycle number, Rheinkalk exhibits a better average $CO_2$ capacity than that of the Northwest Spain and Swabian Alb limestones, which can be attributed again to differences in solid composition and morphological properties.
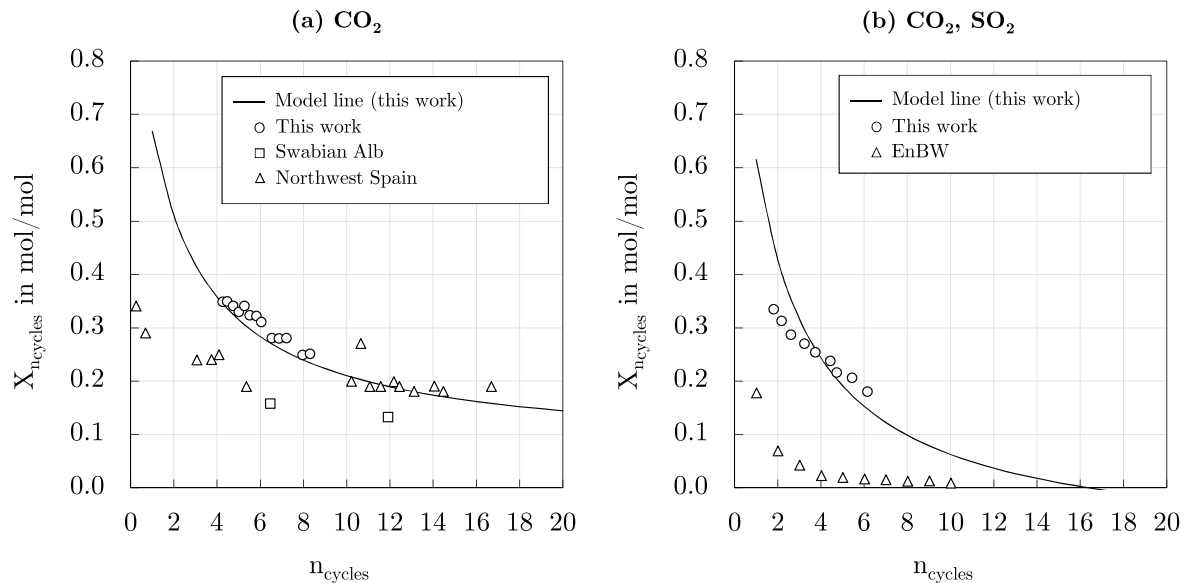


Figure 4.2: Sorbent capacity ($X_{n_{cycles}}$) against number of cycles ($n_{cycles}$) for several limestones without (a) and with (b) the presence of $SO_2$ during carbonation in a DFB system: Rheinkalk (this work), Swabian Alb [45], Northwest Spain [45], and EnBW [51]

The addition of $SO_2$ to the carbonation step entailed an exacerbated deactivation of Rheinkalk compared to the reference case (see figure 4.2b), characterized by a more pro-

nounced decay in the subsequent CaL cycles. While a good correlation between DFB and TGA results was obtained in this work, a poorer agreement was found for EnBW. As anticipated previously, this can be presumably attributed to the different experimental conditions set by the authors [51], particularly during the calcination step (i.e., 940 °C, 20 min), which could ultimately promote a faster degradation of the sorbent. Nevertheless, it can be concluded that the suggested expression seems to estimate the theoretical number of Calcium Looping cycles ($n_{cycles}$) with adequate accuracy, considering the inherent uncertainties of some parameters involved in the process (i.e., $X_{ave}$ and $\dot{N}_{Ca,loop}$).
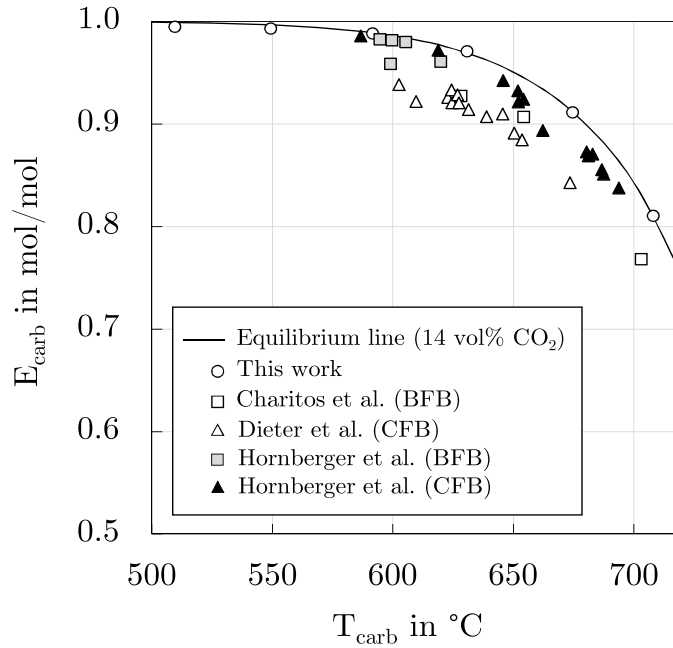


Figure 4.3: Carbonator $CO_2$ capture efficiency ($E_{carb}$) vs temperature ($T_{carb}$) at characteristic power plant flue gas conditions: BFB [43, 106] and CFB [73, 106]

Within the next phase of the experiments included in this chapter, a parametric assessment of the 20 kW$_{th}$ BFB carbonator was conducted. As already anticipated in chapter 4.1, three variables were subjected to analysis, namely: (i) the carbonation temperature, (ii) the $CO_2$ concentration, and (iii) the steam loading. Figure 4.3 displays the carbonator $CO_2$ capture efficiency ($E_{carb}$) against the carbonation temperature ($T_{carb}$), both for the results given in this work and those reported by different authors [43, 73, 106]. In the illustration, the solid line represents the maximum attainable $CO_2$ capture efficiency defined by the chemical equilibrium of the $CaO$-$CO_2$-$CaCO_3$ reaction system [84]. Generally, a satisfactory agreement between the different studies can be found. The results suggest that both BFB and CFB carbonators can enable $CO_2$ capture efficiencies close to equilibrium over a

wide range of temperatures. Of course, it should be noted that the key process variables (e.g., $\xi_{LR}$, $\xi_{MR}$, or $N_{Ca,carb}$) were tailored in each case to attain the proposed $CO_2$ capture targets. For instance, Hornberger et al. reported capture efficiencies between 0.96 and 0.98 mol/mol when operating at a make-up ratio of 0.9 mol/mol [106]. Concurrently, the authors determined $E_{carb}$ values between 0.84 and 0.99 mol/mol when operating the CFB carbonator over a much wider temperature window. Charitos et al. achieved a maximum capture capacity of 0.93 mol/mol when operating at 630 °C [45], while Dieter et al. yielded $E_{carb}$ values of 0.94 mol/mol at a carbonation temperature of 603 °C [73]. Last but not least, the exceptionally high capture values reported in this work are mainly attributed to the relatively low history of the sorbent particles, as this experimental phase was investigated at the very beginning of the test campaign.

Similar to the conclusions drawn by other authors, the results included in this work have shown the positive effect of increased $CO_2$ concentrations on the carbonation process [30, 158, 205]. Operation with an inlet $CO_2$ concentration of 0.06 $m^3/m^3$ led to capture efficiencies of 0.96 mol/mol. On the contrary, $E_{carb}$ values as high as 0.98 mol/mol were yielded at an inlet $CO_2$ concentration of 0.14 $m^3/m^3$. Furthermore, it can be noted that $E_{carb}$ was particularly improved at low $CO_2$ loadings. The latter effect is attributed to the reaction rate being directly proportional to the difference between local and equilibrium $CO_2$ concentrations [30]. Besides, the average maximum carrying capacity was negatively influenced by the increased $CO_2$ loading. As postulated by Sivalingam, the latter effect can be mainly ascribed to an enhanced number of sequential CaL cycles [191]. Higher $CO_2$ concentrations shorten the fast reaction rate phase and thus the carbonator active space time.

The positive effect of steam on the carbonation reaction has been widely reported in the literature [15, 19, 73, 77, 143]. Dieter et al. conducted investigations at different carbonation temperatures with and without steam addition [73]. The authors indicated that steam could comprehensively enhance the carbonation reaction at temperatures close to 600 °C, increasing $E_{carb}$ by about 16 percentage points with respect to the reference case. The latter finding is in line with the conclusions drawn by Dobner et al., who noted that steam could catalyze the reaction between $CO_2$ and CaO, especially at low temperatures (i.e., 550 °C) [75]. Besides, Lindén et al. explored the influence of water vapor on carbonation of CaO in the temperature range 400-550 °C, reporting a weak influence of steam partial pressure with increasing temperature [129]. In contrast, Yang and Xiao showed that steam greatly increases sorbent carbonation conversion up to pressures of 5 MPa between 550-650 °C [205]. A later work by Manovic and Anthony supports the latter assertion, where enhanced sorbent carbonation at 600 °C in a steam concentration range of 0.10-0.20 $m^3/m^3$ is reported. In this chapter, $X_{ave}$ increased slightly from 0.34 to 0.38 mol/mol at $H_2O$ values between 0.07 and 0.13 $m^3/m^3$. Assuming a negligible effect of limestone make-up on

$X_{ave}$, the latter behavior can be associated with the fact that steam does not affect the carbonation rate during the kinetically controlled stage. In contrast, steam addition might enhance diffusion in the product layer, becoming the controlling step when the thicker product layer is formed [83].

# 5 Part-load operation of a novel Calcium Looping system for flexible CO$_2$ capture in coal-fired power plants

## 5.1 Original publication

Article

# Part-Load Operation of a Novel Calcium Looping System for Flexible CO₂ Capture in Coal-Fired Power Plants

Joseba Moreno,* Matthias Hornberger, Max Schmid, and Günter Scheffknecht

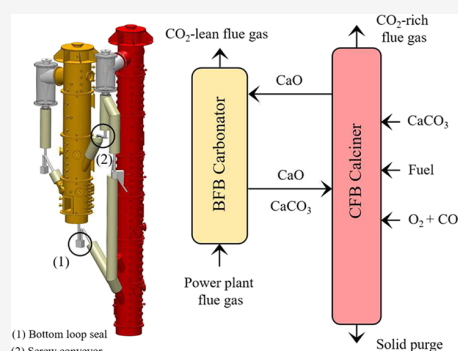Cite This: *Ind. Eng. Chem. Res.* 2021, 60, 7320−7330

Read Online

ACCESS | Metrics & More | Article Recommendations

**ABSTRACT:** The increasing share of renewable energy supply is forcing fossil-fueled power plants to undergo flexible operation, with large load changes during the day and even periods of complete shutdown. Dual circulating fluidized bed (DCFB) calcium looping (CaL) has rapidly emerged as a viable option for efficient post-combustion $CO_2$ capture in baseload coal-fired power stations. However, DCFBs might be unsuitable for flexible carbon capture at very low power plant capacity factors, beyond which the solid entrainment rate becomes insufficient. This work introduces a CaL system featuring the unique option of decoupling the solid circulation from the carbonator flue gas load with a carbonator bottom interlink. The concept has been successfully demonstrated with high $CO_2$ capture efficiency (Hornberger et al. *Fuel Process. Technol.*, **2020**, 106557), but not yet regarding its load flexibility behavior. The carbonator performance has been assessed at partial loads as low as 40%, identifying a minimum active space time of 41 s as a basis to achieve an equilibrium normalized capture efficiency of 90%. In addition, the calciner performance has been evaluated for a variety of oxy-fuel cases (31−55 vol %$_{db}$) and calcination temperatures (850−940 °C). The obtained results endorse the suggested novel CaL system's suitability for the flexible decarbonization of load-following power plants.

(1) Bottom loop seal
(2) Screw conveyor

CO₂-lean flue gas · CaO · CO₂-rich flue gas · BFB Carbonator · CFB Calciner · CaO · CaCO₃ · CaCO₃ · Fuel · O₂ + CO₂ · Power plant flue gas · Solid purge

## 1. INTRODUCTION

Decarbonization of current power and industrial systems is globally regarded as a mandatory step to meet the net-zero emissions goals set by the Paris Climate Agreement.[1,2] Renewable technologies are being rapidly deployed to achieve this goal, although their behavior is still variable, and thus they require the implementation of mid-merit power systems to balance energy supply and demand.[3] Besides the technical challenges associated with high operation flexibility, fossil-fueled power plants still require a methodology to cut energy-related $CO_2$ emissions. Carbon capture and storage (CCS) technologies are increasingly recognized as a viable method as they can be retrofitted to amortized coal-fired power plants with high $CO_2$ capture levels and moderate energy penalties and costs.[4,5] However, the technical requirements for a flexible operation of thermal power plants with CCS are still high and constitute a significant challenge for their development and deployment.[6]

The calcium looping (CaL) technology has gained considerable attention in the last years as a solution for improving the flexibility of $CO_2$ capture units retrofitted to load-following power stations.[7−12] The process uses natural limestone as a calcium oxide (CaO) precursor for $CO_2$ capture.[13−16] The $CO_2$ contained in the power plant flue gas is exothermically absorbed by CaO in a carbonator at around 650 °C (see Figure 1). The $CO_2$-depleted exhaust gas is vented

CO₂-rich flue gas

O₂ → · Make-up → · Fuel → Calciner ≈ 900 °C $CaCO_3 + heat \rightarrow CaO + CO_2$ → Solid purge

CaO, CaCO₃ · CaO

Carbonator ≈ 650 °C $CaO + CO_2 \rightarrow CaCO_3 + heat$ → CO₂-lean flue gas

Power plant flue gas
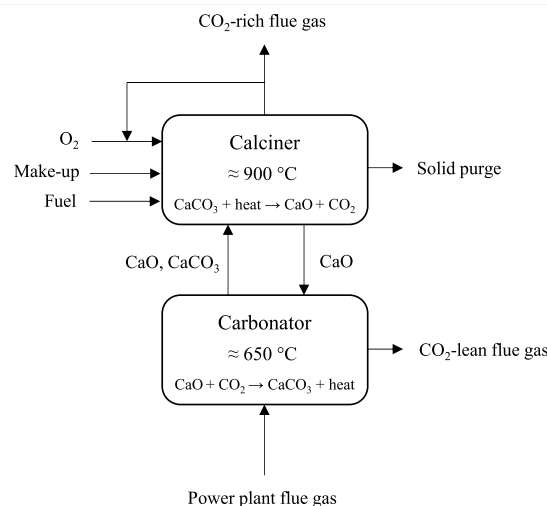
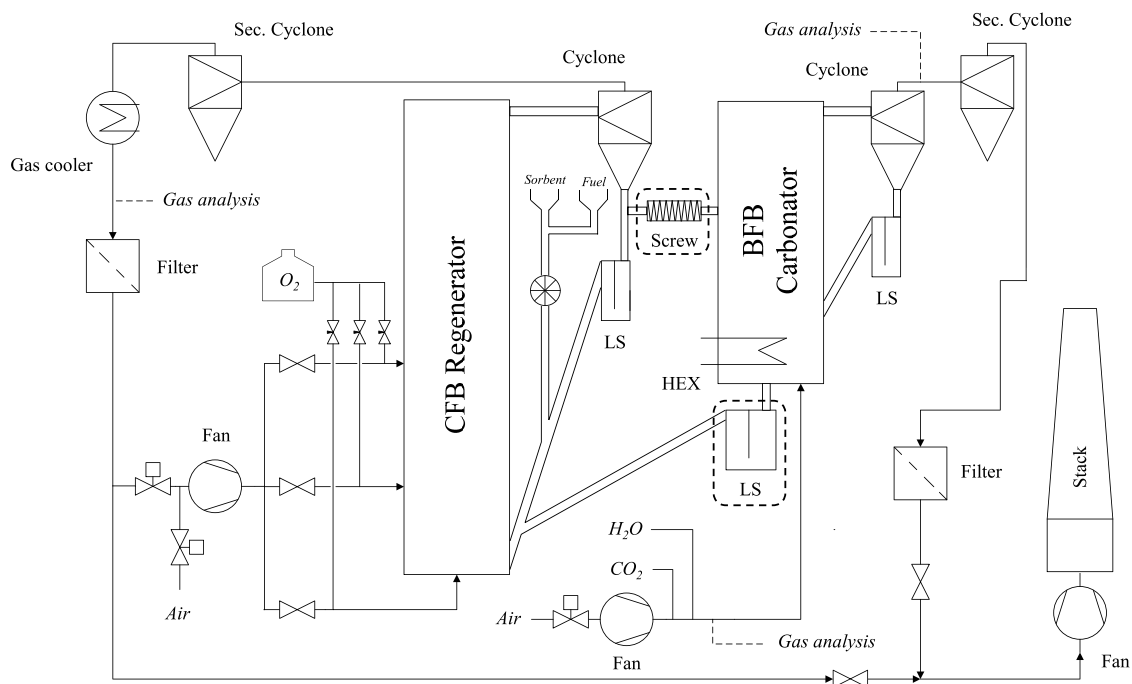**Figure 1.** Simplified scheme of the CaL process.

**Figure 2.** Schematic of the University of Stuttgart's 200 kW$_{th}$ CaL facility (BFB-CFB configuration) with key flexibility components enveloped in dashed squares.

to the environment, whereas the partly carbonated solids are transferred to a calcination reactor (i.e., calciner or regenerator). In the calciner, the $CO_2$ bound in the solid phase is released at around 900 °C. A gas stream highly concentrated in $CO_2$ leaves the reactor, while the regenerated CaO is returned to the carbonator to close the solid loop. The heat for the endothermic calcination reaction is provided by burning supplementary fuel with oxygen from an air separation unit (i.e., oxy-fuel combustion). The $CO_2$-rich regenerator flue gas can be partly recirculated into the system to maintain an appropriate combustion temperature. Due to sorbent deactivation upon cycling, a continuous flow of fresh make-up (i.e., $CaCO_3$) is fed to the process. This is compensated by an equivalent sorbent purge to avoid the accumulation of inerts in the system (e.g., fuel ash and $CaSO_4$).

Since the technology was conceptualized in 1999 by Shimizu et al.,[17] the process has progressed steadily, being its feasibility demonstrated up to the MW$_{th}$ scale with several pilot plants worldwide.[18−25] Despite this significant development, most research has focused on investigating the process performance at baseload operating conditions, overlooking the flexibility potential of CaL systems coupled to mid-merit fossil-fueled power units. CaL plants retrofitted to existing power stations are expected to exhibit a high degree of versatility in terms of load variations. The frequent changes resulting from the load-following operation of coal-fired power blocks are translated into changes in the flue gas flow rate and, hence, in the superficial flue gas velocity entering the carbonator unit. This directly impacts on the contact time between the sorbent and the $CO_2$ and, thereby, on the $CO_2$ capture performance. Hence, modifications in relevant process parameters (e.g., solid circulation rate, and make-up flow) are required to adjust the bed inventory and ensure sufficient reaction times between CaO and $CO_2$ in the carbonator. Few studies to date have focused on evaluating different integration possibilities for

facilitating the development of highly flexible CaL plants retrofitted to coal-fired power stations.[10−12,26] However, to our best knowledge, only one article has been published on the experimental investigation of a dual CFB CaL system's flexible performance at different carbonator load levels.[27] In the study, the authors indicated that a conventional CFB carbonator design might be unsuitable to effectively accommodate very low flue gas superficial velocities (i.e., thermal loads). This was attributed to the resulting low solid entrainment rates that ultimately affect the hydrodynamic stability of the CaL system and, hence, the carbonator $CO_2$ capture efficiency.

The present work introduces a CaL reactor concept based on a BFB carbonator and a CFB calciner that can respond to a wide range of flue gas load changes. This reactor arrangement has been investigated in the context of a recent European project (FlexiCaL), which aimed at developing novel calcium looping systems with improved process flexibility. The proposed CaL configuration performance has been assessed during steady-state operation at full- and part-load conditions, where the main process variables have been tailored to achieve sufficiently high carbonator $CO_2$ capture efficiencies. A simple carbon mass balance is applied for a preliminary validation of the carbonator performance, whereas a basic reactor model approach, successfully implemented in experimental facilities of different sizes,[18,21,24,28,29] is proposed to interpret the results with more detail.

## 2. EXPERIMENTAL SETUP

The 200 kW$_{th}$ pilot facility is located at the Institute of Combustion and Power Plant Technology (IFK) of the University of Stuttgart. It consists of three refractory-lined reactors that can be interconnected into two different reactor arrangements, namely, CFB-CFB and BFB-CFB. While the regenerator is always operated in CFB mode, the carbonator can be operated either in CFB mode or in BFB mode. For a

**Table 1. Chemical Composition of the Utilized Fuel**

| | kg/kg, waf | | | | | kg/kg, wf | kg/kg, ad |
|---|---|---|---|---|---|---|---|
| | $\gamma_C$ | $\gamma_H$ | $\gamma_O$ | $\gamma_N$ | $\gamma_S$ | $\gamma_{ash}$ | $\gamma_{H_2O}$ |
| Colombian hard coal | 0.776 | 0.052 | 0.145 | 0.016 | 0.011 | 0.091 | 0.019 |

detailed description of the CFB-CFB configuration, please refer elsewhere.[30,31]

The schematic representation of the 200 kW$_{th}$ BFB-CFB reactor concept is shown in Figure 2. The CFB calciner is 10 m high and has an average internal diameter of 200 mm, whereas the BFB carbonator consists of a 6 m reactor with an internal diameter of 330 mm. The pilot plant is equipped with typical industrial fluidized bed system components, i.e., a start-up natural gas burner, air-quenching devices to cool down the off-gases, and induced draft fans. The key feature of this CaL arrangement for improved load flexibility lies in the solid interconnection between both reactors. This is achieved by the combination of a screw feeder and a carbonator bottom loop seal. The screw conveyor's rotational speed controls the looping rate from the regenerator to the carbonator. The bottom loop seal in the carbonator, on the other hand, ensures the flexible operation of the pilot plant as it allows the decoupling of the solid circulation from the carbonator to the regenerator from the carbonator fluidization velocity. The proposed reactor system (i.e., BFB-CFB) offers the unique possibility to test an alternative configuration in which the carbonator operates in a broad range of fluidization regimes ranging from bubbling, over turbulent, to circulating conditions. Hence, compared with a conventional CFB-CFB arrangement, the concept is highly flexible with respect to flue gas load changes. Both reactors are connected to high-efficiency primary cyclones, in which the exhaust gas is separated from the entrained solids in a preliminary step. A part of the solids separated from the regenerator's primary cyclone supplies the screw feeder. The remaining particles overflow the screw and are recirculated into the calciner. Any sorbent entrained in the carbonator will be separated by the primary cyclone and internally recirculated via the upper loop seal. The flue gas is then passed through protective cyclones and bag filters, mainly for fly ash and dust removal. The purified regenerator flue gas can be partly recirculated using a blower at this stage, whereas the carbonator exhaust gas is vented to the outside air using an induced draft (ID) fan. The carbonator is fluidized with a synthetic mixture of air, steam, and $CO_2$ from a storage tank, which allows investigating different types of flue gas compositions. The calciner is capable of operating in either air-blown or oxy-combustion mode. During oxy-fuel combustion, the oxygen delivered from a storage tank is diluted with the regenerator flue gas and is partly recirculated into the system at different stages. Dry gas compositions are measured by non-dispersive infrared spectroscopy ($CO_2$, CO, and $SO_2$) and paramagnetism ($O_2$) in the off-gas lines after both reactors, as well as at the carbonator inlet. The volume fractions of $NO_x$ and water vapor in the regenerator exhaust gas are measured by non-dispersive infrared spectroscopy and impact jet psychrometry, respectively.

Fuel (see Table 1) and sorbent (see Table 2) dosing is achieved by gravimetric screw feeders. The dosing system is connected to the regenerator by a rotary valve, which decouples the reactor pressure from the atmospheric metering system and feeds the solids at the regenerator bottom.

**Table 2. Chemical Composition of the Utilized Sorbent**

| | kg/kg, wf | | | | | |
|---|---|---|---|---|---|---|
| | $x_{CaO}$ | $x_{MgO}$ | $x_{SiO_2}$ | $x_{Al_2O_3}$ | $x_{CO_2}$ | $x_{others}$ |
| German limestone | 0.551 | 0.007 | 0.004 | 0.001 | 0.435 | 0.002 |

Additionally, the calciner counts with a purge removal system made up of a bottom drain valve. The solid circulation between reactors is continuously measured by a high-temperature microwave sensor and is verified by manual solid flow measurements. This consists of measuring the time required for solids of known bulk density to fill a circulation pipe's known volume. The solids sampled from the loop seals, secondary cyclones, and bag filters of each reactor are subsequently analyzed in terms of chemical composition, $CO_2$ carrying capacity, and particle size distribution.

## 3. EVALUATION METHODOLOGY

**3.1. Carbonator Carbon Mass Balance.** An essential tool for the validation of the carbonation process is the closure of the carbon mass balance. During steady-state operation, where there is no accumulation of $CaCO_3$ in the reactor bed, the mass of $CO_2$ disappearing from the gas phase has to equal the mass of $CO_2$ being bound as carbonate in the CaO stream circulating between the two reactors:

$$\dot{N}_{CO_2,carb,in}E_{carb} = \dot{N}_{Ca}(X_{carb} - X_{calc}) \tag{1}$$

The amount of $CO_2$ captured from the gas phase ($\dot{N}_{CO_2,carb,in}E_{carb}$) can be calculated by the continuous online measurement of volume flow and gas composition at carbonator inlet and outlet. This left term is thus the most reliable. For calculating the amount of $CO_2$ appearing in the solid phase, the looping rate ($\dot{N}_{Ca}$) is estimated according to the measured solid circulation rate and the circulating solids' calcium content. Once $\dot{N}_{Ca}$ is known, it is possible to calculate the amount of solids entering the carbonator with a molar carbonate content $X_{calc}$ after regeneration (i.e., $\dot{N}_{Ca}X_{calc}$) and those leaving the carbonator after $CO_2$ absorption with a molar carbonate content $X_{carb}$ (i.e., $\dot{N}_{Ca}X_{carb}$), assuming that both reactors are perfectly mixed. The comparison between both equation terms is a useful indicator of the experimental information's consistency, which is the basis for analyzing the carbonator performance.

**3.2. Active Space Time and Basic Carbonator Model Validation.** Another relevant methodology for assessing the carbonation process is based on a basic reactor model and simplified particle reaction rate model:[21,32]

$$\left(\frac{dX_{carb}}{dt}\right)_{reactor} = k_s \varphi X_{ave}(\overline{y_{CO_2,carb} - y_{CO_2,carb,eq}}) \tag{2}$$

In eq 2, $k_s$ is the surface reaction rate constant for the utilized limestone, ($\overline{y_{CO_2,carb} - y_{CO_2,carb,eq}}$) refers to the difference between the logarithmic average and the equilibrium $CO_2$ volume fraction in the carbonator, $\varphi$ indicates the gas–solid

contacting factor, and $X_{ave}$ states the sorbent's average maximum $CO_2$ carrying capacity. This simplified approach allows to solve the following mass balance for the amount of $CO_2$ removed in the gas phase and the $CO_2$ captured by the CaO particles in the carbonator bed (see ref 21 for more details):

$$E_{carb} = N_{Ca,carb} f_{active} k_s \varphi X_{ave} (\overline{y_{CO_2,carb} - y_{CO_2,carb,eq}}) / \dot{N}_{CO_2,carb,in} \quad (3)$$

The apparent carbonation rate constant ($k_s\varphi$) can be calculated as a fitting parameter from eq 3, whereas the surface carbonation rate constant ($k_s$) can be determined by thermogravimetric analysis. $N_{Ca,carb}$ refers to the carbonator total calcium inventory, $f_{active}$ corresponds to the fraction of active particles reacting in the fast reaction rate (where $X_{carb} < X_{ave}$), and $\dot{N}_{CO_2,carb,in}$ is the molar flow of $CO_2$ entering the carbonator. Equation 3 constitutes a reactor design equation model and links all calcium looping parameters directly or indirectly with the carbonator $CO_2$ capture efficiency ($E_{carb}$) for the given set of operating conditions. The key parameter of this model is the active space time ($\tau_{active} = N_{Ca,carb} f_{active} X_{ave} / \dot{N}_{CO_2,carb,in}$), which is indicative of both the sorbent inventory and the reaction rate of such inventory.

## 4. RESULTS

The results presented in this paper involved experimental work conducted with the BFB-CFB CaL reactor configuration in various pilot campaigns. These added up to 225 h of operation with interconnected reactors, from which 155 h were achieved in $CO_2$ capture mode with stable oxy-fuel combustion of coal in the regenerator. Each experiment was operated for at least 1 h (although in general 2 h) after steady-state conditions were reached. The robustness of the proposed reactor design was also demonstrated for about 17 h during full-load conditions and 10 h during partial load conditions, respectively.

Throughout the presented experiments, the pilot facility was operated over a wide range of experimental conditions (see Table 3). While the regenerator was always operated with a

**Table 3. Experimental Range of Operating Conditions**

| parameter | symbol | value/range | unit |
|---|---|---|---|
| carbonator temperature | $T_{carb}$ | 591−704 | °C |
| carbonator solid inventory | $W_{s,carb}$ | 422−1063 | kg/m² |
| carbonator inlet $CO_2$ concentration | $y_{CO_2,carb,in}$ | 14 | vol % |
| carbonator superficial gas velocity | $u_{carb}$ | 0.8−2.0 | m/s |
| carbonator $CO_2$ capture efficiency | $E_{carb}$ | 38−97 | % |
| calciner temperature | $T_{calc}$ | 851−940 | °C |
| calciner solid inventory | $W_{s,calc}$ | 881−1414 | kg/m² |
| calciner inlet $O_2$ concentration | $y_{O_2,calc,in}$ | 31−55 | vol %$_{db}$ |
| make-up ratio | $\xi_{MR}$ | 0.09−0.11 | mol/mol |
| looping ratio | $\xi_{LR}$ | 10.2−12.2 | mol/mol |

similar bed inventory (i.e., 28−40 kg or 881−1414 kg/m²), the carbonator solid inventory was varied to evaluate its impact on the $CO_2$ capture efficiency (i.e., 36−91 kg or 422−1063 kg/ m²). Similarly, dedicated experiments were conducted in the carbonator to assess the influence of the reactor bed temperature on the capture of $CO_2$. The flexibility potential of the BFB carbonator was evaluated at gas superficial velocities as low as 0.8 m/s, which corresponded to thermal loads of about 40% from the established baseload case. For

comparison purposes, an intermediate load case (i.e., 60%) was also investigated. The calciner was operated at realistic oxy-fuel conditions, using recirculated calciner flue gas with an inlet oxygen concentration between 31 and 55 vol %$_{db}$. The calciner temperature was also varied to evaluate the impact on sorbent calcination and off-gas composition. The make-up ratio and looping ratio were kept constant between the tests (i.e., 0.09 mol/mol and 10.2 mol/mol, respectively), although two complementary experiments with slightly higher values (by about 20%) were investigated for comparative purposes.

Figure 3 introduces the carbonator and calciner temperatures against the respective $CO_2$ outlet concentrations. The
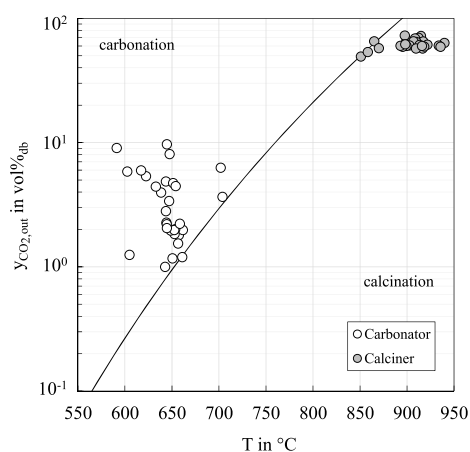
**Figure 3.** Dry outlet $CO_2$ reactor concentration ($y_{CO_2,out}$) vs average reactor temperature ($T$).

depicted solid line corresponds to the chemical $CO_2$ equilibrium concentration at the given temperature.[33] According to the illustration, successful carbonation conditions were achieved for all investigated experiments, with $y_{CO_2,out}$ yielding between 1.0 and 9.7 vol %$_{db}$. Within the investigated temperature window, the outlet $CO_2$ calciner concentration ranged from 49 up to 73 vol %$_{db}$. As this concentration is given on a dry basis, the remaining gas species in the calciner exhaust gas refer mainly to nitrogen and oxygen. The nitrogen dilution is mostly related to inert gas flushing of the coal feeding system and loop seal fluidization (here by 20 vol %$_{db}$). The amount of oxygen corresponds to the required oxygen excess to ensure complete oxidation of the fuel.

**4.1. Carbonator Operation.** *4.1.1. Influence of Temperature and Solid Bed Inventory.* The performance achieved in a calcium looping carbonator depends mostly on the reactor design, sorbent activity, solid inventory, and defined operating conditions (e.g., operation temperature and $CO_2$ concentration). In practice, as the $CO_2$ loading is mainly imposed by the nature of the combustion flue gas, the carbonator $CO_2$ capture efficiency can only be adjusted by altering the carbonation conditions (e.g., temperature), the sorbent loading, and the sorbent activity. The $CO_2$ capture efficiencies achieved for all experiments investigated in this study are presented in Figure 4a. It can be seen for most tests that the carbonator $CO_2$ capture performance is very close to the theoretical maximum achievable $CO_2$ capture (i.e., black solid line). For such operation conditions, capture efficiencies over 85% were achieved in the carbonator at temperatures close to 650 °C. The satisfactory carbonation performance here can be
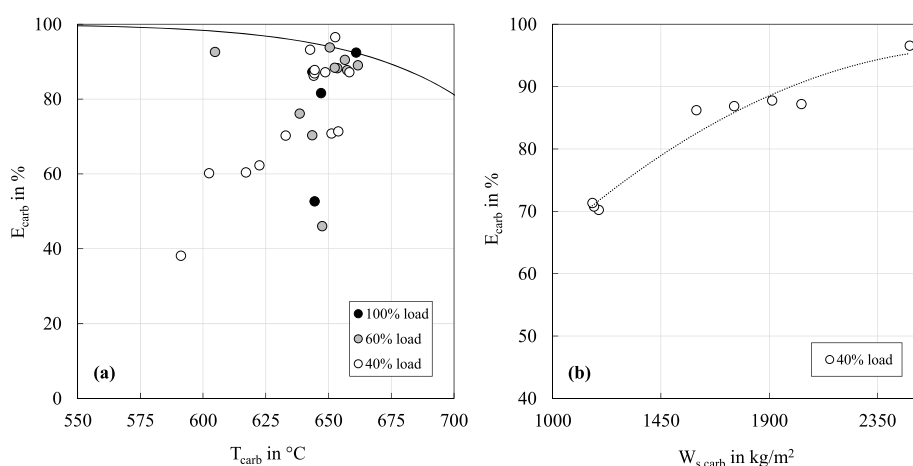
**Figure 4.** (a) Carbonator $CO_2$ capture efficiency ($E_{carb}$) vs carbonation temperature ($T_{carb}$) for all experiments investigated in this study. (b) Carbonator $CO_2$ capture efficiency ($E_{carb}$) vs carbonator solid inventory ($W_{s,carb}$) for selected 40% load experiments under the same process conditions with corresponding trend line.
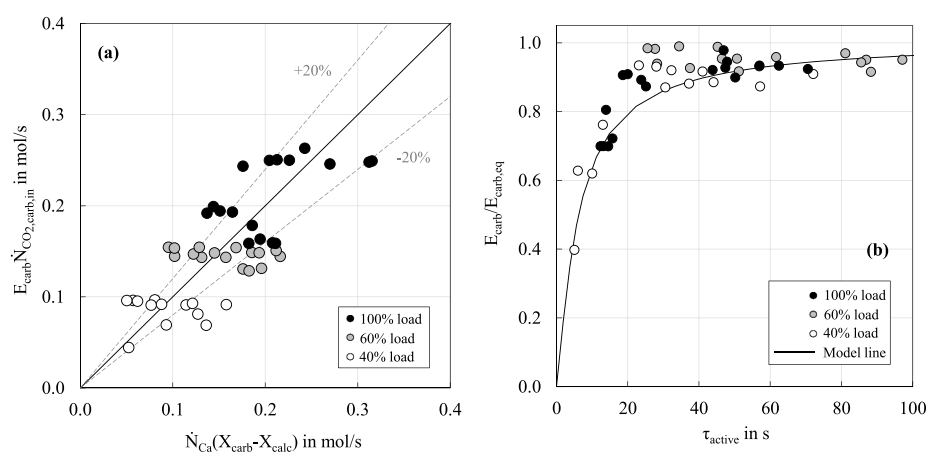


**Figure 5.** (a) Comparison of the carbonator carbon balance for the gas phase and solid phase. (b) Equilibrium normalized carbonator $CO_2$ capture efficiency ($E_{carb}/E_{carb,eq}$) vs carbonator active space time ($\tau_{active}$).

ascribed to the sorbent's high $CO_2$ carrying capacity, as well as to the sufficiently high sorbent inventory and satisfactory carbonation conditions. However, some other data points introduced in Figure 4a indicate a significant deviation from the equilibrium limited $CO_2$ capture efficiency. The relatively low carbonator solid inventory applied in such experiments limited the quantity of CaO in the bed, thus affecting the carbonation performance. The effect was purposely investigated at 40% load operation (see Figure 4b). Dedicated experiments were conducted with diverse carbonator solid inventories under similar carbonator temperature conditions (i.e., 635–655 °C). The illustration shows that differences as high as 1350 kg/m$^2$ (or 41 kg) can increase the $CO_2$ capture efficiency by about 25 percentage points, given that all remaining process conditions remain unchanged. This latter finding correlates well with the conclusions drawn by Chen et al. at a 3 kW$_{th}$ bench-scale unit, in which the inventory of solids was postulated as a major parameter affecting the carbonator capture efficiency.[34] Moreover, investigations at a considerably higher scale revealed that the capture performance attained in the carbonator was significantly influenced by the amount of solid bed inventory.[19,28,35]

**4.1.2. Carbon Mass Balance and Active Space Time Model.** As previously anticipated, the carbonator carbon balance constitutes a crucial key metric for evaluating the CaL process performance. Figure 5a depicts the carbonator carbon balance for all experiments with available gas and solid sample measurements. According to the gas balance, the amount of $CO_2$ absorbed in the carbonator ranged from 0.05 mol/s at 40% load up to 0.25 mol/s under 100% load conditions. In most cases, there is a reasonable agreement between the $CO_2$ removed from the gas phase and the $CO_2$ bound as carbonate in the circulating CaO solid stream. Nonetheless, the values derived from the solid balance tend to show higher deviations than the numbers obtained from the gas balance. This is mostly ascribed to the intrinsic uncertainties in the measurement of the hot circulating solids. Moreover, it should be noted that the sampled solids represent only a minor share of the total amount of the solids in the CaL system and may thus also influence the analysis of the solid phase balance. The evaluation of the carbonator performance through the simplified active space time model is introduced in Figure 5b. The illustration shows the equilibrium normalized carbonator $CO_2$ capture efficiency ($E_{carb}/E_{carb,eq}$) against the carbonator active space time ($\tau_{active}$), both for the experimental
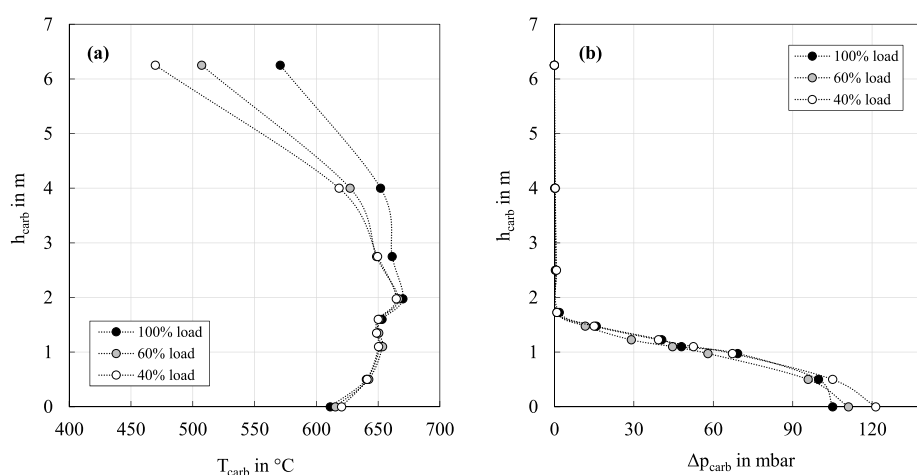
**Figure 6.** Carbonator temperature ($T_{carb}$) (a) and pressure ($\Delta p_{carb}$) (b) profiles over the carbonator height ($h_{carb}$) at a reference carbonator temperature of 660 °C.
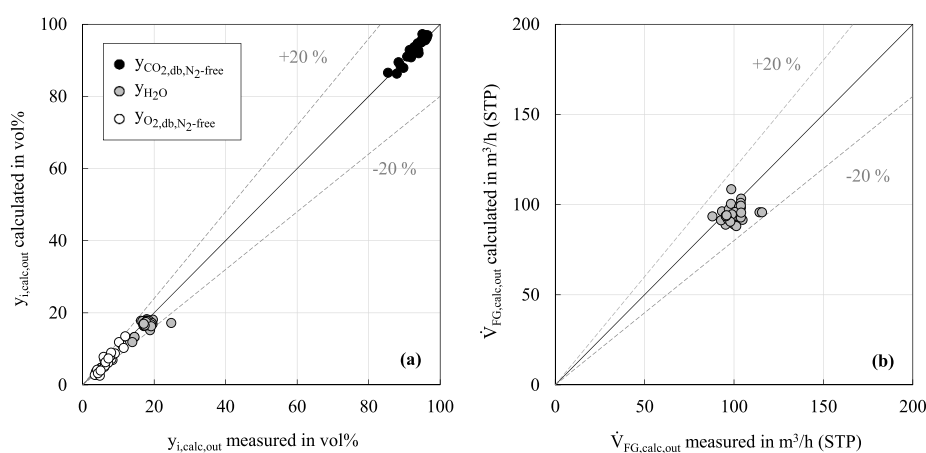


**Figure 7.** Comparison of the calciner mass balance for calculated and measured flue gas concentrations ($y_i$) (a) and flue gas volume flow ($\dot{V}_{FG}$) (b).

and calculated (i.e., model) values. The plot shows a good correlation between the model line and the experimental data, considering the inherent uncertainties in the experimental determination of $\tau_{active}$.[29,36] For the experiments in this study, $k_s\varphi$ averaged 0.16 s$^{-1}$. While this apparent carbonation rate constant is lower than the typical values observed in CFB carbonators (i.e., 0.30−0.43 s$^{-1}$),[21,37,38] it is still substantially higher than the reaction rates reported for conventional BFB units operated at much lower gas superficial velocities (i.e., 0.05−0.09 s$^{-1}$).[38,39] Hence, the results in this study show that a BFB carbonator operated with sufficient gas throughput can still provide an efficient gas−solid interaction, enabling high CO$_2$ capture efficiencies both during full- and part-load operation.

*4.1.3. Carbonator Hydrodynamics.* The hydrodynamic behavior of the CaL system is essential for the stable operation of the facility. Figure 6 introduces the temperature (a) and pressure (b) profiles of the BFB carbonator during the long-term full- and part-load investigations. The values represent the average measurements taken at each reactor height. The temperature profile described by the carbonator is character-istic of the bubbling to turbulent fluidization regime. The reactor region containing most of the solid inventory (i.e., 2 m) shows typical carbonation temperatures in the three m)

investigated cases, with values ranging between 665 and 670 °C. The upper part of the reactor exhibits lower temperatures during partial load operation, which is ascribed to the lower solid entrainment rates achieved under modest superficial gas velocities. This statement becomes evident when comparing the temperatures measured at the reactor top in the three load cases (i.e., 6.2 m), in which differences as high as 100 °C were observed between 100 and 40% load operating conditions. However, this effect is expected to have a minor influence on the carbonator CO$_2$ capture efficiency as the main part of the reaction is assumed to take place in the dense part of the reactor.[21]

The pressure profile described by the carbonator resembles the typical behavior of a BFB unit (see Figure 6b). This is characterized by a high-pressure drop in the reactor's bottom zone (i.e., up to 2 m), where most of the solid inventory is located. The pressure difference across the reactor accounted for 104 mbar during full-load operation, whereas at 40% load conditions, 120 mbar was measured. This slight increase is attributed to the lower gas superficial velocities applied during partial load operation. In addition, the pressure difference measured above the freeboard region (i.e., above 2 m) was negligible for all three investigated load cases.

The results presented in this section endorse the feasibility of operating a BFB carbonator at realistic low coal-fired power plant loads (i.e., 40%), achieving high $CO_2$ capture efficiencies over a wide range of process temperatures and solid bed inventories. The demonstration of even lower load factors might still be attainable with the proposed reactor configuration. However, its application is not straightforward as it needs to be balanced by criteria of reactor hydrodynamics and $CO_2$ capture efficiency. Hence, modifications to relevant process variables (i.e., solid circulation rate and make-up flow) may be required in some cases to compensate for the hydrodynamic changes and to guarantee adequate $CO_2$ absorption. Furthermore, the characterization of dynamic CaL behavior is essential for gaining an in-depth knowledge of the process to sustain smooth plant operation during load changes. The experimental information presented in this chapter contributes to a better understanding of the operation of flexible CaL carbonators, which is a key aspect for the deployment of the technology in future energy scenarios.

**4.2. Calciner Operation.** Within a preliminary evaluation phase of the calciner performance, the reactor material balance was assessed using the gas concentration, volume flow, and solid flow data measured in the pilot facility. Combined combustion and calcination calculations were employed to assess the experimental results' quality by estimating the flue gas composition and off-gas volume flow. The elementary combustion calculations were performed by stoichiometric relations assuming complete fuel combustion. The calcination estimations were conducted by analyzing the collected solid samples, the flow of circulating solids, and the sorbent make-up. The comparison between the calculated and experimental data is introduced in Figure 7.

The calculated steam, $CO_2$, and $O_2$ concentrations correlate well with the measured values, indicating a satisfactory closure of the calciner material balance. Deviation of the measured and calculated values for such gas components averaged 6, 0.1, and 7%, respectively. Moreover, the measured and calculated off-gas volume flows yielded deviations around 5%. This disparity can be regarded as marginal, considering the modest flue gas duct's cross section and the impeller anemometer's accuracy within the measured volume flow range. In addition, the very similar off-gas concentrations and volume flows indicate that the calciner operation was not substantially affected by the thermal load case applied in the carbonator.

*4.2.1. Influence of Inlet Oxygen Concentration.* The oxygen concentration of the combustion gas mixture is a significant parameter to influence and control the calciner's fuel combustion efficiency. Figure 8 introduces the dry oxygen inlet concentration against the share of recirculated calciner flue gas.

As can be expected, the achievement of high oxygen inlet partial pressures requires a reduction in the recirculated flue gas volume flow to avoid the dilution of oxygen. The calciner was operated over a wide range of inlet oxygen concentrations that ranged between 31 and 55 vol %$_{db}$. Despite the low flue gas recirculation rates employed to achieve such high oxy-fuel cases, the temperature profile described by the calciner reactor was always uniform, without the presence of hotspots. The investigation of even higher oxy-fuel levels may still be conceivable at the 200 kW$_{th}$ pilot facility. However, this evaluation was out of the present work's scope. In addition, as the looping ratio and make-up ratio were kept unchanged throughout the tests, the calciner's heat demand was reduced
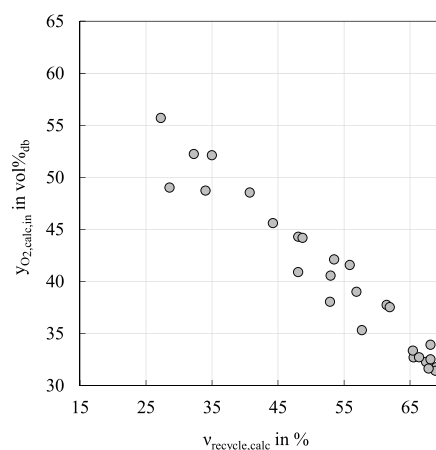


**Figure 8.** Dry oxygen inlet concentration ($y_{O_2,calc,in}$) vs calciner flue gas recirculation rate ($\nu_{recycle,calc}$).

with decreasing carbonator's flue gas load. In consequence, the rate of recirculated flue gas was accordingly increased to maintain the desired gas superficial velocity (i.e., solid entrainment) in the reactor during part-load operation, posing a dilution effect on the inlet oxygen concentration.

A major aspect that conditions the subsequent storage or utilization of the $CO_2$-rich calciner flue gas is its purity. This is mainly related to the concentration of excess oxygen, nitrogen oxides ($NO_x$), and sulfur oxides ($SO_2$) in the off-gas stream. Figure 9a displays the dry $NO_x$ volume fraction in the flue gas for different oxy-fuel cases within a temperature range of 910−940 °C. Generally, CFB boilers are characterized by low $NO_x$ emissions due to the moderate combustion temperatures that prevent thermal $NO_x$ formation.[40] Consequently, the major share of $NO_x$ formation in fluidized beds is related to the fuel-bound nitrogen. The linearity of $NO_x$ formation with excess oxygen has already been reported in previous works.[40,41] This can be attributed to a decreased reducing zone in the combustor, which results in the reduction of $NO_x$ to $N_2$. Furthermore, Figure 9a indicates the promoting effect of the inlet oxygen concentration on $NO_x$ formation. As indicated by different authors, it is presumable that when the combustion agent's oxygen concentration is increased, volatile matters and char are more likely to be oxidized. Hence, the combustion circumstance tends to be more oxidative to accelerate fuel-N conversion into $NO_x$.[42,43]

The concentration of $SO_2$ in the calciner exhaust gas is significantly reduced under typical operating conditions prevailing in CaL applications (see Figure 9b). The favorable oxy-fuel combustion temperatures, together with the continuous supply of fresh limestone, constitute a favorable framework for efficient flue gas desulfurization.[31] The increased calcium availability for sulfur retention (i.e., Ca/S ratio) in CaL systems is of several magnitudes higher than the amounts applied for the retention of sulfur during fluidized bed combustion.[44] This ensures an almost $SO_2$ free flue gas in the calciner. For the experiments in this study, the $SO_2$ concentration averaged at 5 ppmv in most cases and was neither influenced by the excess oxygen amount nor the oxy-fuel level applied.

*4.2.2. Influence of Combustion Temperature.* The combustion temperature is another major variable that influences the fuel's conversion degree and, thus, the
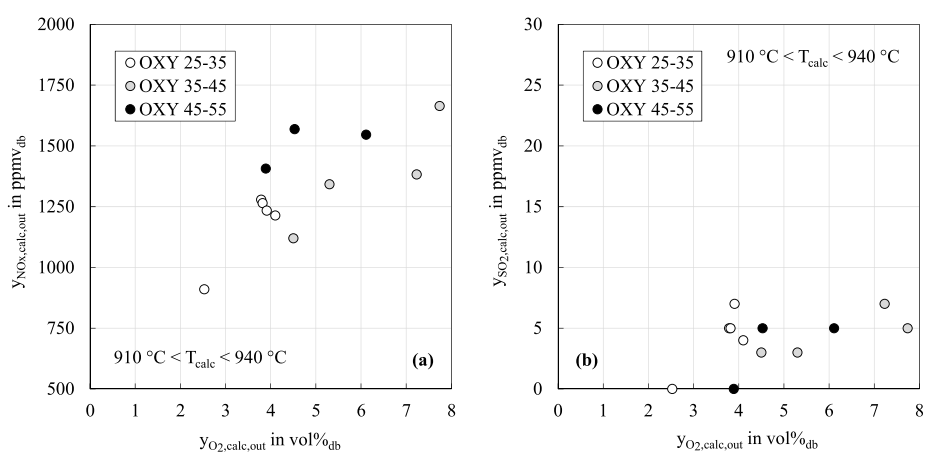
**Figure 9.** Influence of inlet oxygen concentration: dry concentrations of $NO_x$ ($y_{NO_x,calc,out}$) (a) and $SO_2$ ($y_{SO_2,calc,out}$) (b) vs excess oxygen ($y_{O_2,calc,out}$) in the calciner off-gas.



**Figure 10.** Influence of combustion temperature: dry concentrations of $NO_x$ ($y_{NO_x,calc,out}$) (a) and $SO_2$ ($y_{SO_2,calc,out}$) (b) vs excess oxygen ($y_{O_2,calc,out}$) in the calciner off-gas.
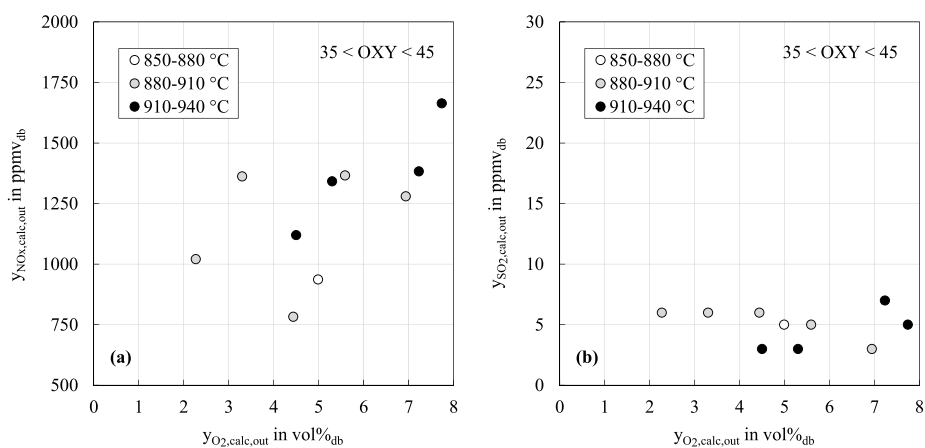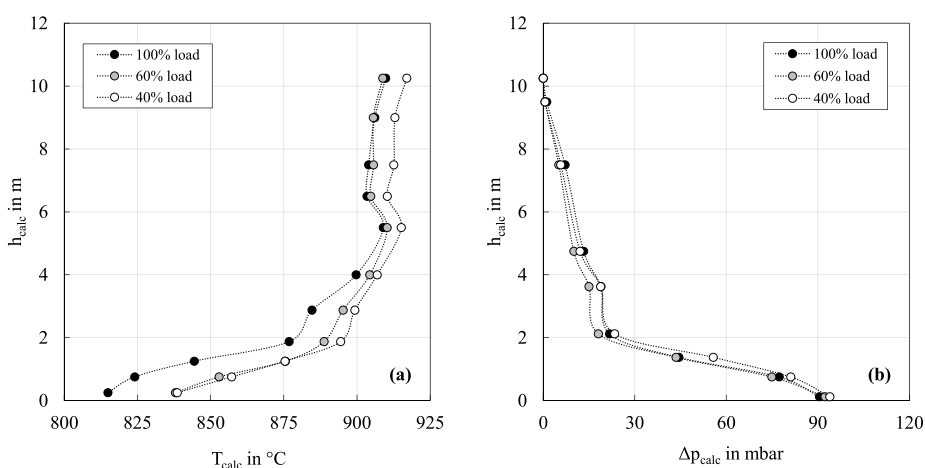


**Figure 11.** Calciner temperature ($T_{calc}$) (a) and pressure ($\Delta p_{calc}$) (b) profiles over the calciner height ($h_{calc}$) at a reference calciner temperature of 910 °C.

combustion flue gas composition. Figure 10a shows the effect of combustion temperature on $NO_x$ formation for an oxygen inlet concentration between 35 and 45 vol %$_{db}$. The three trends introduced in the plot confirm the excess oxygen's promoting effect on the fuel-N conversion to $NO_x$. The $NO_x$ formation behavior does not seem to be significantly affected by the applied combustion temperature. This can be linked to the homogeneous temperature profile described by the

calciner. Although it is not showed here, the reactor temperature gradients obtained in these experiments were almost identical, particularly in the bottom reactor section. These findings are consistent with the results reported by Hofbauer in a similar study.[42] The effect of the combustion temperature on $SO_2$ formation is introduced in Figure 10b. From the values obtained with an oxygen excess of 4 vol %$_{db}$, the illustration indicates a slight improvement in the sulfur retention rate at increased reactor temperatures (i.e., $T_{calc}$ > 910 °C). These results correlate well with the observations made in previous works, where a temperature range of 900−925 °C was proposed as most suitable for efficient fluidized bed in situ desulfurization.[45]

*4.2.3. Calciner Hydrodynamics.* Figure 11 introduces the temperature and pressure profiles described by the CFB calciner for the different carbonator thermal loads under study. The calciner temperature evolution in the three load experiments falls into the typical pattern described by a CFB combustor. This is characterized by stable temperatures in the upper part of the riser and lower temperatures in the bottom region, which are attributed to the inlet flow of colder solids coming from the carbonator. The uniform temperature profile described by the CFB calciner indicates the absence of hot spots. This is indispensable for efficient sorbent calcination and is achieved by staged oxygen addition and flue gas recirculation. With minor differences observed among the three considered carbonator thermal loads, the average calciner temperature measured at a middle-upper height (i.e., 7.5 m) ranged between 909 and 917 °C.

In addition, the pressure drop introduced by the calciner shows a shaped curve in the bottom region with an almost linear gradient in the riser, indicating a uniform distribution of the bed inventory along with the reactor height in each investigated load case.

The results introduced in this chapter envisage that calciner operation can be detached from the thermal load applied in the carbonator, providing that certain requirements are fulfilled, e.g., sufficient solid inventory, sorbent circulation rate, and make-up flow. Other variables such as fuel mass flow rate and oxygen demand are accordingly adjusted to provide the required calciner's heat duty. Under constant looping ratio and make-up ratio conditions, the heat demand in the calciner reduces with decreasing carbonator thermal load. This can be expected as a result of the lower amount of solids coming from the carbonator in combination with a decreased supply of fresh limestone. Despite the reduced heat duty, the calciner has shown to guarantee stable operation at all investigated carbonator loads, both in terms of off-gas compositions (see Figure 7) and hydrodynamic conditions (see Figure 11). The latter observations are in line with the conclusions drawn by Arias et al. in a recent study, which characterized a flexible CaL system for the power sector with a high temperature sorbent storage.[46] The authors postulated that the CaL calciner can be operated continuously in steady-state mode when the load-following power plant enters into operation. Furthermore, the resulting decrease in oxygen flow required to burn supplementary fuel at part-load conditions can be compensated by recirculated flue gas to maintain constant solid entrainment (i.e., gas superficial velocity) in the calciner. However, this latter aspect is not straightforward as it poses a dilution effect on the oxygen concentration at calciner inlet (Figure 8). It is furthermore true that operating the calciner under extreme oxy-fuel combustion conditions can be advantageous to further

reduce the heat demand in the reactor and hence the energy penalty of the whole CaL system.[37] However, the investigation of this last aspect was out of the scope of the present work. The experimental data introduced in this section suggest that the calciner of such a reactor system (i.e., BFB-CFB) can operate over a wide range of process conditions without posing significant changes on the reactor coupling, which is essential to ensure the flexible operation of future large-scale CaL systems.

## 5. CONCLUSIONS

This work has analyzed the performance of a novel CaL reactor arrangement with enhanced load flexibility. The proposed configuration (i.e., BFB-CFB) has been tested at the University of Stuttgart's 200 kW$_{th}$ pilot plant applying industrially relevant process conditions (TRL6). Several experimental campaigns have been conducted to evaluate the steady-state operation of the CaL system at different carbonator flue gas loads. It has been shown that the proposed reactor arrangement can be operated stably with carbonator gas superficial velocities ranging from 0.8 m/s up to 2.0 m/s, without affecting the solid circulation between reactors, and thus the hydrodynamic stability of the system. A simple carbon mass balance has been applied for a preliminary validation of the carbonator performance, and a carbonator model based on the active time approach has been proposed for a more detailed result interpretation. According to the model calculations, an active space time of 41 s is sufficient to achieve an equilibrium normalized carbonator capture efficiency of 90%. The calciner operation has shown to be independent of the thermal load applied in the carbonator. The reactor has been successfully operated with recirculation rates as low as 27% and inlet oxygen concentrations up to 55 vol %$_{db}$. The CFB calciner has described a very uniform temperature profile in all investigated experiments, without the presence of hotspots. The results included in this study endorse the suitability of the proposed novel CaL arrangement for efficient post-combustion $CO_2$ capture at realistic low coal-fired power plant capacity factors (i.e., 40%).

## ■ AUTHOR INFORMATION

**Corresponding Author**

　**Joseba Moreno** − *University of Stuttgart, Institute of Combustion and Power Plant Technology (IFK), 70569 Stuttgart, Germany;* ⊙ orcid.org/0000-0002-6756-4404; Phone: + 49 711 685-63562; Email: joseba.moreno@ifk.uni-stuttgart.de

**Authors**

　**Matthias Hornberger** − *University of Stuttgart, Institute of Combustion and Power Plant Technology (IFK), 70569 Stuttgart, Germany*
　**Max Schmid** − *University of Stuttgart, Institute of Combustion and Power Plant Technology (IFK), 70569 Stuttgart, Germany*
　**Günter Scheffknecht** − *University of Stuttgart, Institute of Combustion and Power Plant Technology (IFK), 70569 Stuttgart, Germany*

Complete contact information is available at:
https://pubs.acs.org/10.1021/acs.iecr.1c00155

## ■ NOMENCLATURE

| | |
|---|---|
| $E$ | $CO_2$ capture efficiency (%) |
| $f_{active}$ | active fraction of particles reacting in the fast reaction regime (-) |
| $h$ | height (m) |
| $k_s$ | surface carbonation rate constant ($s^{-1}$) |
| $k_s\varphi$ | apparent carbonation rate constant ($s^{-1}$) |
| $N$ | molar content of component "$i$" (kmol) |
| $\dot{N}_i$ | molar flow of component "$i$" (kmol/h or mol/s) |
| $\xi_{LR}$ | looping ratio (mol/mol) |
| $\xi_{MR}$ | make-up ratio (mol/mol) |
| $T$ | temperature (°C) |
| $u$ | gas superficial velocity (m/s) |
| $\dot{V}_i$ | volume flow of component "$i$" (m³/h, STP) |
| $W_s$ | solid bed inventory (kg or kg/m²) |
| $X$ | conversion degree (mol/mol) |
| $x_i$ | mass fraction of component "$i$" in sorbent (kg/kg) |
| $y_i$ | volume fraction of component "$i$" in gas (vol %) |

### Greek Letters

| | |
|---|---|
| $\Delta p$ | pressure difference (mbar) |
| $\nu_{recycle}$ | flue gas recirculation rate (%) |
| $\gamma_i$ | mass fraction of component "$i$" in fuel (kg/kg) |
| $\varphi$ | gas−solid contacting effectivity factor (-) |
| $\tau_{active}$ | active space time (s) |

### Acronyms

| | |
|---|---|
| BFB | bubbling fluidized bed |
| CaL | calcium looping |
| CCS | carbon capture and storage |
| CFB | circulating fluidized bed |
| DCFB | dual circulating fluidized bed |
| HEX | heat exchanger |
| ID | induced draft |
| LS | loop seal |
| TRL | technology readiness level |

### Subscripts

| | |
|---|---|
| ad | air dried |
| ave | average |
| calc | calciner |
| carb | carbonator |
| db | dry basis |
| eq | equilibrium |
| FG | flue gas |
| in | inlet |
| out | outlet |
| waf | water and ash free |
| wf | water free |

## ■ REFERENCES

(1) Global CCS Institute *CCS: A solution to climate change right beneath our feet*; Global CCS Institute: Melbourne, Australia, 2018.

(2) International Energy Agency (IEA) *Energy Technology Perspectives 2017: Catalysing Energy Technology Transformations*; IEA: Paris, France, 2017.

(3) International Energy Agency (IEA) *Status of Power System Transformation 2018: Advanced Power Plant Flexibility*; IEA: Paris, France, 2018.

(4) Abanades, J. C.; Arias, B.; Lyngfelt, A.; Mattisson, T.; Wiley, D. E.; Li, H.; Ho, M. T.; Mangano, E.; Brandani, S. Emerging $CO_2$ capture systems. *Int. J. Greenhouse Gas Control* **2015**, *40*, 126−166.

(5) Guandalini, G.; Romano, M. C.; Ho, M.; Wiley, D.; Rubin, E. S.; Abanades, J. C. A sequential approach for the economic evaluation of new $CO_2$ capture technologies for power plants. *Int. J. Greenhouse Gas Control* **2019**, *84*, 219−231.

(6) IEA Greenhouse Gas R&D Programme (IEAGHG) *Operating Flexibility of Power Plants With CCS*; IEAGHG: Cheltenham, UK, 2012.

(7) Arias, B.; Criado, Y. A.; Sanchez-Biezma, A.; Abanades, J. C. Oxy-fired fluidized bed combustors with a flexible power output using circulating solids for thermal energy storage. *Appl. Energy* **2014**, *132*, 127−136.

(8) Astolfi, M.; de Lena, E.; Romano, M. C. Improved flexibility and economics of Calcium Looping power plants by thermochemical energy storage. *Int. J. Greenhouse Gas Control* **2019**, *83*, 140−155.

(9) Chalmers, H.; Leach, M.; Lucquiaud, M.; Gibbins, J. Valuing flexible operation of power plants with $CO_2$ capture. *Energy Procedia* **2009**, *1*, 4289−4296.

(10) Cormos, A.-M.; Simon, A. Assessment of $CO_2$ capture by calcium looping (CaL) process in a flexible power plant operation scenario. *Appl. Therm. Eng.* **2015**, *80*, 319−327.

(11) Criado, Y. A.; Arias, B.; Abanades, J. C. Calcium looping $CO_2$ capture system for back-up power plants. *Energy Environ. Sci.* **2017**, *10*, 1994−2004.

(12) Hanak, D. P.; Biliyok, C.; Manovic, V. Calcium looping with inherent energy storage for decarbonisation of coal-fired power plant. *Energy Environ. Sci.* **2016**, *9*, 971−983.

(13) Abanades, J. C.; Anthony, E. J.; Wang, J.; Oakey, J. E. Fluidized bed combustion systems integrating $CO_2$ capture with CaO. *Environ. Sci. Technol.* **2005**, *39*, 2861−2866.

(14) Abanades, J. C. The maximum capture efficiency of $CO_2$ using a carbonation/calcination cycle of $CaO/CaCO_3$. *Chem. Eng. J.* **2002**, *90*, 303−306.

(15) Dean, C. C.; Blamey, J.; Florin, N. H.; Al-Jeboori, M. J.; Fennell, P. S. The calcium looping cycle for $CO_2$ capture from power generation, cement manufacture and hydrogen production. *Chem. Eng. Res. Des.* **2011**, *89*, 836−855.

(16) Blamey, J.; Anthony, E. J.; Wang, J.; Fennell, P. S. The calcium looping cycle for large-scale $CO_2$ capture. *Prog. Energy Combust. Sci.* **2010**, *36*, 260−279.

(17) Shimizu, T.; Hirama, T.; Hosoda, H.; Kitano, K.; Inagaki, M.; Tejima, K. A Twin Fluid-Bed Reactor for Removal of $CO_2$ from Combustion Processes. *Chem. Eng. Res. Des.* **1999**, *77*, 62−68.

(18) Arias, B.; Alonso, M.; Abanades, C. $CO_2$ Capture by Calcium Looping at Relevant Conditions for Cement Plants: Experimental Testing in a 30 kW_th Pilot Plant. *Ind. Eng. Chem. Res.* **2017**, *56*, 2634−2640.

(19) Arias, B.; Diego, M. E.; Abanades, J. C.; Lorenzo, M.; Diaz, L.; Martínez, D.; Alvarez, J.; Sánchez-Biezma, A. Demonstration of steady

state $CO_2$ capture in a 1.7MW$_{th}$ calcium looping pilot. *Int. J. Greenhouse Gas Control* **2013**, *18*, 237−245.

(20) Charitos, A.; Hawthorne, C.; Bidwe, A. R.; Sivalingam, S.; Schuster, A.; Spliethoff, H.; Scheffknecht, G. Parametric investigation of the calcium looping process for $CO_2$ capture in a 10 kW$_{th}$ dual fluidized bed. *Int. J. Greenhouse Gas Control* **2010**, *4*, 776−784.

(21) Charitos, A.; Rodríguez, N.; Hawthorne, C.; Alonso, M.; Zieba, M.; Arias, B.; Kopanakis, G.; Scheffknecht, G.; Abanades, J. C. Experimental Validation of the Calcium Looping $CO_2$ Capture Process with Two Circulating Fluidized Bed Carbonator Reactors. *Ind. Eng. Chem. Res.* **2011**, *50*, 9685−9695.

(22) Dieter, H.; Beirow, M.; Schweitzer, D.; Hawthorne, C.; Scheffknecht, G. Efficiency and Flexibility Potential of Calcium Looping $CO_2$ Capture. *Energy Procedia* **2014**, *63*, 2129−2137.

(23) Dieter, H.; Hawthorne, C.; Zieba, M.; Scheffknecht, G. Progress in Calcium Looping Post Combustion $CO_2$ Capture: Successful Pilot Scale Demonstration. *Energy Procedia* **2013**, *37*, 48−56.

(24) Hilz, J.; Helbig, M.; Haaf, M.; Daikeler, A.; Ströhle, J.; Epple, B. Long-term pilot testing of the carbonate looping process in 1 MW$_{th}$ scale. *Fuel* **2017**, *210*, 892−899.

(25) Ströhle, J.; Junk, M.; Kremer, J.; Galloy, A.; Epple, B. Carbonate looping experiments in a 1 MW$_{th}$ pilot plant and model validation. *Fuel* **2014**, *127*, 13−22.

(26) Lara, Y.; Romeo, L. M. On the flexibility of coal-fired power plants with integrated Ca-looping $CO_2$ capture process. *Energy Procedia* **2017**, *114*, 6552−6562.

(27) Diego, M. E.; Arias, B. Impact of load changes on the carbonator reactor of a 1.7 MW$_{th}$ calcium looping pilot plant. *Fuel Process. Technol.* **2020**, *200*, 106307.

(28) Alonso, M.; Rodríguez, N.; González, B.; Grasa, G.; Murillo, R.; Abanades, J. C. Carbon dioxide capture from combustion flue gases with a calcium oxide chemical loop. Experimental results and process development. *Int. J. Greenhouse Gas Control* **2010**, *4*, 167−173.

(29) Rodríguez, N.; Alonso, M.; Abanades, J. C. Experimental investigation of a circulating fluidized-bed reactor to capture $CO_2$ with CaO. *AIChE J.* **2011**, *57*, 1356−1366.

(30) Dieter, H.; Bidwe, A. R.; Varela-Duelli, G.; Charitos, A.; Hawthorne, C.; Scheffknecht, G. Development of the calcium looping $CO_2$ capture technology from lab to pilot scale at IFK, University of Stuttgart. *Fuel* **2014**, *127*, 23−37.

(31) Hornberger, M.; Moreno, J.; Schmid, M.; Scheffknecht, G. Experimental investigation of the calcination reactor in a tail-end calcium looping configuration for $CO_2$ capture from cement plants. *Fuel* **2021**, *284*, 118927.

(32) Alonso, M.; Rodríguez, N.; Grasa, G.; Abanades, J. C. Modelling of a fluidized bed carbonator reactor to capture $CO_2$ from a combustion flue gas. *Chem. Eng. Sci.* **2009**, *64*, 883−891.

(33) Barin, I. Thermochemical Data of Pure Substances. *VCH* **1995**, *102*, 1523.

(34) Chang, M.-H.; Huang, C.-M.; Liu, W.-H.; Chen, W.-C.; Cheng, J.-Y.; Chen, W.; Wen, T.-W.; Ouyang, S.; Shen, C.-H.; Hsu, H.-W. Design and Experimental Investigation of Calcium Looping Process for 3-kW$_{th}$ and 1.9-MW$_{th}$ Facilities. *Chem. Eng. Technol.* **2013**, *36*, 1525−1532.

(35) Sánchez-Biezma, A.; Paniagua, J.; Diaz, L.; Lorenzo, M.; Alvarez, J.; Martínez, D.; Arias, B.; Diego, M. E.; Abanades, J. C. Testing postcombustion $CO_2$ capture with CaO in a 1.7 MW$_{th}$ pilot facility. *Energy Procedia* **2013**, *37*, 1−8.

(36) Rodríguez, N.; Alonso, M.; Abanades, J. C.; Charitos, A.; Hawthorne, C.; Scheffknecht, G.; Lu, D. Y.; Anthony, E. J. Comparison of experimental results from three dual fluidized bed test facilities capturing $CO_2$ with CaO. *Energy Procedia* **2011**, *4*, 393−401.

(37) Arias, B.; Diego, M. E.; Méndez, A.; Alonso, M.; Abanades, J. C. Calcium looping performance under extreme oxy-fuel combustion conditions in the calciner. *Fuel* **2018**, *222*, 711−717.

(38) Hornberger, M.; Moreno, J.; Schmid, M.; Scheffknecht, G. Experimental investigation of the carbonation reactor in a tail-end Calcium Looping configuration for $CO_2$ capture from cement plants. *Fuel Process. Technol.* **2020**, *210*, 106557.

(39) Charitos, A. *Experimental Characterization of the Calcium Looping Process for CO2 Capture*; University of Stuttgart, 2013, DOI: 10.18419/opus-2174.

(40) Krzywanski, J.; Czakiert, T.; Shimizu, T.; Majchrzak-Kuceba, I.; Shimazaki, Y.; Zylka, A.; Grabowska, K.; Sosnowski, M. NO$_x$ Emissions from Regenerator of Calcium Looping Process. *Energy Fuels* **2018**, *32*, 6355−6362.

(41) Pang, L.; Shao, Y.; Zhong, W.; Gong, Z.; Liu, H. Experimental study of NO$_x$ emissions in a 30 kW$_{th}$ pressurized oxy-coal fluidized bed combustor. *Energy* **2020**, *194*, 116756.

(42) Hofbauer, G. *Experimentelle Untersuchung der Oxy-Fuel-Verbrennung von Steinkohle in einer zirkulierenden Wirbelschichtfeuerung*; University of Stuttgart, 2017, DOI: 10.18419/opus-9129.

(43) Pu, G.; Zan, H.; Du, J.; Zhang, X. Study on NO Emission in the Oxy-Fuel Combustion of Co-Firing Coal and Biomass in a Bubbling Fluidized Bed Combustor. *BioResources* **2016**, *12*, 1890−1902.

(44) Basu, P. *Combustion and gasification in fluidized beds*; CRC/Taylor & Francis: Boca Ranton, 2006.

(45) de Diego, L. F.; Rufas, A.; García-Labiano, F.; de las Obras-Loscertales, M.; Abad, A.; Gayán, P.; Adánez, J. Optimum temperature for sulphur retention in fluidised beds working under oxy-fuel combustion conditions. *Fuel* **2013**, *114*, 106−113.

(46) Arias, B.; Criado, Y. A.; Abanades, J. C. Thermal Integration of a Flexible Calcium Looping $CO_2$ Capture System in an Existing Back-Up Coal Power Plant. *ACS Omega* **2020**, *5*, 4844−4852. Published Online: Mar. 3, 2020.

## ■ NOTE ADDED AFTER ASAP PUBLICATION

This paper was originally published ASAP on May 5, 2021. Additional corrections, including revisions to eqs 2 and 3, were received, and the revised version was reposted on May 6, 2021.

## 5.2 Result discussion and contextualization

This section explores the performance of a novel CaL reactor arrangement when operated under part-load conditions. The proposed reactor configuration is based on a BFB carbonator and offers a unique option for decoupling the solid circulation between reactors from the amount of fluidizing gas.

To date, different studies have been reported on investigating high $CO_2$ efficiencies using the BFB-CFB reactor system, both for power plant [72, 73] and cement plant application [105, 106]. The first experimental campaigns at the 200 kW$_{th}$ CaL facility focused on demonstrating the system's feasibility [72, 73]. Under conditions typical of power plant application, Dieter et al. explored the process' performance using both carbonator settings (i.e., BFB and CFB). Years later, Hornberger et al. conducted investigations to demonstrate the viability of capturing $CO_2$ from cement plants [105, 106]. Here as well, both carbonation options were deployed to investigate different integration levels between the cement plant and the CaL process, assessing the system's performance over a wide range of operating conditions (see table 5.1). More recently, Moreno et al. explored the BFB-CFB reactor concept regarding its load flexibility behavior [155]. Here as well, a broad range of operating conditions was deployed, demonstrating successful CaL performance even at realistic minimum power plant load cases (i.e., 40 %). The following section presents a detailed discussion on the latter study.

Table 5.1: Experimental range of operation conditions at the 200 kW$_{th}$ CaL facility

| Symbol | Unit | Dieter et al. | Hornberger et al. | Moreno et al. |
|---|---|---|---|---|
| $T_{carb}$ | °C | 600-700 | 585-700 | 591-704 |
| $W_{s,carb}$ | kg/m$^2$ | | 680-1270 | 422-1063 |
| $y_{CO_2,carb,in}$ | m$^3$/m$^3$ | 0.14 | 0.13-0.35 | 0.14 |
| $E_{carb}$ | mol/mol | 0.78-0.94 | 0.45-0.98 | 0.38-0.97 |
| $T_{calc}$ | °C | 850-950 | 890-930 | 851-940 |
| $W_{s,calc}$ | kg/m$^2$ | | 290-840 | 881-1414 |
| $y_{O_2,calc,in}$ (wet basis) | m$^3$/m$^3$ | $< 0.5$ | 0.42-0.65 | 0.19-0.46 |
| $\xi_{MR}$ | mol/mol | 0-0.3 | 0.08-0.9 | 0.09-0.11 |
| $\xi_{LR}$ | mol/mol | 4-14 | 4-14 | 10.2-12.2 |
| Reference | | [72, 73] | [105, 106] | [155] |

Generally, two approaches are employed to characterize the carbon balance of the CaL cycle. The first expression (i.e., equation 2.9) is based on comparing the $CO_2$ disappearing from the gas phase with the $CO_2$ captured by the solids during or after carbonation. The results presented in chapter 5.1 indicate a satisfactory closure of the balance, taking into account inherent uncertainties in the measurement of the hot circulating solids as well as the comparatively low amount of sampled sorbent [17, 95]. The second approach (i.e.,

equation 2.11) is based on a simplified reactor and particle reaction rate model applied to the solid phase around the carbonator [11, 45]. The key parameter of the latter model is the active space time ($\tau_{active}$), which is indicative of both the sorbent inventory and the reaction rate of such inventory. The findings included in this chapter indicate an adequate correlation between the model calculations and the experimental data, considering the inherent uncertainties in the determination of $\tau_{active}$ [169, 170].
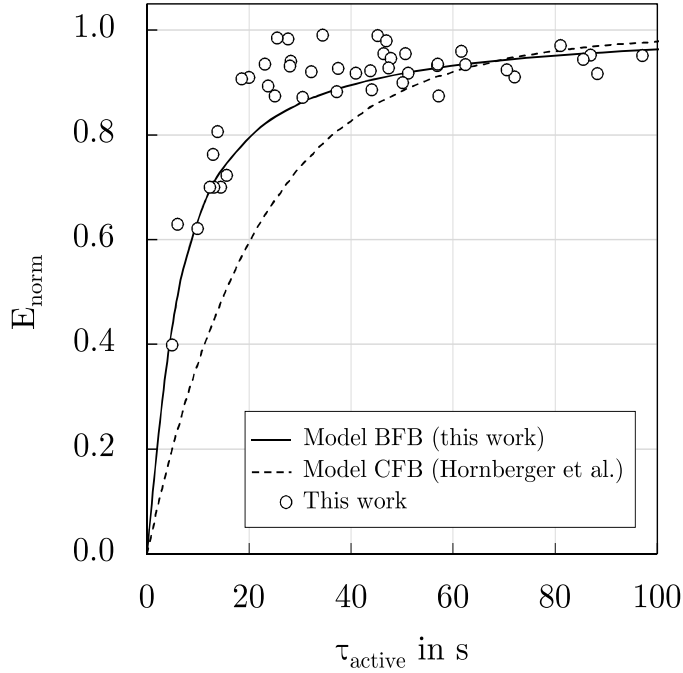


Figure 5.1: Normalized carbonator CO$_2$ capture efficiency (E$_{norm}$) vs active space time ($\tau_{active}$) for characteristic CaL power plant operating conditions. CFB model according to Hornberger et al. [106]

Figure 5.1 displays the normalized carbonator CO$_2$ capture efficiency against the carbonator active space time for characteristic power plant conditions. In addition to the experimental values, a model line for each carbonator setting (i.e., CFB [106] and BFB [155]) is plotted. Generally, there is a good agreement between the BFB model line and the experimental data despite the aforementioned difficulties about solid phase analysis. This work determined an apparent carbonation rate ($k_S\varphi$) of 0.16 s$^{-1}$ with a gas-solid contact factor ($\varphi$) of 0.72. It should be noted that this $k_S\varphi$ is lower than the typical values achieved in CFB carbonators (i.e., 0.30-0.43 s$^{-1}$) [18, 45, 106]. Nevertheless, the calculated $k_S\varphi$ is substantially larger than the apparent carbonation rates determined in conventional BFB units operated at much lower gas superficial velocities (i.e., 0.05-0.09 s$^{-1}$) [42, 106]. In parallel, the determined gas-solid contact factor agrees well with the values obtained for

turbulent fluidized beds (i.e., 0.6-0.8) [89]. Thus, the latter results indicate that a BFB reactor operated with sufficient gas throughput can still provide efficient gas-solid interaction both during full- and part-load operation.
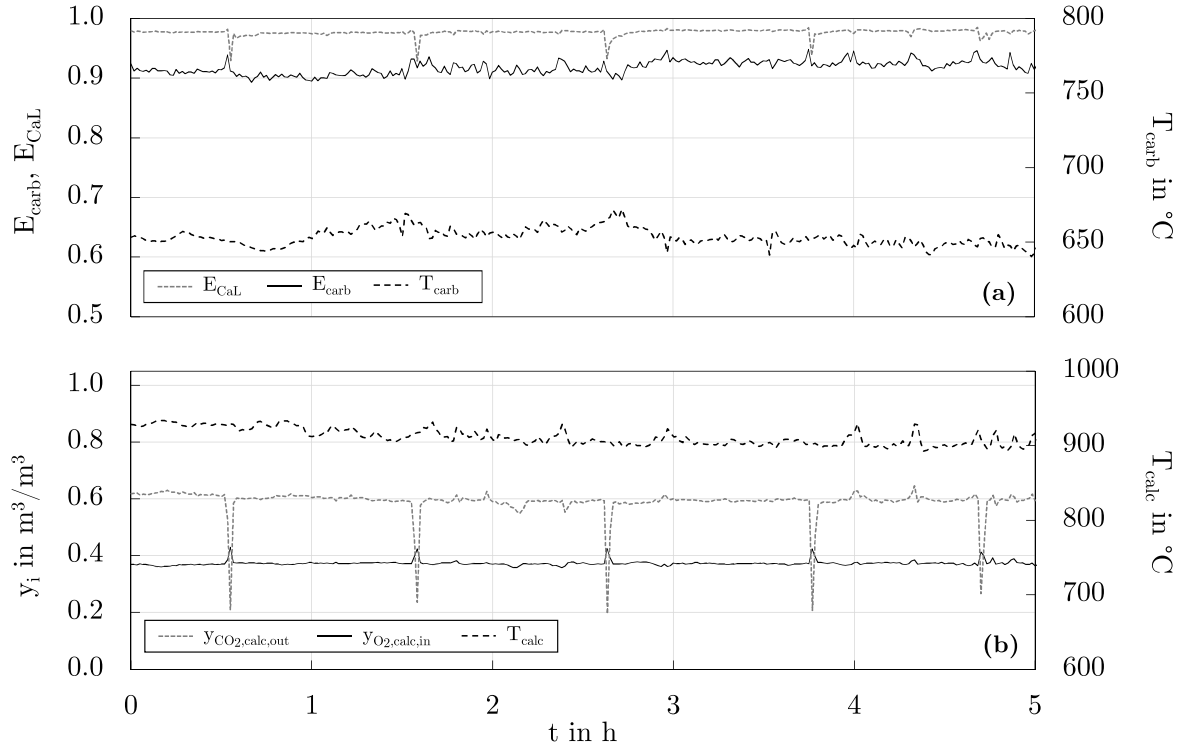


Figure 5.2: Exemplary data plot of the 40 % load case with key process parameters for carbonator (a) and calciner (b)

In figure 5.2, a time trend of an exemplary 40 % load experiment is displayed. The upper plot represents the time evolution of the main carbonator variables. The total $CO_2$ capture efficiency ($E_{CaL}$) has been defined elsewhere [95] and averaged 0.98 mol/mol during the long-term experiment. $E_{carb}$ and $T_{carb}$, in turn, yielded 0.92 mol/mol and 653 °C, respectively. In the bottom graph, the calciner operation is depicted. During the test, $y_{O_2,calc,in}$ averaged at 0.37 m³/m³, whereas $y_{CO_2,calc,out}$ yielded 0.59 m³/m³. Please note that the latter value is greatly influenced by the amount of nitrogen required in the pilot facility for fluidization and flushing purposes. On a nitrogen-free basis, $y_{CO_2,calc,out}$ would account for 0.89 m³/m³. Besides, $T_{calc}$ averaged at 911 °C. Please recall that the peaks observed in the illustration are related to the cleaning of the gas measurement filters, which need to be hourly flushed to guarantee the proper functioning.

Similar to chapter 4, the influence of carbonation temperature upon $CO_2$ absorption efficiency is discussed in this section. Concerning $E_{carb}$, chapter 5 indicates a twofold behavior, depending on the amount of solids contained in the BFB carbonator ($W_{s,carb}$). In practice,

W$_{s,carb}$ is limited by fluid-dynamic restraints. Consequently, the necessary amount of active CaO is usually achieved by increasing the carrying capacity of the sorbent (X$_{ave}$). Nevertheless, the results included in this work indicate that the same objective can be achieved by increasing the bed inventory. Under suitable carbonation conditions (i.e., T$_{carb}$ and X$_{ave}$) and sufficient solid inventories, E$_{carb}$ values over 85 % were obtained. In contrast, experiments conducted with a limited quantity of CaO in the carbonator led to considerably lower E$_{carb}$ values. To this end, the influence of W$_{s,carb}$ on E$_{carb}$ was investigated at 40 % load operation, setting similar process conditions. Results showed that differences as high as 1350 kg/m$^2$ (or 41 kg) could affect E$_{carb}$ by about 25 percentage points. While the latter behavior agrees well with the observations made by Rodriguez et al. in an early work [169], other authors have also reported the strong influence of W$_{s,carb}$ on E$_{carb}$ [10, 17, 41, 180].
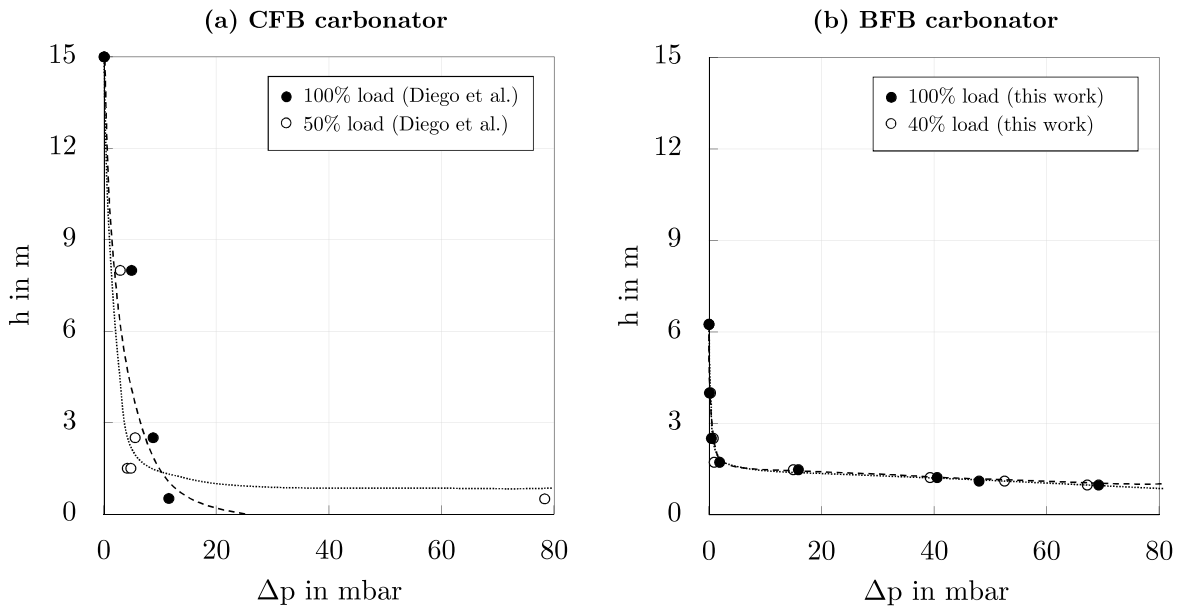


Figure 5.3: Pressure profile of the solids in a CFB (a) and in a BFB (b) carbonator during nominal and minimum part-load operation conditions. CFB data according to Diego and Arias [68]

As anticipated in chapter 3, the hydrodynamic behavior of the CaL system is essential for the stable operation of the facility. The temperature profiles of the BFB carbonator displayed in chapter 5.1 correlate well with the results found in previous works [73, 106]. Independent of the investigated load case, the reactor zone containing most of the solid inventory (i.e., up to 2 m) indicated stable temperature conditions yielding values between 665-670 °C. In contrast, the upper reactor part showed to be strongly influenced by the amount of entrained solids, which increased together with the fluidization velocity. More precisely, differences as high as 100 °C were measured in the upper reactor zone (i.e.,

6.25 m) between 100 and 40 % load operating conditions. The relatively high $E_{carb}$ values achieved in this work both at full- and part-load operation corroborate the assertion that the main part of the carbonation reaction is assumed to occur in the dense part of the reactor [45]. With regard to operation flexibility, figure 5.3 shows the advantages of the proposed BFB carbonator in front of a conventional CFB reactor setting. In this work, the pressure difference across the BFB unit was hardly influenced by the selected load operation case. In contrast, a load reduction of 50 % in a conventional CFB carbonator setting posed significant differences in the solid pressure profile [68]. Operation at minimum CFB loads (i.e., 50 %) led to the formation of a dense bed in the lower part of the reactor, penalizing the solid entrainment rate heavily. According to the authors, an increase in carbonator bed inventory of about six times larger might be expected when operating at characteristic minimum CFB load conditions. Consequently, the presented results endorse the suitability of the proposed BFB-CFB CaL arrangement for both load-flexible and efficient $CO_2$ capture in a load-following power plant scenario.
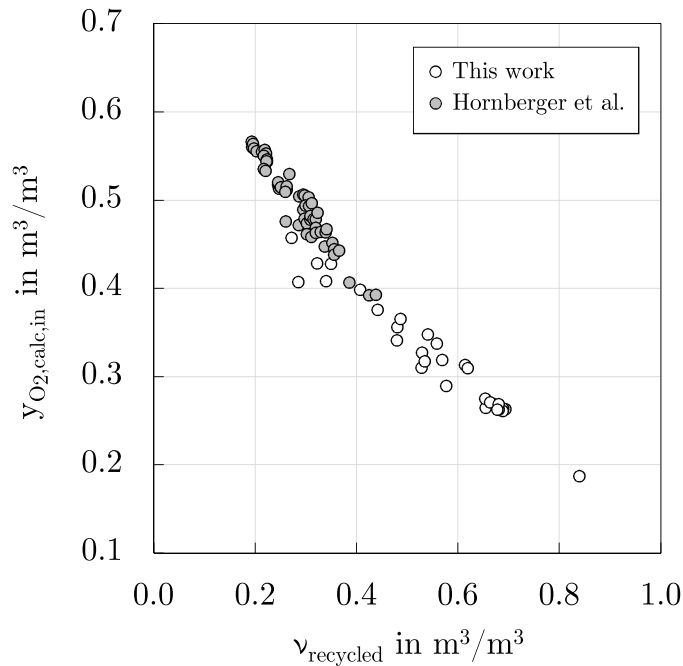


Figure 5.4: Inlet oxygen concentration ($y_{O_2,calc,in}$) vs calciner flue gas recirculation rate ($\nu_{recycled}$) over a wide range of operation conditions. Comparison with data presented by Hornberger et al. [106]

Besides, this work analyzes the calciner performance upon changes in the carbonator flue gas load. Within a preliminary phase of the assessment, the reactor material balance is evaluated. To this end, combined combustion and calcination calculations are conducted

to investigate the experimental results' quality by estimation of flue gas composition and off-gas volume flow. The results displayed in this chapter indicate a satisfactory correlation with the measured plant data. A maximum deviation of 7 % is anticipated for the investigated gas concentrations (i.e., steam, $CO_2$, and $O_2$). The deviation introduced by the off-gas volume flow, in turn, accounted for 5 % in most cases. In parallel, the good agreement between measured and calculated values indicates that the oxy-fuel CFB calciner can be operated within a broad range of operation conditions, as required by the flue gas load selected in the carbonator.

An evidence of such operating flexibility is given through figure 5.4. The illustration compares the inlet concentration of $O_2$ in the calciner with the ratio of recirculated flue gas, both for the results included in this work and those included in a previous publication [105]. Despite the very distinct operation conditions of the CFB calciner in each case, a satisfactory correlation between both studies can be observed. As characteristic for cement plant operation, the increased make-up flows utilized by Hornberger et al. required higher inlet $O_2$ concentrations in the calciner. The present study, in contrast, enabled operation over a broader range of $y_{O_2,calc,in}$ values due to the modest limestone make-up rates selected for power plant application. Similar to the work by Hornberger et al. [105], the investigation of high oxy-fuel cases did not lead to the presence of localized hot spots. Yet if the achievement of even higher $y_{O_2,calc,in}$ values may be feasible at the 200 $kW_{th}$ CaL pilot facility, its investigation was outside the scope of the present study.

The purity of the $CO_2$-rich calciner flue gas is a major aspect conditioning its subsequent storage or utilization. In this work, the behavior of nitrogen oxides ($NO_x$) and sulfur dioxide ($SO_2$) is evaluated. Similar to the observations made by Hornberger et al., the concentration of $SO_2$ in the calciner exhaust gas was found to be significantly reduced under typical CaL operation conditions. The latter effect can be ascribed to the combination of favorable process temperatures and continuous limestone addition. In this work, $SO_2$ averaged 5 ppmv in most cases and was neither influenced by the excess oxygen amount nor the oxy-fuel level applied. Nitrogen oxides, in contrast, showed to be greatly influenced by both $y_{O_2,calc,in}$ and $y_{O_2,calc,out}$. Increased $y_{O_2,calc,out}$ values led to higher $NO_x$ following a linear trend as already described in the literature [106, 123, 164]. Inlet oxygen, in turn, tends to promote $NO_x$ formation by enhanced oxidation of volatile matters and char. Thus, fuel-N conversion into $NO_x$ is further accelerated [103, 166]. Besides, $T_{calc}$ posed a more negligible effect on $NO_x$ formation due to the smooth temperature gradients achieved throughout the CFB calciner [103]. The considerably high $NO_x$ concentrations introduced in this work will most certainly require subsequent treatment in the $CO_2$ processing unit (CPU), depending on the requested $CO_2$ specifications. Nevertheless, $NO_x$ can be easily removed during compression in the CPU [187]. Furthermore, it should be noted that $NO_x$ concentrations tend to be promoted when using CaO as bed material due to the catalyzing

effect that CaO poses on $NO_x$ formation and $N_2O$ decomposition [130].

The hydrodynamic behavior described by the CFB calciner in this chapter evidences the suitability of this reactor to cope with distinct carbonator flue gas loads. The uniform temperature profile measured within the reactor indicated the absence of localized hot spots. Similar to the trends introduced in previous works, the temperature evolution fell into the typical pattern of a CFB boiler, characterized by stable temperatures in the upper zone and lower values at the bottom [73, 105]. In parallel, the pressure drop measured across the CFB riser proved not to be affected by the selected carbonator load case, indicating a uniform distribution of the bed inventory along with the riser height in all experiments.

# 6 Oxy-fuel Combustion of Hard Coal, Wheat Straw, and Solid Recovered Fuel in a 200 kW$_{th}$ Calcium Looping CFB Calciner

## 6.1 Original publication

# Oxy-Fuel Combustion of Hard Coal, Wheat Straw, and Solid Recovered Fuel in a 200 kW$_{th}$ Calcium Looping CFB Calciner

**Joseba Moreno *** [ORCID], **Matthias Hornberger, Max Schmid and Günter Scheffknecht**

University of Stuttgart, Institute of Combustion and Power Plant Technology (IFK), Pfaffenwaldring 23, 70569 Stuttgart, Germany; matthias.hornberger@ifk.uni-stuttgart.de (M.H.); max.schmid@ifk.uni-stuttgart.de (M.S.); guenter.scheffknecht@ifk.uni-stuttgart.de (G.S.)
* Correspondence: joseba.moreno@ifk.uni-stuttgart.de

**Abstract:** The fluidized bed combustion (FBC) of biomass and solid recovered fuel (SRF) is globally emerging as a viable solution to achieve net-negative carbon emissions in the heat and power sector. Contrary to conventional fossil fuels, alternative fuels are highly heterogeneous, and usually contain increased amounts of alkaline metals and chlorine. Hence, experimental studies are mandatory in order to thoroughly characterize the combustion behavior and pollutant formation of non-conventional fuels in novel applications. This work gives an overview of experimental investigations on the oxy-fuel combustion of hard coal, wheat straw, and SRF with a limestone bed in a semi-industrial circulating fluidized bed (CFB) pilot plant. The CFB combustor was able to be operated under different fuel blending ratios and inlet O$_2$ concentrations, showing a stable hydrodynamic behavior over many hours of continuous operation. The boundary conditions introduced in this study are expected to prevail in carbon capture and storage (CCS) processes, such as the oxy-fuel combustion in the CFB calciner of a Calcium Looping (CaL) cycle for post-combustion CO$_2$ capture.

**Keywords:** oxy-fuel combustion; carbon capture; biomass combustion; SRF combustion; fluidized bed combustion; co-firing

## 1. Introduction

Incineration is a well-established strategy for the valorization of refuse biomass and waste materials. The thermal utilization of alternative fuels allows the reduction of the volume of solids dumped in landfills, thereby decreasing greenhouse gas emissions and adverse health and environmental impacts. Processing residual waste to produce fuel is a common method applied to gain an increased value from refuse materials. The so-called solid recovered fuels (SRF) are standardized fuels produced from non-hazardous waste, intentionally prepared for quality criteria such as their calorific value, and mercury or chlorine content [1]. Today, biomass and biomass-based SRF are typically combusted in cement and power plants, either in stand-alone units or by co-firing them with fossil fuels [2,3]. Considering the challenges resulting from the intrinsic fuel characteristics (e.g., form and particle size, ash and moisture content), combustion systems need to be carefully designed in order to guarantee reliable plant operation and effective emissions control.

Circulating fluidized bed (CFB) systems are particularly well suited for the combustion of low-grade quality fuels due to their high fuel adaptability (i.e., low fuel processing efforts), increased solid residence time, and low pollutant emission. Moreover, CFB units might be applied within the framework of second-generation carbon capture and storage (CCS) processes. Carbon capture technologies collect the CO$_2$ emitted from the flue gases of power stations and industrial sites in order to provide a CO$_2$-rich stream suitable for capture after prior purification and compression. When applied to combustion processes, CCS technologies can be categorized into three groups: pre-combustion, post-combustion, and oxy-fuel. Besides this, the combination of biogenic fuels or fuels with a biogenic share (e.g., SRF) with carbon sequestration techniques enables net negative carbon emissions by

the sequestration of 'biogenic' $CO_2$. This approach is usually referred to as bioenergy with CCS (BECCS), which is gaining increasing popularity as a viable solution to counteract a potential overshoot of $CO_2$ emissions and meet the 2050 zero-carbon emission targets [4–8].

Over the past decades, Calcium Looping (CaL) has rapidly emerged as one of the most attractive second-generation $CO_2$ capture technologies. The CaL process uses natural limestone as a calcium oxide precursor (CaO) for $CO_2$ capture. The solid sorbent is continuously cycled between two interconnected fluidized bed reactors, utilizing the reversible carbonation reaction of CaO and the subsequent calcination of the formed $CaCO_3$ [9,10]. The $CO_2$ contained in the power plant's flue gas is exothermically absorbed by CaO in a carbonator at around 650 °C (see Figure 1). The $CO_2$-depleted flue gas is vented to the environment, whereas the partly-carbonated solids are transferred to a regeneration reactor (i.e., calciner). In the calciner, the $CO_2$ bound in the solid phase is released at around 900 °C. A gas stream highly concentrated in $CO_2$ leaves the regenerator, while the calcined sorbents are returned to the carbonator in order to close the solid loop. The heat required for the endothermic calcination reaction is provided by burning supplementary fuel with oxygen from an air separation unit (i.e., oxy-fuel combustion). The $CO_2$-rich regenerator flue gas can be partly recirculated into the system in order to maintain an appropriate combustion temperature. Due to sorbent deactivation upon cycling, a continuous flow of fresh make-up (i.e., $CaCO_3$) is fed to the process. This make-up flow is compensated by an equivalent sorbent purge in order to avoid the accumulation of inerts in the system (e.g., fuel ash and $CaSO_4$). So far, the CaL process has progressed steadily, being its feasibility demonstrated up to the $MW_{th}$ scale using hard coal, lignite, and alternative fuels [11–15].
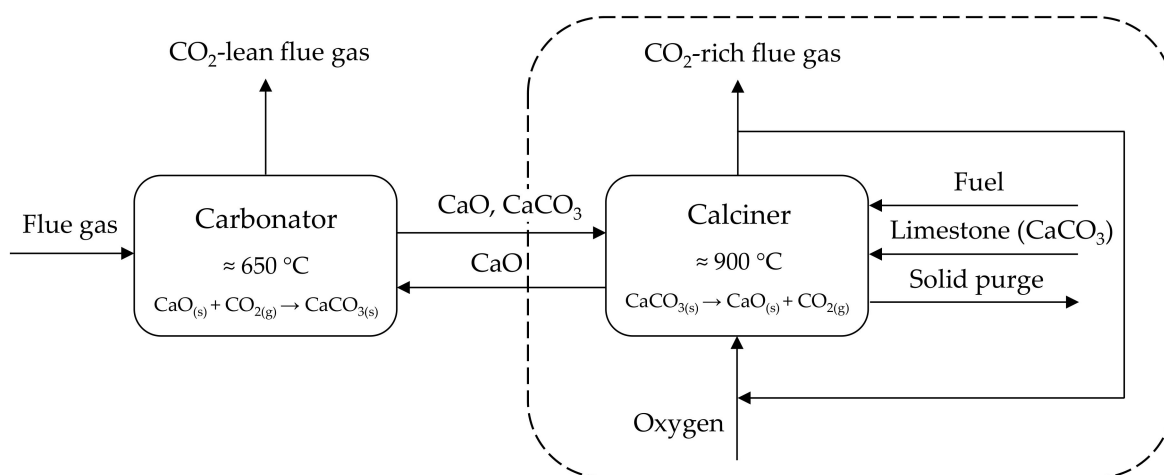


**Figure 1.** Schematic of the Calcium Looping process with the calciner enveloped in a dashed line.

Nitrogen oxides ($NO_x$) are critical components for the sequestration or utilization of $CO_2$, as they may cause corrosion due to the formation of nitric acid during the flue gas compression step [16]. In combustion systems, the main share of $NO_x$ refers to NO, with the balance being $NO_2$ [17]. There are three routes which are responsible for $NO_x$ formation (e.g., thermal, fuel, and prompt) [18]. Generally, CFB boilers are characterized by low $NO_x$ emissions due to the moderate combustion temperatures, which prevent thermal $NO_x$ formation [19,20]. Compared with CFB air combustion systems, the concentration of $NO_x$ in the oxy-fuel case tends to be higher, whereas the specific $NO_x$ conversion per fuel decreases [21]. This is derived from the significant reduction of the combustion flue gas due to the absence of airborne nitrogen. Compared with conventional oxy-fuel combustion, sorbent calcination in a Calcium Looping calciner might lead to enhanced $NO_x$ emissions due to (i) the catalytic effect of CaO on $NO_x$ formation and $N_2O$ decomposition [22], (ii) the elevated temperature required for sorbent regeneration, and (iii) the increased oxygen concentration promoting the oxidation of nitrogen compounds and reducing the amount

of recirculated flue gas [21,23]. While $NO_x$ formation during coal combustion in a CaL regenerator has been widely addressed in the past, much less attention has been devoted to $NO_x$ emissions arising from a CaL calciner employing alternative fuels. To the best of the author's knowledge, there are no published studies which aimed to experimentally investigate the oxy-fuel mono-combustion of a non-woody biomass at a relevant CaL scale (TRL6). Moreover, at the time of writing, only one study has been reported on the investigation of $NO_x$ formation under the stand-alone oxy-fuel combustion of SRF at a semi-industrial scale [24]. In the cited study, Haaf et al. aimed to compare two types of SRF, both under air-firing and oxy-fuel combustion conditions. The authors concluded that the specific NO emissions tend to be lower in the oxy-fuel case for both types of SRF and bed materials (i.e., sand and limestone), which was mainly attributed to the effect of flue gas recirculation during the oxy-fuel case.

Apart from $CO_2$ purity, utility boilers using alternative fuels might suffer severe problems such as slagging, fouling, and corrosion in heat exchangers. During combustion, alkali metals (M) and chloride are easily vaporized and released as alkali chlorides (MCl) into the flue gas. The gaseous alkali chlorides are then converted to alkali sulfates ($M_2SO_4$) through a homogeneous reaction with sulfur oxides and water vapor with or without oxygen (please refer to [25] for more details):

$$2\,MCl + SO_2 + H_2O + 1/2O_2 \rightarrow M_2SO_4 + 2\,HCl \tag{1}$$

$$2\,MCl + SO_3 + H_2O \rightarrow M_2SO_4 + 2\,HCl \tag{2}$$
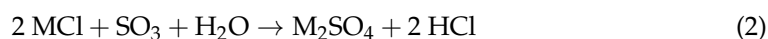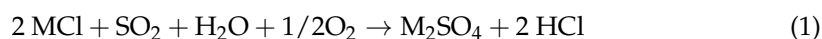
The sulfation of such alkali chlorides releases chlorine as HCl, which is responsible for chlorine-induced high temperature corrosion [26]. In Calcium Looping applications, this problem is overcome to a great extent due to the capacity of limestone to absorb HCl at specific process conditions. The reaction of HCl with limestone in CFB systems is a complex, multi-layered process which mainly depends on the boiler temperature profile, prevailing gas atmosphere, and gas-solid contacting time [27–29]. To date, the absorption of HCl by Ca-species in fluidized beds has been mostly investigated at the laboratory scale [30,31], and only one pilot-scale study has been reported on the investigation of the fate of chlorine under oxy-fuel SRF combustion conditions [13].

The present work investigates the combustion characteristics of hard coal, wheat straw, and SRF under boundary conditions similar to those prevailing in an oxy-fuel CFB calciner of a Calcium Looping cycle. The study focuses on the implications of the fuel (blending) and inlet oxygen concentration on the emissions of $NO_x$ and acidic gases (i.e., $SO_2$ and HCl), as well as on the process hydrodynamics. While $NO_x$ emissions are discussed on the basis of the $CO_2$ purity criteria expected in compression and purification units (CPU), the focus with acidic gases is set on the ability of Calcium Looping solids to retain HCl. Throughout the introduced experiments, the CFB pilot plant demonstrated a high degree of fuel adaptability, allowing for many hours of continuous operation with stable hydrodynamic behavior. The experimental studies were carried out at the 200 $kW_{th}$ CFB pilot plant of the University of Stuttgart, with industrially-relevant process conditions (i.e., recirculated flue gas and technically-pure oxygen).

## 2. Experimental Section

The University of Stuttgart's 200 $kW_{th}$ CaL pilot facility consists of three refractory-lined fluidized bed reactors connected by a solid flow transport system [15,23]. For the experiments involved in this work, the CFB oxy-fuel combustor was used. A schematic of the installation is depicted in Figure 2.
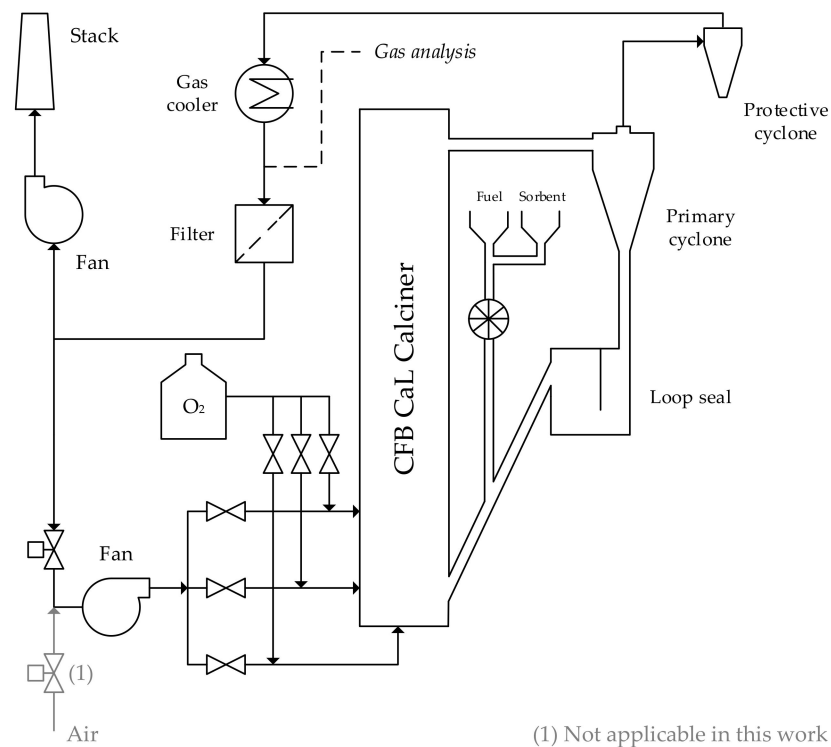
**Figure 2.** Schematic of the 200 kW$_{th}$ Calcium Looping calciner.

The fully refractory lined CFB reactor has an average inner diameter of 200 millimeters and a total height of 10 meters. Sorbent particles are separated from the combustion flue gas in a primary cyclone, and are recirculated back to the reactor riser via a loop seal. The flue gas is then passed through a protective cyclone in order to ensure efficient solid separation before the gas cooler. After cooling the exhaust gas to approximately 180 °C, the gas undergoes particle clean-up in a baghouse filter before it is released to the environment or partly recirculated to the riser inlet. The combustion gas might consist of air, oxygen-enriched air, or recirculated flue gas and technically-pure oxygen. The gas mixture can be fed in three stages for the efficient control of the combustion temperature and pollutant formation. Solids (i.e., fuel and sorbent) are fed into the CFB unit using gravimetrically-controlled screw feeders. Bottom ash might be discharged by a bottom drain valve. Solid samples can be collected from the circulating solids in the loop seal, fly ash, and bottom ash. The flue gas composition is continuously measured by non-dispersive infrared spectroscopy (NDIR) (CO, $CO_2$, $SO_2$, $NO_x$), paramagnetism ($O_2$), and impact jet psychometry ($H_2O$) using online gas analyzers. Furthermore, other gas species of interest (e.g., HCl) can be measured by Fourier-transform infrared spectroscopy (FTIR). The volume fractions of $CO_2$, $O_2$, CO, $SO_2$ and $NO_x$ are continously monitored using an ABB EL 3020, whereas continuous FTIR measurements are achieved using a portable system from Gasmet (DX4000). Gas sampling is conducted according to DIN EN 14792 [32] using a heated candle filter to separate particles from the sample gas, as well as a heated polytetrafluoroethylene (PTFE) hose and a heated pump in order to avoid condensation before the gas measuring unit. The particle filters are periodically cleaned by flushing nitrogen counter-currently. Throughout an experimental campaign, both the NDIR and the paramagnetic $O_2$ sensors are calibrated on a daily basis, and are recalibrated during the day if necessary. Within the first phase of the process, a zero calibration step with pure nitrogen is conducted. Subsequently, the gas analyzers are calibrated through a two-point procedure using gas cylinders of suitable composition. The calibration of the FTIR system is performed externally, and on a yearly basis. The gas sampling frequency is generally 1 s for the ABB EL 3020 and 20 s for the Gasmet DX4000.

The chemical composition ($\gamma_i$) and net calorific value ($H_u$) of the three fuels utilized in this work are introduced in Table 1. These consist of hard coal with a low sulfur content ('La Loma' mine, Colombia), pelletized and non-treated wheat straw (Agrarhandel Müller GbR, Germany), and pelletized SRF produced by steam-treating municipal solid waste (MSW) (ECONWARD, Spain). Table 2 summarizes the chemical composition of the limestone ($x_i$) used in the tests. The limestone type 'Messinghausener Sand 0.1–0.3' was obtained from Lhoist Germany Rheinkalk GmbH.

**Table 1.** Chemical composition ($\gamma_i$) and net calorific value ($H_u$) of the utilized fuels (waf: water and ash free; wf: water free; ad: air dried).

| | $\gamma_C$ | $\gamma_H$ | $\gamma_O$ | $\gamma_N$ | $\gamma_S$ | $\gamma_{Cl}$ | $\gamma_{ash}$ | $\gamma_{H_2O}$ | $H_u$ |
|---|---|---|---|---|---|---|---|---|---|
| | kg/kg, waf | | | | | | kg/kg, wf | kg/kg, ad | MJ/kg, ad |
| Colombian hard coal | 0.776 | 0.052 | 0.145 | 0.016 | 0.011 | 0.000 | 0.091 | 0.019 | 27.5 |
| German wheat straw | 0.497 | 0.066 | 0.425 | 0.010 | 0.001 | 0.001 | 0.059 | 0.081 | 15.6 |
| Spanish SRF | 0.515 | 0.067 | 0.377 | 0.026 | 0.006 | 0.009 | 0.261 | 0.067 | 14.3 |

**Table 2.** Chemical composition ($x_i$) of the utilized sorbent (wf: water free).

| | $x_{CaO}$ | $x_{MgO}$ | $x_{SiO_2}$ | $x_{Al_2O_3}$ | $x_{CO_2}$ | $x_{others}$ |
|---|---|---|---|---|---|---|
| | kg/kg, wf | | | | | |
| German limestone | 0.551 | 0.007 | 0.004 | 0.001 | 0.435 | 0.002 |

## 3. Evaluation Methodology

The concentration of the individual species in the flue gas can be introduced in multiple ways. The two approaches used throughout this publication are briefly explained below:

- $y_i$ in ppmv: the volume fractions of $NO_x$, $SO_2$ and HCl measured in the flue gas at standard temperature and pressure (STP) conditions are presented in parts-per-million. $y_{NO_x}$ and $y_{SO_2}$ are given in dry conditions, whereas $y_{HCl}$ is introduced on a wet basis.
- $e_i$ in mg/MJ$_{th}$: in combustion processes, the emission factor of a gas pollutant '$i$' is commonly described as the mass of pollutant released per unit of fuel burned [33]:

$$e_i = \frac{\dot{M}_i}{\dot{Q}_{th,H_u}} = \frac{\dot{V}_{FG,STP} \cdot y_i \cdot \rho_{n,i}}{H_u \cdot \dot{M}_B} \tag{3}$$

where the mass flow ($\dot{M}_i$) is calculated as the product of the flue gas volume flow in STP conditions ($\dot{V}_{FG,STP}$), and the volume fraction ($y_i$) and standard density ($\rho_{n,i}$) of the desired gas pollutant. The flue gas volume flow is continuously measured using an impeller anemometer, and is accordingly converted to STP conditions. Moreover, $\dot{Q}_{th,H_u}$ represents the thermal duty of a CFB combustor based on the mass flow ($\dot{M}_B$) and net calorific value ($H_u$) of the fuel.

Besides this, it is well known that limestone can absorb HCl under the operation conditions characteristic for fluidized bed boilers. Knowing the outlet volume fraction of HCl in the calciner flue gas, the chlorine retention rate ($\eta_{HCl}$) can be calculated according to Equation (4):

$$\eta_{HCl} = 1 - \frac{\dot{N}_{HCl,FG}}{\dot{N}_{Cl,B}} = 1 - \frac{(\dot{V}_{FG,STP} \cdot y_{HCl,FG} / V_{mn,HCl})}{(\dot{M}_B \cdot \gamma_{Cl,B} / \widetilde{M}_{Cl})} \tag{4}$$

where $\dot{N}_{HCl,FG}$ indicates the molar flow of HCl in the calciner flue gas, defined as the quotient between the product of the flue gas volume flow in STP conditions ($\dot{V}_{FG,STP}$) and the volume fraction of HCl in the exhaust gas ($y_{HCl,FG}$), and the standard molar volume of

HCl ($V_{mn,HCl}$). Furthermore, $\dot{N}_{Cl,B}$ represents the molar flow of chlorine entering the CFB unit, calculated according to the fuel mass flow ($\dot{M}_B$), the mass fraction of chlorine in the fuel ($\gamma_{Cl,B}$), and the molar mass of chlorine ($\widetilde{M}_{Cl}$).

## 4. Results

This study focused on the experimental evaluation of the oxy-fuel combustion characteristics of hard coal, wheat straw, and SRF under boundary conditions similar to those anticipated for the oxy-fuel CFB calciner of a Calcium Looping cycle. The results presented in this work are related to the CFB combustor's performance under different hard coal and biomass blending ratios and inlet oxygen concentrations in the oxidant gas. Additionally, the feasibility of the process under stand-alone SRF combustion is demonstrated. The evaluation of the CaL process concerning the $CO_2$ capture efficiency is out of the scope of this work.

### 4.1. Combustion of Hard Coal and Wheat Straw

Within the first phase of this study, a series of combustion tests were carried out by firing Columbian hard coal and non-woody German biomass (i.e., wheat straw). The effects of the combustion atmosphere and fuel blending ratio were systematically studied, maintaining the overall excess oxygen coefficient roughly constant throughout the tests. The different fuel blending ratios were defined according to the net calorific value of the different fuels, and were subsequently investigated at a similar temperature and oxy-fuel level (i.e., $910 \pm 10$ °C and 25 vol% $O_2$). Additionally, the impact of the inlet oxygen concentration was assessed at a temperature of $910 \pm 10$ °C with 30% biomass blending. Each experiment was conducted for at least 1 h (typically 2 h) under steady-state operating conditions. Moreover, the experiment with the mono-combustion of biomass was conducted for about 9 h, in order to assess the process performance on a longer-term basis.

### 4.1.1. Nitrogen Oxides ($NO_x$)

Figure 3a introduces the specific emission of nitrogen oxides ($e_{NO_x}$) measured during the investigation of four different hard coal and wheat straw combustion experiments. The depicted values refer to the average gas measurements obtained with NDIR and FTIR sensors, both placed at the same location (i.e., the sampling port) of the exhaust gas duct. The error bars represent the standard deviation of the measured value range.
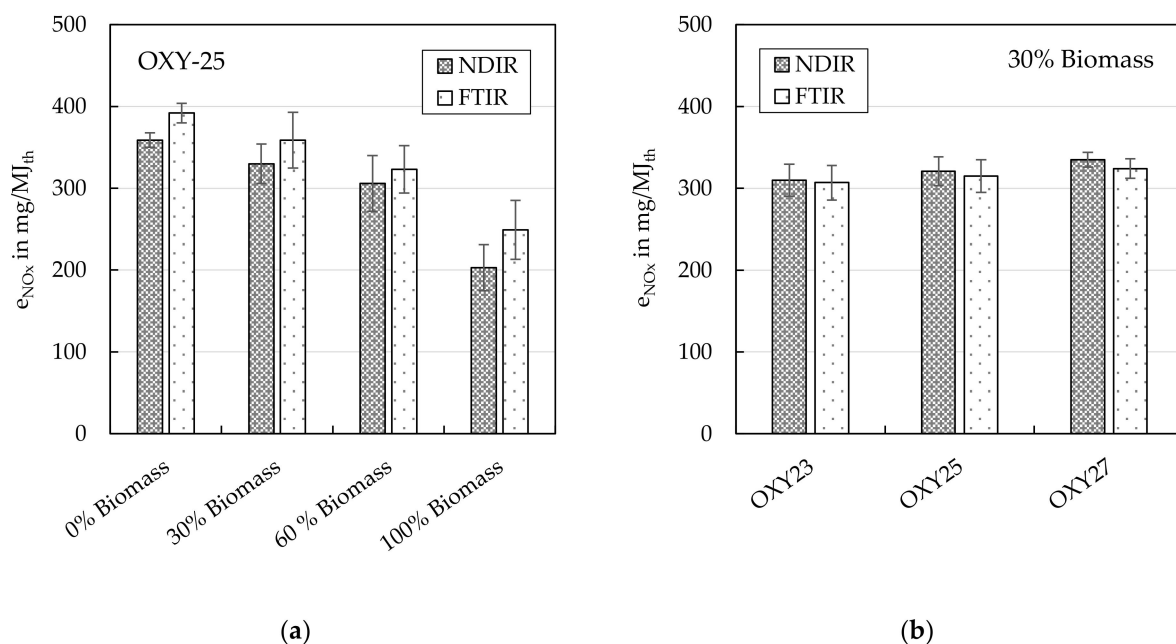


(**a**)  (**b**)

**Figure 3.** Specific $NO_x$ emissions ($e_{NO_x}$) as a function of the biomass share ratio (**a**) and the oxy-fuel case (**b**).

According to the NDIR results, the specific $NO_x$ levels ranged from 359 mg/$MJ_{th}$ during combustion with 100% hard coal down to 203 mg/$MJ_{th}$ with stand-alone biomass firing. As the fuel–$NO_x$ formation mechanism is the dominating route under CFB conditions [34], this decrease can be ascribed to the reduced nitrogen content of the wheat straw (1.0 wt%$_{waf}$) when compared to the fuel-N contained in the hard coal (1.6 wt%$_{waf}$). This explanation is in line with the conclusions drawn by Riaza et al., who evaluated the NO emissions of blends of two distinct coal types with 10 wt% and 20 wt% olive waste under oxy-fuel conditions [35]. Riaza et al. concluded that the NO concentrations under an oxy-fuel atmosphere of both coals decreased after the addition of biomass, and reported an enhanced decrease as the biomass share was raised. Moreover, Figure 3b shows the specific $NO_x$ emissions measured at different oxy-fuel levels under 30% biomass blending. From left to right, the depicted oxy-fuel cases correspond to inlet calciner dry oxygen concentrations of 23 vol%, 25 vol%, and 27 vol%, respectively. As no active cooling could be applied throughout the tests, the maximum attainable oxy-fuel case was limited by the target process temperature. Hence, an inlet oxygen concentration of 27 vol% was found to be the maximum in order to keep the desired reactor temperature of 910 °C. Moreover—as an attempt of maximizing the operating range—a minimum oxy-fuel case of 23 vol% was established. Furthermore, an oxy-fuel case of 25 vol% was evaluated for comparative purposes. The three different oxy-fuel cases in this study were established by adjusting the amount of recirculated flue gas. As the CFB calciner was operated under pure oxy-fuel combustion conditions, the air valve depicted in Figure 2 was kept closed during the tests. Within the investigated oxy-fuel range, the increased inlet oxygen concentrations led to slightly higher $NO_x$ emissions (see Figure 3b). More precisely, an increase in the inlet oxygen volume fraction of about four percentage points caused a marginal increase in the specific $NO_x$ NDIR emissions from 310 mg/$MJ_{th}$ up to 335 mg/$MJ_{th}$. Providing a uniform temperature distribution along the reactor, the promoting effect of the inlet oxygen on $NO_x$ emissions can be typically attributed to (i) the increased oxygen concentration intensifying the oxidation of the nitrogen components in the fuel [21,34], and (ii) the reduction in the flue gas recirculation rate causing the reducing zone of the calciner to be decreased [21]. However, within the relatively narrow investigated oxy-fuel range, it cannot be excluded that such deviations were, at least, partly attributable to fuel-N variations other than the aforementioned two reasons. In any case, the high $NO_x$ emissions achieved in the CFB combustor operating at CaL calciner conditions will most certainly require an $NO_x$ removal step before the $CO_2$ processing unit, depending on the required $CO_2$ specifications. Nevertheless, $NO_x$ can be easily removed during compression in the CPU [16]. Elevated pressure favors the conversion from $NO_x$ to $NO_2$, and $NO_2$ holds a high solubility, allowing it to form nitric acid by dissolving $NO_2$ in water after compression at around 30 bar in a dedicated contact column.

### 4.1.2. Acidic Gases ($SO_2$ and HCl)

The acidic gases emitted from combustion units may play a role in the corrosion of boiler components. In situ sulfur and halogen capture by limestone is one of the most important advantages of fluidized bed combustion (FBC). The use of a calcium-based sorbent (e.g., limestone) in fluidized bed boilers to reduce $SO_2$ emissions is a well-established technique. Limestone is introduced into the fluidized bed combustor at temperatures between 800 and 925°C, at which limestone is rapidly calcined to porous CaO, which can subsequently react with $SO_2$ to form calcium sulfite and calcium sulfate [36]. Furthermore, the addition of limestone can capture hydrogen chloride (HCl) to form liquid or solid phase calcium chloride under the relatively low combustion temperatures used in an FBC system [29]. The absorption of HCl by limestone can subsequently suppress the corrosion of heat exchanger tubes caused by chloride components, particularly when firing municipal solid waste or fuels with a high chlorine content. In Calcium Looping applications, both $SO_2$ and HCl are strongly suppressed due to (i) operation in a very favorable absorption temperature window [27,36] and (ii) an exceptionally high supply of calcium. The supply

of calcium which is available for $SO_2$ and HCl absorption is several magnitudes higher than that generally foreseen to remove $SO_2$ [25] and HCl [37] in fluidized bed combustion systems, yielding an almost sulfur- and chlorine-free flue gas.

Figure 4 depicts the specific emissions of $SO_2$ ($e_{SO_2}$) as a function of the biomass substitution ratio (graph a) and the oxy-fuel level applied (graph b). According to Figure 4a, there is a slight tendency in $SO_2$ emissions to decrease with increasing biomass substitution. Such a decreasing trend can be explained by (i) the significantly lower sulfur content of the wheat straw (0.001 wt%$_{waf}$) compared with that of the hard coal (0.011 wt%$_{waf}$), and (ii) the (partial) sulfation of alkali metal species contained in the fuel. Still, the decreasing tendency of $e_{SO_2}$ in Figure 4a can be regarded as marginal. Because the thermal input to the reactor was maintained between the different tests, the stable behavior of $e_{SO_2}$ can be ascribed to the mostly-constant $SO_2$ concentrations measured in the flue gas, which ranged between 1.9 mg/MJ$_{th}$ and 2 mg/MJ$_{th}$ (i.e., 3 ppmv) as a result of the very effective desulphurization rate achieved by the wide limestone availability ($\eta_{SO_2} > 99$ %). As far as the inlet oxygen concentration is concerned, it has been postulated that specific $SO_2$ emissions tend to be promoted in higher oxy-fuel cases [21,38]. However, the results obtained in this work (see Figure 4b) introduce a rather constant behavior of $e_{SO_2}$ with increasing inlet $O_2$ as a result of the very effective in-situ flue gas desulphurization. With marginal differences between the investigated cases, $e_{SO_2}$ averaged at 2 mg/MJ$_{th}$.
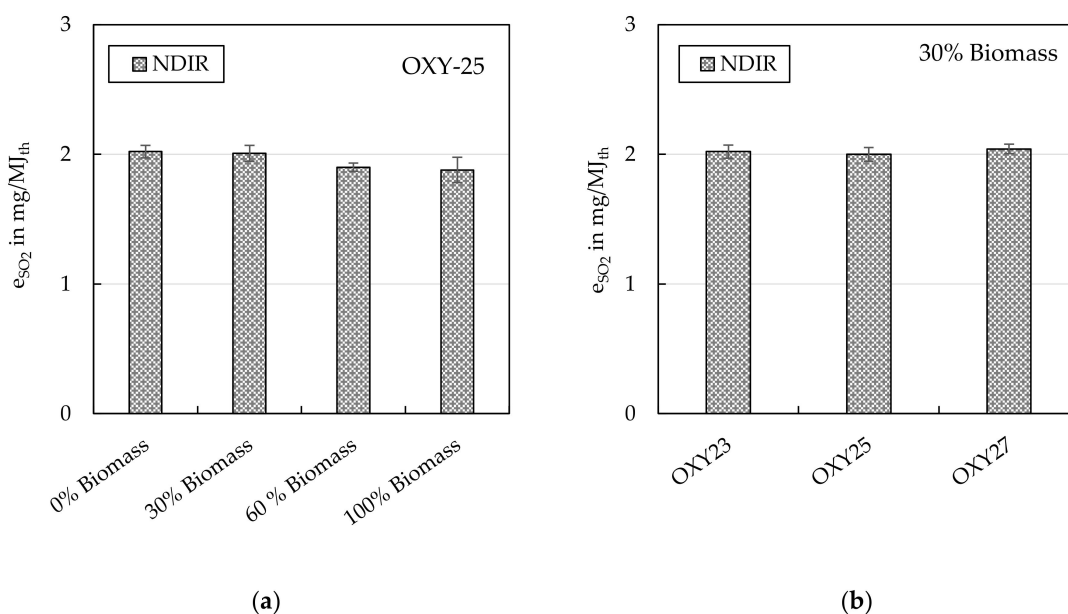


|     |     |
| :-: | :-: |
| (**a**) | (**b**) |

**Figure 4.** Specific $SO_2$ emissions ($e_{SO_2}$) as a function of the biomass share ratio (**a**) and the oxy-fuel case (**b**).

Figure 5 introduces the specific emissions of HCl ($e_{HCl}$) as a function of the biomass blending ratio (graph a) and the oxy-fuel level (graph b). According to Figure 5a, the specific HCl emissions increased from 1.8 mg/MJ$_{th}$, when no wheat straw was fired, up to 3.9 mg/MJ$_{th}$, with the mono-combustion of biomass. Here, as well, the explanation lies in the chlorine content of the fuels. Because the chlorine content in the biomass (0.1 wt%$_{waf}$) is considerably higher than that in the hard coal (0.02 wt%$_{waf}$), blending biomass increases the total chlorine content of the combusted fuel mix. These observations correlate well with the conclusions drawn by Wolf et al., who reported constantly-increasing HCl concentrations with growing shares of biomass when investigating the effect of the co-combustion of bituminous coal and straw in a CFB boiler [39]. Moreover, Figure 5b indicates a marginal increase in the specific HCl emissions during operation at higher inlet oxygen concentrations. However, as HCl is not an oxidation product, this behavior must be attributed to slight differences in the mass flow rates of hard coal and wheat straw between the tests.
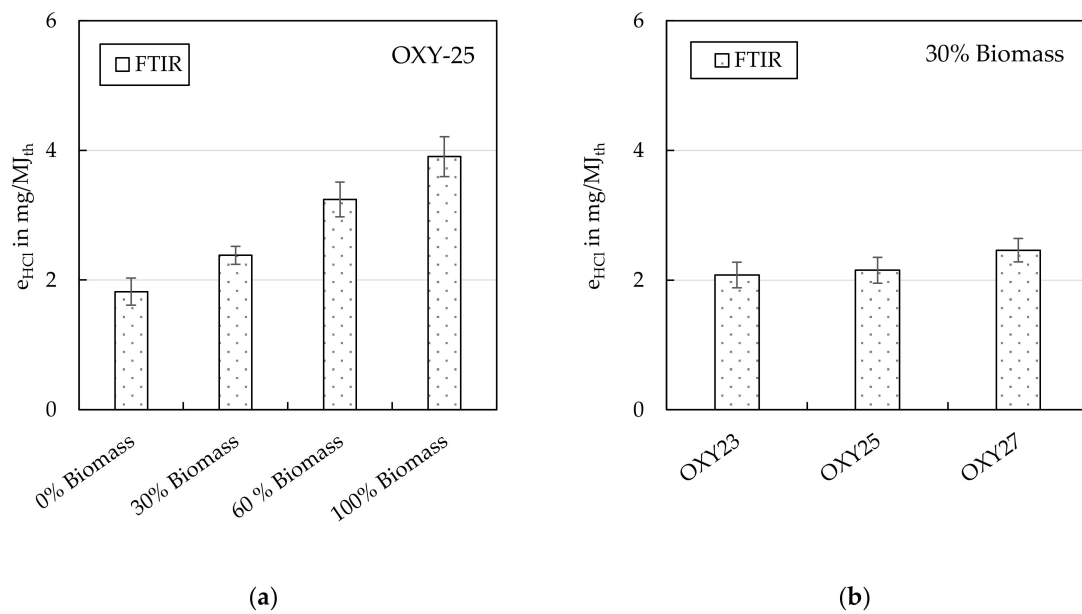
**Figure 5.** Specific HCl emissions ($e_{HCl}$) as a function of the biomass share ratio (**a**) and the oxy-fuel case (**b**).

Besides this, the relatively low specific HCl emissions introduced in this study are greatly influenced by the capability of limestone to absorb HCl under specific Calcium Looping conditions. As anticipated previously, limestone can provide the efficient retention of $SO_2$ and HCl despite having different temperature regimes. Some authors have investigated the competitive mechanism between the sulfation and chlorination of calcined limestone, suggesting that the $SO_2$ retention efficiency is markedly promoted in the presence of HCl, while the concurrent chlorination reaction is suppressed [29,40]. As shown in Figures 4 and 5, both $SO_2$ and HCl emissions are strongly inhibited by the high calcium availability in the CFB calciner, which makes it difficult to provide a thorough assessment of the interaction between $SO_2$ and HCl in the system. Nonetheless, and recalling the capability of Calcium Looping solids to absorb hydrogen chloride, it is of practical interest to look into the chlorine retention rate achieved in each experiment (see Figure 6).
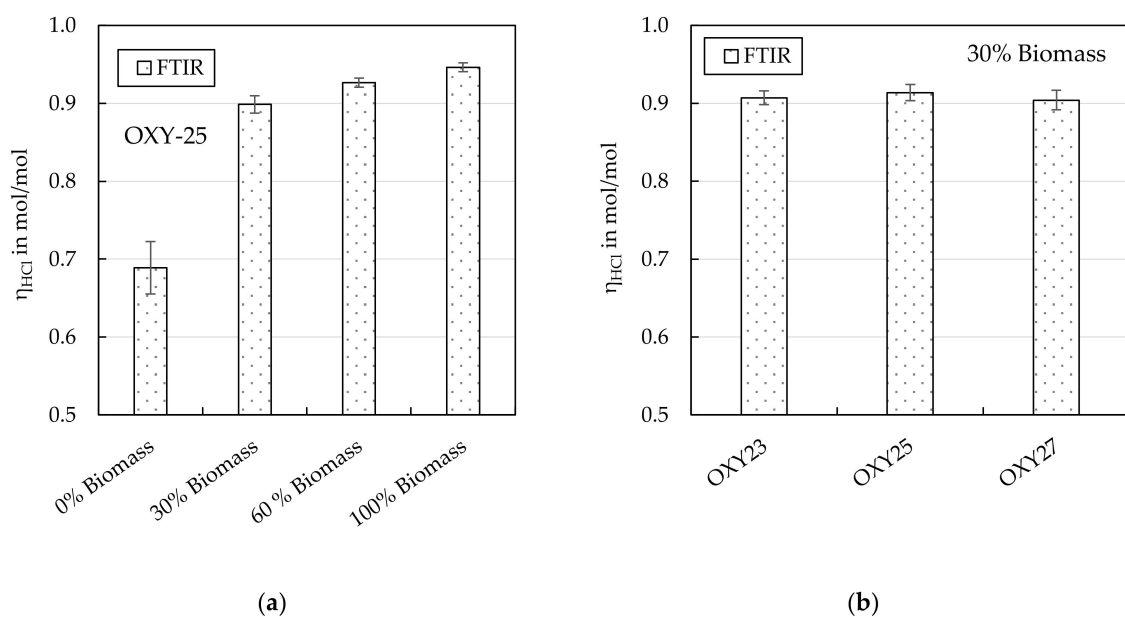


**Figure 6.** HCl retention rate ($\eta_{HCl}$) as a function of the biomass share ratio (**a**) and the oxy-fuel case (**b**).

Figure 6a displays the average chlorine retention rate ($\eta_{HCl}$) calculated for all of the investigated fuel blending experiments. $\eta_{HCl}$ averaged at 0.68 mol/mol during the stand-alone hard coal combustion, whereas 0.95 mol/mol was yielded during the mono-combustion of biomass. The comparatively high HCl retention efficiency achieved in the presence of biomass is presumably attributable to the increased content of alkali metal vapors, which can lead to more condensation nuclei during combustion and hence a higher absorption surface (i.e., limestone and/or ash) than pure hard coal combustion [41]. As can be observed in Figure 6a, chlorine retention rates above 0.90 mol/mol were obtained with at least 30% biomass substitution. The retention rate of HCl by limestone was also evaluated by Haaf et al. in a recent publication [13]. Haaf et al. investigated the mono-combustion of two SRF types at different temperatures in the calciner, and they reported retention values over 0.90 mol/mol for most of the conducted experiments. Moreover, the authors postulated that minimum calciner temperatures of around 860 °C are desirable to maximize chlorine retention ($\eta_{HCl}$ > 0.90 mol/mol). Besides this, Figure 6b displays the marginal influence of the inlet oxygen concentration on the chlorine retention rate. Similarly to Figure 5b, this behavior can be attributed to slight differences in the respective coal and wheat straw flow rates, as HCl formation is not favored by the oxidizing atmosphere. Furthermore, it is true that HCl can react with $O_2$ under excessive oxygen atmospheres, releasing chlorine and water vapor according to the exothermic Deacon reaction [40]. Nevertheless, this latter effect was assumed to play a minor role in the present study, in which the high calciner temperatures will cause the equilibrium to move towards the reactants, which will lower the conversion of HCl to $Cl_2$. In view of the last results, it can be concluded that a Calcium Looping calciner can provide an appropriate framework for the reduction of HCl emissions originated by supplementary fuel combustion, lessening the associated impacts on equipment corrosion and the formation of polychlorinated dioxins and furans [42].

### 4.1.3. Reactor Profiles

Figure 7 shows the temperature (graphs a and c) and pressure (graphs b and d) profiles along the CFB riser for the different fuel blending and oxy-fuel cases investigated in this work. The riser height refers to the wind box nozzle top located at 0 m. Generally, the characteristics of the temperature profiles obtained for the different biomass share ratios correlate well with each other, showing average reference riser temperatures (i.e., 7.5 m) in the range of 914 to 918 °C (see Figure 7a). Besides this, while the temperature distributions obtained for 0%, 30%, and 60% biomass shares in the bottom section are comparable with each other, minor deviations were introduced at 100% biomass operation. The observed effect is attributed to the very distinct volatile matter of the hard coal (38.1 wt%$_{wf}$) and the biomass (76.6 wt%$_{wf}$). Like solid carbon, volatile components are not retained in the dense phase, which means that a major portion of the combustion reaction is taking place in the upper reactor zone. In consequence, wheat straw promotes high temperatures in the upper part and lower temperatures in the bottom section. Besides this, the temperature profiles observed during the investigation of the different oxy-fuel levels introduce the effect of increased oxygen addition (see Figure 7c). In order to evaluate this aspect, it is necessary to compare the gradual temperature increase observed between the lowest point where the oxidant is introduced (i.e., 0.25 m), and the height at which all of the oxidant has been added and adequately mixed (i.e., 5.5 m). After the subsequent comparison, temperature differences of 43 °C, 65 °C, and 68 °C were obtained for inlet oxygen concentrations of 23 vol%, 25 vol% and 27 vol%, respectively. As the fuel flow rate was kept constant between the tests, such temperature differences can be ascribed to an enhanced combustion thermal output arising from an increased inlet oxygen concentration. Despite the introduced deviations, the temperature profiles observed during the investigation of the diverse fuel blending and oxy-fuel experiments are smooth, and resemble a typical CFB combustor's uniform behavior without the presence of hot spots [23,43]. The influence of biomass co-firing on the CFB system's hydrodynamics can be observed in Figure 7b. The measured

pressure drop of the riser during biomass mono-combustion averaged at 40 mbar, which deviates considerably from the average value (i.e., 14 mbar) observed when no biomass was co-fired. For 100% biomass combustion, the pressure increases sharply in the dense zone, while above that, the decrease of the pressure blunts. Similarly to Figure 7a, this behavior can be ascribed to the higher amount of volatile matter contained in the biomass [44]. The increased volatile content of the wheat straw presumably causes a segregation in the solids along the reactor height, in which the reactor hydrodynamics range from the superposition of a bubble bed formed by coarser particles in the lower region, over a turbulent middle section with smaller particles, to a fast bed formed by fine particles in the upper part. Apart from this, it should not be ignored that the mono-combustion of biomass was investigated for 9 h of continuous operation. During this time, no material was drained from the system. Therefore, the described pressure increase can also be attributed, at least partially, to the effect of ash accumulation. Increased oxygen inlet concentrations did not have a significant influence on the pressure difference across the CFB riser (see Figure 7d). The pressure drop observed along the bed is very similar for all three investigated oxy-fuel cases, and indicates the absence of bed agglomeration effects.
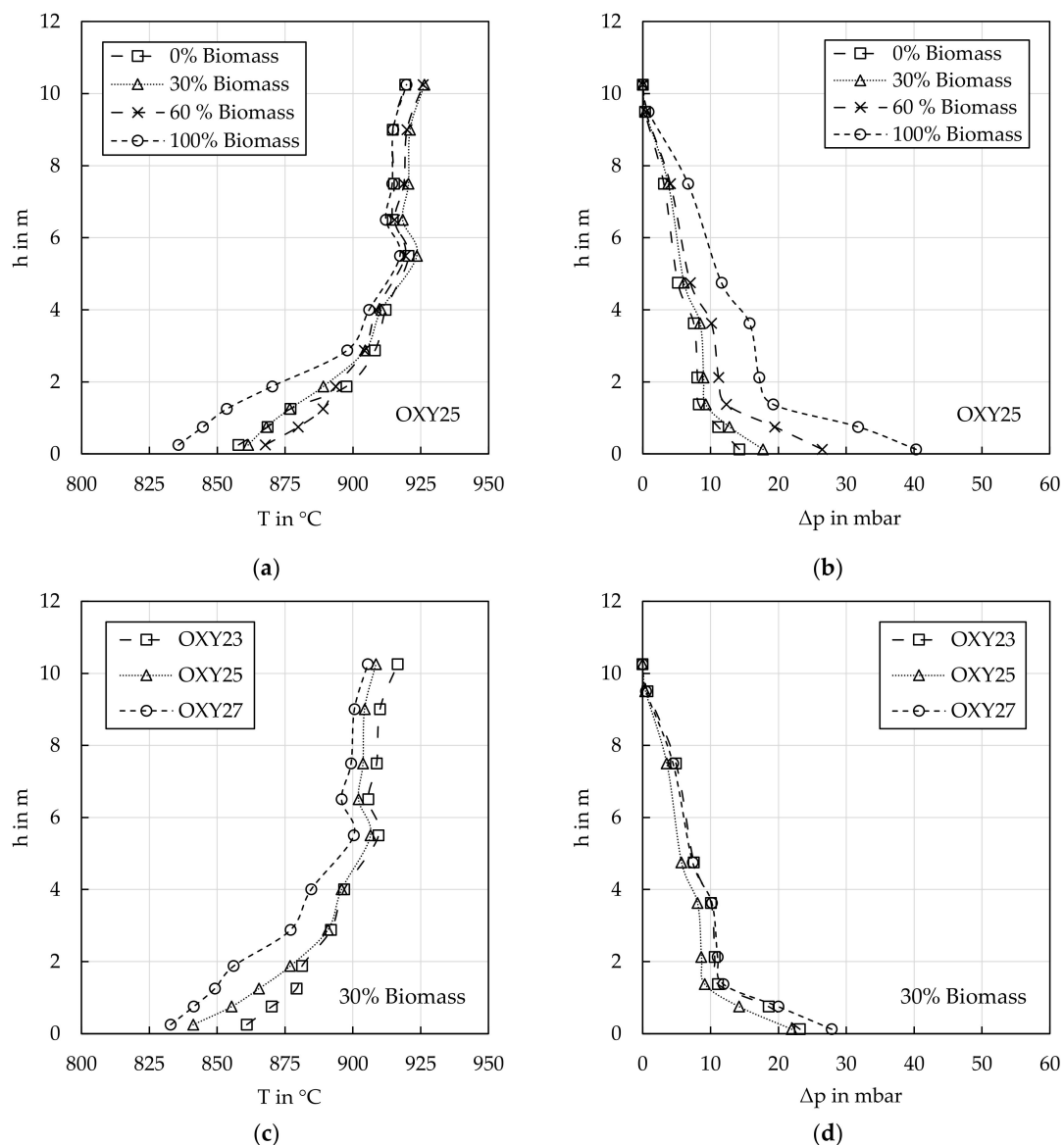


**Figure 7.** Calciner temperature (**a,c**) and pressure (**b,d**) profiles measured during the investigation of different fuel blending ratios and oxy-fuel cases.

### 4.2. Mono-Combustion of SRF

The overall goal of the following experiment was to demonstrate the feasibility of continuous and stable oxy-fuel SRF mono-combustion as a supplementary heat source in the CFB calciner. Table 3 provides an overview of the operating conditions throughout the experimental test. Generally, the selected conditions were similar to those defined for the investigation of the hard coal and biomass co-firing experiments, except for the combustion temperature. A technical limitation in the fuel dosing system constrained the maximum attainable temperature in the riser to approximately 865 °C. Accordingly, a reactor temperature of 850 °C was defined, aiming at exploiting the boundary conditions prevailing in municipal solid waste incinerators [45]. Of course, from the CaL sorbent calcination standpoint, temperatures above 900 °C are usually required to achieve efficient sorbent regeneration. In the 200 kW$_{th}$ CFB calciner, this inconvenience can still be overcome due to the dilution of the $CO_2$ product stream in the reactor required for practical reasons, such as the flushing of pressure transducers, loop seal fluidization, and sealing purposes in the fuel feeding system. Hence, a sufficient sorbent calcination is feasible even at a calciner operation temperature in the range of 835 to 852 °C. The evolution of SRF stand-alone combustion is introduced in Figure 8. The left y-axis refers to the gas volume fractions of NO$_x$ ($y_{NO_x}$), HCl ($y_{HCl}$), and SO$_2$ ($y_{SO_2}$), whereas the right y-axis shows the average riser temperature ($T$). The experimental time ($t$) is depicted in the x-axis.

**Table 3.** Experimental range of the operating conditions.

| Parameter | Symbol | Value/Range | Unit |
|---|---|---|---|
| Temperature | $T$ | 835–852 | °C |
| Thermal input | $\dot{Q}_{th}$ | 93–112 | kW$_{th}$ |
| Superficial gas velocity | $u_0$ | 3.9–4.1 | m/s |
| Solid inventory | $W_s$ | 971–1479 | kg/m$^2$ |
| O$_2$ inlet volume fraction | $y_{O_2,in}$ | 0.21–0.22 | m$^3$/m$^3$ |
| Experimental duration | $t$ | 3.5 | h |
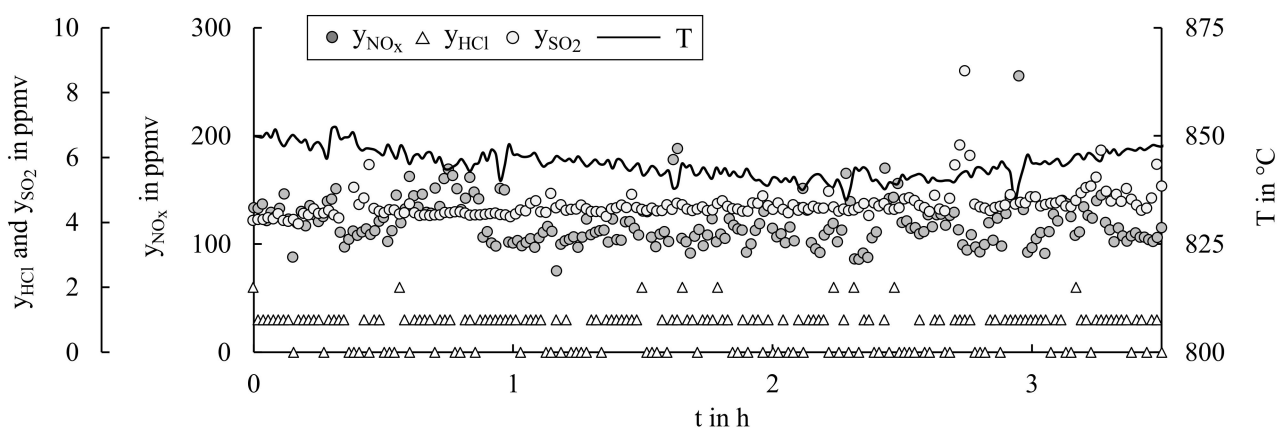


**Figure 8.** Volume fractions of NO$_x$ ($y_{NO_x}$), HCl ($y_{HCl}$), SO$_2$ ($y_{SO_2}$), and temperature ($T$) against time ($t$) during solid recovered fuel mono-combustion. $y_{NO_x}$ and $y_{SO_2}$ were measured by non-dispersive infrared spectroscopy; $y_{HCl}$ was measured by Fourier-transform infrared spectroscopy.

During the investigated period, the inlet oxygen concentration was close to 0.22 m$^3$/m$^3$. The oxygen excess at the calciner outlet was between 0.03 and 0.10 m$^3$/m$^3$, and averaged at 0.06 m$^3$/m$^3$ (on a dry basis). This relatively large oxygen excess was required in order to ensure the adequate burnout of the SRF. The thermal duty throughout the test averaged at 102 kW$_{th}$, and was similar to those investigated during the diverse co-firing experiments. The temperature fluctuations of the calciner were mainly caused by the inhomogeneous nature of the SRF. Moreover, several peaks can be observed roughly every 30 min, which

were ascribed to punctual irregularities in the fuel mass flow every time the dosing tank was re-filled. As can be observed, this effect did not have any significant influence on the stable and uniform evolution of the investigated gas species. HCl volume fractions up to 2 ppmv were measured downstream of the calciner, yielding an almost chlorine-free exhaust gas. The very low measured HCl concentrations in combination with the increased chlorine content of the SRF led to exceptionally high chlorine retention rates in the system, which yielded around 0.999 mol/mol. The $SO_2$ and $NO_x$ concentrations showed a stable evolution throughout the test, and averaged at 4 ppmv and 127 ppmv, respectively. The minor fluctuations observed in Figure 8 are explained by side-effects caused by the re-filling of the fuel dosing unit (i.e., punctual changes in the excess oxygen level). Due to substantial differences in the combustion temperature, the $NO_x$ concentrations displayed in Figure 8 cannot be directly referred to the trends obtained from the co-firing of hard coal and biomass. Nonetheless, the results introduced in this section are in line with the NO concentrations measured by Haaf et al. [13], considering the slight variations of the fuel composition and in the range of experimental conditions set for the respective tests.

Figure 9 shows the reactor temperature and pressure profiles measured during the mono-combustion of SRF. Similarly to Figure 7, the depicted temperature gradient is smooth, and resembles the operation of a typical CFB combustor (see Figure 9a). This is characterized by stable temperatures in the upper part and a gradual temperature increase in the bottom region. On the other hand, the solid induced pressure drop over the riser increased notably in the course of the experiment (see Figure 9b). More precisely, at the beginning of the test ($t$=0 h), the riser pressure drop was about 93 mbar, whereas this value averaged at 125 mbar after 3 h of continuous operation. Similarly to the mono-combustion of wheat straw, the depicted experiment was conducted without draining any solid bed material from the riser. Therefore, the increased bed pressure observed in this case can be attributed to ash accumulation effects. Moreover, the reactor pressure drops measured during the SRF mono-combustion were significantly higher than the differential riser pressures achieved during the investigation of the different biomass share ratios (see Figure 7b). This behavior can be explained by the different ash contents of the fuels. As introduced in Table 1, the ash content of the SRF (26.1 wt%$_{wf}$) is considerably higher than the mass fraction of ash contained in the hard coal (9.1 wt%$_{wf}$) and in the biomass (5.9 wt%$_{wf}$). In any case, and in line with the observations made from the stand-alone biomass combustion, ash accumulation was found not to be a limiting aspect in this case either, and the CFB calciner was able to be fired with SRF under realistic oxy-fuel combustion conditions for several hours of continuous operation. Still, ash accumulation and agglomeration might constitute a major challenge for the stable and long term operation of industrial CFB boilers employing alternative fuels [46]. The common proposed measures to counteract ash-related issues include (i) operation at lower process temperatures, when possible; (ii) the dilution or renewal of the bed material; (iii) operation at increased fluidization velocities; and (iv) the incorporation of additives (e.g., kaolin). Furthermore, a reliable online monitoring system for the detection of early stages of ash-induced problems is crucial for the successful implementation of all of these measures [47]. However, the application of the proposed actions is not straightforward, as they need to be balanced by the criteria of CFB combustion efficiency and pollutant emission. In consequence, further investigation is still needed to cope with various challenges associated with ash accumulation effects.
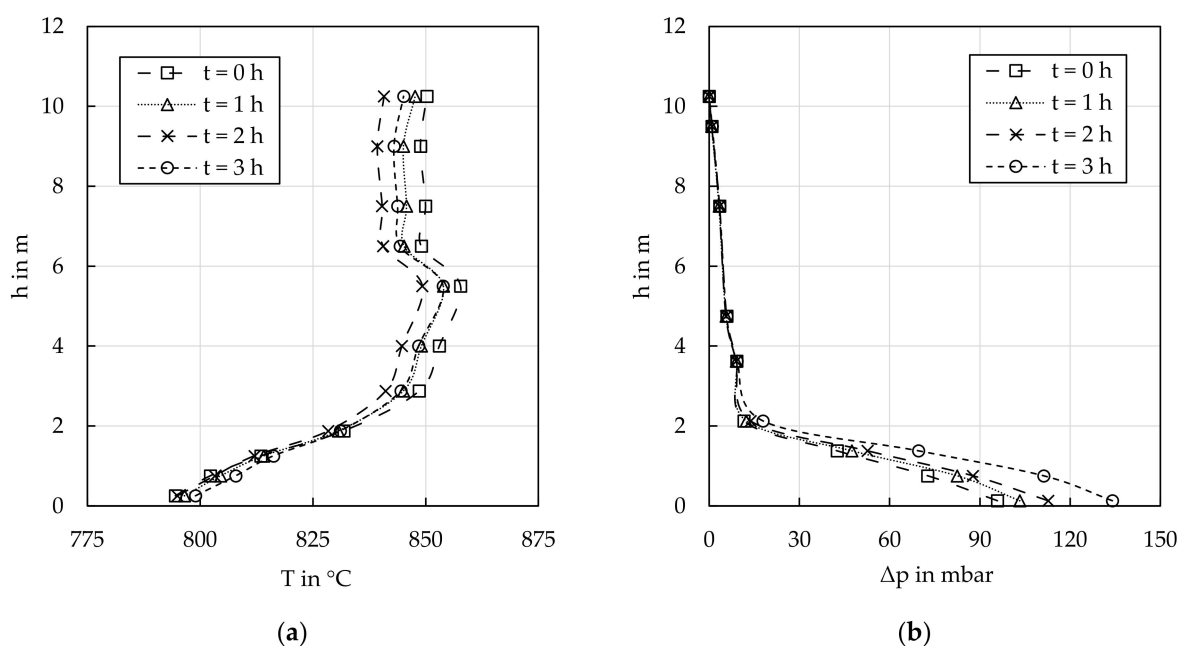
**Figure 9.** Calciner temperature (**a**) and pressure (**b**) profiles measured during solid recovered fuel mono-combustion.

## 5. Conclusions

In this work, the oxy-fuel combustion of hard coal, wheat straw, and solid recovered fuel was assessed at a semi-industrial 200 kW$_{th}$ CFB test facility, under boundary conditions prevailing in the calciner of a CaL process. In the course of the pilot testing (of about 43 h), a wide range of experimental conditions were established. The fuel blending ratio and the inlet oxygen concentration were varied in order to derive implications about gaseous emissions of NO$_x$ and acidic species such as SO$_2$ and HCl, as well as temperature and pressure reactor profiles. Fuel blending was found to hardly influence the pollution formation process. Nonetheless, biomass substitution directly affected the pollutant emissions by modifying the fuel mixture's nitrogen and chlorine content. HCl specific emissions were significantly reduced by the presence of Ca-species in the calciner, yielding chlorine retention rates above 0.90 mol/mol for all of the investigated experiments with biomass substitution. Moreover, the high NO$_x$ emissions achieved in the CaL calciner will most certainly require a NO$_x$ removal step before the CPU, depending on the required CO$_2$ specifications. The pilot reactor's temperature profile resembled the typical pattern described by conventional CFB units with no hot spots. Ash accumulation was found to significantly increase the pressure drop along the reactor not only at high biomass substitution rates but also during the mono-combustion of SRF. For the experiments in this study, the increased riser differential pressure was not a limiting aspect. Nevertheless, ash accumulation still constitutes a key challenge to be addressed in fluidized beds employing low-grade quality fuels in order to ensure reliable and long-term plant operation in novel CCS applications.

**Author Contributions:** Conceptualization, J.M.; methodology, J.M.; formal analysis, J.M.; investigation, J.M.; data curation, J.M.; writing—original draft preparation, J.M.; writing—review and editing, M.H., M.S. and G.S.; supervision, G.S. All authors have read and agreed to the published version of the manuscript.

**Conflicts of Interest:** The authors declare no conflict of interest.

## Abbreviations

| | |
|---|---|
| ad | air dried |
| B | fuel |
| BECCS | bio-energy with CCS |
| CaL | calcium looping |
| CCS | carbon capture and storage |
| CFB | circulating fluidized bed |
| CPU | compression and purification unit |
| FBC | fluidized bed combustion |
| FG | flue gas |
| FTIR | fourier-transform infrared spectroscopy |
| MSW | municipal solid waste |
| NDIR | non-dispersive infrared spectroscopy |
| PTFE | polytetrafluoroethylene |
| SRF | solid recovered fuel |
| STP | standard temperature and pressure |
| th | thermal |
| waf | water and ash free |
| wf | water free |

## Symbols

| | |
|---|---|
| $e_i$ | emission factor of gas component $i$ (mg/MJ$_{th}$) |
| $h$ | height (m) |
| $H_u$ | net calorific value (MJ/kg) |
| $\dot{M}$ | mass flow (kg/h or kg/s) |
| $\widetilde{M}_i$ | molar mass of component $i$ (kg/kmol) |
| $\dot{N}$ | molar flow (kmol/h or kmol/s) |
| $\Delta p$ | differential pressure (mbar) |
| $\dot{Q}$ | heat flow (kW) |
| $T$ | temperature (°C) |
| $t$ | time, experimental duration (h) |
| $u_0$ | superficial gas velocity (m/s) |
| $\dot{V}$ | volume gas flow (m$^3$/h) |
| $V_{mn}$ | standard molar volume (22.4 l/mol) |
| $W_s$ | cross-sectional area based solid inventory (kg/m$^2$) |
| $x_i$ | mass fraction of component $i$ (kg/kg) |
| $y_i$ | outlet gas volume fraction of component $i$ (ppmv) |
| $y_{i,in}$ | inlet gas volume fraction of component $i$ (m$^3$/m$^3$) |
| $\eta_i$ | retention rate of component $i$ (mol/mol) |
| $\gamma_i$ | fuel mass fraction of component $i$ (kg/kg) |
| $\rho_{n,i}$ | standard density of component $i$ (kg/m$^3$) |

## References

1. RAL-GZ 724. *Sekundärbrennstoffe-Gütesicherung*; RAL Deutsches Institut für Gütesicherung und Kennzeichnung e. V.: Münster, Germany, 2012.
2. Sarc, R.; Lorber, K.E.; Pomberger, R. Manufacturing of Solid Recovered Fuels (SRF) for Energy Recovery Processes. *Waste Manag.* **2016**, *6*, 401–416.
3. Iacovidou, E.; Hahladakis, J.; Deans, I.; Velis, C.; Purnell, P. Technical properties of biomass and solid recovered fuel (SRF) co-fired with coal: Impact on multi-dimensional resource recovery value. *Waste Manag.* **2018**, *73*, 535–545. [CrossRef] [PubMed]
4. United Nations Treaty Collection. *The Paris Agreement*; Chapter XXVII 7 d; United Nations Framework Convention on Climate Change (UNFCCC): Paris, France, 2015.
5. Bui, M.; Fajardy, M.; Mac Dowell, N. Thermodynamic Evaluation of Carbon Negative Power Generation: Bio-energy CCS (BECCS). *Energy Procedia* **2017**, *114*, 6010–6020. [CrossRef]
6. Gough, C.; Upham, P. Biomass energy with carbon capture and storage (BECCS or Bio-CCS). *Greenh. Gases Sci. Technol.* **2011**, *1*, 324–334. [CrossRef]
7. Ditaranto, M.; Becidan, M.; Stuen, J. Opportunities for CO$_2$ Capture in the Waste-to-Energy Sector. *Waste Manag.* **2019**, *9*, 319–328.

8.　Wienchol, P.; Szlęk, A.; Ditaranto, M. Waste-to-energy technology integrated with carbon capture—Challenges and opportunities. *Energy* **2020**, *198*, 117352. [CrossRef]

9.　Shimizu, T.; Hirama, T.; Hosoda, H.; Kitano, K.; Inagaki, M.; Tejima, K. A Twin Fluid-Bed Reactor for Removal of $CO_2$ from Combustion Processes. *Chem. Eng. Res. Des.* **1999**, *77*, 62–68. [CrossRef]

10.　Abanades, J.C.; Anthony, E.J.; Wang, J.; Oakey, J.E. Fluidized Bed Combustion Systems Integrating $CO_2$ Capture with CaO. *Environ. Sci. Technol.* **2005**, *39*, 2861–2866. [CrossRef] [PubMed]

11.　Haaf, M.; Hilz, J.; Peters, J.; Unger, A.; Ströhle, J.; Epple, B. Operation of a 1 $MW_{th}$ calcium looping pilot plant firing waste-derived fuels in the calciner. *Powder Technol.* **2020**, *372*, 267–274. [CrossRef]

12.　Arias, B.; Diego, M.; Abanades, J.; Lorenzo, M.; Diaz, L.; Martínez, D.; Alvarez, J.; Sánchez-Biezma, A. Demonstration of steady state $CO_2$ capture in a 1.7$MW_{th}$ calcium looping pilot. *Int. J. Greenh. Gas Control.* **2013**, *18*, 237–245. [CrossRef]

13.　Haaf, M.; Peters, J.; Hilz, J.; Unger, A.; Ströhle, J.; Epple, B. Combustion of solid recovered fuels within the calcium looping process—Experimental demonstration at 1 $MW_{th}$ scale. *Exp. Therm. Fluid Sci.* **2020**, *113*, 110023. [CrossRef]

14.　Vorrias, I.; Atsonios, K.; Nikolopoulos, A.; Nikolopoulos, N.; Grammelis, P.; Kakaras, E. Calcium looping for $CO_2$ capture from a lignite fired power plant. *Fuel* **2013**, *113*, 826–836. [CrossRef]

15.　Dieter, H.; Bidwe, A.R.; Varela-Duelli, G.; Charitos, A.; Hawthorne, C.; Scheffknecht, G. Development of the calcium looping $CO_2$ capture technology from lab to pilot scale at IFK, University of Stuttgart. *Fuel* **2014**, *127*, 23–37. [CrossRef]

16.　Shah, M.; Degenstein, N.; Zanfir, M.; Kumar, R.; Bugayong, J.; Burgers, K. Near zero emissions oxy-combustion $CO_2$ purification technology. *Energy Procedia* **2011**, *4*, 988–995. [CrossRef]

17.　Scheffknecht, G.; Al-Makhadmeh, L.; Schnell, U.; Maier, J. Oxy-fuel coal combustion—A review of the current state-of-the-art. *Int. J. Greenh. Gas Control.* **2011**, *5*, S16–S35. [CrossRef]

18.　Stanger, R.; Wall, T.; Spörl, R.; Paneru, M.; Grathwohl, S.; Weidmann, M.; Scheffknecht, G.; McDonald, D.; Myöhänen, K.; Ritvanen, J.; et al. Oxyfuel combustion for $CO_2$ capture in power plants. *Int. J. Greenh. Gas Control.* **2015**, *40*, 55–125. [CrossRef]

19.　Pang, L.; Shao, Y.; Zhong, W.; Gong, Z.; Liu, H. Experimental study of $NO_x$ emissions in a 30 $kW_{th}$ pressurized oxy-coal fluidized bed combustor. *Energy* **2020**, *194*, 116756. [CrossRef]

20.　Krzywanski, J.; Czakiert, T.; Shimizu, T.; Majchrzak-Kuceba, I.; Shimazaki, Y.; Zylka, A.; Grabowska, K.; Sosnowski, M. $NO_x$ Emissions from Regenerator of Calcium Looping Process. *Energy Fuels* **2018**, *32*, 6355–6362. [CrossRef]

21.　Hofbauer, G. Experimentelle Untersuchung der Oxy-Fuel-Verbrennung von Steinkohle in einer zirkulierenden Wirbelschicht-feuerung. *Univ. Stuttg.* **2017**. [CrossRef]

22.　Liu, H.; Gibbs, B. The influence of calcined limestone on $NO_x$ and $N_2O$ emissions from char combustion in fluidized bed combustors. *Fuel* **2001**, *80*, 1211–1215. [CrossRef]

23.　Hornberger, M.; Moreno, J.; Schmid, M.; Scheffknecht, G. Experimental investigation of the calcination reactor in a tail-end calcium looping configuration for $CO_2$ capture from cement plants. *Fuel* **2021**, *284*, 118927. [CrossRef]

24.　Haaf, M.; Müller, A.; Unger, A.; Ströhle, J.; Epple, B. Combustion of solid recovered fuels in a semi-industrial circulating fluid-ized bed pilot plant—Implications of bed material and combustion atmosphere on gaseous emissions. *VGB PowerTech.* **2020**, *3*, 51–56.

25.　Lupiáñez, C.; Mayoral, M.C.; Díez, L.I.; Pueyo, E.; Espatolero, S.; Andrés, J.M. The role of limestone during fluidized bed oxy-combustion of coal and biomass. *Appl. Energy* **2016**, *184*, 670–680. [CrossRef]

26.　Spliethoff, H. *Power Generation from Solid Fuels*; Springer: Berlin, Germany, 2010; ISBN 9783642028557.

27.　Partanen, J.; Backman, P.; Backman, R.; Hupa, M. Absorption of HCl by limestone in hot flue gases. Part I: The effects of temperature, gas atmosphere and absorbent quality. *Fuel* **2005**, *84*, 1664–1673. [CrossRef]

28.　Partanen, J.; Backman, P.; Backman, R.; Hupa, M. Absorption of HCl by limestone in hot flue gases. Part II: Importance of calcium hydroxychloride. *Fuel* **2005**, *84*, 1674–1684. [CrossRef]

29.　Partanen, J.; Backman, P.; Backman, R.; Hupa, M. Absorption of HCl by limestone in hot flue gases. Part III: Simultaneous absorption with $SO_2$. *Fuel* **2005**, *84*, 1685–1694. [CrossRef]

30.　Piao, G.; Aono, S.; Kondoh, M.; Yamazaki, R.; Mori, S. Combustion test of refuse derived fuel in a fluidized bed. *Waste Manag.* **2000**, *20*, 443–447. [CrossRef]

31.　Desroches-Ducarne, E.; Marty, E.; Martin, G.; Delfosse, L.; Nordin, A. Effect of Operating Conditions on HCl Emissions from Municipal Solid Waste Combustion in a Laboratory-Scale Fluidized Bed Incinerator. *Environ. Eng. Sci.* **1998**, *15*, 279–289. [CrossRef]

32.　DIN EN 14792. In *Stationary Source Emissions—Determination of Mass Concentration of Nitrogen Oxides—Standard Reference Method: Chemiluminescence*; DIN German Institute for Standardization: Berlin, Germany, 2017.

33.　Trozzi, C. *EMEP/EEA Air Pollution Emission Inventory Guidebook 2019: Energy Industries*; European Environment Agency: Copenhagen, Denmark, 2019.

34.　Pu, G.; Zan, H.; Du, J.; Zhang, X. Study on NO Emission in the Oxy-Fuel Combustion of Co-Firing Coal and Biomass in a Bub-bling Fluidized Bed Combustor. *BioResources* **2016**, *12*, 1890–1902. [CrossRef]

35.　Riaza, J.; Gil, M.; Álvarez, L.; Pevida, C.; Pis, J.; Rubiera, F. Oxy-fuel combustion of coal and biomass blends. *Energy* **2012**, *41*, 429–435. [CrossRef]

36.　De Diego, L.; Rufas, A.; García-Labiano, F.; Obras-Loscertales, M.D.L.; Abad, A.; Gayán, P.; Adánez, J. Optimum temperature for sulphur retention in fluidised beds working under oxy-fuel combustion conditions. *Fuel* **2013**, *114*, 106–113. [CrossRef]

37. Cai, Y.; Ma, Z.; Yan, J.; Zhang, Y.; Chen, Z.; Gao, R.; Zhong, P. Dichlorination in a circulating fluidized-bed incinerator for municipal solid waste incineration system. *Waste Dispos. Sustain. Energy* **2019**, *1*, 207–212. [CrossRef]
38. Hu, Y.; Naito, S.; Kobayashi, N.; Hasatani, M. $CO_2$, $NO_x$ and $SO_2$ emissions from the combustion of coal with high oxygen concentration gases. *Fuel* **2000**, *79*, 1925–1932. [CrossRef]
39. Wolf, C.; Leino, T.J.; Stephan, A.R.; Aho, M.J.; Spliethoff, H. Online Corrosion Measurements in Combination with Deposit and Aerosol Analysis during the Co-firing of Straw with Coal in Electrically Heated, Small-Scale Pulverized Fuel and Circulating Fluidized Bed Systems. *Energy Fuels* **2018**, *32*, 2506–2516. [CrossRef]
40. Xie, W.; Liu, K.; Pan, W.-P.; Riley, J. Interaction between emissions of $SO_2$ and HCl in fluidized bed combustors. *Fuel* **1999**, *78*, 1425–1436. [CrossRef]
41. Hu, G.; Dam-Johansen, K.; Wedel, S.; Hansen, J.P. Enhancement of the Direct Sulfation of Limestone by Alkali Metal Salts, Calcium Chloride, and Hydrogen Chloride. *Ind. Eng. Chem. Res.* **2007**, *46*, 5295–5303. [CrossRef]
42. Addink, R.; Bakker, W.C.M.; Olie, K. Influence of HCl and $Cl_2$ on the Formation of Polychlorinated Diben-zo-p-dioxins/Dibenzofurans in a Carbon/Fly Ash Mixture. *Environ. Sci. Technol.* **1995**, *29*, 2055–2058. [CrossRef] [PubMed]
43. Dieter, H.; Hawthorne, C.; Zieba, M.; Scheffknecht, G. Progress in Calcium Looping Post Combustion $CO_2$ Capture: Successful Pilot Scale Demonstration. *Energy Procedia* **2013**, *37*, 48–56. [CrossRef]
44. Scala, F.; Salatino, P. Modelling fluidized bed combustion of high-volatile solid fuels. *Chem. Eng. Sci.* **2002**, *57*, 1175–1196. [CrossRef]
45. Dri, M.; Canfora, P.; Antonopoulos, I.S.; Gaudillat, P. Best Environmental Management Practice for the Waste Management Sector. *JRC Sci. Policy Rep.* **2018**. [CrossRef]
46. Bolhàr-Nordenkampf, M.; Nummelin, T.; Luomaharju, T.; Viljanen, J. Operating Experience from the World´s Largest Waste Fired Circulating Fluidized Bed Reactor in Västerås. *Waste Manag.* **2015**, *5*, 167–178.
47. Gatternig, B. *Predicting Agglomeration in Biomass Fired Fluidized Beds*; University of Erlangen-Nürnberg: Erlangen, Germany, 2015.

## 6.2 Result discussion and contextualization

The present chapter offers a discussion on the oxy-fuel combustion characteristics of hard coal, wheat straw, and SRF under conditions typical for the CaL process.

Most of the investigations reported on CaL to date have considered coal as auxiliary fuel to sustain the endothermicity of the calcination step. However, as more and more biomass and waste-derived materials are now being combusted in stationary power plants, the oxy-fuel operation of CaL calciners with alternative fuels is receiving increasing attention. Concurrently, the combination of oxy-fuel combustion with non-conventional fuels can effectively provide a method for avoiding further $CO_2$ emissions into the atmosphere and reducing the overall carbon footprint.

Table 6.1: Range of experimental conditions for semi-industrial CaL calciners powered by alternative fuels

| Symbol | Unit | Haaf et al. | Moreno et al. |
|---|---|---|---|
| $T_{calc}$ | °C | 750-920 | 835-940 |
| $W_{s,calc}$ | kg/m$^2$ | 150-400 | 566-1479 |
| $y_{O_2,calc,in}$ (dry basis) | m$^3$/m$^3$ | 0.4-0.65 | 0.21-0.31 |
| $u_{0,calc}$ | m/s | 4.5-5.5 | 3.1-4.1 |
| Fuel type | | SRF | Wheat straw, SRF |
| Reference | | [95, 96] | [150] |

The mono-combustion of alternative fuels within the CaL cycle has been scarcely addressed in the past. To date, three studies have been published on this topic [95, 96, 150]. These are summarized in table 6.1. In their first work, Haaf et al. aimed at demonstrating the combustion of two SRFs at a 1 MW$_{th}$ CaL facility [96]. To this end, the authors chose $CO_2$ concentrations typical for WtE units fueled by municipal solid waste (MSW). Within the scope of the study, the calciner performance and the fate of chlorine were assessed. In contrast, the second work offers an evaluation of the carbonator performance and the overall hydrodynamic behavior of the process [95]. Haaf et al. concluded that the utilization of SRF as CaL supplementary fuel has no significant disadvantage on the $CO_2$ capture efficiency. Nonetheless, attention should be paid to the accumulation of coarse inert ash fractions, as it can severely affect the hydrodynamic stability of the system. Besides, the publication included in this chapter evaluated the calciner performance under mono-combustion of hard coal, wheat straw, and SRF. Also, the co-firing behavior of hard coal and biomass and the influence of inlet oxygen concentration upon combustion were assessed. The preliminary scope of the work aimed at conducting an overall assessment of the CaL cycle, including the carbonator performance. However, the latter could not be completed due to the damage of the external solid circulation pipe connecting both

reactors.
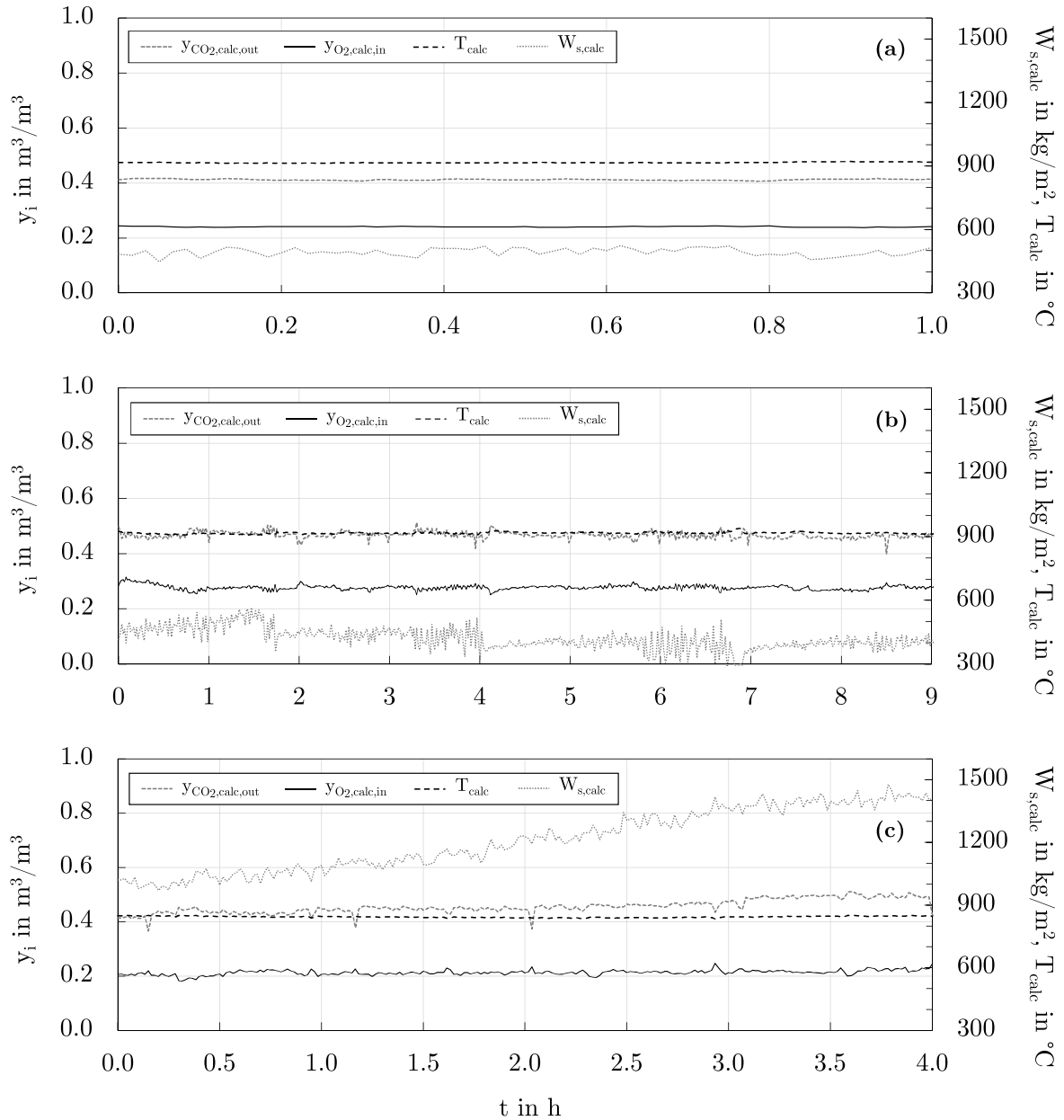


Figure 6.1: Exemplary data plots of the CFB calciner during mono-combustion of various solid fuels: hard coal (a), wheat straw (b), and SRF (c)

Figure 6.1 displays the time evolution of the main calciner variables when utilizing the aforementioned three fuels. Generally, the illustration indicates stable oxy-fuel combustion of all fuels. While coal firing was evaluated in a shorter term, mono-combustion of wheat straw and SRF was investigated for 9 h and 4 h, respectively. During the experiments, a maximum inlet oxygen concentration ($y_{O_2,calc,in}$) of 0.27 m³/m³ was employed. Please note that higher oxy-fuel cases could not be investigated due to technical constraints.

In parallel, outlet $CO_2$ concentrations ($y_{CO_2,calc,out}$) in the range of 0.41-0.47 $m^3/m^3$ were yielded. As anticipated in a previous passage, the latter values are significantly diluted by the continuous nitrogen inflow required for fluidization and flushing purposes (by about 0.20 $m^3/m^3$). Oxy-fuel combustion of coal and wheat straw aimed at investigating typical calcination temperatures (i.e., 900 °C). In contrast, mono-combustion of SRF targeted at exploiting the boundary conditions defined for waste incineration systems (i.e., 850 °C). Besides, the lowest subplot indicates an increase in solid inventory during the test. As explained in the publication, standalone SRF combustion was explored without draining any solids from the reactor. Therefore, the increase in $W_{s,calc}$ can be mostly attributed to ash accumulation effects.
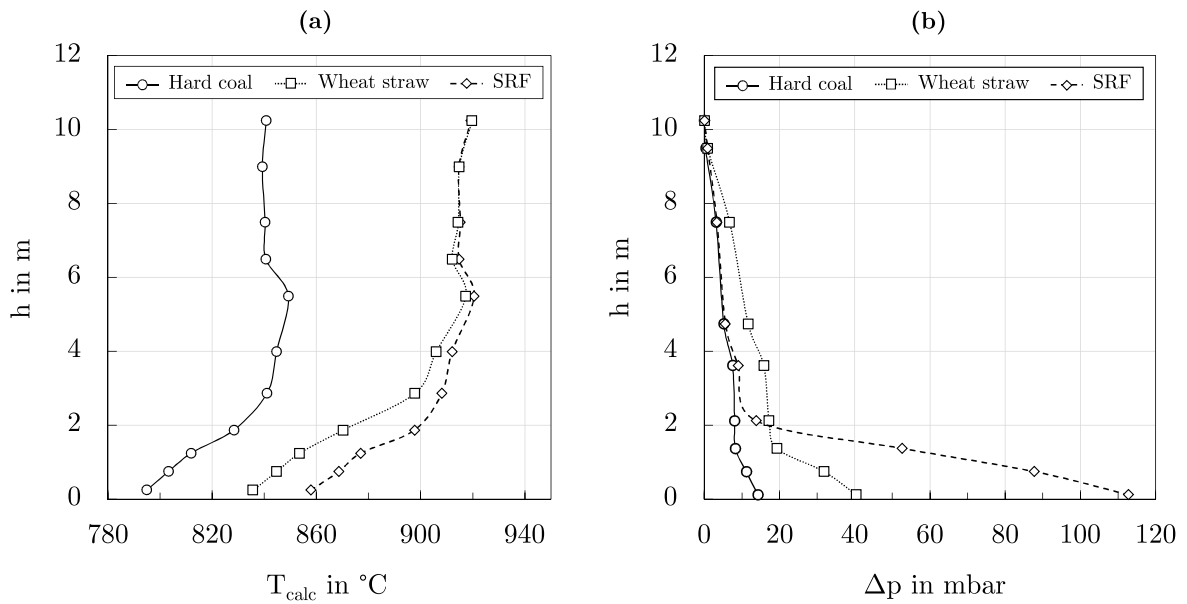


Figure 6.2: Temperature (a) and pressure (b) profiles of the CFB calciner during mono-combustion of various solid fuels

Fuel blending with biomass substantially decreased the specific $NO_x$ emissions ($e_{NO_x}$). While 359 $mg/MJ_{th}$ were measured during oxy-combustion of hard coal, 203 $mg/MJ_{th}$ were yielded at 100 % biomass firing. Considering the relatively low-temperature combustion occurring in CFB boilers [123, 164], the latter behavior can presumably be explained by the lower nitrogen content of the biomass. The latter assertion seems to be in line with the conclusions drawn by Riaza et al., who also reported a decrease in $NO_x$ concentrations with increasing biomass share. An increase in inlet oxygen concentration from 0.23 to 0.27 $m^3/m^3$ posed only a marginal increase in $e_{NO_x}$. Considering the limited operation window, it cannot be excluded that such differences were caused, at least partly, by variations in fuel mass flow rather than by the increased oxygen availability [103, 166].

In parallel, $e_{SO_2}$ displayed a slightly decreasing tendency with increasing biomass substitution. As anticipated in the paper, the latter effect can be ascribed to the lower biomass sulfur content combined with the (partial) sulfation of fuel alkali metal species. In addition, it should be noted that the shallow $e_{SO_2}$ values depicted in the illustration were caused by efficient flue gas desulfurization (i.e., wide limestone availability), which led to $SO_2$ capture rates ($\eta_{SO_2}$) over 0.99 mol/mol. Contrary to what has been published in the literature [103, 108], an increase in $y_{O_2,calc,in}$ did not cause an appreciable effect on $e_{SO_2}$, presumably due to the very effective in-situ flue gas desulfurization yielded in this study. Besides, biomass substitution posed an increasing tendency in fuel-specific HCl emissions ($e_{HCl}$). The higher values observed in this work are in line with an early study by Wolf et al. [203] and are attributed to the comparatively high chlorine content of the wheat straw. $y_{O_2,calc,in}$ showed to slightly promote $e_{HCl}$. As HCl is not an oxidation product, the observed marginal effect can be presumably attributed to small differences in the respective fuel mass flow rates. In line with the presented $e_{SO_2}$ results, $e_{HCl}$ was greatly suppressed by calcium-containing species in the CaL calciner. Consequently, this work cannot give a thorough assessment of the interaction between $SO_2$ and HCl. Contrary to $SO_2$, fuel blending showed to influence the chlorine retention rate significantly ($\eta_{HCl}$). Oxy-combustion of hard coal led to an average $\eta_{HCl}$ of 0.68 mol/mol, whereas 100 % biomass firing yielded values around 0.95 mol/mol. According to Hu et al., the latter behavior can be explained by the increased content of alkali metal vapors, which can lead to more condensation nuclei during combustion, creating a higher absorption surface [107]. The effect of temperature on $\eta_{HCl}$ was evaluated by Haaf et al. in a recent study [95]. According to the authors, calciner temperatures of at least 860 °C are desirable to maximize chlorine retention ($\eta_{HCl}$ > 0.90 mol/mol). However, the results of this work indicate that $\eta_{HCl}$ values over 0.90 mol/mol can be achieved when operating with at least 30 % biomass substitution in the calciner at temperatures close to 910 °C.

As anticipated at the beginning of this passage, the utilization of alternative fuels within the CaL system should be accompanied by stable reactor hydrodynamics. Figure 6.2 displays the temperature (a) and differential pressure (b) profiles achieved during mono-combustion of the aforementioned fuels. All three experiments indicate the absence of localized hotspots. The temperature gradient described by the CFB calciner shows a gradual increase from the reactor bottom to the last stage of oxidant feeding (i.e., 4 m). At this point, all oxidant is being fed to the calciner, and the temperature remains mostly constant. As introduced in chapter 5, the lower temperatures at the bottom are mainly attributed to the sensible heat of recirculated solids. Also, the effect of continuous sorbent calcination should be considered. The oxy-combustion of both wheat straw and SRF led to a substantial increase in the differential reactor pressure. During mono-combustion of hard coal, 14 mbar were measured. In contrast, standalone combustion of wheat straw and SRF yielded

40 mbar and 113 mbar, respectively. As discussed in the paper, the higher pressure drop obtained with alternative fuels can be partly described by ash accumulation effects. Both experiments were investigated on a longer-term basis, without draining any solids from the calciner. Concerning the biomass test, the higher volatile content of the fuel might have also contributed to the observed effect. High-volatile fuels, such as wheat straw, have been reported to cause fuel particle fragmentation and volatile matter segregation and post-combustion above the dense reactor zone [184]. In the case of SRF, the latter effect is exacerbated by the comparatively higher ash content of the fuel. Despite ash accumulation effects, the 200 $kW_{th}$ CFB calciner could be operated under realistic oxy-fuel combustion conditions for several hours of continuous operation. However, further research is needed to thoroughly characterize the long-term influence of low-grade fuels within the CaL cycle, both in terms of gas and solid balance.

# 7 Summary and conclusions

Recent developments in climate change and increasing carbon dioxide ($CO_2$) emissions worldwide evidence the urgent need to rapidly decarbonize the energy sector. Generally, the proposed strategies include a substantial deployment of renewable energy sources. Nonetheless, climate change might influence renewable energy generation through long-term alterations in various environmental conditions. For instance, solar power production may be impaired by reduced surface solar radiation. Also, wind power production might be influenced by changes in wind speed and density patterns. As reviewed by the Intergovernmental Panel on Climate Change (IPCC), most decarbonization scenarios will require large investments in renewable energy, particularly under assumptions of limited or no deployment of carbon capture and storage (CCS). Moreover, the International Energy Agency (IEA) has categorized CCS as essential to achieving the goal of net-zero emissions by 2050. Within the framework of this thesis, the Calcium Looping (CaL) technology has been assessed as a promising post-combustion $CO_2$ capture option for power plants. The present work offers a multiscale assessment of the process, ranging from laboratory to pilot scale (TRL6).

As reviewed by several authors, there are two major technical aspects that currently hinder the commercialization of the technology, namely sorbent stability and process flexibility. In the past, CaO-based sorbents have been widely employed due to the numerable advantages they offer. However, the natural-based sorbents typically suffer from a rapid decline in $CO_2$ capture performance, particularly in the presence of realistic flue gas species such as $SO_2$. Furthermore, the flexible operation of CaL systems in future energy scenarios has been recently reviewed. In this context, CaL units coupled to power plants are expected to show a high degree of flexibility both in terms of flue gas loads (i.e., carbonator) and the utilization of alternative fuels (i.e., calciner), being the latter essential to achieving net-negative carbon emissions. The present thesis offers a methodology to individually address each of the aforementioned process challenges. In the following, a summary of each study is given.

Within the first phase of the sorbent evaluation experiments, the cyclic deactivation behavior of three distinct limestones was evaluated in a thermogravimetric analyzer (TGA) using realistic flue gas compositions upon carbonation. In the presence of $SO_2$ and $H_2O$, both Rheinkalk and Riyadh showed the typical behavior of unmetamorphosed limestones.

Saabar, in contrast, proved to be negatively influenced by the addition of steam, while the presence of $SO_2$ showed to improve the carbonation conversion. Subsequently, the cyclic decay behavior of Rheinkalk was evaluated in a 20 $kW_{th}$ dual fludized bed (DFB) facility, both with and without the presence of $SO_2$ during carbonation. The proposed mathematical expression to describe the evolution of carrying capacity upon cycling correlated with the TGA experiments adequately. This work determined an apparent carbonation rate ($k_S\varphi$) of 0.09 $s^{-1}$, which correlates well with the values obtained in other BFB units operated at similar conditions. Furthermore, the performance of a BFB carbonator upon changes in temperature, $CO_2$ loading, and steam concentration was evaluated. While the attained $CO_2$ absorption efficiency ($E_{carb}$) decreased with increasing carbonation temperature, a higher $CO_2$ loading resulted in increased equilibrium normalized $E_{carb}$ values ($E_{norm}$) due to the enhanced carbonation driving force. In contrast, $E_{norm}$ proved to be particularly favored at low $H_2O$ concentrations because of the enhanced pore network $CO_2$ diffusivity. The high carbonation performance attained in this work, in combination with the relatively low gas superficial velocities employed, postulate this reactor configuration as suitable for the decarbonization of load-following power plants (see chapter 5). Furthermore, the present study contributes to a better understanding of the influence of both $SO_2$ and $H_2O$ on scarcely investigated metamorphosed limestones.

Following operation with a BFB carbonator unit, the flexible performance of a BFB-CFB reactor arrangement was investigated at the IFK's 200 $kW_{th}$ CaL facility. A total of three experimental campaigns were devoted to evaluating the steady-state behavior of the system upon changes in carbonator flue gas loads. Results indicated that the proposed reactor setting could be stably operated with carbonator velocities ranging between 0.8-2.0 m/s, provided that other key variables remained unchanged. Results were successfully validated using two different approaches. With the use of the active space time ($\tau_{active}$) model, a $\tau_{active}$ of 41 s was identified as necessary to achieve a $E_{norm}$ of 90 %. Also, the influence of carbonator solid inventory ($W_{s,carb}$) upon $E_{carb}$ was investigated at 40 % load operation. It was found that differences as high as 1350 $kg/m^2$ (or 41 kg) can affect $E_{carb}$ by about 25 percentage points. Concerning the carbonator hydrodynamics, operation at part-load led to decreased temperatures in the upper region due to the decreased sorbent entrainment. Concurrently, decreased gas superficial velocities slightly increased the pressure difference across the BFB unit. Calciner operation proved to be independent of the selected carbonator flue gas load. The CFB calciner was successfully operated over a broad range of process conditions, with inlet dry oxygen concentrations as high as 0.55 $m^3/m^3$. The hydrodynamic behavior described by the CFB unit was stable and smooth, without the presence of localized hot spots. In short, results indicate that the proposed BFB-CFB CaL arrangement can enable both efficient and load-flexible $CO_2$ capture in load-following power plants, even at characteristic minimum part-load conditions (i.e., 40 %).

The impact of fuel selection was evaluated using three different fuels, namely hard coal, wheat straw, and SRF. Due to the failure of the external circulation pipe, only the calciner operation could be addressed. In the course of the pilot testing (of about $43\,h$), a broad range of experimental conditions was established. The effect of coal-biomass blending ratio and inlet oxygen concentration on emissions and hydrodynamic behavior was evaluated. Biomass substitution showed to affect pollutants emission by changes in the fuel mixture. In parallel, both $SO_2$ and HCl-specific emissions were significantly reduced by the presence of Ca-species in the calciner, yielding chlorine retention rates over $0.90$ mol/mol with biomass substitution rates higher or equal to $30\,\%$. Concurrently, $NO_x$ emissions decreased at increased biomass shares due to the lower biomass nitrogen content. However, the relatively high values reported in this study suggest that an additional $NO_x$-removal step will probably be required. Concerning reactor hydrodynamics, no localized hot spots were detected. The measured reactor differential pressure increased both during mono-combustion of wheat straw and SRF. In the case of biomass, the latter behavior can be explained by the higher volatile content of the fuel. Regarding SRF, the comparatively high ash fraction of the fuel should also be considered. Besides, it should be noted that both experiments were investigated in a longer term, without draining any solid material from the calciner. Hence, the increased pressure drop can, at least, be partly attributed to ash accumulation effects. Overall, the latter results envisage that such a CFB calciner can also be effectively operated using low-grade quality fuels.

**Recommendations for further research**

From a practical standpoint, only the initial fast carbonation regime of CaO is considered relevant for $CO_2$ capture. Exploiting the diffusion-controlled reaction stage would comprehensively increase the solid residence times in the carbonator, enlarging the carbonator design step disproportionately. However, Grasa et al. demonstrated that $SO_2$ could also react with CaO unavailable for carbonation, leading to an activity greater than that usually estimated (Grasa et al. *Industrial & Engineering Chemistry Research* 47(5): 1630-1635, 2008). Besides, available studies justify the absence of a flue gas desulfurization (FGD) installation based on the extent of sulfation, with sulfation conditions playing an irrelevant role. Given these facts, it is advisable to develop a sulfation model that also accounts for the influence of flue gas steam content on deactivation, correcting the reactivating effect experienced by sorbents when carbonation is allowed to surpass the kinetically controlled range. Such a model should help verify that the extent of sulfation per cycle number is determinant rather than the sulfation mode employed.

Future studies on flexible CaL behavior should characterize the transient behavior between specific load cases, as these are essential to develop control strategies to sustain smooth plant operation. Extensive studies are required to define such control concepts, ranging

from the fuel feed rate in the regenerator, through the solid circulation rate, up to the temperature control by heat extraction in the carbonator. Besides, the achievement of even lower part-load operating scenarios with the proposed BFB-CFB reactor setting should be revised with more detail. Additional plant changes might be required to overcome the challenges in reactor hydrodynamics and $CO_2$ absorption rate. For commercial BFB carbonators with a larger cross-section, multiple bottom loop seals might be necessary to allow uniform sorbent extraction from the carbonator. As for the calciner, operation with extreme oxy-fuel combustion conditions is recommended to further reduce the heat demand in the calciner, and hence the overall energy penalty.

Concerning fuel flexibility aspects, extended operation with low-grade fuels is strongly recommended to characterize the process thoroughly. Process evaluation in terms of pollutant formation and ash accumulation behavior is anticipated to ensure reliable and long-term plant operation at a commercial scale. Furthermore, the impact of fuel selection on carbonation performance should be carefully addressed. Similarly, the investigation of corrosive depositions within the CaL unit should not be overlooked, mainly when operating with non-conventional fuels.

# A Appendix: Sorbent analysis

The following appendix presents complementary results derived from the analysis of the three sorbents employed in this work: Rheinkalk, Riyadh, and Saabar. Each limestone type was characterized in terms of particle size distribution (Appendix A.1), cyclic reactivity (Appendix A.2), and microscopy imaging (Appendices A.3 and A.4). Additional information on X-ray diffraction as well as $N_2$ adsorption and mercury intrusion porosimetry can be found elsewhere [104].

## A.1 Grain size distribution of utilized sorbents

The particle size distribution (PSD) of each limestone was measured using a Malvern Mastersizer 3000 equipped with an Aero S dry particle dispersion unit. Figures A.1 and A.2 give the size distribution of all three limestones in the range of 100-400 µm and 400-1000 µm, respectively.
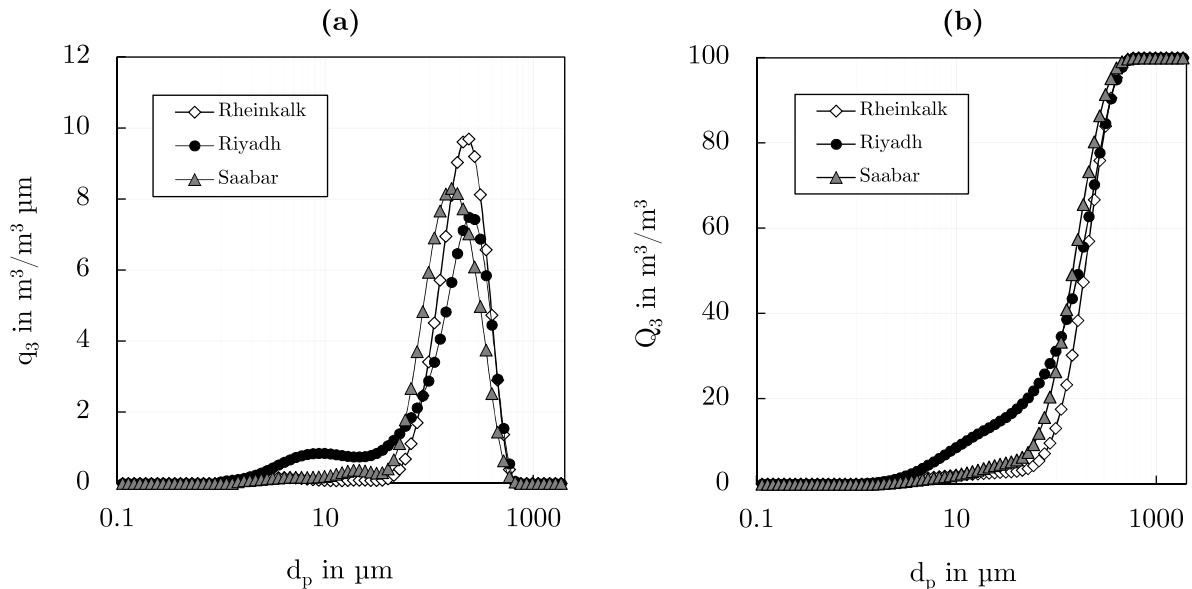


Figure A.1: Size distribution of all tested sorbents in the range between 100-400 µm: (a) frequency distribution, (b) cumulative distribution
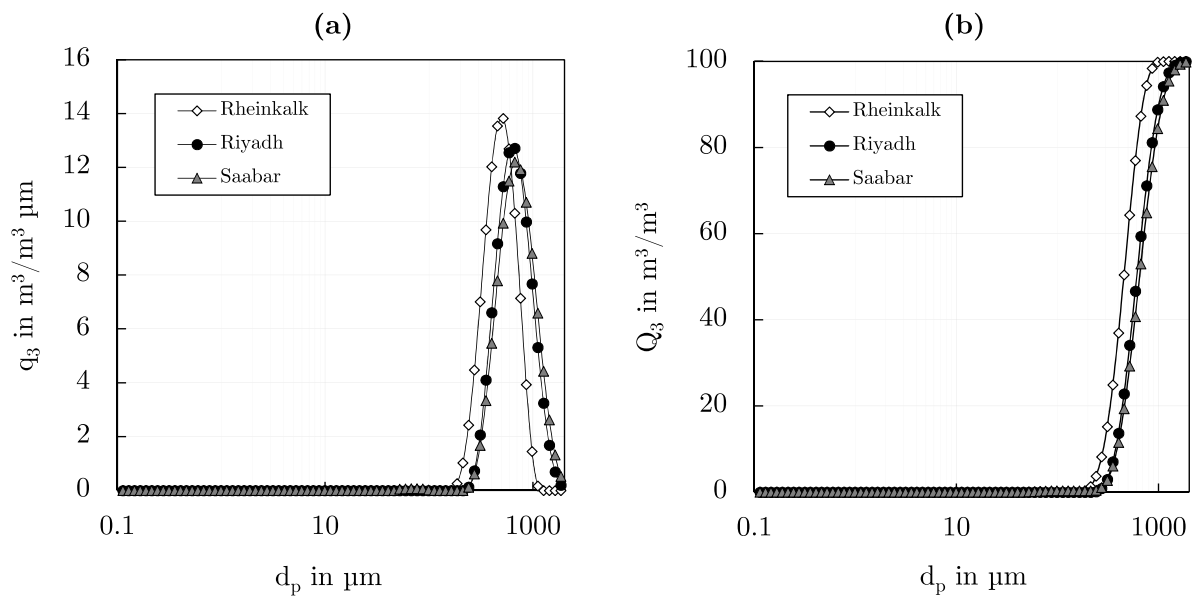
Figure A.2: Size distribution of all tested sorbents in the range between 400-1000 µm: (a) frequency distribution, (b) cumulative distribution

# A.2 Sorbent cycling experiments by thermogravimetric analysis (TGA)

As anticipated in chapter 4, the cyclic activity of each sorbent was evaluated using a Linseis PT1100 custom-built thermogravimetric analyzer (TGA). Figures A.3 to A.5 depict the conversion degree of each limestone upon the first carbonation cycle. Moreover, figure A.3a shows the influence of sample mass on sorbent conversion.



Figure A.3: Sorbent conversion (X) against time (t) for the Rheinkalk limestone during the first carbonation cycle. Carbonation and calcination routines as described in chapter 4

Similar to the results presented in chapter 4, the latter tests were completed using four different carbonation routines that include $SO_2$ and steam. For a detailed description of each routine, please refer to chapter 4.



**(a) $CO_2$**

**(b) $CO_2$, $H_2O$**

**(c) $CO_2$, $SO_2$**

**(d) $CO_2$, $SO_2$, $H_2O$**

Figure A.4: Sorbent conversion (X) against time (t) for the Riyadh limestone during the first carbonation cycle. Carbonation and calcination routines as described in chapter 4
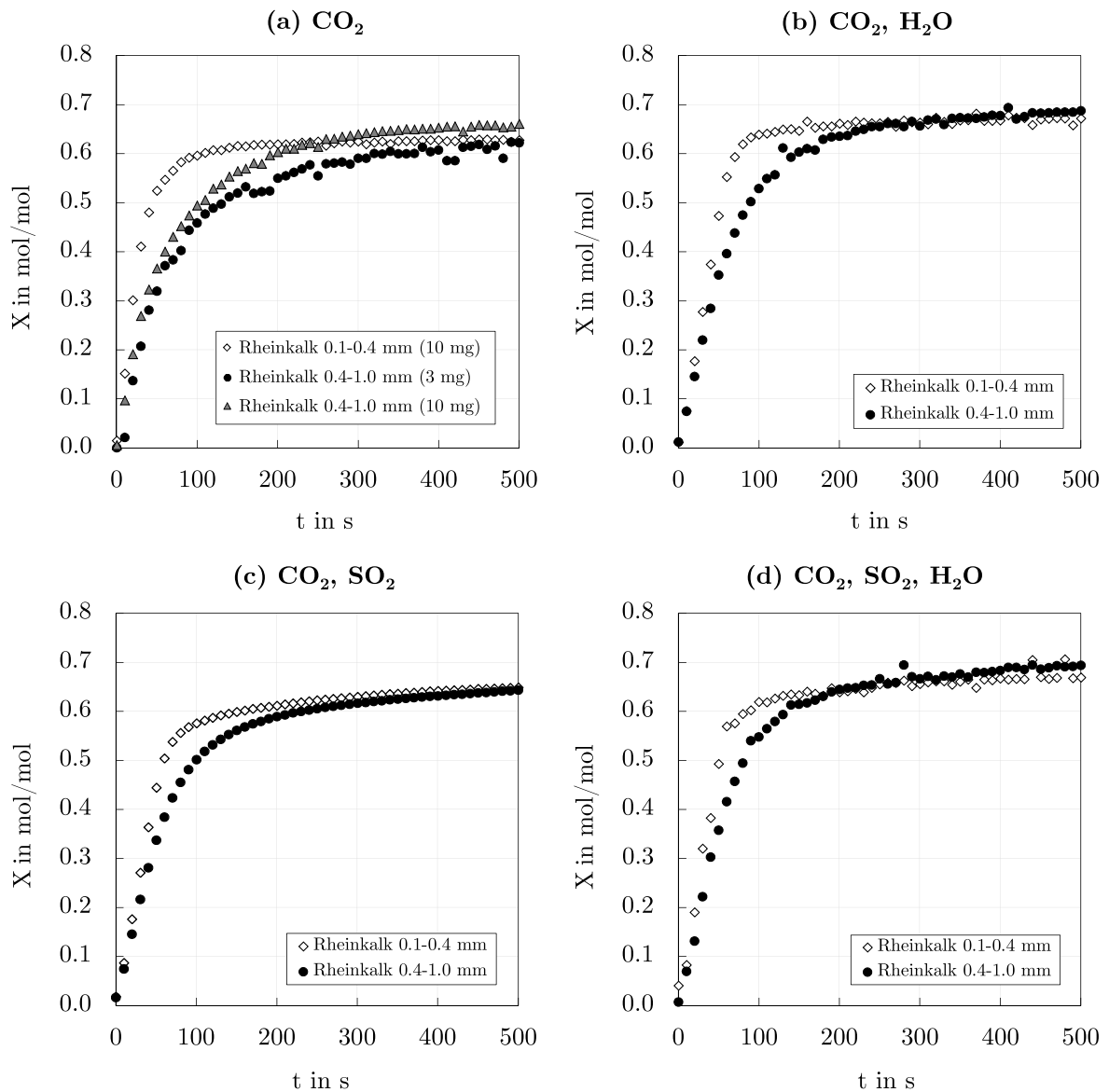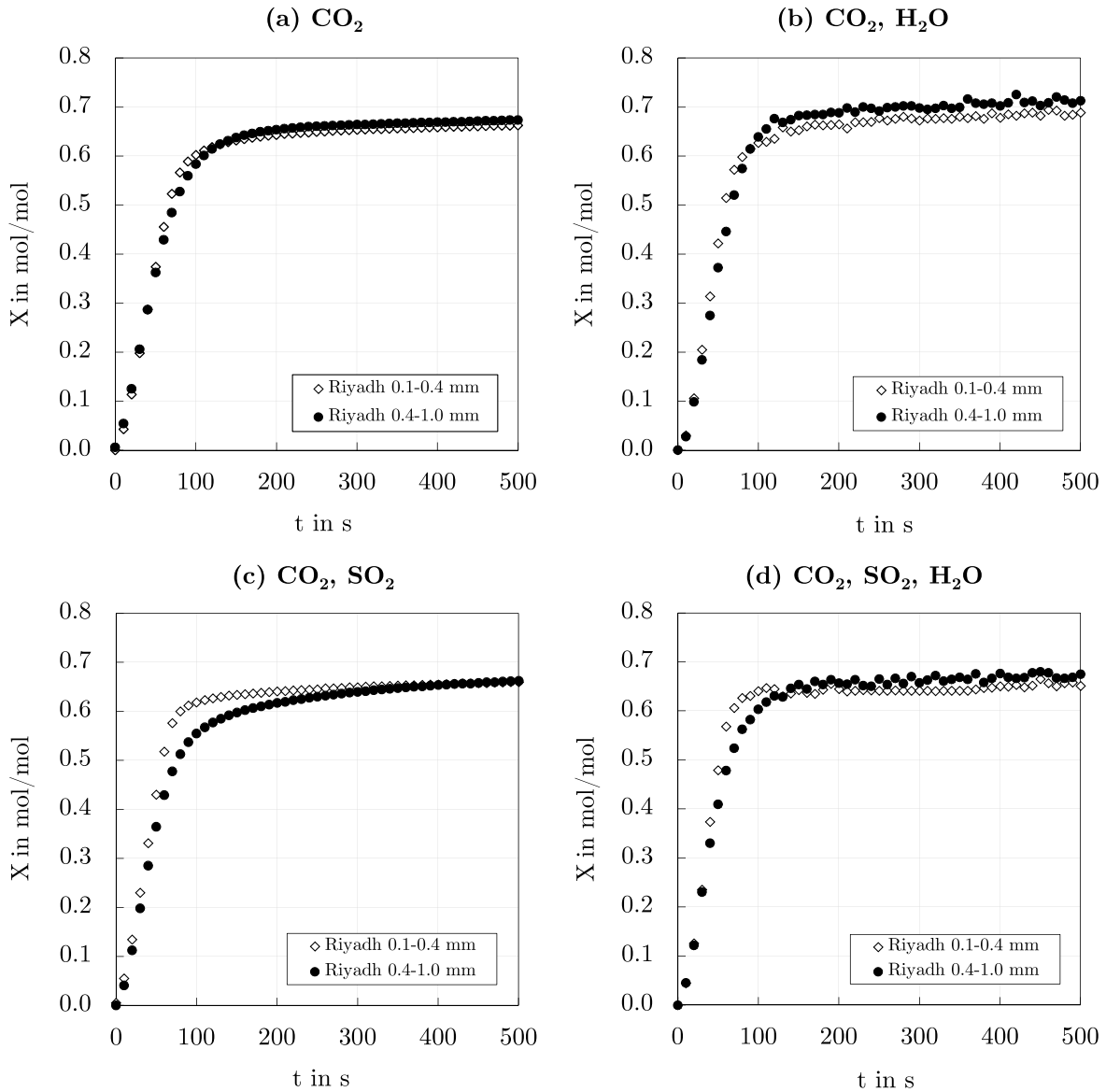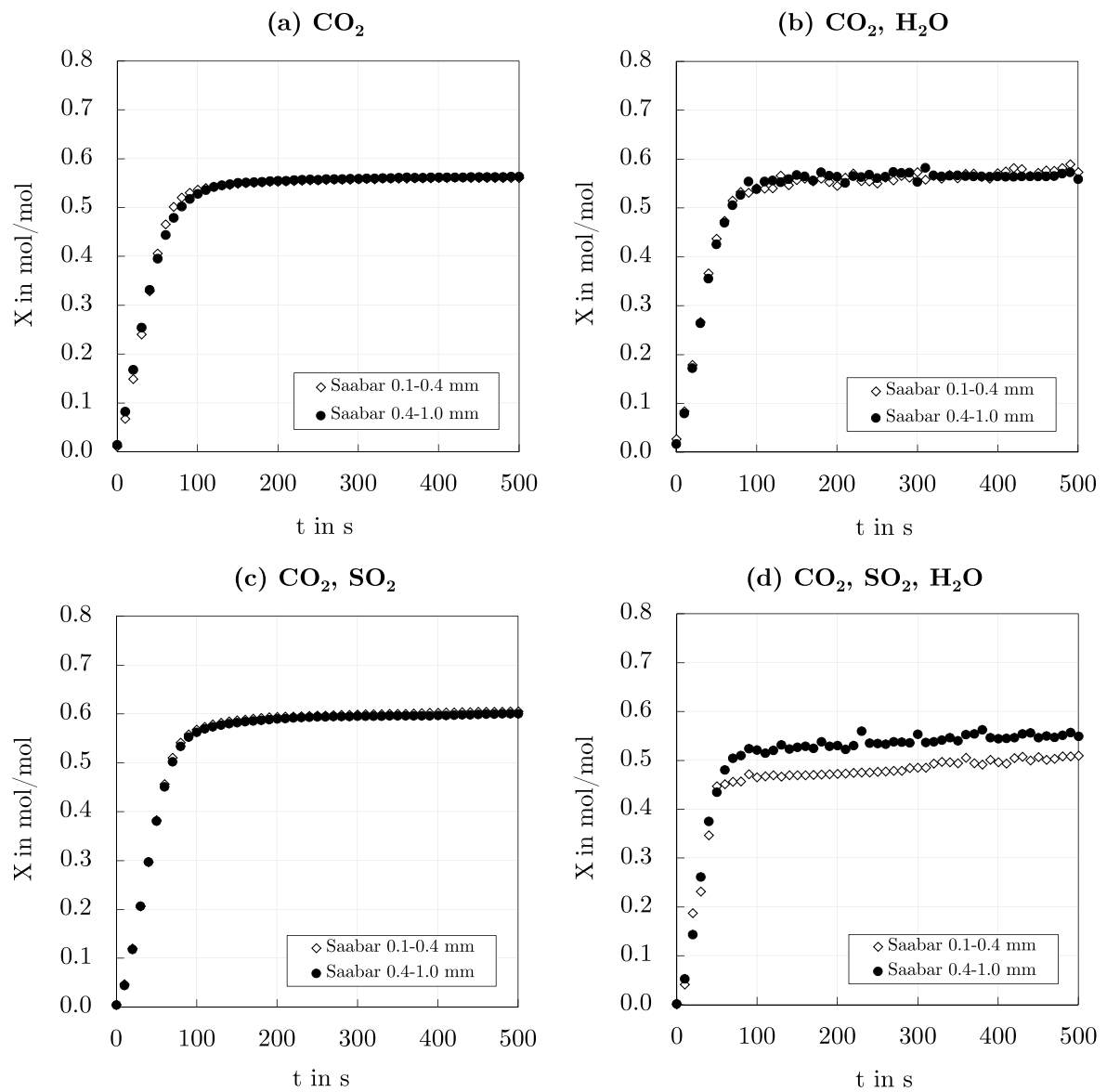
Figure A.5: Sorbent conversion (X) against time (t) for the Saabar limestone during the first carbonation cycle. Carbonation and calcination routines as described in chapter 4

The influence of carbonation conditions on the cyclic behavior of each limestone is shown in figures A.6 to A.8. Please note that the results displayed for the finer size fraction (i.e., 0.1-0.4 mm) correspond to those presented in chapter 4. These are reproduced here to enable comparison with the trends given for the coarser fraction (i.e., 0.4-1.0 mm).



Figure A.6: Sorbent capacity ($X_{n_{cycles}}$) against number of cycles ($n_{cycles}$) for the Rheinkalk limestone. Carbonation and calcination routines as described in chapter 4

Figure A.7: Sorbent capacity ($X_{n_{cycles}}$) against number of cycles ($n_{cycles}$) for the Riyadh limestone. Carbonation and calcination routines as described in chapter 4

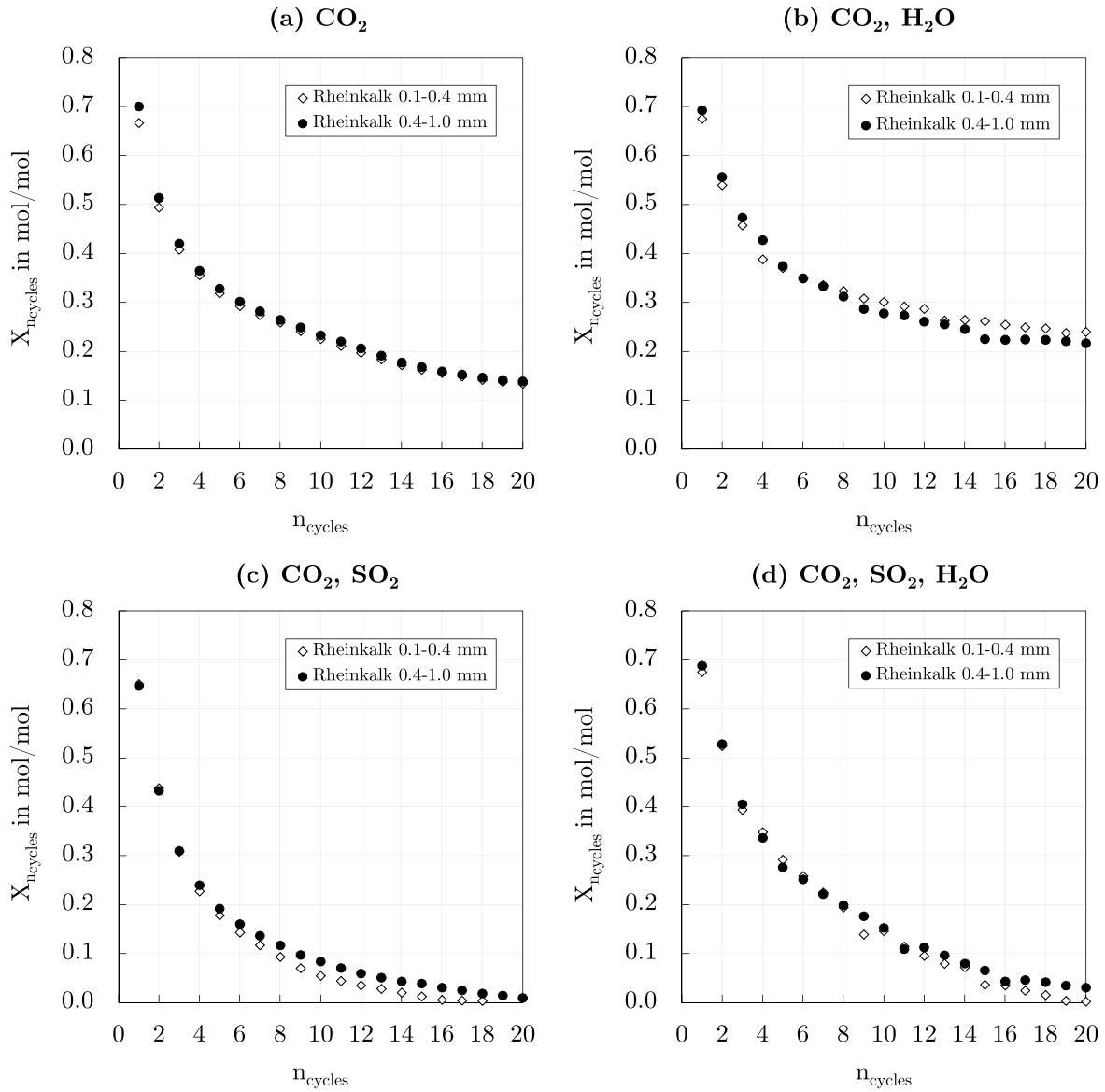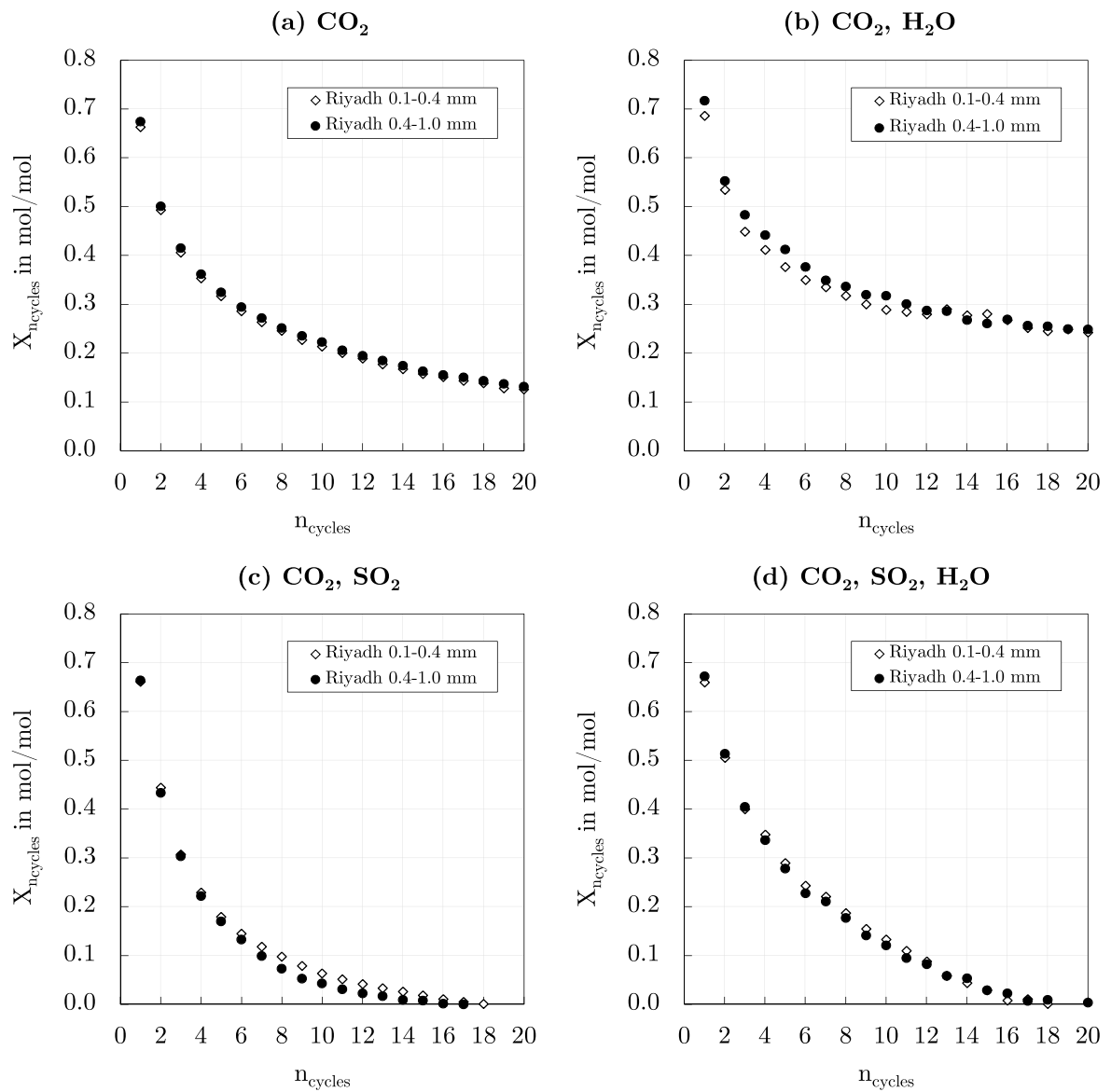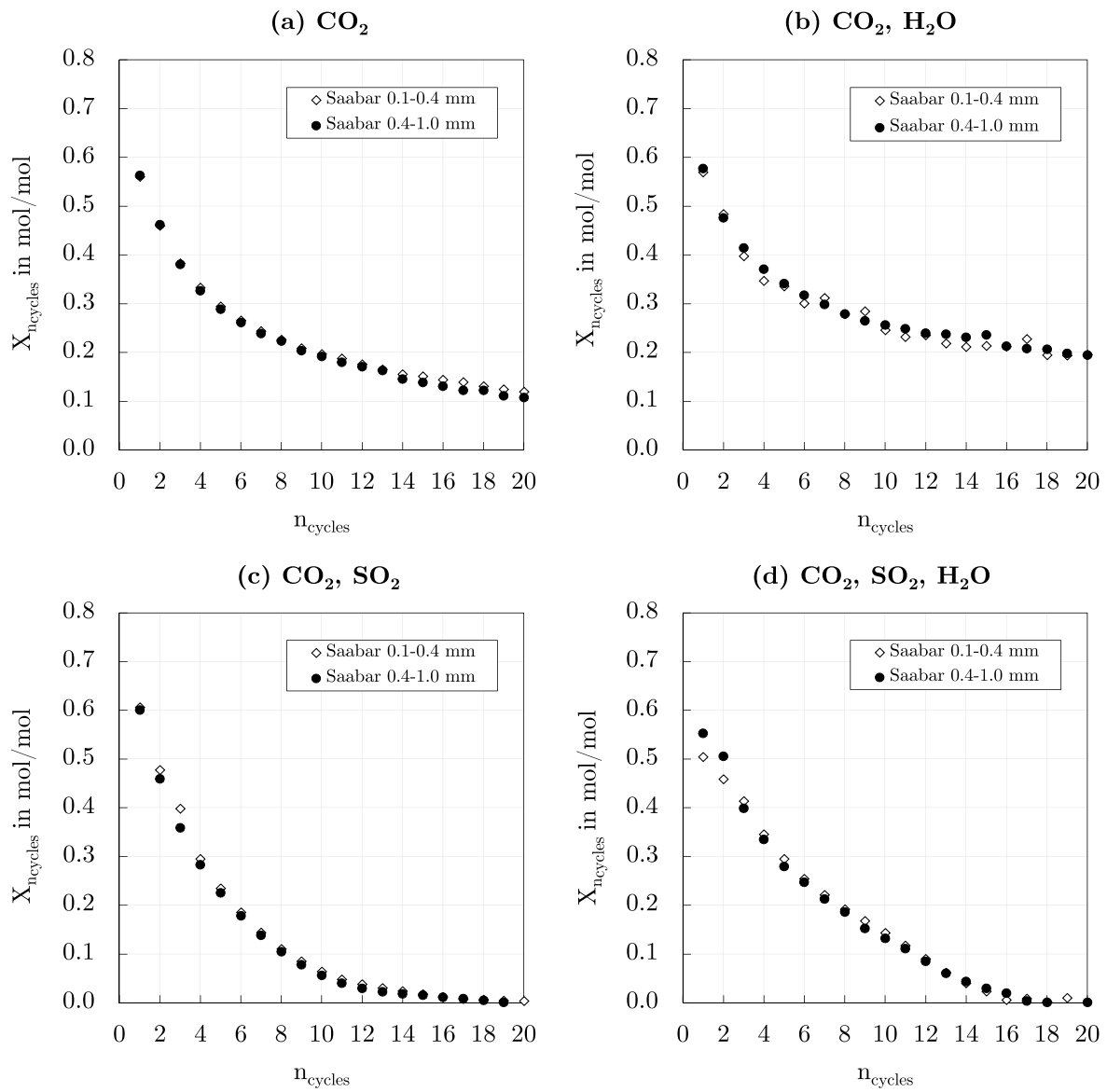Figure A.8: Sorbent capacity ($X_{n_{cycles}}$) against number of cycles ($n_{cycles}$) for the Saabar limestone. Carbonation and calcination routines as described in chapter 4

# A.3 Scanning Electron Microscopy (SEM)

Figures A.9 to A.12 give information about the surface topography and composition of the Rheinkalk limestone when subjected to one or multiple cycles. Please note that the results related to the first cycle correspond to sorbent regeneration in an inert atmosphere. In contrast, sorbent particles subjected to multiple CaL cycles were (partly) sulfated because of the sulfur oxides originating from the combustion of the auxiliary fuel in the calciner.

(a)                                                                     (b)
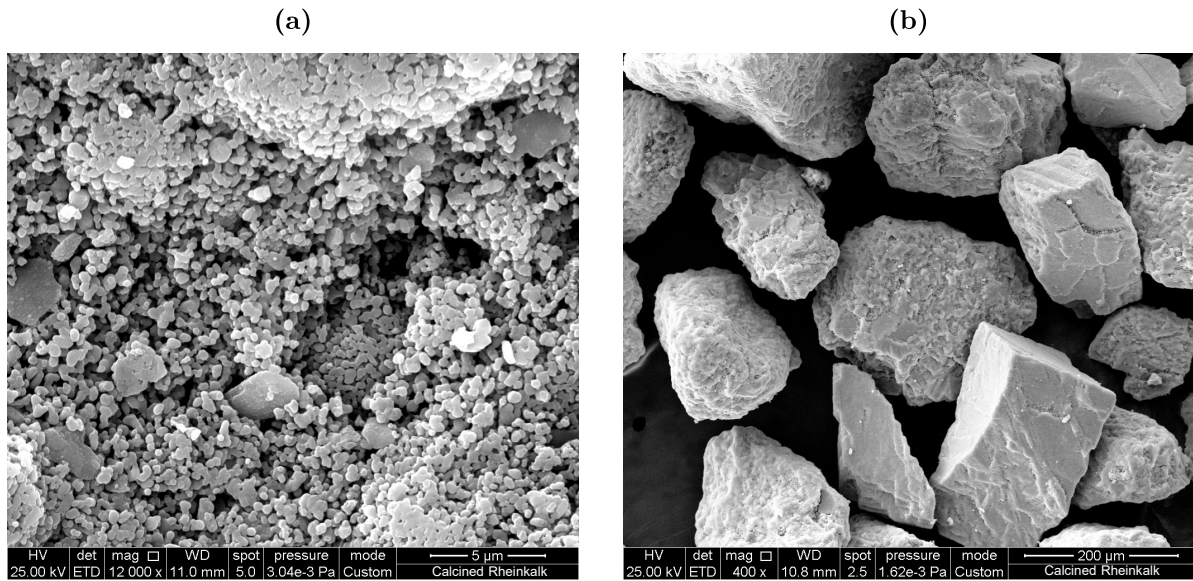


Figure A.9: SEM images of the Rheinkalk limestone after the first calcination cycle: (a) at 5 μm resolution, (b) at 200 μm resolution

The depicted microstructural results were obtained using a Quanta FEG 650 SEM instrument equipped with a S/TEM detector. Furthermore, an Ametek-EDAX analyzer (Apollo X) was employed to obtain a distribution map of the sample's composition. The quantification of the EDX results was performed using the ZAF correction method in which corrections for atomic number (Z), absorption (A) and fluorescence (F) effects are calculated separately from suitable physical models and solved iteratively (see Appendix A.4).

(a)                                                                                      (b)
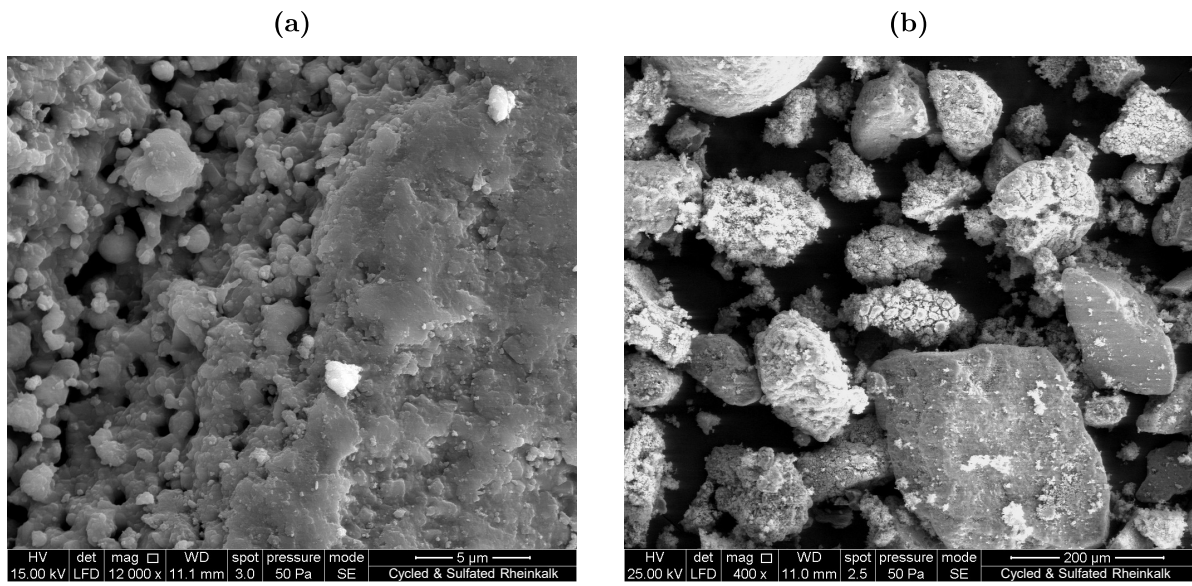


Figure A.10: SEM imaging of the Rheinkalk limestone after multiple CaL cycles: (a) at 5 μm resolution, (b) at 200 μm resolution

# A.4 Energy Dispersive X-Ray Analysis (EDX)

Table A.1: Weight (wt%) and atomic (at%) EDX computation of the Rheinkalk limestone after the first calcination cycle. ZAF correction method

| Element | $x_i$ (wt%) | $x_i$ (at%) |
|---------|-------------|-------------|
| C       | 2.60        | 6.13        |
| O       | 23.41       | 41.51       |
| Ca      | 73.99       | 52.36       |

(a)  (b)
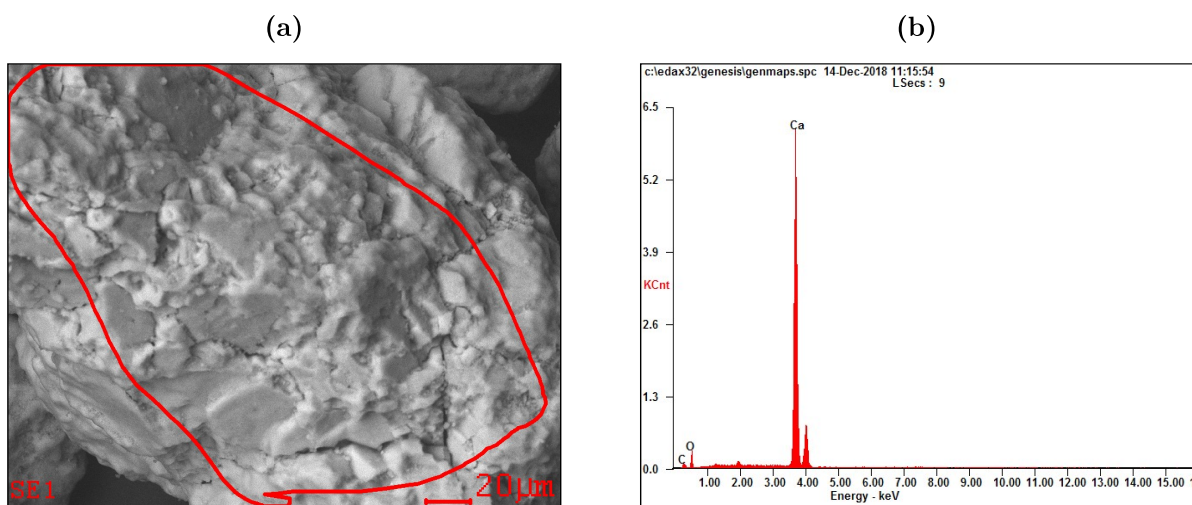


Figure A.11: EDX imaging of the Rheinkalk limestone after the first calcination cycle: (a) SEM micrograph, (b) EDX intensity spectrum

Table A.2: Weight (wt%) and atomic (at%) EDX computation of the sulfated Rheinkalk limestone after multiple CaL cycles. ZAF correction method

| Element | $x_i$ (wt%) | $x_i$ (at%) |
|---------|-------------|-------------|
| C       | 2.74        | 5.70        |
| O       | 34.65       | 54.14       |
| Mg      | 0.91        | 0.93        |
| Al      | 0.87        | 0.81        |
| Si      | 0.95        | 0.85        |
| S       | 1.33        | 1.03        |
| Ca      | 58.55       | 36.54       |

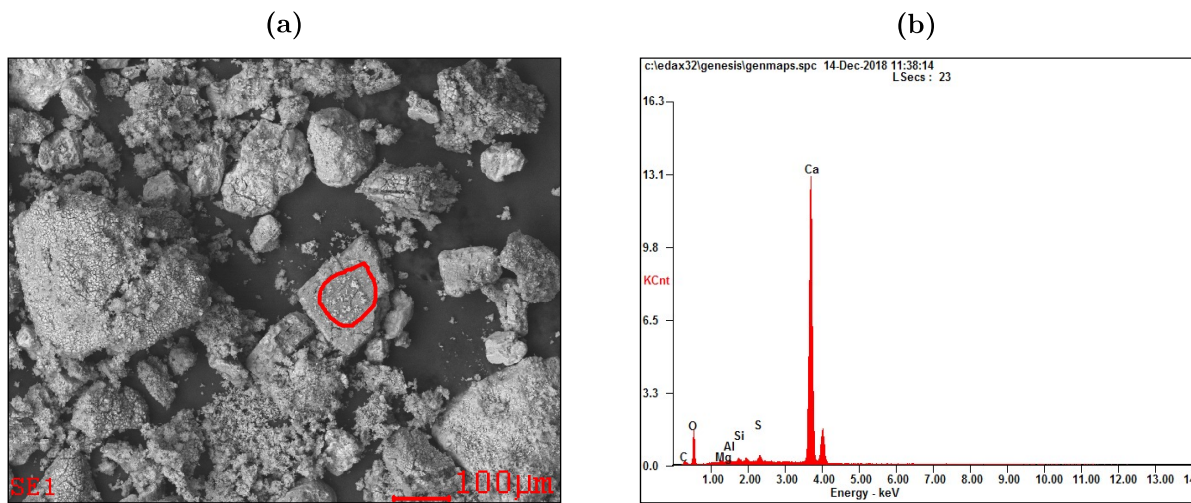**(a)**                                         **(b)**



Figure A.12: EDX imaging of the sulfated Rheinkalk limestone after multiple CaL cycles: (a) SEM micrograph, (b) EDX intensity spectrum

# Bibliography

[1] ABANADES, J. C.: The maximum capture efficiency of $CO_2$ using a carbonation/calcination cycle of $CaO/CaCO_3$. *Chemical Engineering Journal* (90): 303–306, 2002. – DOI: http://dx.doi.org/10.1016/S1385-8947(02)00126-2

[2] ABANADES, J. C.; ALVAREZ, D.: Conversion Limits in the Reaction of $CO_2$ with Lime. *Energy & Fuels* 17(2): 308–315, 2003. – DOI: http://dx.doi.org/10.1021/ef020152a

[3] ABANADES, J. C.; ANTHONY, E. J.; LU, D. Y.; SALVADOR, C.; ALVAREZ, D.: Capture of $CO_2$ from combustion gases in a fluidized bed of CaO. *AIChE Journal* 50(7): 1614–1622, 2004. – DOI: http://dx.doi.org/10.1002/aic.10132

[4] ABDILAHI, A. M.; MUSTAFA, M. W.; ABUJARAD, S. Y.; MUSTAPHA, M.: Harnessing flexibility potential of flexible carbon capture power plants for future low carbon power systems: Review. *Renewable & Sustainable Energy Reviews* 81: 3101–3110, 2018. – DOI: http://dx.doi.org/10.1016/j.rser.2017.08.085

[5] AL-JEBOORI, M. J.; NGUYEN, M.; DEAN, C.; FENNELL, P. S.: Improvement of Limestone-Based $CO_2$ Sorbents for Ca Looping by HBr and Other Mineral Acids. *Industrial & Engineering Chemistry Research* 52(4): 1426–1433, 2013. – DOI: http://dx.doi.org/10.1021/ie302198g

[6] AL-JEBOORI, M. J.; FENNELL, P. S.; NGUYEN, M.; FENG, K.: Effects of Different Dopants and Doping Procedures on the Reactivity of CaO-based Sorbents for $CO_2$ Capture. *Energy & Fuels* 26(11): 6584–6594, 2012. – DOI: http://dx.doi.org/10.1021/ef301153b

[7] ALBRECHT, K. O.; WAGENBACH, K. S.; SATRIO, J. A.; SHANKS, B. H.; WHEELOCK, T. D.: Development of a CaO-Based $CO_2$ Sorbent with Improved Cyclic Stability. *Industrial & Engineering Chemistry Research* 47(20): 7841–7848, 2008. – DOI: http://dx.doi.org/10.1021/ie8007743

[8] ALONSO, M.; ARIAS, B.; FERNÁNDEZ, J. R.; BUGHIN, O.; ABANADES, C.: Measuring attrition properties of calcium looping materials in a 30 kW pilot plant. *Powder Technology* 336: 273–281, 2018. – DOI: http://dx.doi.org/10.1016/j.powtec.2018.06.011

[9] ALONSO, M.; CORDERO, J. M.; ARIAS, B.; ABANADES, J. C.: Sulfation Rates of Particles in Calcium Looping Reactors. *Chemical Engineering & Technology* 37(1): 15–19, 2014. – DOI: http://dx.doi.org/10.1002/ceat.201200614

[10] ALONSO, M.; RODRÍGUEZ, N.; GONZÁLEZ, B.; GRASA, G.; MURILLO, R.; ABANADES, J. C.: Carbon dioxide capture from combustion flue gases with a

calcium oxide chemical loop. Experimental results and process development. *International Journal of Greenhouse Gas Control* 4(2): 167–173, 2010. – DOI: http://dx.doi.org/10.1016/j.ijggc.2009.10.004

[11] ALONSO, M.; RODRÍGUEZ, N.; GRASA, G.; ABANADES, J. C.: Modelling of a fluidized bed carbonator reactor to capture $CO_2$ from a combustion flue gas. *Chemical Engineering Science* 64(5): 883–891, 2009. – DOI: http://dx.doi.org/10.1016/j.ces.2008.10.044

[12] ALONSO, M.; RODRÍGUEZ, N.; GONZÁLEZ, B.; ARIAS, B.; ABANADES, J. C.: Biomass Combustion with in Situ $CO_2$ Capture by CaO. II. Experimental Results. *Industrial & Engineering Chemistry Research* 50(11): 6982–6989, 2011. – DOI: http://dx.doi.org/10.1021/ie102355e

[13] ALVAREZ, D.; ABANADES, J. C.: Determination of the Critical Product Layer Thickness in the Reaction of CaO with $CO_2$. *Industrial & Engineering Chemistry Research* 44(15): 5608–5615, 2005. – DOI: http://dx.doi.org/10.1021/ie050305s

[14] ANTHONY, E. J.; GRANATSTEIN, D. L.: Sulfation phenomena in fluidized bed combustion systems. *Fuel and Energy Abstracts* 43(3): 209, 2002. – DOI: http://dx.doi.org/10.1016/S0140-6701(02)85919-7

[15] ARIAS, B.; ALONSO, M.; ABANADES, J. C.: $CO_2$ Capture by Calcium Looping at Relevant Conditions for Cement Plants: Experimental Testing in a 30 kW$_{th}$ Pilot Plant. *Industrial & Engineering Chemistry Research* 56(10): 2634–2640, 2017. – DOI: http://dx.doi.org/10.1021/acs.iecr.6b04617

[16] ARIAS, B.; CORDERO, J. M.; ALONSO, M.; DIEGO, M. E.; ABANADES, J. C.: Investigation of $SO_2$ Capture in a Circulating Fluidized Bed Carbonator of a Ca Looping Cycle. *Industrial & Engineering Chemistry Research* 52(7): 2700–2706, 2013. – DOI: http://dx.doi.org/10.1021/ie3026828

[17] ARIAS, B.; DIEGO, M. E.; ABANADES, J. C.; LORENZO, M.; DIAZ, L.; MARTÍNEZ, D.; ALVAREZ, J.; SÁNCHEZ-BIEZMA, A.: Demonstration of steady state $CO_2$ capture in a 1.7 MW$_{th}$ calcium looping pilot. *International Journal of Greenhouse Gas Control* 18: 237–245, 2013. – DOI: http://dx.doi.org/10.1016/j.ijggc.2013.07.014

[18] ARIAS, B.; DIEGO, M. E.; MÉNDEZ, A.; ALONSO, M.; ABANADES, J. C.: Calcium looping performance under extreme oxy-fuel combustion conditions in the calciner. *Fuel* 222: 711–717, 2018. – DOI: http://dx.doi.org/10.1016/j.fuel.2018.02.163

[19] ARIAS, B.; GRASA, G.; ABANADES, J. C.; MANOVIC, V.; ANTHONY, E. J.: The Effect of Steam on the Fast Carbonation Reaction Rates of CaO. *Industrial & Engineering Chemistry Research* 51(5): 2478–2482, 2012. – DOI: http://dx.doi.org/10.1021/ie202648p

[20] ARIAS, B.; GRASA, G. S.; ABANADES, J. C.: Effect of sorbent hydration on the average activity of CaO in a Ca-looping system. *Chemical Engineering Journal* 163(3): 324–330, 2010. – DOI: http://dx.doi.org/10.1016/j.cej.2010.08.009

[21] ARIAS, B.; GRASA, G. S.; ALONSO, M.; ABANADES, J. C.: Post-combustion calcium looping process with a highly stable sorbent activity by recarbonation. *Energy & Environmental Science* 5(6): 7353, 2012. – DOI: http://dx.doi.org/10.1039/c2ee03008j

[22] ARIAS, B.; CRIADO, Y. A.; ABANADES, J. C.: Thermal Integration of a Flexible Calcium Looping $CO_2$ Capture System in an Existing Back-Up Coal Power Plant. *ACS omega* 5(10): 4844–4852, 2020. – DOI: http://dx.doi.org/10.1021/acsomega.9b03552

[23] ASTOLFI, M.; DE LENA, E.; ROMANO, M. C.: Improved flexibility and economics of Calcium Looping power plants by thermochemical energy storage. *International Journal of Greenhouse Gas Control* 83: 140–155, 2019. – DOI: http://dx.doi.org/10.1016/j.ijggc.2019.01.023

[24] ATSONIOS, K.; ZENELI, M.; NIKOLOPOULOS, A.; NIKOLOPOULOS, N.; GRAMMELIS, P.; KAKARAS, E.: Calcium looping process simulation based on an advanced thermodynamic model combined with CFD analysis. *Fuel* 153: 370–381, 2015. – DOI: http://dx.doi.org/10.1016/j.fuel.2015.03.014

[25] BARKER, R.: The reversibility of the reaction $CaCO_3 \rightleftharpoons CaO+CO_2$. *Journal of Applied Chemistry and Biotechnology* 23(10): 733–742, 1973. – DOI: http://dx.doi.org/10.1002/jctb.5020231005

[26] BEMROSE, C. R.; BRIDGWATER, J.: A review of attrition and attrition test methods. *Powder Technology* 49(2): 97–126, 1987. – DOI: http://dx.doi.org/10.1016/0032-5910(87)80054-2

[27] BENEDETTI, A.; ILAVSKY, J.; SEGRE, C.; STRUMENDO, M.: Analysis of textural properties of CaO-based $CO_2$ sorbents by ex situ USAXS. *Chemical Engineering Journal* 355: 760–776, 2019. – DOI: http://dx.doi.org/10.1016/j.cej.2018.07.164

[28] BENITEZ-GUERRERO, M.; VALVERDE, J. M.; PEREJON, A.; SANCHEZ-JIMENEZ, P. E.; PEREZ-MAQUEDA, L. A.: Effect of milling mechanism on the $CO_2$ capture performance of limestone in the Calcium Looping process. *Chemical Engineering Journal* 346: 549–556, 2018. – DOI: http://dx.doi.org/10.1016/j.cej.2018.03.146

[29] BERSTAD, D.; ANANTHARAMAN, R.; JORDAL, K.: Post-combustion $CO_2$ capture from a natural gas combined cycle by $CaO/CaCO_3$ looping. *International Journal of Greenhouse Gas Control* 11: 25–33, 2012. – DOI: http://dx.doi.org/10.1016/j.ijggc.2012.07.021

[30] BHATIA, S. K.; PERLMUTTER, D. D.: Effect of the product layer on the kinetics of the $CO_2$–lime reaction. *AIChE Journal* 29(1): 79–86, 1983. – DOI: http://dx.doi.org/10.1002/aic.690290111

[31] BLAMEY, J.; ANTHONY, E. J.; WANG, J.; FENNELL, P. S.: The calcium looping cycle for large-scale $CO_2$ capture. *Progress in Energy and Combustion Science* 36(2): 260–279, 2010. – DOI: http://dx.doi.org/10.1016/j.pecs.2009.10.001

[32] BLAMEY, J.; PATERSON, N. M.; DUGWELL, D. R.; FENNELL, P. S.: Mechanism of Particle Breakage during Reactivation of CaO-Based Sorbents for $CO_2$ Capture. *Energy & Fuels* 24(8): 4605–4616, 2010. – DOI: http://dx.doi.org/10.1021/ef100476d

[33] BORGWARDT, R. H.: Calcination kinetics and surface area of dispersed limestone particles. *AIChE Journal* 31(1): 103–111, 1985. – DOI: http://dx.doi.org/10.1002/aic.690310112

[34] BORGWARDT, R. H.: Sintering of nascent calcium oxide. *Chemical Engineering Science* 44(1): 53–60, 1989. – DOI: http://dx.doi.org/10.1016/0009-2509(89)85232-7

[35] BORGWARDT, R. H.: Calcium oxide sintering in atmospheres containing water and carbon dioxide. *Industrial & Engineering Chemistry Research* 28(4): 493–500, 1989. – DOI: http://dx.doi.org/10.1021/ie00088a019

[36] BOUQUET, E.; LEYSSENS, G.; SCHÖNNENBECK, C.; GILOT, P.: The decrease of carbonation efficiency of CaO along calcination–carbonation cycles: Experiments and modelling. *Chemical Engineering Science* 64(9): 2136–2146, 2009. – DOI: http://dx.doi.org/10.1016/j.ces.2009.01.045

[37] BRODA, M.; MÜLLER, C. R.: Sol–gel-derived, CaO-based, $ZrO_2$-stabilized $CO_2$ sorbents. *Fuel* 127: 94–100, 2014. – DOI: http://dx.doi.org/10.1016/j.fuel.2013.08.004

[38] BUI, M.; ADJIMAN, C. S.; BARDOW, A.; ANTHONY, E. J.; BOSTON, A.; BROWN, S.; FENNELL, P. S.; FUSS, S.; GALINDO, A.; HACKETT, L. A.; HALLETT, J. P.; HERZOG, H. J.; JACKSON, G.; KEMPER, J.; KREVOR, S.; MAITLAND, G. C.; MATUSZEWSKI, M.; METCALFE, I. S.; PETIT, C.; PUXTY, G.; REIMER, J.; REINER, D. M.; RUBIN, E. S.; SCOTT, S. A.; SHAH, N.; SMIT, B.; TRUSLER, J. M.; WEBLEY, P.; WILCOX, J.; MAC DOWELL, N.: Carbon capture and storage (CCS): the way forward. *Energy & Environmental Science* 11(5): 1062–1176, 2018. – DOI: http://dx.doi.org/10.1039/c7ee02342a

[39] CAESAR PROJECT: D 4.9 – European Best Practice Guidelines for Assessment of $CO_2$ Capture Technologies. https://www.ctc-n.org/sites/www.ctc-n.org/files/resources/d_4_9_best_practice_guide.pdf, Last checked: January 2022

[40] CHALMERS, H.; GIBBINS, J.; LEACH, M.: Valuing power plant flexibility with CCS: the case of post-combustion capture retrofits. *Mitigation and Adaptation Strategies for Global Change* 17(6): 621–649, 2012. – DOI: http://dx.doi.org/10.1007/s11027-011-9327-5

[41] CHANG, M.; HUANG, C.; LIU, W.; CHEN, W.; CHENG, J.; CHEN, W.; WEN, T.; OUYANG, S.; SHEN, C.; HSU, H.: Design and Experimental Investigation of Calcium Looping Process for 3-$kW_{th}$ and 1.9-$MW_{th}$ Facilities. *Chemical Engineering & Technology* 36(9): 1525–1532, 2013. – DOI: http://dx.doi.org/10.1002/ceat.201300081

[42] CHARITOS, A.: Experimental characterization of the calcium looping process for $CO_2$ capture, Dissertation. University of Stuttgart, 2013. – DOI: http://dx.doi.org/10.18419/opus-2174

[43] CHARITOS, A.; HAWTHORNE, C.; BIDWE, A. R.; KOROVESIS, L.; SCHUSTER, A.; SCHEFFKNECHT, G.: Hydrodynamic analysis of a 10 kW$_{th}$ Calcium Looping Dual Fluidized Bed for post-combustion $CO_2$ capture. *Powder Technology* 200(3): 117–127, 2010. – DOI: http://dx.doi.org/10.1016/j.powtec.2010.02.012

[44] CHARITOS, A.; HAWTHORNE, C.; BIDWE, A. R.; SIVALINGAM, S.; SCHUSTER, A.; SPLIETHOFF, H.; SCHEFFKNECHT, G.: Parametric investigation of the calcium looping process for $CO_2$ capture in a 10 kW$_{th}$ dual fluidized bed. *International Journal of Greenhouse Gas Control* 4(5): 776–784, 2010. – DOI: http://dx.doi.org/10.1016/j.ijggc.2010.04.009

[45] CHARITOS, A.; RODRÍGUEZ, N.; HAWTHORNE, C.; ALONSO, M.; ZIEBA, M.; ARIAS, B.; KOPANAKIS, G.; SCHEFFKNECHT, G.; ABANADES, J. C.: Experimental Validation of the Calcium Looping $CO_2$ Capture Process with Two Circulating Fluidized Bed Carbonator Reactors. *Industrial & Engineering Chemistry Research* 50(16): 9685–9695, 2011. – DOI: http://dx.doi.org/10.1021/ie200579f

[46] CHEN, Z.; SONG, H. S.; PORTILLO, M.; LIM, C. J.; GRACE, J. R.; ANTHONY, E. J.: Long-Term Calcination/Carbonation Cycling and Thermal Pretreatment for $CO_2$ Capture by Limestone and Dolomite. *Energy & Fuels* 23(3): 1437–1444, 2009. – DOI: http://dx.doi.org/10.1021/ef800779k

[47] CHI, C.; LI, Y.; MA, X.; DUAN, L.: $CO_2$ capture performance of CaO modified with by-product of biodiesel at calcium looping conditions. *Chemical Engineering Journal* 326: 378–388, 2017. – DOI: http://dx.doi.org/10.1016/j.cej.2017.05.163

[48] CHRISSAFIS, K.; DAGOUNAKI, C.; PARASKEVOPOULOS, K. M.: The effects of procedural variables on the maximum capture efficiency of $CO_2$ using a carbonation/calcination cycle of carbonate rocks. *Thermochimica Acta* 428(1-2): 193–198, 2005. – DOI: http://dx.doi.org/10.1016/j.tca.2004.10.010

[49] CONNELL, D. P.; LEWANDOWSKI, D. A.; RAMKUMAR, S.; PHALAK, N.; STATNICK, R. M.; FAN, L.: Process simulation and economic analysis of the Calcium Looping Process (CLP) for hydrogen and electricity production from coal and natural gas. *Fuel* 105: 383–396, 2013. – DOI: http://dx.doi.org/10.1016/j.fuel.2012.07.006

[50] COPPOLA, A.; ALLOCCA, M.; MONTAGNARO, F.; SCALA, F.; SALATINO, P.: The effect of steam on $CO_2$ uptake and sorbent attrition in fluidised bed calcium looping: The influence of process conditions and sorbent properties. *Separation and Purification Technology* 189: 101–107, 2017. – DOI: http://dx.doi.org/10.1016/j.seppur.2017.08.001

[51] COPPOLA, A.; ESPOSITO, A.; MONTAGNARO, F.; IULIANO, M.; SCALA, F.; SALATINO, P.: The combined effect of $H_2O$ and $SO_2$ on $CO_2$ uptake and sorbent attrition during fluidised bed calcium looping. *Proceedings of the Combustion Institute* 37(4): 4379–4387, 2019. – DOI: http://dx.doi.org/10.1016/j.proci.2018.08.013

[52] COPPOLA, A.; MONTAGNARO, F.; SALATINO, P.; SCALA, F.: Fluidized bed calcium looping: The effect of $SO_2$ on sorbent attrition and $CO_2$ capture capacity. *Chemical Engineering Journal* 207-208: 445–449, 2012. – DOI: http://dx.doi.org/10.1016/j.cej.2012.06.149

[53] COPPOLA, A.; SALATINO, P.; MONTAGNARO, F.; SCALA, F.: Reactivation by water hydration of the $CO_2$ capture capacity of a calcium looping sorbent. *Fuel* 127: 109–115, 2014. – DOI: http://dx.doi.org/10.1016/j.fuel.2013.09.059

[54] COPPOLA, A.; SCALA, F.; SALATINO, P.; MONTAGNARO, F.: Fluidized bed calcium looping cycles for $CO_2$ capture under oxy-firing calcination conditions: Part 1. Assessment of six limestones. *Chemical Engineering Journal* 231: 537–543, 2013. – DOI: http://dx.doi.org/10.1016/j.cej.2013.07.113

[55] COPPOLA, A.; SCALA, F.; SALATINO, P.; MONTAGNARO, F.: Fluidized bed calcium looping cycles for $CO_2$ capture under oxy-firing calcination conditions: Part 2. Assessment of dolomite vs. limestone. *Chemical Engineering Journal* 231: 544–549, 2013. – DOI: http://dx.doi.org/10.1016/j.cej.2013.07.112

[56] CORDERO, J. M.; ALONSO, M.; ARIAS, B.; ABANADES, J. C.: Sulfation Performance of CaO Purges Derived from Calcium Looping $CO_2$ Capture Systems. *Energy & Fuels* 28(2): 1325–1330, 2014. – DOI: http://dx.doi.org/10.1021/ef402384z

[57] CORMOS, A.; SIMON, A.: Dynamic Modelling of $CO_2$ Capture by Calcium-Looping Cycle. *Chemical Engineering Transactions* 35: 421–426, 2013. – DOI: http://dx.doi.org/10.3303/CET1335070

[58] CORMOS, A.; SIMON, A.: Assessment of $CO_2$ capture by calcium looping (CaL) process in a flexible power plant operation scenario. *Applied Thermal Engineering* 80: 319–327, 2015. – DOI: http://dx.doi.org/10.1016/j.applthermaleng.2015.01.059

[59] CORMOS, C.: Assessment of chemical absorption/adsorption for post-combustion $CO_2$ capture from Natural Gas Combined Cycle (NGCC) power plants. *Applied Thermal Engineering* 82: 120–128, 2015. – DOI: http://dx.doi.org/10.1016/j.applthermaleng.2015.02.054

[60] CRIADO, Y. A.; ARIAS, B.; ABANADES, J. C.: Calcium looping $CO_2$ capture system for back-up power plants. *Energy & Environmental Science* 10(9): 1994–2004, 2017. – DOI: http://dx.doi.org/10.1039/C7EE01505D

[61] CRIADO, Y. A.; ARIAS, B.; ABANADES, J. C.: Effect of the Carbonation Temperature on the $CO_2$ Carrying Capacity of CaO. *Industrial & Engineering Chemistry Research* 57(37): 12595–12599, 2018. – DOI: http://dx.doi.org/10.1021/acs.iecr.8b02111

[62] CURRAN, G. P.; FINK, C. E.; GORIN, E.: $CO_2$ Acceptor Gasification Process in: Shora, F. C., Fuel Gasification. American Chemical Society, 1967. – ISBN: 0–8412–0070–X. – DOI: http://dx.doi.org/10.1021/ba-1967-0069.ch010

[63] DAVISON, J.: Flexible CCS plants–A key to near-zero emission electricity systems. *Energy Procedia* 4: 2548–2555, 2011. – DOI: http://dx.doi.org/10.1016/j.egypro.2011.02.152

[64] DAVISON, J.; ARIENTI, S.; COTONE, P.; MANCUSO, L.: Co-production of hydrogen and electricity with $CO_2$ capture. *Energy Procedia* 1(1): 4063–4070, 2009. – DOI: http://dx.doi.org/10.1016/j.egypro.2009.02.213

[65] DE LENA, E.; SPINELLI, M.; GATTI, M.; SCACCABAROZZI, R.; CAMPANARI, S.; CONSONNI, S.; CINTI, G.; ROMANO, M. C.: Techno-economic analysis of calcium looping processes for low $CO_2$ emission cement plants. *International Journal of Greenhouse Gas Control* 82: 244–260, 2019. – DOI: http://dx.doi.org/10.1016/j.ijggc.2019.01.005

[66] DE LENA, E.; SPINELLI, M.; MARTÍNEZ, I.; GATTI, M.; SCACCABAROZZI, R.; CINTI, G.; ROMANO, M. C.: Process integration study of tail-end Ca-Looping process for $CO_2$ capture in cement plants. *International Journal of Greenhouse Gas Control* 67: 71–92, 2017. – DOI: http://dx.doi.org/10.1016/j.ijggc.2017.10.005

[67] DIEGO, M. E.; ALONSO, M.: Operational feasibility of biomass combustion with in situ $CO_2$ capture by CaO during 360 h in a 300 $kW_{th}$ calcium looping facility. *Fuel* 181: 325–329, 2016. – DOI: http://dx.doi.org/10.1016/j.fuel.2016.04.128

[68] DIEGO, M. E.; ARIAS, B.: Impact of load changes on the carbonator reactor of a 1.7 $MW_{th}$ calcium looping pilot plant. *Fuel Processing Technology* 200: 106307, 2020. – DOI: http://dx.doi.org/10.1016/j.fuproc.2019.106307

[69] DIEGO, M. E.; ARIAS, B.; ABANADES, J. C.: Investigation of the dynamic evolution of the $CO_2$ carrying capacity of solids with time in La Pereda 1.7 $MW_{th}$ calcium looping pilot plant. *International Journal of Greenhouse Gas Control* 92: 102856, 2020. – DOI: http://dx.doi.org/10.1016/j.ijggc.2019.102856

[70] DIEGO, M. E.; ARIAS, B.; MÉNDEZ, A.; LORENZO, M.; DÍAZ, L.; SÁNCHEZ-BIEZMA, A.; ABANADES, J. C.: Experimental testing of a sorbent reactivation process in La Pereda 1.7 $MW_{th}$ calcium looping pilot plant. *International Journal of Greenhouse Gas Control* 50: 14–22, 2016. – DOI: http://dx.doi.org/10.1016/j.ijggc.2016.04.008

[71] DIEGO, M. E.; ARIAS, B.; GRASA, G.; ABANADES, J. C.: Design of a Novel Fluidized Bed Reactor To Enhance Sorbent Performance in $CO_2$ Capture Systems Using CaO. *Industrial & Engineering Chemistry Research* 53(24): 10059–10071, 2014. – DOI: http://dx.doi.org/10.1021/ie500630p

[72] DIETER, H.; BEIROW, M.; SCHWEITZER, D.; HAWTHORNE, C.; SCHEFFKNECHT, G.: Efficiency and Flexibility Potential of Calcium Looping $CO_2$ Capture. *Energy Procedia* 63: 2129–2137, 2014. – DOI: http://dx.doi.org/10.1016/j.egypro.2014.11.230

[73] DIETER, H.; BIDWE, A. R.; VAREL, G. D.; CHARITOS, A.; HAWTHORNE, C.; SCHEFFKNECHT, G.: Development of the calcium looping $CO_2$ capture technology from lab to pilot scale at IFK, University of Stuttgart. *Fuel* 127: 23–37, 2014. – DOI: http://dx.doi.org/10.1016/j.fuel.2014.01.063

[74] DIETER, H.; HAWTHORNE, C.; ZIEBA, M.; SCHEFFKNECHT, G.: Progress in Calcium Looping Post Combustion $CO_2$ Capture: Successful Pilot Scale Demonstration. *Energy Procedia* 37: 48–56, 2013. – DOI: http://dx.doi.org/10.1016/j.egypro.2013.05.084

[75] DOBNER, S.; STERNS, L.; GRAFF, R. A.; SQUIRES, A. M.: Cyclic Calcination and Recarbonation of Calcined Dolomite. *Industrial & Engineering Chemistry Process Design and Development* 16(4): 479–486, 1977. – DOI: http://dx.doi.org/10.1021/i260064a008

[76] DOMENICHINI, R.; MANCUSO, L.; FERRARI, N.; DAVISON, J.: Operating Flexibility of Power Plants with Carbon Capture and Storage (CCS). *Energy Procedia* 37: 2727–2737, 2013. – DOI: http://dx.doi.org/10.1016/j.egypro.2013.06.157

[77] DONAT, F.; FLORIN, N. H.; ANTHONY, E. J.; FENNELL, P. S.: Influence of high-temperature steam on the reactivity of CaO sorbent for $CO_2$ capture. *Environmental Science & Technology* 46(2): 1262–1269, 2012. – DOI: http://dx.doi.org/10.1021/es202679w

[78] DUELLI, G.; CHARITOS, A.; ARMBRUST, N.; DIETER, H.; SCHEFFKNECHT, G.: Analysis of the calcium looping system behavior by implementing simple reactor and attrition models at a 10 $kW_{th}$ dual fluidized bed facility under continuous operation. *Fuel* 169: 79–86, 2016. – DOI: http://dx.doi.org/10.1016/j.fuel.2015.11.070

[79] ERANS, M.; BEISHEIM, T.; MANOVIC, V.; JEREMIAS, M.; PATCHIGOLLA, K.; DIETER, H.; DUAN, L.; ANTHONY, E. J.: Effect of $SO_2$ and steam on $CO_2$ capture performance of biomass-templated calcium aluminate pellets. *Faraday Discussions* 192: 97–111, 2016. – DOI: http://dx.doi.org/10.1039/c6fd00027d

[80] ERANS, M.; MANOVIC, V.; ANTHONY, E. J.: Calcium looping sorbents for $CO_2$ capture. *Applied Energy* 180: 722–742, 2016. – DOI: http://dx.doi.org/10.1016/j.apenergy.2016.07.074

[81] ERANS, M.; JEREMIAS, M.; MANOVIC, V.; ANTHONY, E. J.: Operation of a 25 $kW_{th}$ Calcium Looping Pilot-plant with High Oxygen Concentrations in the Calciner. *Journal of Visualized Experiments* 128: 1–10, 2017. – DOI: http://dx.doi.org/10.3791/56112

[82] FENNELL, P. S.; DAVIDSON, J. F.; DENNIS, J. S.; HAYHURST, A. N.: Regeneration of sintered limestone sorbents for the sequestration of $CO_2$ from combustion and other systems. *Journal of the Energy Institute* 80(2): 116–119, 2007. – DOI: http://dx.doi.org/10.1179/174602207X189175

[83] FENNELL, P. S.; PACCIANI, R.; DENNIS, J. S.; DAVIDSON, J. F.; HAYHURST, A. N.: The Effects of Repeated Cycles of Calcination and Carbonation on a Variety of Different Limestones, as Measured in a Hot Fluidized Bed of Sand. *Energy & Fuels* 21(4): 2072–2081, 2007. – DOI: http://dx.doi.org/10.1021/ef060506o

[84] GARCÍA-LABIANO, F.; ABAD, A.; DIEGO, L. F.; GAYÁN, P.; ADÁNEZ, J.: Calcination of calcium-based sorbents at pressure in a broad range of $CO_2$ concentrations. *Chemical Engineering Science* 57(13): 2381–2393, 2002. – DOI: http://dx.doi.org/10.1016/S0009-2509(02)00137-9

[85] GECOS: Group of Energy Conversion Systems. http://www.gecos.polimi.it/research-areas/carbon-capture-technologies/, Last checked: January 2022

[86] GONZÁLEZ, B.; ALONSO, M.; ABANADES, J. C.: Sorbent attrition in a carbonation/calcination pilot plant for capturing $CO_2$ from flue gases. *Fuel* 89(10): 2918–2924, 2010. – DOI: http://dx.doi.org/10.1016/j.fuel.2010.01.019

[87] GONZÁLEZ, B.; BLAMEY, J.; MCBRIDE-WRIGHT, M.; CARTER, N.; DUGWELL, D.; FENNELL, P.; ABANADES, J. C.: Calcium looping for $CO_2$ capture: sorbent enhancement through doping. *Energy Procedia* 4: 402–409, 2011. – DOI: http://dx.doi.org/10.1016/j.egypro.2011.01.068

[88] GOUGH, C.; UPHAM, P.: Biomass energy with carbon capture and storage (BECCS or Bio-CCS). *Greenhouse Gases: Science and Technology* 1(4): 324–334, 2011. – DOI: http://dx.doi.org/10.1002/ghg.34

[89] GRASA, G.; ABANADES, J. C.: $CO_2$ Capture Capacity of CaO in Long Series of Carbonation/Calcination Cycles. *Industrial & Engineering Chemistry Research* 45(26): 8846–8851, 2006. – DOI: http://dx.doi.org/10.1021/ie0606946

[90] GRASA, G.; ABANADES, J. C.; ALONSO, M.; GONZÁLEZ, B.: Reactivity of highly cycled particles of CaO in a carbonation/calcination loop. *Chemical Engineering Journal* 137(3): 561–567, 2008. – DOI: http://dx.doi.org/10.1016/j.cej.2007.05.017

[91] GRASA, G.; ABANADES, J. C.; ANTHONY, E. J.: Effect of Partial Carbonation on the Cyclic CaO Carbonation Reaction. *Industrial & Engineering Chemistry Research* 48(20): 9090–9096, 2009. – DOI: http://dx.doi.org/10.1021/ie900443y

[92] GRASA, G.; ALONSO, M.; ABANADES, J. C.: Sulfation of CaO Particles in a Carbonation/Calcination Loop to Capture $CO_2$. *Industrial & Engineering Chemistry Research* 47(5): 1630–1635, 2008. – DOI: http://dx.doi.org/10.1021/ie070937+

[93] GRASA, G.; MARTÍNEZ, I.; DIEGO, M. E.; ABANADES, J. C.: Determination of CaO Carbonation Kinetics under Recarbonation Conditions. *Energy & Fuels* 28(6): 4033–4042, 2014. – DOI: http://dx.doi.org/10.1021/ef500331t

[94] GUPTA, H.; FAN, L.: Carbonation−Calcination Cycle Using High Reactivity Calcium Oxide for Carbon Dioxide Separation from Flue Gas. *Industrial & Engineering Chemistry Research* 41(16): 4035–4042, 2002. – DOI: http://dx.doi.org/10.1021/ie010867l

[95] HAAF, M.; HILZ, J.; PETERS, J.; UNGER, A.; STRÖHLE, J.; EPPLE, B.: Operation of a 1 $MW_{th}$ calcium looping pilot plant firing waste-derived fuels in the calciner. *Powder Technology* 372: 267–274, 2020. – DOI: http://dx.doi.org/10.1016/j.powtec.2020.05.074

[96] HAAF, M.; PETERS, J.; HILZ, J.; UNGER, A.; STRÖHLE, J.; EPPLE, B.: Combustion of Solid Recovered Fuels within the Calcium Looping Process - Experimental Demonstration at 1 $MW_{th}$ Scale. *Experimental Thermal and Fluid Science* 113: 110023, 2019. – DOI: http://dx.doi.org/10.1016/j.expthermflusci.2019.110023

[97] HAN, L.; ZHANG, Y.; LIN, K.; JIA, X.; ZHANG, H.; ZHONG, Y.; WANG, Q.; LI, Z.: Developing a Novel CaO-Based Sorbent for Promoted $CO_2$ Capture and Tar Reduction. *Energy & Fuels* 31(5): 5306–5317, 2017. – DOI: http://dx.doi.org/10.1021/acs.energyfuels.6b03409

[98] HANAK, D. P.; BILIYOK, C.; MANOVIC, V.: Calcium looping with inherent energy storage for decarbonisation of coal-fired power plant. *Energy & Environmental Science* 9(3): 971–983, 2016. – DOI: http://dx.doi.org/10.1039/C5EE02950C

[99] HANAK, D. P.; POWELL, D.; MANOVIC, V.: Techno-economic analysis of oxy-combustion coal-fired power plant with cryogenic oxygen storage. *Applied Energy* 191: 193–203, 2017. – DOI: http://dx.doi.org/10.1016/j.apenergy.2017.01.049

[100] HAWTHORNE, C.; CHARITOS, A.; PEREZ-PULIDO, C. A.; BING, Z.; SCHEFFKNECHT, G.: Design of a dual fluidised bed system for the post-combustion removal of $CO_2$ using CaO. Part I: CFB carbonator reactor model. Proceedings of the 9$^{th}$ International Conference on Circulating Fluidized Beds. TuTech Innovation GmbH, 2008. – ISBN: 393040057X

[101] HAWTHORNE, C.; TROSSMANN, M.; GALINDO CIFRE, P.; SCHUSTER, A.; SCHEFFKNECHT, G.: Simulation of the carbonate looping power cycle. *Energy Procedia* 1(1): 1387–1394, 2009. – DOI: http://dx.doi.org/10.1016/j.egypro.2009.01.182

[102] HILZ, J.; HELBIG, M.; HAAF, M.; DAIKELER, A.; STRÖHLE, J.; EPPLE, B.: Long-term pilot testing of the carbonate looping process in 1 $MW_{th}$ scale. *Fuel* 210: 892–899, 2017. – DOI: http://dx.doi.org/10.1016/j.fuel.2017.08.105

[103] HOFBAUER, G.: Experimentelle Untersuchung der Oxy-Fuel-Verbrennung von Steinkohle in einer zirkulierenden Wirbelschichtfeuerung, Dissertation. University of Stuttgart, 2017. – DOI: http://dx.doi.org/10.18419/opus-9129

[104] HOMSY, S. L.; MORENO, J.; DIKHTIARENKO, A.; GASCON, J.; DIBBLE, R. W.: Calcium Looping: On the Positive Influence of $SO_2$ and the Negative Influence of $H_2O$ on $CO_2$ Capture by Metamorphosed Limestone-Derived Sorbents. *ACS omega* 5(50): 32318–32333, 2020. – DOI: http://dx.doi.org/10.1021/acsomega.0c04157

[105] HORNBERGER, M.; MORENO, J.; SCHMID, M.; SCHEFFKNECHT, G.: Experimental investigation of the calcination reactor in a tail-end calcium looping configuration for $CO_2$ capture from cement plants. *Fuel* 284: 118927, 2021. – DOI: http://dx.doi.org/10.1016/j.fuel.2020.118927

[106] HORNBERGER, M.; MORENO, J.; SCHMID, M.; SCHEFFKNECHT, G.: Experimental investigation of the carbonation reactor in a tail-end Calcium Looping configuration for $CO_2$ capture from cement plants. *Fuel Processing Technology* 210: 106557, 2020. – DOI: http://dx.doi.org/10.1016/j.fuproc.2020.106557

[107] HU, G.; DAM-JOHANSEN, K.; WEDEL, S.; HANSEN, J. P.: Enhancement of the Direct Sulfation of Limestone by Alkali Metal Salts, Calcium Chloride, and Hydrogen Chloride. *Industrial & Engineering Chemistry Research* 46(16): 5295–5303, 2007. – DOI: http://dx.doi.org/10.1021/ie070208u

[108] HU, Y.; NAITO, S.; KOBAYASHI, N.; HASATANI, M.: $CO_2$, $NO_x$ and $SO_2$ emissions from the combustion of coal with high oxygen concentration gases. *Fuel* 79(15): 1925–1932, 2000. – DOI: http://dx.doi.org/10.1016/S0016-2361(00)00047-8

[109] HUGHES, R. W.; LU, D.; ANTHONY, E. J.; WU, Y.: Improved Long-Term Conversion of Limestone-Derived Sorbents for In Situ Capture of $CO_2$ in a Fluidized Bed Combustor. *Industrial & Engineering Chemistry Research* 43(18): 5529–5539, 2004. – DOI: http://dx.doi.org/10.1021/ie034260b

[110] HURST, T. F.; COCKERILL, T. T.; FLORIN, N. H.: Life cycle greenhouse gas assessment of a coal-fired power station with calcium looping $CO_2$ capture and offshore geological storage. *Energy & Environmental Science* 5(5): 7132–7150, 2012. – DOI: http://dx.doi.org/10.1039/c2ee21204h

[111] IEA 2011: Harnessing Variable Renewables: A Guide to the Balancing Challenge. International Energy Agency (IEA), 2011

[112] IEA 2016: 20 Years of Carbon Capture and Storage: Accelerating Future Deployment. International Energy Agency (IEA), 2016

[113] IEA 2016: Ready for CCS Retrofit: The potential for equipping China's existing coal fleet with carbon capture and storage. International Energy Agency (IEA), 2016

[114] IEA 2017: Energy Technology Perspectives 2017: Catalysing Energy Technology Transformations. International Energy Agency (IEA), 2017

[115] IEA 2018: Global Energy and $CO_2$ Status Report 2018. International Energy Agency (IEA), 2018

[116] IEA 2019: Global Energy and $CO_2$ Status Report 2019. International Energy Agency (IEA), 2019

[117] IEA 2020: CCUS in Clean Energy Transitions. International Energy Agency (IEA), 2020

[118] IEA 2021: Technology Roadmap: Energy storage. International Energy Agency (IEA), 2021

[119] IEAGHG 2012: Operating Flexibility of Power Plants With CCS. IEA Greenhouse Gas R&D Programme (IEAGHG), 2012

[120] IPCC 2019: Global warming of 1.5 °C. Intergovernmental Panel on Climate Change (IPCC), 2019

[121] KEATLEY, P.; SHIBLI, A.; HEWITT, N. J.: Estimating power plant start costs in cyclic operation. *Applied Energy* 111: 550–557, 2013. – DOI: http://dx.doi.org/10.1016/j.apenergy.2013.05.033

[122] KNOWLEDGE CENTRE 2018: The Shand CCS Feasibility Study Public Report. International CCS Knowledge Centre, 2018

[123] KRZYWANSKI, J.; CZAKIERT, T.; SHIMIZU, T.; MAJCHRZAK-K., I.; SHIMAZAKI, Y.; ZYLKA, A.; GRABOWSKA, K.; SOSNOWSKI, M.: $NO_x$ Emissions from Regenerator of Calcium Looping Process. *Energy & Fuels* 32(5): 6355–6362, 2018. – DOI: http://dx.doi.org/10.1021/acs.energyfuels.8b00944

[124] LARA, Y.; ROMEO, L. M.: On the Flexibility of Coal-fired Power Plants with Integrated Ca-looping $CO_2$ Capture Process. *Energy Procedia* 114: 6552–6562, 2017. – DOI: http://dx.doi.org/10.1016/j.egypro.2017.03.1791

[125] LASHERAS, A.; STRÖHLE, J.; GALLOY, A.; EPPLE, B.: Carbonate looping process simulation using a 1D fluidized bed model for the carbonator. *International Journal of Greenhouse Gas Control* 5(4): 686–693, 2011. – DOI: http://dx.doi.org/10.1016/j.ijggc.2011.01.005

[126] LAURSEN, K.: Sulfation and reactivation characteristics of nine limestones. *Fuel* 79(2): 153–163, 2000. – DOI: http://dx.doi.org/10.1016/S0016-2361(99)00147-7

[127] LI, Z.; FANG, F.; TANG, X.; CAI, N.: Effect of Temperature on the Carbonation Reaction of CaO with $CO_2$. *Energy & Fuels* 26(4): 2473–2482, 2012. – DOI: http://dx.doi.org/10.1021/ef201543n

[128] LI YUEN FONG, J. C.; ANDERSON, C. J.; XIAO, G.; WEBLEY, P. A.; HOADLEY, A. F.: Multi-objective optimisation of a hybrid vacuum swing adsorption and low-temperature post-combustion $CO_2$ capture. *Journal of Cleaner Production* 111(A): 193–203, 2016. – DOI: http://dx.doi.org/10.1016/j.jclepro.2015.08.033

[129] LINDÉN, I.; BACKMAN, P.; BRINK, A.; HUPA, M.: Influence of Water Vapor on Carbonation of CaO in the Temperature Range 400–550 °C. *Industrial & Engineering Chemistry Research* 50(24): 14115–14120, 2011. – DOI: http://dx.doi.org/10.1021/ie2009795

[130] LIU, H.; GIBBS, B.: The influence of calcined limestone on $NO_x$ and $N_2O$ emissions from char combustion in fluidized bed combustors. *Fuel* 80(9): 1211–1215, 2001. – DOI: http://dx.doi.org/10.1016/S0016-2361(00)00212-X

[131] LIU, R.; SHI, X.; WANG, C.; GAO, Y.; XU, S.; HAO, G.; CHEN, S.; LU, A.: Advances in Post-Combustion $CO_2$ Capture by Physical Adsorption: From Materials Innovation to Separation Practice. *ChemSusChem* 14(6): 1428–1471, 2021. – DOI: http://dx.doi.org/10.1002/cssc.202002677

[132] LIU, W.; DENNIS, J. S.; SULTAN, D. S.; REDFERN, S. A.; SCOTT, S. A.: An investigation of the kinetics of $CO_2$ uptake by a synthetic calcium based sorbent. *Chemical Engineering Science* 69(1): 644–658, 2012. – DOI: http://dx.doi.org/10.1016/j.ces.2011.11.036

[133] LÓPEZ, J. M.; GRASA, G.; MURILLO, R.: Evaluation of the effect of inert support on the carbonation reaction of synthetic CaO-based $CO_2$ sorbents. *Chemical Engineering Journal* 350: 559–572, 2018. – DOI: http://dx.doi.org/10.1016/j.cej.2018.05.014

[134] LU, D. Y.; HUGHES, R. W.; ANTHONY, E. J.: Ca-based sorbent looping combustion for $CO_2$ capture in pilot-scale dual fluidized beds. *Fuel Processing Technology* 89(12): 1386–1395, 2008. – DOI: http://dx.doi.org/10.1016/j.fuproc.2008.06.011

[135] LUCQUIAUD, M.; HERRAIZ, L.; SU, D.; THOMSON, C.; CHALMERS, H.; BECIDAN, M.; DITARANTO, M.; ROUSSANALY, S.; ANANTHARAMAN, R.; MORENO, J.; SCHMID, M.; FINNEY, K. N.; POURKASHANIAN, M.; VAN OS, P.; VERONEZI

FIGUEIREDO, R.; GARCIA MORETZ-SOHN MONTEIRO, J.; GOETHEER, E.: Negative Emissions in the Waste-to-Energy Sector: An Overview of the Newest-CCUS Programme. Proceedings of the 15th Greenhouse Gas Control Technologies Conference (GHGT), Abu Dhabi, UAE, 2021. – DOI: http://dx.doi.org/10.2139/ssrn.3812571

[136] LUU, M. T.; ABDUL MANAF, N.; ABBAS, A.: Dynamic modelling and control strategies for flexible operation of amine-based post-combustion $CO_2$ capture systems. *International Journal of Greenhouse Gas Control* 39: 377–389, 2015. – DOI: http://dx.doi.org/10.1016/j.ijggc.2015.05.007

[137] LYSIKOV, A. I.; SALANOV, A. N.; OKUNEV, A. G.: Change of $CO_2$ Carrying Capacity of CaO in Isothermal Recarbonation−Decomposition Cycles. *Industrial & Engineering Chemistry Research* 46(13): 4633–4638, 2007. – DOI: http://dx.doi.org/10.1021/ie0702328

[138] MA, X.; LI, Y.; DUAN, L.; ANTHONY, E. J.; LIU, H.: $CO_2$ capture performance of calcium-based synthetic sorbent with hollow core-shell structure under calcium looping conditions. *Applied Energy* 225: 402–412, 2018. – DOI: http://dx.doi.org/10.1016/j.apenergy.2018.05.008

[139] MAC DOWELL, N.; STAFFELL, I.: The role of flexible CCS in the UK's future energy system. *International Journal of Greenhouse Gas Control* 48(2): 327–344, 2016. – DOI: http://dx.doi.org/10.1016/j.ijggc.2016.01.043

[140] MANOVIC, V.; ANTHONY, E. J.: Thermal Activation of CaO-Based Sorbent and Self-Reactivation during $CO_2$ Capture Looping Cycles. *Environmental Science & Technology* 42(11): 4170–4174, 2008. – DOI: http://dx.doi.org/10.1021/es800152s

[141] MANOVIC, V.; LU, D.; ANTHONY, E. J.: Steam hydration of sorbents from a dual fluidized bed $CO_2$ looping cycle reactor. *Fuel* 87(15-16): 3344–3352, 2008. – DOI: http://dx.doi.org/10.1016/j.fuel.2008.04.035

[142] MANOVIC, V.; ANTHONY, E. J.: Parametric Study on the $CO_2$ Capture Capacity of CaO-Based Sorbents in Looping Cycles. *Energy & Fuels* 22(3): 1851–1857, 2008. – DOI: http://dx.doi.org/10.1021/ef800011z

[143] MANOVIC, V.; ANTHONY, E. J.: Carbonation of CaO-Based Sorbents Enhanced by Steam Addition. *Industrial & Engineering Chemistry Research* 49(19): 9105–9110, 2010. – DOI: http://dx.doi.org/10.1021/ie101352s

[144] MANOVIC, V.; ANTHONY, E. J.; GRASA, G.; ABANADES, J. C.: $CO_2$ Looping Cycle Performance of a High-Purity Limestone after Thermal Activation/Doping. *Energy & Fuels* 22(5): 3258–3264, 2008. – DOI: http://dx.doi.org/10.1021/ef800316h

[145] MARTÍNEZ, A.; LARA, Y.; LISBONA, P.; ROMEO, L. M.: Operation of a Cyclonic Preheater in the Ca-looping for $CO_2$ Capture. *Environmental Science & Technology* 47(19): 11335–11341, 2013. – DOI: http://dx.doi.org/10.1021/es401601k

[146] MARTÍNEZ, I.; GRASA, G.; PARKKINEN, J.; TYNJÄLÄ, T.; HYPPÄNEN, T.; MURILLO, R.; ROMANO, M. C.: Review and research needs of Ca-Looping systems modelling for post-combustion $CO_2$ capture applications. *International Journal of*

*Greenhouse Gas Control* 50: 271–304, 2016. – DOI: http://dx.doi.org/10.1016/j.ijggc.2016.04.002

[147] MARTÍNEZ, I.; ROMANO, M. C.; FERNÁNDEZ, J. R.; CHIESA, P.; MURILLO, R.; ABANADES, J. C.: Process design of a hydrogen production plant from natural gas with $CO_2$ capture based on a novel Ca/Cu chemical loop. *Applied Energy* 114: 192–208, 2014. – DOI: http://dx.doi.org/10.1016/j.apenergy.2013.09.026

[148] MATERIĆ, B. V.; SHEPPARD, C.; SMEDLEY, S. I.: Effect of Repeated Steam Hydration Reactivation on CaO-based Sorbents for $CO_2$ Capture. *Environmental Science & Technology* 44(24): 9496–9501, 2010. – DOI: http://dx.doi.org/10.1021/es102623k

[149] MONTAÑÉS, R. M.; KORPÅS, M.; NORD, L. O.; JAEHNERT, S.: Identifying Operational Requirements for Flexible CCS Power Plant in Future Energy Systems. *Energy Procedia* 86: 22–31, 2016. – DOI: http://dx.doi.org/10.1016/j.egypro.2016.01.003

[150] MORENO, J.; HORNBERGER, M.; SCHMID, M.; SCHEFFKNECHT, G.: Oxy-Fuel Combustion of Hard Coal, Wheat Straw, and Solid Recovered Fuel in a 200 kW$_{th}$ Calcium Looping CFB Calciner. *Energies* 14(8): 2162, 2021. – DOI: http://dx.doi.org/10.3390/en14082162

[151] MORENO, J.; SPÖRL, R.; SCHEFFKNECHT, G.: Flexible operation of the calcium looping $CO_2$ capture process with a BFB/TFB carbonator. Oral presentation at the 7$^{th}$ High Temperature Solid Looping Cycles Network (HTSLCN), Luleå, Sweden, 2017

[152] MORENO, J.; SPÖRL, R.; SCHEFFKNECHT, G.: Increased load flexibility of the Calcium Looping $CO_2$ capture process with a bubbling/turbulent fluidized bed carbonator. Proceedings of the 23$^{rd}$ International Conference on Fluidized Bed Conversion (FBC), Seoul, Korea, 2018. – ISBN: 978–89–950005–7–1

[153] MORENO, J.; SPÖRL, R.; SCHEFFKNECHT, G.: $CO_2$ Capture with a Highly Flexible Calcium Looping System Using a BFB/TFB Carbonator. Proceedings of the 14$^{th}$ Greenhouse Gas Control Technologies Conference (GHGT), Melbourne, Australia, 2019. – DOI: http://dx.doi.org/10.2139/ssrn.3332625

[154] MORENO, J.; HOMSY, S. L.; SCHMID, M.; SCHEFFKNECHT, G.: Calcium Looping: Sorbent and Process Characterization in a 20 kW$_{th}$ Dual Fluidized Bed. *Energy & Fuels* 35(20): 16693–16704, 2021. – DOI: http://dx.doi.org/10.1021/acs.energyfuels.1c01734

[155] MORENO, J.; HORNBERGER, M.; SCHMID, M.; SCHEFFKNECHT, G.: Part-Load Operation of a Novel Calcium Looping System for Flexible $CO_2$ Capture in Coal-Fired Power Plants. *Industrial & Engineering Chemistry Research* 60(19): 7320–7330, 2021. – DOI: http://dx.doi.org/10.1021/acs.iecr.1c00155

[156] NIKOLOPOULOS, A.; NIKOLOPOULOS, N.; CHARITOS, A.; GRAMMELIS, P.; KAKARAS, E.; BIDWE, A. R.; VARELA, G.: High-resolution 3-D full-loop simulation of a CFB carbonator cold model. *Chemical Engineering Science* 90: 137–150, 2013. – DOI: http://dx.doi.org/10.1016/j.ces.2012.12.007

[157] NIKOLOPOULOS, A.; STROH, A.; ZENELI, M.; ALOBAID, F.; NIKOLOPOULOS, N.; STRÖHLE, J.; KARELLAS, S.; EPPLE, B.; GRAMMELIS, P.: Numerical investigation and comparison of coarse grain CFD – DEM and TFM in the case of a 1 $MW_{th}$ fluidized bed carbonator simulation. *Chemical Engineering Science* 163: 189–205, 2017. – DOI: http://dx.doi.org/10.1016/j.ces.2017.01.052

[158] OAKESON, W. G.; CUTLER, I. B.: Effect of $CO_2$ Pressure on the Reaction with CaO. *Journal of the American Ceramic Society* 62(11-12): 556–558, 1979. – DOI: http://dx.doi.org/10.1111/j.1151-2916.1979.tb12729.x

[159] ORTIZ, C.; ROMANO, M. C.; VALVERDE, J. M.; BINOTTI, M.; CHACARTEGUI, R.: Process integration of Calcium-Looping thermochemical energy storage system in concentrating solar power plants. *Energy* 155: 535–551, 2018. – DOI: http://dx.doi.org/10.1016/j.energy.2018.04.180

[160] ORTIZ, C.; VALVERDE, J. M.; CHACARTEGUI, R.; BENÍTEZ-GUERRERO, M.; PEREJÓN, A.; ROMEO, L. M.: The Oxy-CaL process: A novel $CO_2$ capture system by integrating partial oxy-combustion with the Calcium-Looping process. *Applied Energy* 196: 1–17, 2017. – DOI: http://dx.doi.org/10.1016/j.apenergy.2017.03.120

[161] ORTIZ, C.; VALVERDE, J. M.; CHACARTEGUI, R.: Energy Consumption for $CO_2$ Capture by means of the Calcium Looping Process: A Comparative Analysis using Limestone, Dolomite, and Steel Slag. *Energy Technology* 4(10): 1317–1327, 2016. – DOI: http://dx.doi.org/10.1002/ente.201600390

[162] ORTIZ, C.; VALVERDE, J. M.; CHACARTEGUI, R.; PÉREZ-MAQUEDA, L. A.; GIMENEZ-GAVARRELL, P.: Scaling-up the Calcium-Looping Process for $CO_2$ Capture and Energy Storage. *KONA Powder and Particle Journal* 38(0): 189–208, 2021. – DOI: http://dx.doi.org/10.14356/kona.2021005

[163] OZCAN, D. C.; ALONSO, M.; AHN, H.; ABANADES, J. C.; BRANDANI, S.: Process and Cost Analysis of a Biomass Power Plant with in Situ Calcium Looping $CO_2$ Capture Process. *Industrial & Engineering Chemistry Research* 53(26): 10721–10733, 2014. – DOI: http://dx.doi.org/10.1021/ie500606v

[164] PANG, L.; SHAO, Y.; ZHONG, W.; GONG, Z.; LIU, H.: Experimental study of $NO_x$ emissions in a 30 $kW_{th}$ pressurized oxy-coal fluidized bed combustor. *Energy* 194: 116756, 2020. – DOI: http://dx.doi.org/10.1016/j.energy.2019.116756

[165] POUR, N.; WEBLEY, P. A.; COOK, P. J.: Potential for using municipal solid waste as a resource for bioenergy with carbon capture and storage (BECCS). *International Journal of Greenhouse Gas Control* 68: 1–15, 2018. – DOI: http://dx.doi.org/10.1016/j.ijggc.2017.11.007

[166] PU, G.; ZAN, H.; DU, J.; ZHANG, X.: Study on NO Emission in the Oxy-Fuel Combustion of Co-Firing Coal and Biomass in a Bubbling Fluidized Bed Combustor. *BioResources* 12(1): 1890–1902, 2017. – DOI: http://dx.doi.org/10.15376/biores.12.1.1890-1902

[167] RASMUSSEN, M. H.; WEDEL, S.; PEDERSEN, K. H.; ILLERUP, J. B.; DAM-JOHANSEN, K.: Initial reaction between CaO and $SO_2$ under carbonating and non-carbonating conditions. *Chemical Engineering Science* 134: 169–177, 2015. – DOI: http://dx.doi.org/10.1016/j.ces.2015.04.051

[168] RIDHA, F. N.; WU, Y.; MANOVIC, V.; MACCHI, A.; ANTHONY, E. J.: Enhanced $CO_2$ capture by biomass-templated $Ca(OH)_2$-based pellets. *Chemical Engineering Journal* 274: 69–75, 2015. – DOI: http://dx.doi.org/10.1016/j.cej.2015.03.041

[169] RODRÍGUEZ, N.; ALONSO, M.; ABANADES, J. C.: Experimental investigation of a circulating fluidized-bed reactor to capture $CO_2$ with CaO. *AIChE Journal* 57(5): 1356–1366, 2011. – DOI: http://dx.doi.org/10.1002/aic.12337

[170] RODRÍGUEZ, N.; ALONSO, M.; ABANADES, J. C.; CHARITOS, A.; HAWTHORNE, C.; SCHEFFKNECHT, G.; LU, D. Y.; ANTHONY, E. J.: Comparison of experimental results from three dual fluidized bed test facilities capturing $CO_2$ with CaO. *Energy Procedia* 4: 393–401, 2011. – DOI: http://dx.doi.org/10.1016/j.egypro.2011.01.067

[171] ROMANO, M.: Coal-fired power plant with calcium oxide carbonation for post-combustion $CO_2$ capture. *Energy Procedia* 1(1): 1099–1106, 2009. – DOI: http://dx.doi.org/10.1016/j.egypro.2009.01.145

[172] ROMANO, M. C.: Modeling the carbonator of a Ca-looping process for $CO_2$ capture from power plant flue gas. *Chemical Engineering Science* 69(1): 257–269, 2012. – DOI: http://dx.doi.org/10.1016/j.ces.2011.10.041

[173] ROMANO, M. C.; MARTÍNEZ, I.; MURILLO, R.; ARSTAD, B.; BLOM, R.; OZCAN, D. C.; AHN, H.; BRANDANI, S.: Process simulation of Ca-looping processes: Review and guidelines. *Energy Procedia* 37: 142–150, 2013. – DOI: http://dx.doi.org/10.1016/j.egypro.2013.05.095

[174] ROUSSANALY, S.; ANANTHARAMAN, R.; LINDQVIST, K.; ZHAI, H.; RUBIN, E.: Membrane properties required for post-combustion $CO_2$ capture at coal-fired power plants. *Journal of Membrane Science* 511: 250–264, 2016. – DOI: http://dx.doi.org/10.1016/j.memsci.2016.03.035

[175] RYU, H.; GRACE, J. R.; LIM, C. J.: Simultaneous $CO_2/SO_2$ Capture Characteristics of Three Limestones in a Fluidized-Bed Reactor. *Energy & Fuels* 20(4): 1621–1628, 2006. – DOI: http://dx.doi.org/10.1021/ef050277q

[176] SAASTAMOINEN, J. J.; SHIMIZU, T.; TOURUNEN, A.: Effect of attrition on particle size distribution and $SO_2$ capture in fluidized bed combustion under high $CO_2$ partial pressure conditions. *Chemical Engineering Science* 65(1): 550–555, 2010. – DOI: http://dx.doi.org/10.1016/j.ces.2009.06.023

[177] SAASTAMOINEN, J.; PIKKARAINEN, T.; TOURUNEN, A.; RÄSÄNEN, M.; JÄNTTI, T.: Model of fragmentation of limestone particles during thermal shock and calcination in fluidised beds. *Powder Technology* 187(3): 244–251, 2008. – DOI: http://dx.doi.org/10.1016/j.powtec.2008.02.016

[178] SALAUDEEN, S. A.; ACHARYA, B.; DUTTA, A.: CaO-based $CO_2$ sorbents: A review on screening, enhancement, cyclic stability, regeneration and kinetics modelling. *Journal of $CO_2$ Utilization* 23: 179–199, 2018. – DOI: http://dx.doi.org/10.1016/j.jcou.2017.11.012

[179] SALVADOR, C.; LU, D.; ANTHONY, E. J.; ABANADES, J. C.: Enhancement of CaO for $CO_2$ capture in an FBC environment. *Chemical Engineering Journal* 96(1-3): 187–195, 2003. – DOI: http://dx.doi.org/10.1016/j.cej.2003.08.011

[180] SÁNCHEZ-BIEZMA, A.; PANIAGUA, J.; DIAZ, L.; LORENZO, M.; ALVAREZ, J.; MARTÍNEZ, D.; ARIAS, B.; DIEGO, M. E.; ABANADES, J. C.: Testing postcombustion $CO_2$ capture with CaO in a 1.7 $MW_{th}$ pilot facility. *Energy Procedia* 37: 1–8, 2013. – DOI: http://dx.doi.org/10.1016/j.egypro.2013.05.078

[181] SANCHEZ FERNANDEZ, E.; SANCHEZ DEL RIO, M.; CHALMERS, H.; KHAKHARIA, P.; GOETHEER, E.; GIBBINS, J.; LUCQUIAUD, M.: Operational flexibility options in power plants with integrated post-combustion capture. *International Journal of Greenhouse Gas Control* 48(2): 275–289, 2016. – DOI: http://dx.doi.org/10.1016/j.ijggc.2016.01.027

[182] SCACCIA, S.; VANGA, G.; GATTIA, D. M.; STENDARDO, S.: Preparation of CaO-based sorbent from coal fly ash cenospheres for calcium looping process. *Journal of Alloys and Compounds* 801: 123–129, 2019. – DOI: http://dx.doi.org/10.1016/j.jallcom.2019.06.064

[183] SCALA, F.; CHIRONE, R.; SALATINO, P.: Attrition phenomena relevant to fluidized bed combustion and gasification systems in: Scala, F., Woodhead Publishing Series in Energy. Elsevier, 2013. – ISBN: 978–0–85709–541–1. – DOI: http://dx.doi.org/10.1533/9780857098801.1.254

[184] SCALA, F.; SALATINO, P.: Modelling fluidized bed combustion of high-volatile solid fuels. *Chemical Engineering Science* 57(7): 1175–1196, 2002. – DOI: http://dx.doi.org/10.1016/S0009-2509(02)00004-0

[185] SCALA, F.; MONTAGNARO, F.; SALATINO, P.: Sulphation of limestones in a fluidized bed combustor: The relationship between particle attrition and microstructure. *The Canadian Journal of Chemical Engineering* 86(3): 347–355, 2008. – DOI: http://dx.doi.org/10.1002/cjce.20069

[186] SCHAKEL, W.; HUNG, C. R.; TOKHEIM, L.; STRØMMAN, A. H.; WORRELL, E.; RAMÍREZ, A.: Impact of fuel selection on the environmental performance of post-combustion calcium looping applied to a cement plant. *Applied Energy* 210: 75–87, 2018. – DOI: http://dx.doi.org/10.1016/j.apenergy.2017.10.123

[187] SHAH, M.; DEGENSTEIN, N.; ZANFIR, M.; KUMAR, R.; BUGAYONG, J.; BURGERS, K.: Near zero emissions oxy-combustion $CO_2$ purification technology. *Energy Procedia* 4: 988–995, 2011. – DOI: http://dx.doi.org/10.1016/j.egypro.2011.01.146

[188] SHI, J.; LI, Y.; ZHANG, Q.; MA, X.; DUAN, L.; ZHOU, X.: $CO_2$ capture performance of a novel synthetic CaO/sepiolite sorbent at calcium looping conditions. *Applied*

*Energy* 203: 412–421, 2017. – DOI: http://dx.doi.org/10.1016/j.apenergy.2017.06.050

[189] SHIMIZU, T.; HIRAMA, T.; HOSODA, H.; KITANO, K.; INAGAKI, M.; TEJIMA, K.: A Twin Fluid-Bed Reactor for Removal of $CO_2$ from Combustion Processes. *Chemical Engineering Research and Design* 77(1): 62–68, 1999. – DOI: http://dx.doi.org/10.1205/026387699525882

[190] SILABAN, A.; NARCIDA, M.; HARRISON, D. P.: Characteristics of the reversible reaction between $CO_2(g)$ and calcined dolomite. *Chemical Engineering Communications* 146(1): 149–162, 2007. – DOI: http://dx.doi.org/10.1080/00986449608936487

[191] SIVALINGAM, S.: $CO_2$ separation by calcium looping from full and partial fuel oxidation processes, Dissertation. Technical University of Munich, 2012

[192] STANMORE, B. R.; GILOT, P.: Review—calcination and carbonation of limestone during thermal cycling for $CO_2$ sequestration. *Fuel Processing Technology* 86(16): 1707–1743, 2005. – DOI: http://dx.doi.org/10.1016/j.fuproc.2005.01.023

[193] STRÖHLE, J.; JUNK, M.; KREMER, J.; GALLOY, A.; EPPLE, B.: Carbonate looping experiments in a 1 $MW_{th}$ pilot plant and model validation. *Fuel* 127: 13–22, 2014. – DOI: http://dx.doi.org/10.1016/j.fuel.2013.12.043

[194] SUN, P.; GRACE, J. R.; LIM, C. J.; ANTHONY, E. J.: Removal of $CO_2$ by Calcium-Based Sorbents in the Presence of $SO_2$. *Energy & Fuels* 21(1): 163–170, 2007. – DOI: http://dx.doi.org/10.1021/ef060329r

[195] SUN, P.; GRACE, J. R.; LIM, C. J.; ANTHONY, E. J.: Investigation of Attempts to Improve Cyclic $CO_2$ Capture by Sorbent Hydration and Modification. *Industrial & Engineering Chemistry Research* 47(6): 2024–2032, 2008. – DOI: http://dx.doi.org/10.1021/ie070335q

[196] SUN, P.; LIM, C. J.; GRACE, J. R.: Cyclic $CO_2$ capture by limestone-derived sorbent during prolonged calcination/carbonation cycling. *AIChE Journal* 54(6): 1668–1677, 2008. – DOI: http://dx.doi.org/10.1002/aic.11491

[197] SUN, R.; LI, Y.; LIU, H.; WU, S.; LU, C.: $CO_2$ capture performance of calcium-based sorbent doped with manganese salts during calcium looping cycle. *Applied Energy* 89(1): 368–373, 2012. – DOI: http://dx.doi.org/10.1016/j.apenergy.2011.07.051

[198] TAIT, P.; BUSCHLE, B.; MILKOWSKI, K.; AKRAM, M.; POURKASHANIAN, M.; LUCQUIAUD, M.: Flexible operation of post-combustion $CO_2$ capture at pilot scale with demonstration of capture-efficiency control using online solvent measurements. *International Journal of Greenhouse Gas Control* 71: 253–277, 2018. – DOI: http://dx.doi.org/10.1016/j.ijggc.2018.02.023

[199] UNFCCC 2016: The Paris Agreement. Report of the Conference of the Parties on its twenty-first session, held in Paris from 30 November to 11 December 2015 (FCCC/CP/2015/10). United Nations Framework Convention on Climate Change (UNFCCC), 2016

[200] VALVERDE, J. M.; SANCHEZ-JIMENEZ, P. E.; PEREZ-MAQUEDA, L. A.: Calcium-looping for post-combustion $CO_2$ capture. On the adverse effect of sorbent regeneration under $CO_2$. *Applied Energy* 126: 161–171, 2014. – DOI: http://dx.doi.org/10.1016/j.apenergy.2014.03.081

[201] WANG, J.; ANTHONY, E. J.: On the Decay Behavior of the $CO_2$ Absorption Capacity of CaO-Based Sorbents. *Industrial & Engineering Chemistry Research* 44(3): 627–629, 2005. – DOI: http://dx.doi.org/10.1021/ie0493154

[202] WANG, J.; MANOVIC, V.; WU, Y.; ANTHONY, E. J.: A study on the activity of CaO-based sorbents for capturing $CO_2$ in clean energy processes. *Applied Energy* 87(4): 1453–1458, 2010. – DOI: http://dx.doi.org/10.1016/j.apenergy.2009.08.010

[203] WOLF, C.; LEINO, T. J.; STEPHAN, A. R.; AHO, M. J.; SPLIETHOFF, H.: Online Corrosion Measurements in Combination with Deposit and Aerosol Analysis during the Co-firing of Straw with Coal in Electrically Heated, Small-Scale Pulverized Fuel and Circulating Fluidized Bed Systems. *Energy & Fuels* 32(2): 2506–2516, 2018. – DOI: http://dx.doi.org/10.1021/acs.energyfuels.7b03976

[204] WU, Y.; BLAMEY, J.; ANTHONY, E. J.; FENNELL, P. S.: Morphological Changes of Limestone Sorbent Particles during Carbonation/Calcination Looping Cycles in a Thermogravimetric Analyzer (TGA) and Reactivation with Steam. *Energy & Fuels* 24(4): 2768–2776, 2010. – DOI: http://dx.doi.org/10.1021/ef9012449

[205] YANG, S.; XIAO, Y.: Steam Catalysis in CaO Carbonation under Low Steam Partial Pressure. *Industrial & Engineering Chemistry Research* 47(12): 4043–4048, 2008. – DOI: http://dx.doi.org/10.1021/ie8000265

[206] YAO, J. G.; BOOT-HANDFORD, M. E.; ZHANG, Z.; MAITLAND, G. C.; FENNELL, P. S.: Pressurized In Situ $CO_2$ Capture from Biomass Combustion via the Calcium Looping Process in a Spout-Fluidized-Bed Reactor. *Industrial & Engineering Chemistry Research* 59(18): 8571–8580, 2020. – DOI: http://dx.doi.org/10.1021/acs.iecr.9b06989

[207] YIN, J.; ZHANG, C.; QIN, C.; LIU, W.; AN, H.; CHEN, G.; FENG, B.: Reactivation of calcium-based sorbent by water hydration for $CO_2$ capture. *Chemical Engineering Journal* 198-199: 38–44, 2012. – DOI: http://dx.doi.org/10.1016/j.cej.2012.05.078

[208] YLÄTALO, J.; RITVANEN, J.; ARIAS, B.; TYNJÄLÄ, T.; HYPPÄNEN, T.: 1-Dimensional modelling and simulation of the calcium looping process. *International Journal of Greenhouse Gas Control* 9: 130–135, 2012. – DOI: http://dx.doi.org/10.1016/j.ijggc.2012.03.008

[209] YLÄTALO, J.; PARKKINEN, J.; RITVANEN, J.; TYNJÄLÄ, T.; HYPPÄNEN, T.: Modeling of the oxy-combustion calciner in the post-combustion calcium looping process. *Fuel* 113: 770–779, 2013. – DOI: http://dx.doi.org/10.1016/j.fuel.2012.11.041

[210] YLÄTALO, J.; RITVANEN, J.; TYNJÄLÄ, T.; HYPPÄNEN, T.: Model based scale-up study of the calcium looping process. *Fuel* 115: 329–337, 2014. – DOI: http://dx.doi.org/10.1016/j.fuel.2013.07.036

[211] Yu, F.; Phalak, N.; Sun, Z.; Fan, L.: Activation Strategies for Calcium-Based Sorbents for $CO_2$ Capture: A Perspective. *Industrial & Engineering Chemistry Research* 51(4): 2133–2142, 2012. – DOI: http://dx.doi.org/10.1021/ie200802y

[212] Zhao, X.; Zhou, H.; Sikarwar, V. S.; Zhao, M.; Park, A. A.; Fennell, P. S.; Shen, L.; Fan, L.: Biomass-based chemical looping technologies: the good, the bad and the future. *Energy & Environmental Science* 10(9): 1885–1910, 2017. – DOI: http://dx.doi.org/10.1039/C6EE03718F

[213] Zhou, L.; Duan, L.; Anthony, E. J.: A calcium looping process for simultaneous $CO_2$ capture and peak shaving in a coal-fired power plant. *Applied Energy* 235: 480–486, 2019. – DOI: http://dx.doi.org/10.1016/j.apenergy.2018.10.138

[214] Zhou, Z.; Xu, P.; Xie, M.; Cheng, Z.; Yuan, W.: Modeling of the carbonation kinetics of a synthetic CaO-based sorbent. *Chemical Engineering Science* 95: 283–290, 2013. – DOI: http://dx.doi.org/10.1016/j.ces.2013.03.047